



Doctor Thesis

**Modeling and Characterization of
Conical and Parallel Co-Rotating Twin Screw
Extruders**

Submitted by

Dipl.-Ing. Ramesh Kumar Selvasankar



Univ.Prof. Dipl.-Ing.Dr.mont. Clemens Holzer

Leoben, May 2017

Affidavit

I declare in lieu of oath, that I wrote this thesis and performed the associated research myself, using only the literature cited in this volume.

Location, Date

Signature

Acknowledgements

Foremost, I would like to express my deepest gratitude to my advisor Univ.Prof. Dipl.-Ing.Dr.mont. Clemens Holzer for providing me the opportunity in carrying out my doctoral studies and research at the institute. As a mentor he has been guiding me through all the steps of my career and my PhD research. This accomplishment would have not been possible without his guidance.

I express my deep and sincere gratitude to my team leader Dipl.-Ing. Stephan Schuschnigg, for all the interesting discussions we had over extrusion and for his support, guidance, sound advice, good company and lots of ideas throughout the course of my work.

I would like to thank MAS company (Maschinen- und Anlagenbau Schulz GmbH) for providing me the resources to perform the practical experiments in their technical center and for their financial support in carrying out this project. I also thank the Austrian Research Funding Agency (FFG) for funding this project.

I am deeply indebted to Ass.Prof.Dipl.-Ing.Dr.mont. Walter. Friesenbichler, who gave me the chance to come to Austria and supported me to pursue my studies at the Montanuniversity Leoben.

My sincere thanks to Dr.mont. C. T. Vijayakumar for his mentoring, constant encouragement, help and support throughout my career as a polymer technologist.

Special thanks to all the members and colleagues at department of Polymer Processing and Injection Molding of Polymers for their support, the pleasant working atmosphere and practical help they provided me during my research work at the university. I would like to particularly thank Dipl.-Ing. Dr.mont. Ivica Duretek for helping me with the material data.

Lastly, and most importantly, I wish to thank my parents, family and all my friends, for their emotional support and love. To them I dedicate this thesis.

Abstract

The co-rotating intermeshing twin screw extruders are used widely in processing and compounding of polymers. The development of the first conical tightly intermeshing co-rotating twin screw extruder for processing polymer by the company Maschinen und Anlagenbau Schulz GmbH (M-A-S) in 2007 will change the general classification of the twin screw extruders, which till now excludes the conical co-rotating system. The new conical technology has several advantages over the parallel co-rotating twin screws. The main advantage is the large intake volume in the feeding zone, due to the conicity of the extruder, which facilitates the usage of the conical extruders for processing or recycling or compounding materials with very low bulk density, such as film flakes, recycled bottles or wood plastic composites etc.

For an optimal utilization of the parallel or conical co-rotating extruders an in depth knowledge on the processing characteristics of the plasticizing screws are very important. Moreover the quality of the end product is highly influenced by the screw geometry and the configuration. The configuration of the screw is generally based on experiences or applying the "trail and error" method, which is time and cost consuming. The easiest and faster way is to use mathematical process models to predict the processing behavior of the configured screw without carrying out any practical trails. Such process models are available for parallel co-rotating screws. Since the conical co-rotating twin screw extruders are new to the extrusion sector, until now no studies have been carried out on these conical screws for processing polymer materials.

The main focus of this thesis was to develop mathematical process models for the conical co-rotating twin screws, based on the currently available models for parallel screws and to verify the developed models with practical results. Different screw elements and different processing zones of the parallel and conical twin screw extruders were theoretically and experimentally analyzed.

For an accurate process model, the mathematical description of the geometry of screw elements is very essential. The screw geometric description was done, based on the theoretical model described by Booy for the parallel intermeshing twin screws. Due to conicity of the conical screws the geometry of the screw elements varies over the screw axial length. For this reason the screw was discretized into many small segments

and each segment was considered as parallel screw geometry. The influence of the channel profile (Erdmenger, double shear edge and box profile) of the screw elements on process characteristics was analyzed in detail using three dimensional flow simulation.

To calculate the theoretical maximum throughput of the solid conveying zone a model was developed which includes the bulk density correction and the changes in the solid bed width. With this model the maximum throughput of Erdmenger, shear edge and box profile are determined. For modeling the melting mechanism a modified Tadmor model was used, in which the location dependent melt film thickness was taken into consideration. For determining the material temperature changes in the melting zone the frictional heat and heat changes due to conduction were taken into account. The models for solid conveying and melting were based on the models described by Ansahl and Melish for parallel twin screws. Due to complexity in modeling the different phases of material in these zones no accurate results were achieved. Moreover, due to lack of experimental data like melt temperature inside the barrel or screw pulling experiments, the models could not be verified for its accuracy.

The melt conveying models for both parallel and conical screw elements includes the shear, pressure, leakage and apex flows. In order to make the model simpler the temperature changes of the melt due to dissipation and the barrel temperature influences were neglected. The pressure-throughput behavior (screw characteristics), which is the main criteria for the screw element selection, was determined analytically and also calculated using finite element method for different screw elements. The comparison of the predicted data using the developed model showed a good agreement with the experimental data. The degree of fill and back pressure length calculation was determined in this work using an iterative method and the algorithm for determining the back pressure length works accurate and fast.

With the developed mathematical models for conical screws in this work, a software "NCT" was developed for computing the processing behavior of conical co-rotating twin screws with user defined screw configuration and processing parameters. Similar simulating software "2SX" for parallel co-rotating twin screw extruder, especially for the compounders available at the Chair of Polymer Processing, Montanuniversitaet Leoben was developed as a part of this work. With this software, screw configuration

or individual screw elements can be simulated and optimized prior to experimental trials.

Kurzfassung

Der Doppelschneckenextruder, insbesondere der k ä m m e n d e g l e i c h l ä u f i g e Extruder, wird meist für die Verarbeitung und Aufbereitung von Kunststoffen eingesetzt. Der neue konische k ä m m e n d e g l e i c h l ä u f e n d e Doppelschneckenextruder für die Kunststoffverarbeitung entwickelt von der Firma Maschinen und Anlagenbau Schulz GmbH (M-A-S) im Jahr 2007 wird zu einer neuen Klassifizierung der Extruder führen. Diese neue konische Bauform bietet mehr Vorteile, als der parallele Doppelschneckenextruder. Insbesondere die Konizität des Extruders bietet ein hohes Einzugvolumen, welches für die Verarbeitung von Mahlgut oder die Aufbereitung von Kunststoffen mit niedriger Schüttgutdichte (z. B. Flakes, PET Recycling oder WPC) gut ist.

Für eine optimale Nutzung des parallelen oder konischen gleichlaufenden Extruders ist eine detaillierte Kenntnis vom Prozessverhalten der Plastifizierschnecke sehr wichtig. Eine optimale Schneckenkonfiguration ist erforderlich um eine gute Produktqualität zu erreichen. Grundsätzlich werden die Schnecken durch Erfahrungswissen oder durch die traditionelle „Trail-and-Error“-Methode ausgelegt, welche zeit- und kostenintensiv ist. Eine einfache, schnelle, genaue Methode um Schnecken zu konfigurieren und zu optimieren ohne praktische Versuche durchzuführen, ist die Anwendung von mathematischen Prozessmodellen. Solche Modelle sind für die Charakterisierung des parallelen Doppelschneckenextruders vorhanden, aber das Prozessverhalten der konischen gleichlaufenden Maschinen für die Verarbeitung von Kunststoffen wurde bisher nicht im Detail studiert, weil diese Art von Extrudern neu am Extrudermarkt ist.

Das Hauptziel dieser Doktorarbeit war die Entwicklung neuer Prozessmodelle für die konischen gleichläufigen Schnecken auf Basis bestehender Modelle für parallele Maschinen und die Verifizierung der Modelle durch praktische Versuche. In dieser Arbeit wurden verschiedene Schneckenelemente und Verfahrenszonen empirisch und praktisch für parallele und konische Doppelschnecken analysiert.

Für eine genaue Prozessmodellierung ist die Beschreibung der realen Geometrie von Schneckenelementen sehr wichtig. Auf den Grundlagen von Booy für die parallelen dichtk ä m m e n d e n Doppelschnecken wurde die Geometriebeschreibung von verschiedenen Schneckenelementen aufgebaut. Durch die Konizität ändert sich die Schneckengeometrie in axialer Richtung. Aus diesem Grund wurden die Schnecken in

axialer Richtung differentiell betrachtet und die aufgeteilten einzelnen Schichten wurden als parallele Geometrie angenommen. Der Einfluss von Schneckenkanalprofilen (Erdmenger-, Schubflanken- und Doppelschubflankenprofil) auf das Prozessverhalten wurde mittels 3D Simulation im Detail studiert.

Zur Ermittlung des maximal förderbaren Massestroms der Feststoffförderzone wurde ein Feststofffördermodell vorgestellt. Durch eine Korrektur der Schüttdichte und der maximalen Feststoffbreite wurde der maximale Massestrom für Erdmenger-, Schubflanken- und Doppelschubflankenprofile ermittelt. Für die Modellierung des Aufschmelzverhaltens wurde ein modifiziertes Tadmor-Modell eingesetzt, welches eine ortsabhängige Schmelzfilmdicke berücksichtigt. Die Berechnung der Temperaturänderung des Materials durch Dissipation und Wärmeleitung in der Aufschmelzzone wurde berücksichtigt. Die Modelle für die Feststoffförderzone und die Aufschmelzzone basieren auf den Prozessmodellen für parallel gleichlaufende Doppelschneckenextruder von Anshl und Melish. Aufgrund der Komplexität der Modellierung von unterschiedlichen Materialphasen in diesen Zonen wurden keine genauen Ergebnisse erreicht. Auch wegen fehlender Messdaten von konischen Extrudern, z.B. Massetemperatur in den Schneckenkanälen oder Ergebnissen aus Schneckenziehversuchen, war es nicht möglich die Modelle zu verifizieren.

Das Modell für die Schmelzförderung von verschiedenen Schneckenelementen betrachtet Schlepp-, Druck-, Leck- und Zwickelspalt- Volumenströmung. Um das Modell einfacher zu gestalten wurden keine Temperaturänderungen der Schmelze durch Dissipation oder der Zylinderwandtemperatur auf die Massetemperatur berücksichtigt. Die Fördercharakteristik, welche das wichtigste Kriterium für die Schneckenelementauswahl ist, wurde für unterschiedliche Schneckenelemente analytisch mit der „Finite Element Methode“ ermittelt. Der Vergleich der berechneten Werte mit experimentellen Ergebnissen für die einzelnen Schneckenelemente zeigt die Gültigkeit der gewählten Vorgehensweise. Der Schneckenfüllgrad und die Rückstaulänge wurden durch eine iterative Methode ermittelt. Der entwickelte Algorithmus für die Berechnung der Rückstaulänge ist schnell und genau.

Die entwickelten, teilweise komplexen Modelle wurden im Simulationsprogramm „NCT“ implementiert. Dies ermöglicht die Beurteilung des Prozessverhaltens von konisch gleichlaufenden Doppelschnecken für die konfigurierte Schneckengeometrie und Prozessparametern. Ähnlich wurde eine Schneckenauslegungssoftware „2XS“ für

parallel gleichlaufende Doppelschnecken, insbesondere für die Compoundieranlagen am Lehrstuhl für Kunststoffverarbeitung der Montanuniversität Leoben entwickelt. Mit diesem Schneckenberechnungsprogramm ist es möglich, einzelne Schneckenelemente oder eine Schneckenkonfiguration im Vorfeld zu simulieren und zu optimieren ohne praktische Versuche durchzuführen.

CONTENTS

1	Introduction	1
2	Closely Intermeshing Co-Rotating Twin Screw Extruders	5
2.1	Introduction	5
2.2	Intermeshing Co-Rotating Parallel Twin Screw Extruder.....	5
2.2.1	Processing Zones of Twin Screw Extruders	7
2.2.2	Feed Zone	7
2.2.3	Melting Zone.....	8
2.2.4	Filler Feeding Zone	8
2.2.5	Mixing Zone	9
2.2.6	Devolatilization Zone.....	10
2.2.7	Pressure Build-up or Discharge Zone.....	11
2.3	Intermeshing Co-Rotating Conical Twin Screw Extruder	11
2.3.1	Processing Zones of MAS Extruder	15
2.3.2	Conical Modular Screw.....	17
3	Twin Screw Geometry	18
3.1	Introduction	18
3.2	Design Principles of Intermeshing Co-Rotating Twin Screws	19
3.3	Different Screw Channel Profiles.....	23
Standard or Erdmenger Profile.....		24
Double Shear Edge or Box Profile.....		24
Shear Edge or Schubflanken Profile.....		25
3.4	Flow Simulation of Channel Profiles.....	26
3.5	Areas and Free Volume Calculation of Parallel Extruders.....	27
3.6	Geometry of Conical Twin Screw Extruder	30
3.7	Areas and Free Volume Calculation of Conical Extruders	32
4	Screw Elements	33
4.1	Introduction	33

4.2	Conveying Element.....	34
4.3	Backward or Negative Conveying Element.....	36
4.4	Kneading Element.....	37
4.5	Mixing Elements	39
4.5.1	Conveying Mixing Element.....	39
4.5.2	Gear Tooth Mixing Element	41
4.6	Special Shear Element – Blister Ring.....	42
4.7	Screw Elements Used in MAS Extruder.....	43
5	Solid Conveying	46
5.1	Introduction	46
5.2	Feed Zone Screw Geometry	47
5.3	Maximum Solid Bed	48
5.4	Physical Model of Solid Material Feeding Behavior.....	50
5.5	Maximum Throughput	52
5.6	Tailback Length	53
5.7	Bulk Density Correction	57
6	Melting.....	59
6.1	Introduction	59
6.2	Melting Profile Model.....	60
6.3	Melt Temperature Profile.....	63
7	Melt Conveying.....	67
7.1	Introduction	67
7.2	Throughput Characteristics under Isothermal Conditions.....	67
7.2.1	Groove Model.....	67
7.2.2	Forward Conveying Element - Erdmenger Profile.....	69
7.2.3	Forward Conveying Element - Shear Edge Profile	73
7.2.4	Forward Conveying Element - Double Shear Edge or Box Profile.....	75

7.2.5	Dimensionless Screw Characteristic Curves	77
7.2.6	Kneading Element	78
7.2.7	Conveying Mixing Element.....	80
7.2.8	Blister Ring	81
7.2.9	Backward Conveying Element.....	82
7.3	Back Pressure Length	82
7.4	Degree of Fill (DOF).....	83
8	Experimental	85
8.1	Introduction	85
8.2	Conical Co-Rotating Extruder	85
8.3	Parallel Co-Rotating Extruder.....	92
8.4	Materials and Material Data	98
8.4.1	Material	98
8.4.2	Rheological Data	98
8.4.3	pvT Data	99
8.4.4	Thermal Conductivity	101
8.4.5	Specific Heat Capacity.....	102
9	CAE of Co-Rotating Twin Screw Extruders	104
9.1	Introduction	104
9.2	Extruder Modeling Dimensions.....	105
9.3	Calculation Procedure.....	107
9.4	Co-rotating Twin Screw Modeling Tool.....	110
9.4.1	NCT – Conical Co-Rotating Twin Screw Modeling Tool	110
9.4.2	2XS – Parallel Co-Rotating Twin Screw Modeling Tool.....	117
10	Results and Discussions	126
10.1	Comparison of Different Channel Profiles with Flow Simulation	126
10.1.1	Maximum Flow Rate Comparison	127
10.1.2	Comparison of Pressure	128
10.1.3	Comparison of Shearing and Viscosity	131

10.1.4	Comparison of Flow Velocity.....	135
10.2	Conical Twin Screw	136
10.2.1	Trail 1 – Comparison of Theoretical and Experimental Results	136
10.2.2	Trail 2 – Comparison of Theoretical and Experimental Results	140
10.2.3	Scale Up NCT 90 – Metering Zone.....	148
10.2.4	Solid Conveying and Melting.....	153
10.3	Parallel Twin Screw	159
10.3.1	Screw Element Pressure Characteristics.....	159
10.3.2	Screw Pull Out Study and Degree of Fill.....	166
10.3.3	Pressure Profile over Screw Length	171
11	Conclusions	177
12	Nomenclature	180
12.1	Symbols.....	180
12.2	Greek Symbols.....	186
12.3	Acronyms.....	188
13	List of Tables	189
14	List of Figures	190
15	Bibliography	195
16	Appendix.....	200
	Material Data - PP Bormed™ DM55pharm	200

1 Introduction

Co-rotating twin screw extruders are one of the most commonly used extruders for processing polymers. These extruders are extensively used for compounding, mixing, blending, recycling and continuous processing of plastics. They are also used in other industrial sectors like; rubber, wood plastic composites (WPC) and food processing.

The general classification of screw extruders as in many literatures (Rauwendaal C. , 2001) (Kohlgrueber, 2008) (White & Kim, 2010) (Harold F.G., 2005) (Tadmor Z., 1970) is shown in Figure 1.1.

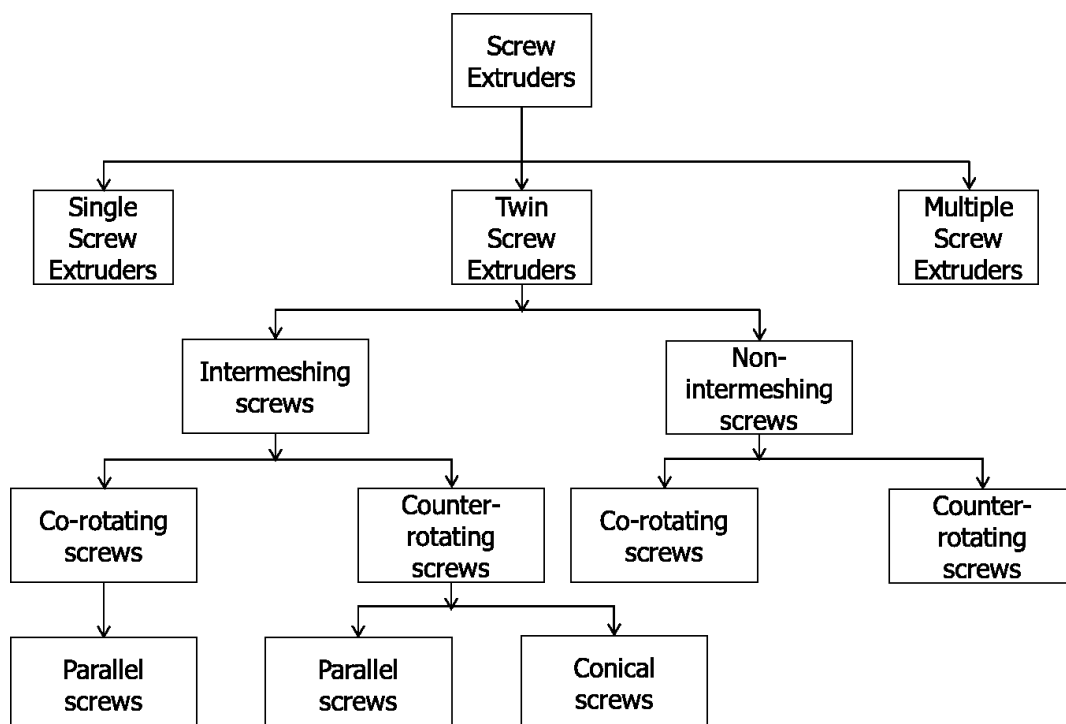


Figure 1.1: Classification of extruders

Extruders can be classified according to the number of screws as single, twin- and multiple screw extruders. The twin screw extruders, which dominate other extruders, can be further classified based on the relative screw rotating as co-rotating (screws rotate in same direction) or counter-rotating twin screw extruders (screws rotate in opposite direction). Referring to the relative closeness of the screws, the twin screw extruders are further classified as intermeshing (partially or fully) and non-intermeshing (separated or tangential) twin screw extruders. Another classification is based on the relative screw diameter at the beginning and at the end of the extruder as parallel and conical twin screw extruders.

In the twin screw family, closely intermeshing, also called as self-cleaning or self-wiping, co-rotating twin screw extruders are widely used because of its good mixing and pumping characteristics and comparatively better residence time than single screw extruders. The twin screw extruders have gained great commercial importance because of its modular construction. Barrel and screws, with different segments and elements can be configured according to the desired processing requirement.

The patent of the first co-rotating, self-cleaning twin screw extruder for polymer extrusion was given in the year 1944 and in 1953 (Erdmenger, Meskat, Dormagen, & Gladbach, 1954); Werner & Pfleiderer obtained the worldwide license (Kohlgrueber, 2008). In the past 60 years, drastic developments were undergone in the processing of polymers using co-rotating twin screw extruders. At present co-rotating twin screw extruders with screw sizes ranging from 16 mm (laboratory size) to 443 mm (mega compounder) are available in market. The maximum output of the currently available largest twin screw extruder is about 100 t/h (Coperion, 2013).

The development of the counter-rotating twin screw extruders for processing polymers (mainly PVCu) started in the year 1939, while the concept of conical counter-rotating screws was developed in 1960's (Schneider, 2005). The counter-rotating twin screws form C-shaped chambers, which convey the material according to the geometry and proportional to screw rotation speed. As there is nearly no interchanging of melt between these chambers the mixing quality is poor. The residence time spectra is very narrow as the particles that enter at a time will be forwarded with the same velocity. Thus the parallel and conical counter-rotating twin screw extruders are mainly used for processing shear and temperature sensitive materials.

In literature, until now no conical co-rotating twin screw extruders is considered under the classification of twin screw extruders. A 2002 patent (Hauck B.W., 2002) to Wenger Manufacturing, Inc. (US), describes the conical intermeshing co-rotating twin screw extruders for pet food processing. The conical screws have only conveying elements, since no plasticization of the material was required. In 2006 the first conical co-rotating intermeshing twin screw extruder, developed and patented (Schulz, 2006) by the company "Maschinen und Anlagen Schulz GmbH" MAS, Austria, was launched at the International Exhibition for Plastics and Rubbers in Duesseldorf in 2007. This extruder is mainly used for recycling, compounding and processing of plastics, WPC and PPC (materials with low bulk density) (Schuschnigg, Klammer, & Holzer, Introduction of the conical co-rotating twin screw extruder, 2010). The extruder comprises modular screws with conveying, mixing and

kneading elements. The concept of conical co-rotating twin screws is also implemented in the field of micro compounding of polymers by Thermo Fisher Scientific Inc. The Thermo Scientific HAAKE MiniCTW micro-conical twin screw compounders are mainly used in laboratories for research and industries that compound expensive or small-scale materials such as nano composites, bio-polymers or pharmaceuticals (Thermo Scientific, 2013).

The successful implementation of the conical co-rotating twin screw extruders by the company MAS, Austria for recycling, processing and compounding of polymers and polymer based composites will lead to the new classification of the screw extruders as shown Figure 1.2:

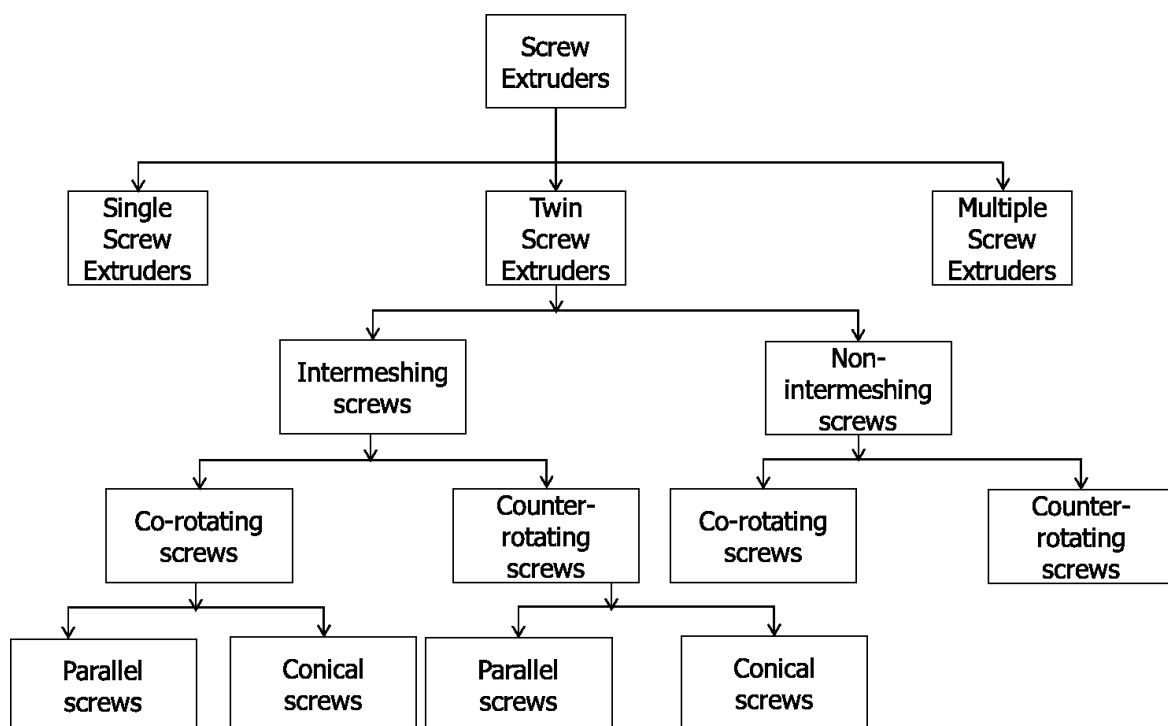


Figure 1.2: New classification of extruders

The basic theoretical studies of the co-rotating twin screw extruders were done based on the Erdmenger's geometry. Booy published a detailed review concerning the twin screw geometry (Booy, 1978) and the flow characteristics in twin screw extruders under fully and partially filled conditions (Booy, 1980). Later several efforts were made by many authors (White & Szydowski, 1987) (Meijer & Elemans, 1988) (Vergnes, Della Valle, & Delamare, 1998) (White, Byong-Jun, Santosh, & Jong, 2001) to study the solid conveying, melting and flow mechanism of non-Newtonian fluids in twin screw elements under isothermal and non-isothermal conditions. Different mathematical models for characterizing the polymer behavior in the different functional zones of a closely intermeshing parallel co-rotating twin screw

extruders have been suggested by the authors. Also several authors used 3D FEM simulations to simulate and study the flow in the conveying, kneading and mixing elements (Gotsis, Ji, & Kalyon, 1990) (Barrera, Vega, & Martinez-Salazar, 2008) (Janssen, et al., 1996) (Bravo, Hrymak, & Wright, 2000). Since MAS conical co-rotating twin screw extruders are the first extruders of this kind, no studies have been done until now on the flow characterization and modeling of this extruder.

The main objective of this dissertation was to model and characterize the different functional zones (solid conveying, melting and melt pumping) of closely intermeshing conical co-rotating twin screw extruders, based on the models developed for parallel co-rotating extruder. Practical experiments were performed on the extruders and the theoretical values were compared with the practical values, in order to verify and optimize the developed model. As a part of this dissertation user friendly software were developed, for modeling the parallel and conical co-rotating twin screw in single dimension (1D). This dissertation is the first effort to study the processing characteristics of conical co-rotating twin screw extruders theoretically and experimentally.

2 Closely Intermeshing Co-Rotating Twin Screw Extruders

2.1 Introduction

The refinement of polymer and its properties are necessary to meet the constantly increasing demands on plastic parts. Modifying the properties of polymers by means of additives and/or blending with other polymers is gaining more importance. Compounding offers a quick, easy and low-cost alternative to discover new grades of plastics.

The modular intermeshing co-rotating twin screw extruder has become the most important of the twin screw machines when it comes to compounding. Also these extruders are probably the most complex of the commercial machines involving several different types of screw elements which are closely intermeshing and self-wiping.

Closely or fully intermeshing means that the screws sit so close to one another in such a manner that, just enough mechanical clearance between the screws is available to avoid the adhesive wear. The top of one screw nests in the root or bottom of the other screw.

They are also self-wiping, since the screws rotate in the opposite direction in the intermeshing region. Thus the tip of one screw wipes or cleans the material from the root of the other screw. This self-cleaning mechanism minimizes the potential for material to stay in one spot of the screw, which may degrade and eventually re-enter the melt as a contaminant.

2.2 Intermeshing Co-Rotating Parallel Twin Screw Extruder

The co-rotating twin screw extruder has the same three basic components as a single screw extruder – drive section, plasticization section and discharge. The length of these extruders is typically described by its L/D ratio (barrel length divided by the diameter of the screw). A typical L/D ratio for a compounder would be between 30 and 40 L/D.

The heart of the extruder is the plasticization unit, barrel and screws (Figure 2.1 a). The extruder barrels are designed as a modular system, which comprises several barrel modules with different openings and inserts for feed of the polymer, additives, venting or degassing. The barrel modules are flanged together depending on the need. Similarly the screw geometry can be tailor made with different screw elements generally like, conveying,

kneading and mixing elements, according to the requirements. Depending on the material processed and the application, various screw elements are slid onto the shaft in the desired configuration. One more major advantage of this modular concept is that the worn out barrel or screw elements could be easily replaced, without replacing the complete plasticization unit and hence reduction in maintenance cost.

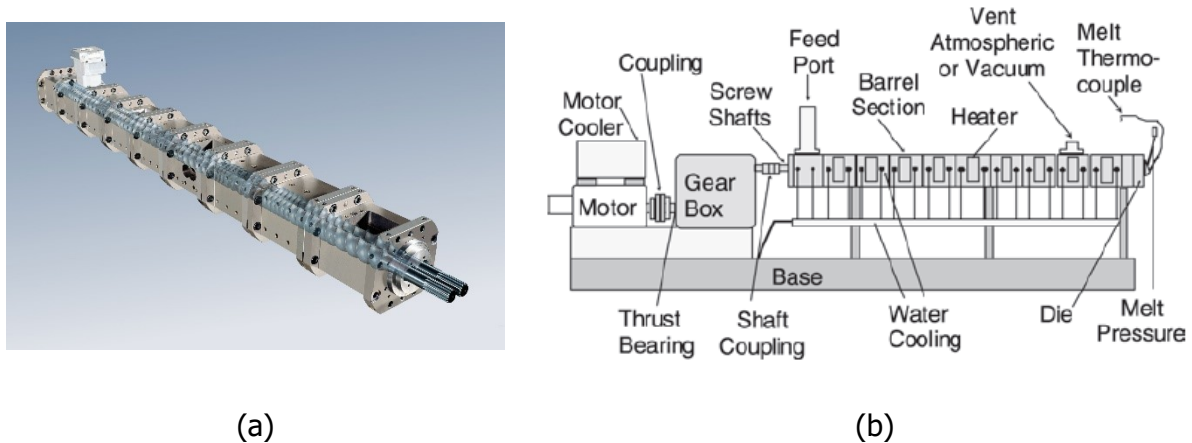


Figure 2.1: a) Construction of segmented screw elements assembled on splined shafts and modular barrel elements (Martin, 2011) b) Main components of a compounder (Harold F.G., 2005)

The other important elements of the extruder, the drive unit (comprising motor, coupling and gear box), cooling system, barrel heaters, die and sensors are shown in Figure 2.1 b. The shafts of the screws are connected to the drive of the extruder. The drive system is composed of a DC Motor, cooling unit for the motor, coupling between motor and the gear box, thrust bearing, gear box, cooling and lubrication for the gear box and shaft coupling. The motor provides the required power and/or torque to the screws, via the gear box and the shaft. The barrel heat is controlled using cooling water, in case the barrel temperature increases due to shear heating or friction.

The die, for producing the required product (pipe, profile or sheet) is connected to the barrel with the help of an adapter. Melt temperature and melt pressure are measure using thermocouple and pressure transducer mounted in the adapter. In some cases screen pack or melt filtration is equipped to remove the foreign particles and to increase back pressure. Also in some cases a gear pump is used between the barrel and die, to generate the required pressure.

2.2.1 Processing Zones of Twin Screw Extruders

The various processing zones of a parallel twin screw compounder are shown in Figure 2.2. The major functional zones of a twin screw extruder are feed zone, plasticization or melting zone, side feed zone, mixing zone, venting zone and discharge or pressure build-up zone. Each processing zone is dependent on the other zone. For example, the incorporation of nano-fillers takes place after melting the matrix polymer and is followed by the mixing zone to disperse the fillers into the polymer matrix.

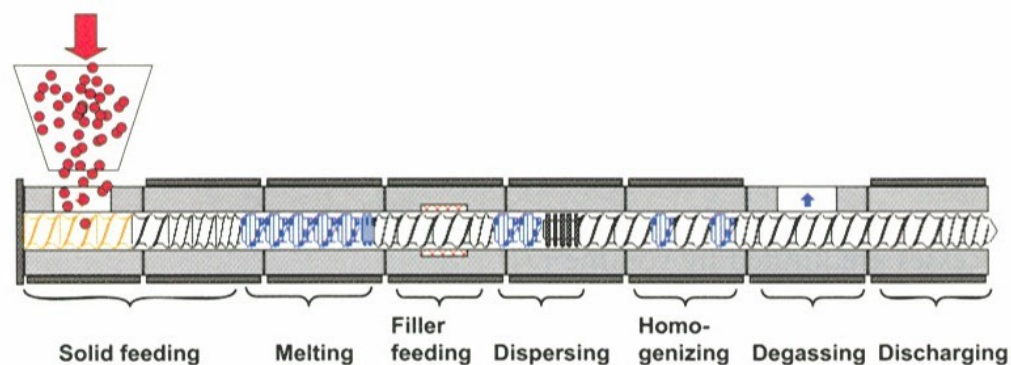


Figure 2.2: Processing zones of parallel twin screw extruder (Kohlgrueber, 2008)

2.2.2 Feed Zone

The main function of the feed zone is to convey the solid material, fed into the barrel from the feed hopper, forward and at the same time compact the solid material, in order to remove the entrapped air that is drawn along with the fed material (Kohlgrueber, 2008). Also in some applications, next to the feed barrel element an atmospheric venting barrel element is used to enhance the removal of trapped air. The friction between the polymer material and the cylinder is one of the main parameters for conveying the material in the forward direction. Due to the frictional heat generation and pre-melting of the polymer in the intake zone, the intake barrel is usually cooled to prevent the sticking of the material to the barrel walls or the feed hopper, affecting the intake characteristics.

The two major feeding methods used for feeding an extruder are force-feeding and starve-feeding. During force-feeding, a reserve of material is maintained in the hopper of the extruder and material is 'positively displaced' or 'forced' into the extruder. Starve-feeding is the condition when an extruder is fed at a rate less than the capacity of the screw feeding

section. The hopper remains empty and functions as a conduit to avoid material from spilling (Padmanabhan, 2008).

The feed capacity depends on the available screw free volume in the intake zone, the screw rotation speed and the bulk density of the polymer. The free volume, which is obtained by subtracting the space occupied by the screw elements inside the 8-shaped barrel, is dependent on the geometry of the screw element used in the feed zone. The modular design of the twin screw allows the configuration of the feed zone with different screw geometries for more free volume or better conveying properties (see chapter 3). In general, for an effective feed, the preferred length of the feed zone is about 4 to 6D (Kohlgrueber, 2008).

2.2.3 Melting Zone

In case of compounding the melting of the polymer matrix takes place before the accession of the filler particles. The melting zone is responsible for transforming the solid material into a melt. The melting process in extruders can be divided into two stages: firstly compacting the bulk material, to reduce the entrapped air between the particles, simultaneously forming a thin melt film on the barrel walls, secondly generating pressure and shearing and mixing the molten and un-molten material (Wang, 2000).

The main factors which influence the melting process are the degree of fill, screw speed, residence time and the throughput. The melting of the polymer begins once the screw elements after the feed zone are completely filled and where the pressure generates. Mostly restrictive screw elements at the end of the melting zone like negative conveying element are used to block the flow in the positive direction, thus improving the fill degree in the melting zone.

2.2.4 Filler Feeding Zone

Once the polymer is completely melted, the incorporation of the fillers is carried out. The side feeding uses either a single screw or double co-rotating screw conveyors for conveying the filler particles from the side into the barrel. The number of screws is dependent on the type, form and bulk density of the filler particles. Also special feeding systems are available for feeding liquid fillers. The filler can be fed either by volumetric or gravimetric feeding system.

2.2.5 Mixing Zone

Mixing is one of the essential functions of a co-rotating twin screw extruder. The goal of the mixing process in an extruder is to increase the uniformity of the composition. Shear and elongation flows are the two common types of flow in a co-rotating twin-screw extruder. Extensional flow can occur as a result of building up of pressure or during its release. Also the usage of mixing elements in fully filled zones is more effective.

The two major types of mixing are dispersive and distributive mixing (Figure 2.3).

In case of distributive mixing the filler particles are just distributed in to the polymer matrix without any agglomeration of the filler particles. For good distributive mixing, the variation in the melt flow directions is necessary. Kneading elements with narrow disc and large staggered angle, conveying element with slots and gear mixing elements are helpful for achieving distributive mixing.

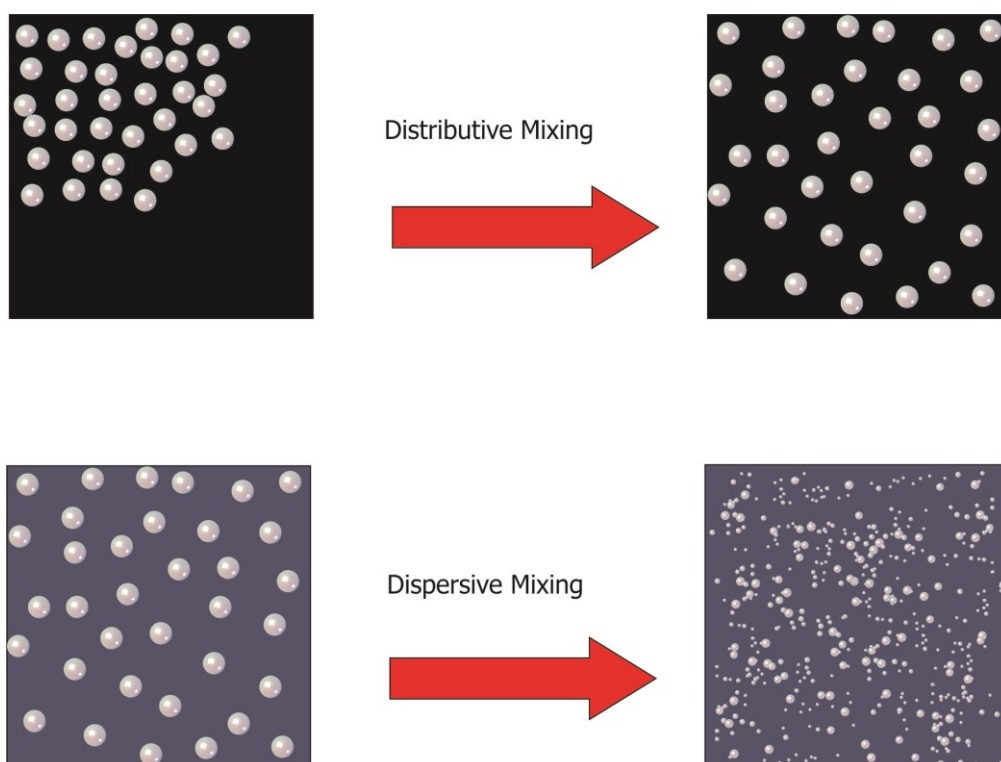


Figure 2.3: Types of mixing in polymer compounding

Dispersive mixing possesses higher shearing in order to disperse the fillers in the matrix. For achieving good dispersiveness, kneading elements with wide discs and with large staggered angle (neutral or negative conveying), negative conveying elements and multiple mixing gears can be used.

The modular concept of twin screw allows the use of different mixing elements according to the needed mixing. The mixing zone is also important for homogenizing the melt.

2.2.6 Devolatilization Zone

The purpose of the venting or degassing zone is to remove the volatiles like, water, residual monomers and other solvents from the melt. Also in some applications vacuum is used for improving the degassing. This zone is partially filled in order to provide large product surface and to prevent the flow of melt through the vent. Figure 2.4 shows the different vent inserts which are available for different materials (Kohlgrueber, 2008).

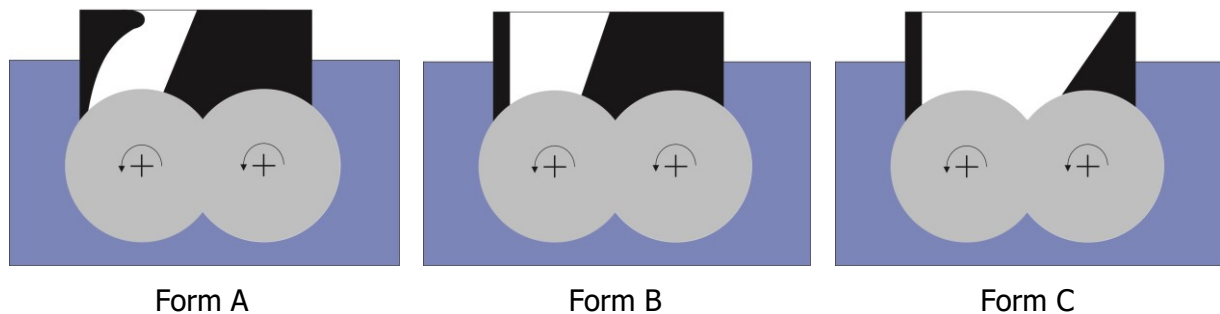


Figure 2.4: Types of venting in twin screw extruders (Kohlgrueber, 2008)

- Form A: Upturning screw and intermeshing area are fully covered, down turning screw is partially covered. Used for polymer melts that do not adhere to the screw (PVC, Polyolefin)
- Form B: Upturning screw and intermeshing area are completely covered. Mainly used for polymer melts that adhere to screw (PA, PET, PC)
- Form C: Upturning screw is partly covered. Implemented mainly for large volume of gas in polymer melt (solvent devolatilization)

A melt seal is the vital requirement for removal of moisture and entrapped air from the melt during compounding at lower than atmospheric pressure. Adequate lengths of vent opening and vent hood design that maximizes the pressure gradient inside the extruder further facilitate this process. The melt seal is achieved by simply ensuring that prior to starting of the vent zone and just after its completion, the melt completely fills up screw channels (degree of fill = 1). Usually a reverse lead element will ensure build-up of a sufficient wall of material behind it. However, depending on the nature of work, adequate melt seal may have

to be build-up to avoid frequent breaking of seal resulting in poor devolatilization. At least "1D" length of the melt seal may be required while running high vacuum with thin melts.

2.2.7 Pressure Build-up or Discharge Zone

The function of the metering or pressure build-up zone is to generate the pressure required in order to overcome the pressure loss when material is flowing through the die or pressure consuming screw elements or any subsequent unit like filters. These zones are located in the discharge zone and upstream of backward pumping elements (Kohlgrueber, 2008). This zone is also called the pumping zone in an extruder. The compounded polymer melt is transported forward by drag flow caused by the rotating action of the screws. Screws with a degree of fill of 1 and with shorter leads are optimum for creating the pumping effect. This zone pumps the homogeneous compounded melt at constant temperature and pressure. The performance of the optimally designed screws is conserved only if the excessive cooling in this zone is avoided.

2.3 Intermeshing Co-Rotating Conical Twin Screw Extruder

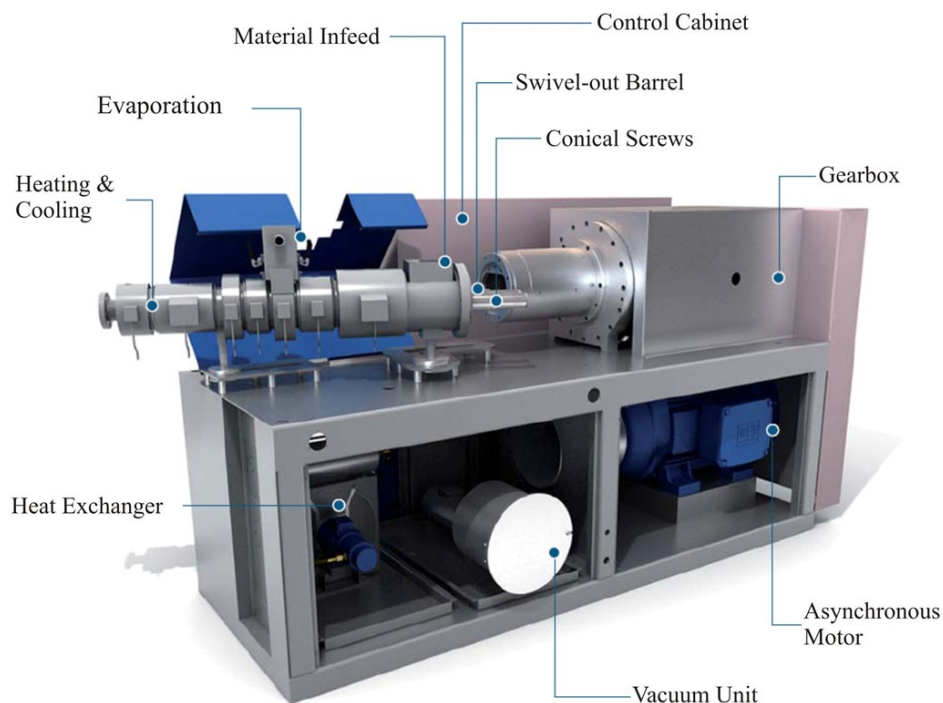


Figure 2.5: MAS 55 conical co-rotating twin screw extruder (MAS Maschinen und Anlagenbau Schulz GmbH, 2016)

The MAS extruder (Figure 2.5) combines the concept of co-rotating twin screw extruder and a conical counter rotating twin screw extruder and combines the advantages of both the systems. The conical design uncouples the geometric relation between diameter and axial spacing and the maximum transferable torque. It gives the possibility to transfer higher torque, roughly four times the torque of parallel co-rotating extruders, and has at the same time a large free volume (Klammer, 2009). The advantage of the conical design is that the feed volume is significantly more than the discharge volume, resulting in high screw fill. Also the large diameter in the melting region benefits high outputs and high melt pressure at even low screw rotation speed (Bittermann & Sykacek, 2007).

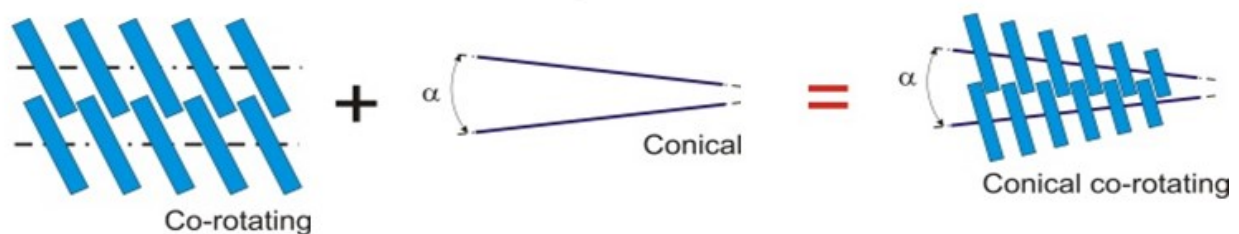


Figure 2.6: Concept of NCT extruder (Klammer G. , 2009)

The technological benefits of the MAS extruder are: (MAS Maschinen und Anlagenbau Schulz GmbH, 2016)

- large input volumes and thus excellent feeding characteristic
- high melt pressure build-up and maximum pressure stability, thus removing the need for a melt pump in most cases
- large shaft diameters allow for high torque
- easy removal of the screw via the rear of the extruder
- excellent homogenization characteristics
- excellent feeding behavior results in a short melt retention time in the extruder at low melt temperature
- extremely low specific energy consumption

The extruder has two tightly intermeshing conical co-rotating screws, which are positioned in the segmented barrel (Figure 2.9). Different screw elements, such as conveying, conveying mixing, kneading and shearing element can be configured modular according to the processing requirements and the material being processed. Special mixing and kneading

elements are used for improving the melt homogeneity. The mixing and plasticizing capacity is set by replacing the screw elements.

The extruder barrel can be swiveled out as shown in Figure 2.5, which eases the screws changing process and the screws can be pulled out from the larger end of the barrel. The material can be fed into the extruder either by a gravimetric or a crammer feeder, depending on the bulk density of the material and the desired throughput. The barrel zones are equipped with heating shells and liquid cooling for regulating the barrel temperature. The barrel is made out of three-parts and can also be modified according to the requirements (with/without degasification, position of degasifying aperture etc.).

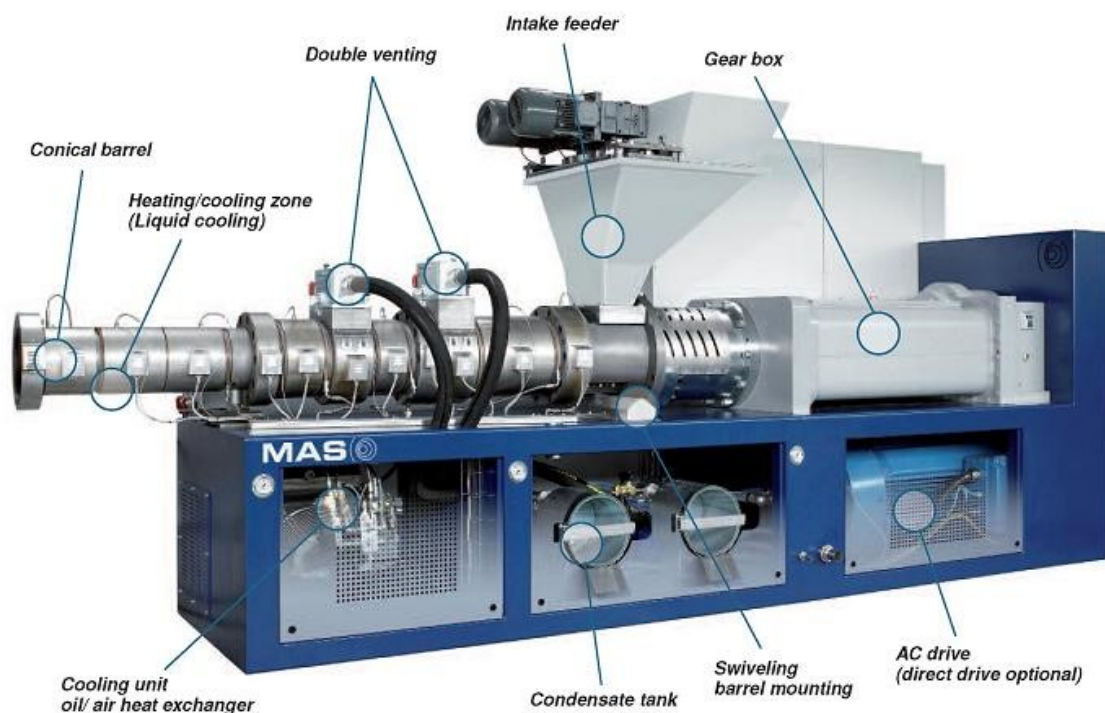


Figure 2.7: MAS 90 extruder with double vent (MAS Maschinen und Anlagenbau Schulz GmbH, 2016)

For most of the polymers processed in an extruder, the evaporation zone is crucial for good product quality. The vacuum venting is present before the metering zone of MAS55 extruder. The vacuum unit of the extruder is placed beneath the barrel. For more effecting venting, in larger size MAS Extruder (for example MAS90) double vent ports are used (Figure 2.7), which is very beneficial during processing materials with high moisture content. The heat exchange for the cooling system is positioned beneath the extruder barrel.

The needed power is provided by a frequency controlled asynchronous motor and transferred via the gearbox to the screw shafts or on newer types via a direct motor.

The conical co-rotating design of the MAS extruder supports a versatile range of applications. The MAS extruder is suitable for any application in the extrusion sector (Figure 2.8):

- recycling of polyolefin, technical plastics and materials that are temperature and shear sensitive
- compounding of plastics, with fillers (CaCO₃, Talcum etc.), fibers, colorant and other additives

The conical, co-rotating MAS extruder offers process stability and economic compounding of plastics with very different characteristics wherever it is necessary to fulfill the quality requirements. Especially in the following areas

- WPC (Wood Plastic Composites)
- PPC (Paper Plastic Composites)
- NFC (Natural Fiber Composites)

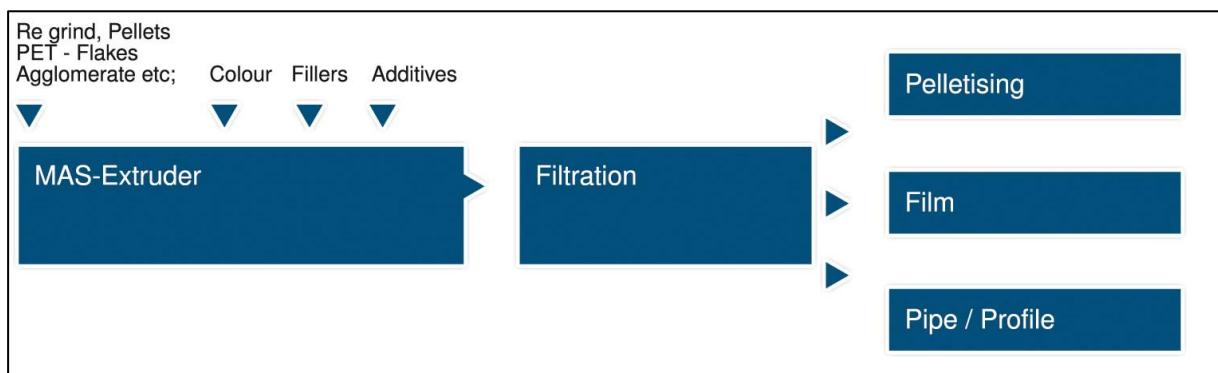


Figure 2.8: Applications of MAS extruder (MAS Maschinen und Anlagenbau Schulz GmbH, 2016)

Generous axis spacing ensures a large intake volume and thus guarantees perfect feeding performance (MAS Maschinen und Anlagenbau Schulz GmbH, 2013). Thanks to its conical design with a substantially larger feed volume, the MAS extruder offers decisive advantages. From a process technology point of view, excellent results are achieved even when compounding high volumes of glass fibers (more than 50 % supported) with a PE/PET or PP melt. A single mixing aperture is used to feed all materials. Complicated multiple dosing, which is typical for cylindrical designs, is unnecessary.

Due to the conical design and the resulting excellent pressure stability of the extruder, process reliability in direct extrusion of WPC/PPC and NFC profiles is ensured. Extruded WPC/PPC/NFC profiles with a wood, paper or fiber content of up to 80 % and at the same time excellent mechanical characteristics are unique selling points in this market sector for MAS's extruders (John Wood & Associates Ltd, 2009).

The different conical extruder series of MAS and their respective throughput capacity is given in Table 2.1.

Table 2.1: MAS Extruder series and throughput (MAS Maschinen und Anlagenbau Schulz GmbH, 2016)

Extruder	Material	Throughput (kg/h)
MAS 24	e.g. PE / PP / PS / PET	20 – 30
MAS 45	e.g. PE / PP / PS / PET	100 – 250
MAS 55L	e.g. PE / PP / PS / PET	300 – 600
MAS 75	e.g. PE / PP / PS / PET	600 – 1100
MAS 90	e.g. PE / PP / PS / PET	900 – 1400
MAS 93	e.g. PE / PP / PS / PET	1200 - 2000

2.3.1 Processing Zones of MAS Extruder

The different functional zones of the MAS extruder plasticizing unit are shown in Figure 2.9. Similar to the conventional parallel twin screw extruders (section 2.2), the plasticizing unit is modular, which allows the flexibility to configure the screw geometry and barrel zones according to the need. The MAS Extruder series in general has a feed, plasticization, mixing, degassing and metering/pressure build-up zone. In case of larger series extruders an atmospheric venting zone is also present.

The solid material fed into the feed zone is conveyed in the extrusion direction by means of positive conveying elements. The channels of the intake and the plasticization zones are partially or fully filled depending on the dosing. The feed opening is positioned in the middle of the two screws. In case of MAS extruders having atmospheric venting after the feed zone, the bulk material is compressed using screw geometry with relatively little volume allowing easy removal of the air enclosed between the bulk particles. This pre-compression of the material leads to pre-plasticization of the material.

The melting of the material occurs in the plasticization zone, where the degree of fill is high. Until the screw channels are not completely filled with the material, there is no pressure

build-up. The use of the conical screws leads to an automatic compression due to the reduction of the free channel volume. Also the usage of flow restrictive elements ahead of the melting zone leads to completely filled channels in the melting region. Once the channels are completely full, because of the high pressures and the friction between the cylinder and material, heat is generated, which leads to the first melting of the polymer. Moreover the large surface area of the screws ensures efficient energy transfer to the material (MAS, 2014).

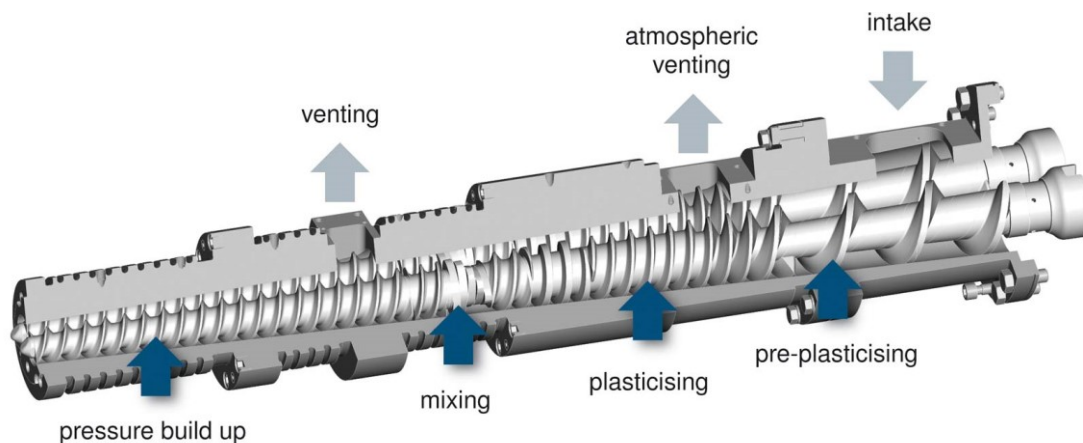


Figure 2.9: Processing zones of MAS extruder (MAS Maschinen und Anlagenbau Schulz GmbH, 2016)

For increasing the degree of fill (DOF) in the melting zone a restricting zone with negative conveying elements or conveying elements with very low free volume (for example single flighted screw elements with small pitch) are used. These elements also help to finish the melting process, so that in the mixing zone only molten polymer will be processed.

The mixing zone can have kneading, screw mixing-, and neutral mixing- or backward pumping mixing elements (Kohlgrueber, 2008). The MAS extruders use kneading, conveying mixing and special shear mixing elements for homogenizing the melt.

The mixing zone is followed by the devolatilization zone, where the volatile substances migrate to the open surface and can be sucked out using vacuum. The degassing zone also permits the processing of damp materials with 2 – 4 % moisture content (MAS, 2014). In order to avoid the melt flowing out the vent, the degree of filling (DOF) is maintained as low as possible. This is achieved by increasing the free channel volume of the screw. The preceding zone comprised of throttle element helps in dropping the pressure level to a minimum and acts as a pressure seal.

After the evaporation zone is the discharge or metering zone, which is responsible for the pressure build-up. Also the conical design is very helpful in building up the pressure, since the free channel volume reduces towards the screw tip. Since the filling degree is high in this zone, further homogenization of the melt can be achieved. Due to the high overlapping of the screw flights a significant pressure build-up, combined with a consistently high output is achieved, even at low screw speeds with high melt pressure at low melt temperatures (MAS, 2014).

2.3.2 Conical Modular Screw

As mentioned before, the plasticization screws of the MAS conical extruders are modularly configured as shown in Figure 2.10.

The two major elements of the screw are the feed zone (P1) and the metering zone (P6) and the rest of the screw elements can be configured according to the application or the need. Different elements such as conveying elements with varying number of flights, mixing elements, kneading elements can be incorporated in the screw configuration.

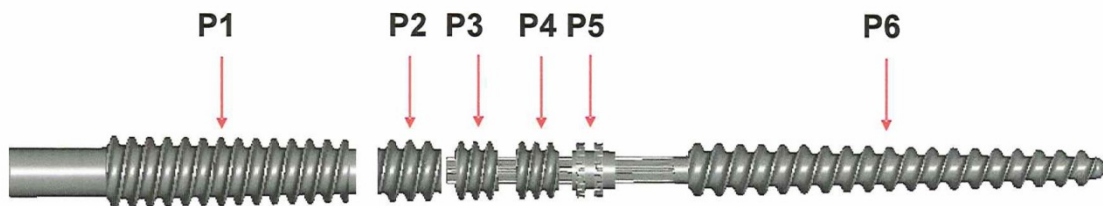


Figure 2.10: Modular screw concept of MAS conical extruder

The screw elements used at the positions P2 to P5 are responsible for melting the polymer, mixing the additives in case of compounding, to get a homogenized melt and to lower the pressure before the melt enters the degassing zone.

3 Twin Screw Geometry

3.1 Introduction

The most commonly used screw geometry is the self-cleaning geometry also called Erdmenger geometry developed and patented by Erdmenger in 1954. Based on the basic Erdmenger geometry, various versions of screw profiles are developed, that can affect the technical result. Essentially, all screw elements (kneading, mixing, forward and backward conveying elements) of the co-rotating twin screw extruder are an adaptation or variation of Erdmenger geometry. The mostly used screw elements for conveying are positive and negative conveying elements with varying number of flights, kneading elements with varying stagger angle (positive, negative and neutral) and different disc thickness. For good mixing, kneading elements and other special mixing elements like gear teeth mixing element and conveying element with grooves are mostly used.

In order to describe the flow of the polymer melt in the screw channel, a detailed understanding of the screw geometry is important. An elaborated description of the intermeshing parallel twin screw geometry was given by Booy (1978). The publication also details the calculation of the specific area and free volume of self-cleaning screw geometry. Based on Booy's work, Rauwendaal (1996) developed the geometric features of screws for both co- and counter-rotating twin screw extruders from the kinematic principles. The important parameter in modeling the flow in co-rotating twin screws are the drag and pressure flows. In case of counter rotating twin screw extruders, leakage flows are much more important, especially in case of large calendar and side gaps. The leakage flow analysis was done by Janssen (1978) for counter-rotating twin screw. Meijer (1988) modeled the flow in co-rotating twin screw elements including the leakage flows.

In case of parallel extruders, the cross sectional geometry of the screw element is the same along the screw length. In the conical intermeshing twin screw extruders the cross-sectional geometry of the screw elements vary according to the tapered axis angle and the conicity of the screw and barrel over the entire screw length. This makes the computation of conical screws more complex. To solve this complexity in this work the screw was discretized along the screw length axis and each discretized element was considered as parallel screw geometry for further computation.

3.2 Design Principles of Intermeshing Co-Rotating Twin Screws

The self-cleaning twin screw geometry developed by Erdmenger is shown in Figure 3.1. Booy (1978) published in detail the geometry of intermeshing self-cleaning twin screws. The main geometric parameters used to define the self-wiping screw elements are:

- D_a Outer screw diameter
- a Centerline distance
- n Number of screw tips
- t The pitch length, the axial length required for one complete thread

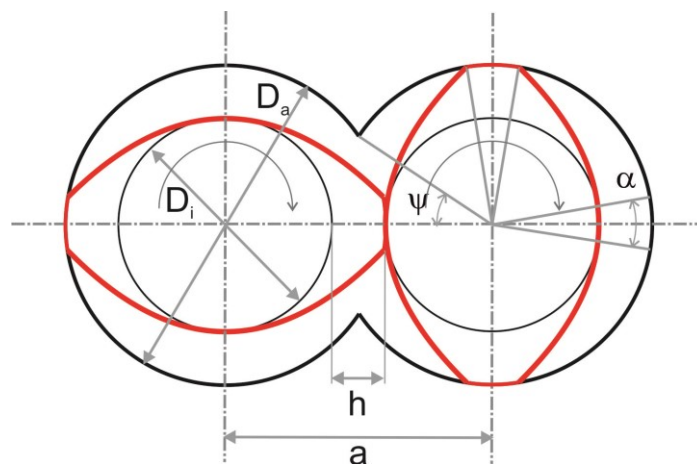


Figure 3.1: Self-cleaning screw element geometry

Both the screw possesses the same outside (D_a) and inside or root diameter (D_i). In most cases the barrel diameter (D) is considered the same as screw outside diameter. In practice there exists a very small clearance between the screw and the barrel wall, called the radial clearance (s_r). This clearance avoids the mechanical contact of the screw flights and the barrel wall. Also clearances between flights (s_f) of the screws in the intermeshing area and clearance between the flight of one screw and ground of other screw, so called calendar gap (s_w) is provided. The main reasons for providing these clearances in the screw elements according to Kohlgrueber (2008) are:

- to prevent metallic erosion
- to compensate for manufacturing tolerances and unevenness
- to compensate for angle discrepancies

- to compensate for uneven heat expansion
- to avoid excessive product stress due to insufficient wide gaps

With the given screw outer and inner diameters, the maximum channel depth (h) of the screw element could be determined using the relation:

$$h = \frac{D_a - D_i}{2} \quad (3.1)$$

The centerline distance (a) is the distance between the two screw axes, which is defined by the extruder manufacturer. This is the major factor in deciding the self-wiping potential of the extruder. For closely intermeshing and self-cleaning property the centerline distance should be less than the outside diameter of the screw. If the centerline distance value is unknown, it can be determined by:

$$a = \frac{D_i}{2} + h + \frac{D_i}{2} = D_i + h = \frac{D_a + D_i}{2} \quad (3.2)$$

The channel depth and the channel cross sectional area decrease with decrease in the centerline distance. The conveying capability of the screw reduces with increase in the centerline distance (Rauwendaal C. , 1996).

The screw element can be single or double or triple flighted. The number of screw tips (n) is the one of the important parameters, responsible for the free volume and the number of flows channels (i). The number of available flow channels is given by:

$$i = 2 \cdot n - 1 \quad (3.3)$$

Here the number 2 indicates the total number of screws. For example a screw element with 3 tips has 5 flow channels and thus more free volume (Figure 3.2).



Figure 3.2: Number of flow channels and free volume in single and multiple-flighted screw elements (Kohlgrueber, 2008)

The intersection of the two barrel bores leads to an intermeshing angle ψ (see Figure 3.1), which can be determined from the screw outer diameter and the centerline distance.

$$\psi = \arccos\left(\frac{a}{D_a}\right) \quad (3.4)$$

As shown in Figure 3.3. the cross sectional geometry of the intermeshing twin screw is composed of three regions: the flight tip, the flight flank and the screw root. In general self-cleaning screws have the same flight tip and root angle (α) shown in Figure 3.1 and it can be given as:

$$\alpha = \frac{\pi}{n} - 2 \cdot \arccos\left(\frac{D_a + D_i}{2 \cdot D_a}\right) = \frac{\pi}{n} - 2 \cdot \psi \quad (3.5)$$

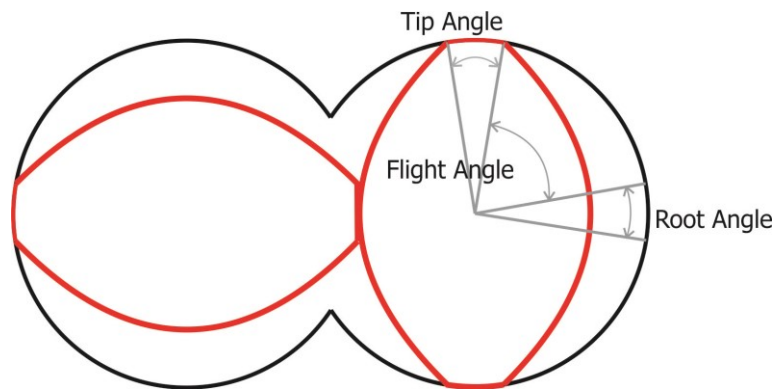


Figure 3.3: Major three angles of intermeshing twin screw element (Rauwendaal C. , 1996)

For screws with same root and tip flank, the following equation is given:

$$n \cdot (\alpha + \psi) = \pi \quad (3.6)$$

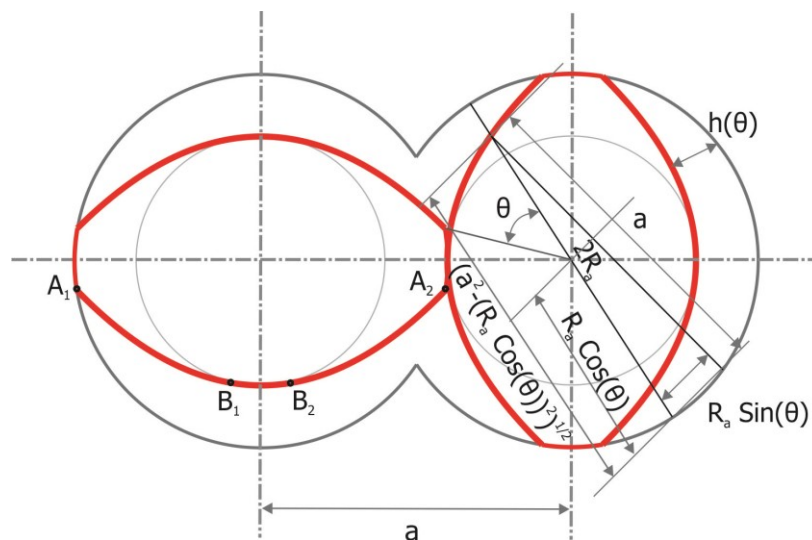


Figure 3.4: Channel depth as a function of angle (θ)

The cross sectional channel depth ($h(\theta)$) of a screw element along the cross channel direction (x -axis), parallel to the screw axis, as a function of the angular coordinate (θ) is given by the following relation according to Booy (1978).

$$h(\theta) = \frac{D_a}{2} \cdot (1 + \cos \theta) - \sqrt{a^2 - D_a^2 \cdot \sin^2 \theta} \quad (3.7)$$

The channel depth ($h(x)$) of an Erdmenger profile as function of the Cartesian co-ordinates x , y and z axis is shown in Figure 3.5. The channel depth could be defined in two segments. As shown in Figure 3.5 the segment between $-e_0/2$ and $+e_0/2$, the channel depth is maximum and constant which is given by:

$$h(x) = h_0 = D_a - a \quad (3.8)$$

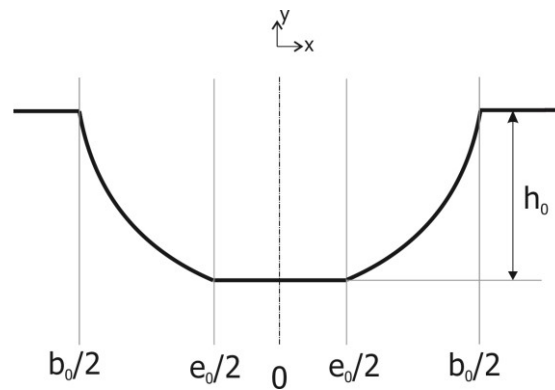


Figure 3.5: Screw cross section view perpendicular to screw axis

In order to describe the channel depth in the parabolic segment (i.e. between $+e_0/2$ and $+b_0/2$) the transformation of the angular coordinate system to the Cartesian coordinate system is required, which is given as:

$$x = \frac{t \cdot \theta \cdot \cos(\varphi_0)}{2 \cdot \pi} + \frac{e_0}{2} \quad (3.9)$$

where φ_0 is the pitch angle, and is given by the following equation:

$$\varphi_0 = \arctan\left(\frac{t}{\pi \cdot D_a}\right) \quad (3.10)$$

and e_0 the maximum width of the flight.

$$e_0 = \frac{t \cdot \alpha \cdot \cos(\varphi_0)}{2 \cdot \pi} \quad (3.11)$$

The maximum width of the channel (b_0) is given as:

$$b_0 = \frac{t \cdot \cos(\varphi_0)}{i} \cdot \left(1 - \frac{\alpha \cdot i}{2 \cdot \pi}\right) \quad (3.12a)$$

which can be simplified to,

$$b_0 = \frac{t \cdot \cos(\varphi_0)}{i} - e_0 \quad (3.12a)$$

The parabolic channel profile between $+e_0/2 < x < +b_0/2$ can be described using equation 3.13.

$$h(x) = \frac{D_a}{2} \left[1 + \cos \left\{ \left(x - \frac{t \cdot \alpha \cdot \cos(\varphi_0)}{4 \cdot \pi} \right) \cdot \frac{2 \cdot \pi}{t \cdot \cos(\varphi_0)} \right\} \right] - \sqrt{\alpha^2 - \left(\frac{D_a}{2}\right)^2 + \cos^2 \left\{ \left(x - \frac{t \cdot \alpha \cdot \cos(\varphi_0)}{4 \cdot \pi} \right) \cdot \frac{2 \cdot \pi}{t \cdot \cos(\varphi_0)} \right\}} \quad (3.13)$$

3.3 Different Screw Channel Profiles

The self-wiping screw channel profile, the Erdmenger profile, could be modified in various ways to gain 15 to 30 % increase in the free volume (Kohlgrueber, 2008) (Schuschnigg, Klammer, & Holzer, Introduction of the conical co-rotating twin screw extruder, 2010). In such cases the parabolic channel profile is avoided and undercuts are made either on the active flights or on both active and passive flights. When using such channel profiles the self-cleaning capability of the screw elements get partially affected in shear edge profile (also called as Schubflanken profile) and no self-wiping is possible in case of double shear edge or box profile. Because of greater free volume of the screw elements with undercuts, these elements are used in the feed and vent zones.

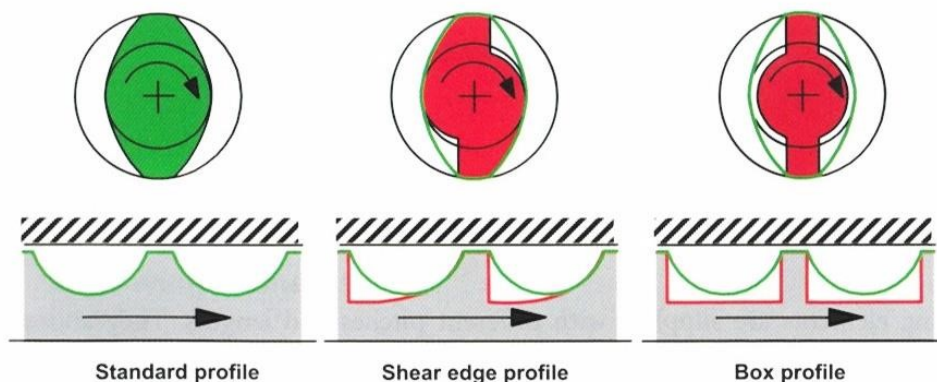


Figure 3.6: Conveying elements with different channel geometries (Kohlgrueber, 2008)

Standard or Erdmenger Profile

The geometry of Erdmenger profile is diagrammatically represented in Figure 3.7. The detailed geometric description of the standard profile is discussed earlier in section 3.2.

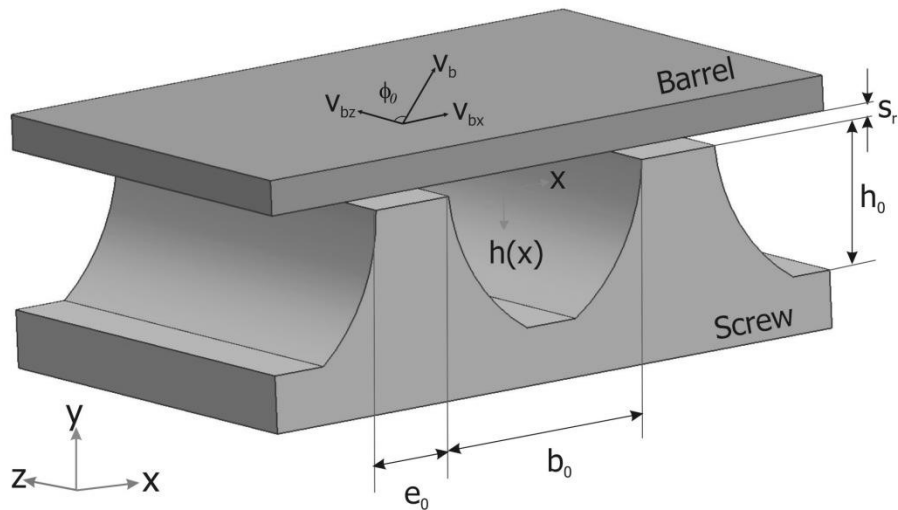


Figure 3.7: Flat plate model of Erdmenger channel profile

Double Shear Edge or Box Profile

The box channel profile (Figure 3.6) possess no parabolic channel profile and the channel depth is constant over the total width of the channel. This leads to an increase in free channel volume of about 30 %. The major advantage of using this screw element is the increase in the conveying capacity. But the self-cleaning function of the screw element is no more possible.

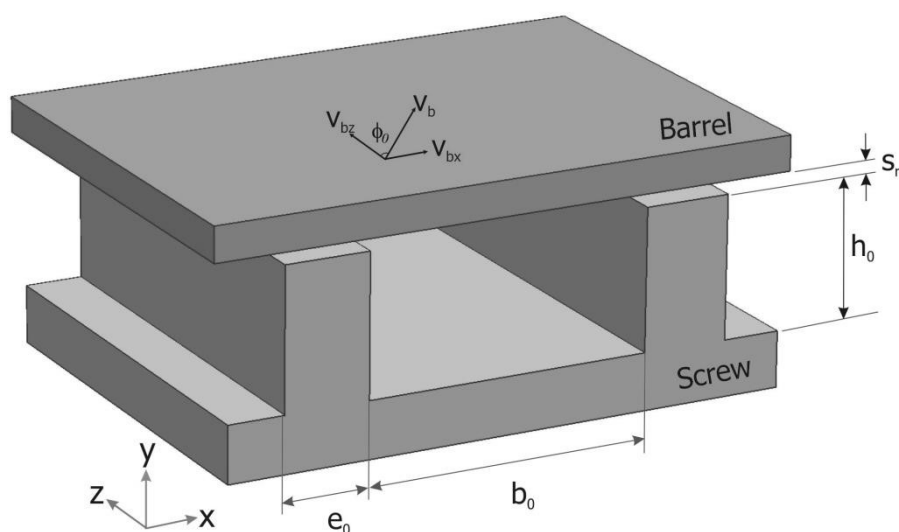


Figure 3.8: Flat plate model of double edge or box profile

The box profile geometry differs from the standard Erdmenger geometry only in the channel depth. The following conditions are applied for calculating the channel depth:

The channel depth over the channel width (b_0) is,

$$h(x) = h_0 \quad (3.14)$$

and over the flight width e_0

$$h(x) = 0 \quad (3.15)$$

The other geometric parameters are described in the similar way as Erdmenger geometry.

Shear Edge or Schubflanken Profile

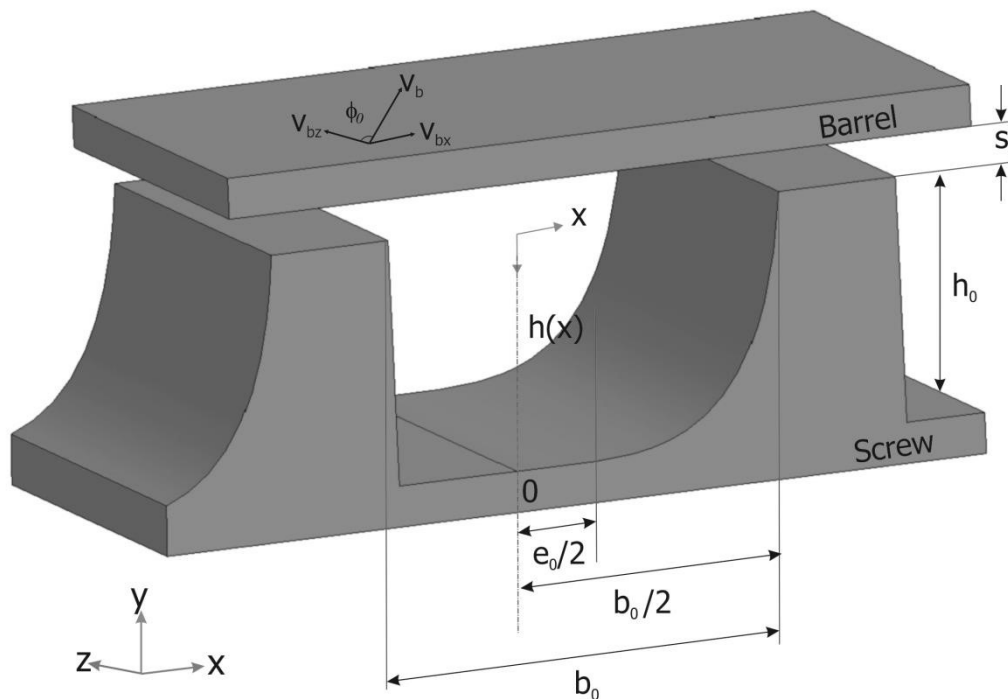


Figure 3.9: Geometry of a shear edge profile

The shear edge profile is the combination of standard and box profile. The following conditions are applied for calculating the channel depth:

The channel depth in segment where, $b_0/2 > x < e_0/2$ is:

$$h(x) = \frac{D_a}{2} \left[1 + \cos \left\{ \left(x - \frac{t \cdot \alpha \cdot \cos(\varphi_0)}{4 \cdot \pi} \right) \cdot \frac{2 \cdot \pi}{t \cdot \cos(\varphi_0)} \right\} \right] - \sqrt{\alpha^2 - \left(\frac{D_a}{2} \right)^2 + \cos^2 \left\{ \left(x - \frac{t \cdot \alpha \cdot \cos(\varphi_0)}{4 \cdot \pi} \right) \cdot \frac{2 \cdot \pi}{t \cdot \cos(\varphi_0)} \right\}} \quad (3.16)$$

The channel depth in segment where, $e_0/2 < x < -b_0/2$ is:

$$h(x) = h_0 \quad (3.17)$$

and over the flight width e_0

$$h(x) = 0 \quad (3.18)$$

3.4 Flow Simulation of Channel Profiles

In order to characterize and compare the three different channel profiles, 3D flow simulation were carried out using Ansys Polyflow. The pressure generation capability of the three different channel profiles, the shearing and the flow velocity are studied under isothermal conditions for a LDPE polymer at different processing conditions like flow rates and screw rotation speeds. The 3D flow simulations were conducted assuming that the elements are completely filled. Screw elements with 60 mm length, pitch 30 mm and 2 flights were used for the simulation.

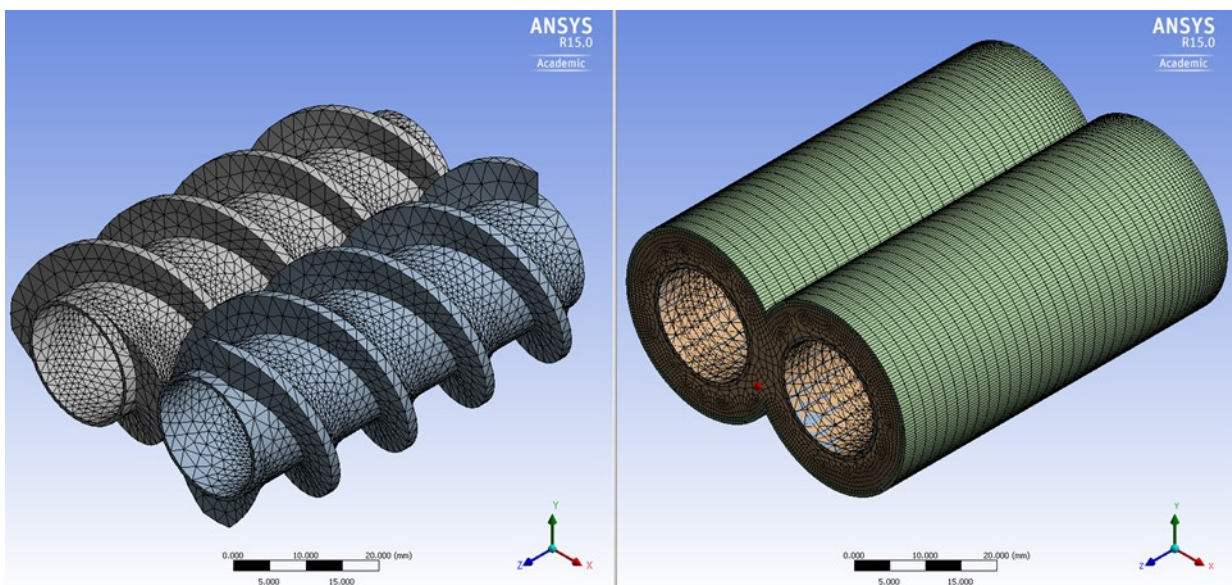


Figure 3.10: Meshing of the Erdmenger screw element and barrel

The meshing was done with fine elements at the outer cylinder and coarser elements in the inner cylinder element. Both elements were meshed with all quad elements which forms a brick structure. The screw were meshed with triangular elements.

Figure 3.10 shows the generated mesh for the Erdmenger Profile. On the left side the two screws and on the right side the meshing of the barrel wall. The barrel for each geometry is equal and has 130 200 Nodes and 94 416 nodes and the barrel volume is 88 845 mm³.

The constructed elements were imported into Ansys Polyflow 15.0. In the model the screw elements were arranged so that a small clearance exist between the screws. The cylinder was constructed in two parts, so that the gap between the screw tips and the cylinder wall can be meshed with a finer grid compared to the inner elements. This is important as we expect higher gradients in velocity and pressure in the flight clearance (Schuschnigg, 2014).

The characteristics of the generated mesh are summarized in the following Table 3.1.

Table 3.1: Nodes, elements and free volume of different channel profiles

Channel profile	Each Screw		
	Nodes	Elements	Volume in mm ³
Erdmenger Profile	9 780	35 597	10 504
Shear Edge Profile	7 004	24 076	8 049
Double Shear Edge Profile	9 492	36 751	4 968

The material data of LDPE type LD159AC from Exxonmobile used for this simulation is given in chapter 8.4.

3.5 Areas and Free Volume Calculation of Parallel Extruders

The surface area of the screw flights, roots and barrel and the free volume between the barrel and the screws are important for studying the melt flow, heat and mass transfer in the twin screw extruders (Booy, 1978) (Potente, Ansahl, & Klarholz, 1994). In case of parallel screws the calculation of the area and free volume is relatively easier compared to the conical screws, due to the constant cross sectional geometry along the screw axis

Booy (1978) has derived the basic equations for calculating the specific area and the specific surface areas for parallel fully intermeshing screws. For characterizing the areas and volumes, Booy introduced geometric constants. Also Booy published in 1980 a detailed

description for calculating the free volume in the nip zone of the fully intermeshing twin screw geometry.

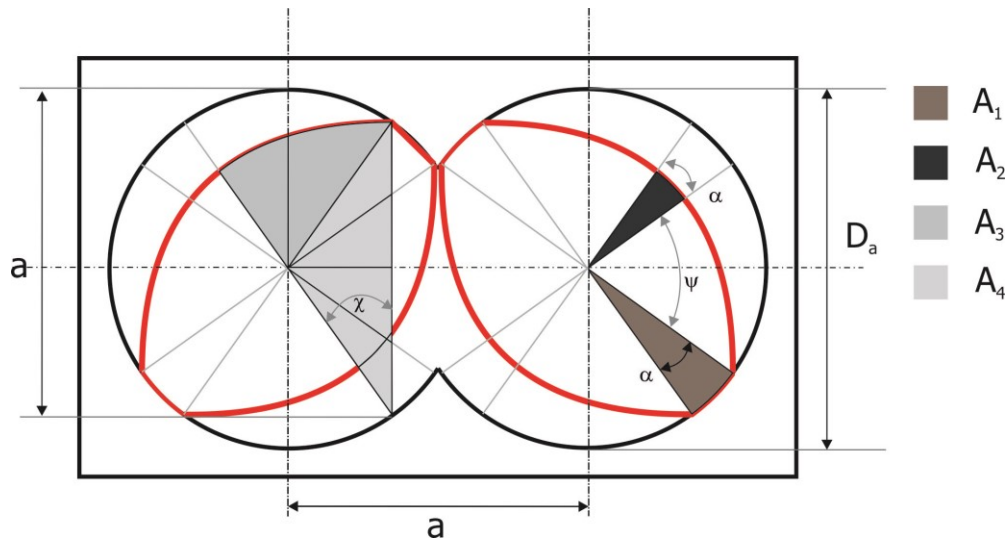


Figure 3.11: Free cross-sectional area of self-wiping twin screw geometry (Ansahl, 1993)

Potente and Ansahl (1994) proposed some simplified equations, using Booy's equations, to calculate the free axial cross-sectional area of self-wiping twin screw geometry. The calculated area can be integrated over the length of the screw element to achieve the specific volumes. The simplified equations (Booy, 1978) (Ansahl, 1993) for calculating the free cross sectional area for Erdmenger geometry are given as:

the flight tip area A_1

$$A_1 = \frac{1}{8} \cdot \alpha \cdot D_a^2 \quad (3.19)$$

the root area A_2 :

$$A_2 = \frac{1}{8} \cdot \alpha \cdot (2 \cdot a - D_a)^2 \quad (3.20)$$

$$A_3 + A_4 = \frac{1}{4} \cdot 2 \cdot \psi \cdot a^2 \quad (3.21)$$

In Figure 3.11 χ is given as:

$$\chi = \arcsin\left(\frac{D_a}{2 \cdot a} \cdot \sin\left(\frac{\psi}{2}\right)\right) \quad (3.22)$$

and the triangular area A_4 is given by:

$$A_4 = \frac{1}{4} \cdot a \cdot D_a \cdot \sin(\psi) \quad (3.23)$$

The area of one profile can be determined as:

$$A_{profile} = (A_1 + A_2) \cdot n + A_3 \cdot 2 \cdot n \quad (3.24)$$

The cross sectional area of the 8 shaped barrel, with barrel diameter D :

$$A_{barrel} = \frac{1}{4} \cdot \left(2 \cdot \pi - \frac{\psi}{2}\right) \cdot D^2 + \frac{1}{2} \cdot a \cdot D \cdot \sin(\psi) \quad (3.25)$$

Using equations 3.24 and 3.25 the free cross-sectional area of the screw can be determined as:

$$A_{free} = A_{barrel} - 2 \cdot A_{profile} \quad (3.26)$$

The free volume between the screws and barrel is

$$V_{free} = \int_0^L A_{free} \cdot dL \quad (3.27)$$

where L is the length of the screw.

The free area in the nip zone of the screws is given according to Booy (1980) as:

$$A_{nip} = \frac{1}{2} \cdot a \cdot D \cdot \sin(\psi) - \frac{A_{profile} \cdot \psi}{\pi} \quad (3.28)$$

The flight tip and root surface area is given by (Booy, 1978):

$$S_{nip} = \frac{D_a}{2} \cdot \alpha \cdot L \quad (3.29a)$$

$$S_{root} = \frac{D_i}{2} \cdot \alpha \cdot L \quad (3.29b)$$

The flight flank surface area is:

$$S_{flank} = \frac{2 \cdot \pi}{t} \cdot L \cdot \int_0^{\theta=\frac{\psi}{2}} \sqrt{\left(\frac{\partial h}{\partial \theta}\right)^2 \cdot h(\theta)^2 - \left(\frac{\partial h}{\partial \theta}\right)^2 \cdot \left(\frac{t}{2 \cdot \pi}\right)^2 + h(\theta)^2 \cdot \left(\frac{t}{2 \cdot \pi}\right)^2} \cdot d\theta \quad (3.30)$$

The surface area of the screw profile is given as:

$$S_{profile} = n \cdot (S_{tip} + S_{root} + 2 \cdot S_{flank}) \quad (3.31)$$

The surface area of the barrel is:

$$S_{barrel} = 2 \cdot L \cdot \left(\pi - \frac{\psi}{2}\right) \cdot D \quad (3.32)$$

3.6 Geometry of Conical Twin Screw Extruder

The conical extruders can be simple conical or double conical or negative conical. The difference between these three systems is mainly the change in the channel depth along the screw axis (Figure 3.12). The simple or single conical is the commonly used standard system. Here the inner and outer diameter of the screws change simultaneously providing the same channel depth from the feed zone until the discharge zone. The output capacity of the conical system can be improved by using double conical concept, where the channel depth is larger in the feed zone and decreases along the screw length. This system leads to problems like melt inhomogeneity and increased wear (Seifert, 2005). These problems can be avoided by using an active conical system, where the channel depth increases from feed end towards screw tip.

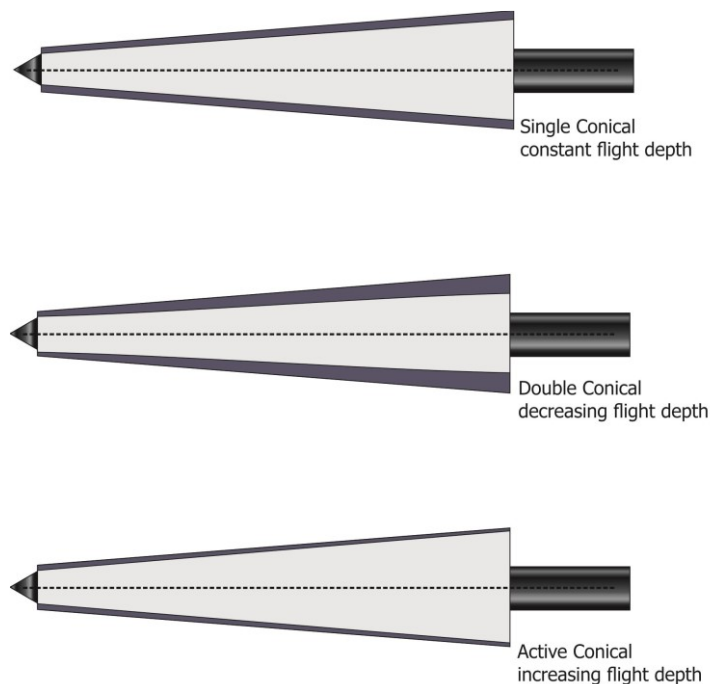


Figure 3.12: Concept of conical extruders (Seifert, 2005)

The MAS conical extruders have a double conical system, where the channel depth changes along the screw axis. The two major angles needed for describing the geometry of the conical screws are (Hensen, Knappe, & Potente, 1989):

- Cone angle of centerline distance (δ)
- Cone angle of barrel (γ)

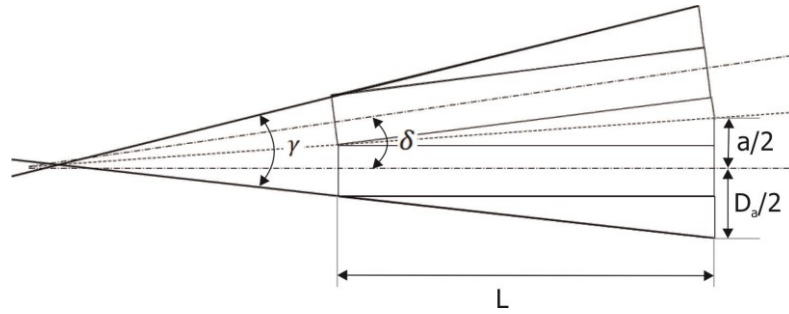


Figure 3.13: Conical extruder screw geometry (Hensen, Knappe, & Potente, 1989)

In case of single conical system, both the cone angles are the same ($\delta = \gamma$)

In case of double conical system, $\delta = 0.5 \cdot \gamma$

The main screw geometric parameters that vary over the screw length (L) (along the x axis) are diameter and centerline distance.

$$D(L) = D_a + 2 \cdot L \cdot \tan \frac{1}{2} \cdot (\gamma - \delta) \quad (3.33)$$

$$a(L) = a + 2 \cdot L \cdot \tan \frac{\delta}{2} \quad (3.34)$$

$$h(L) = D(L) - a(L) \quad (3.35)$$

With given cone angle, screw outer diameter and total screw length, the other geometric parameters, at different points over the length can be determined using the equations given for parallel twin screw geometry (section 3.2).

For example the intermeshing angle (ψ) at a position x is given by:

$$\psi(L = x) = \arccos \left(\frac{a(L = x)}{D(L = x)} \right) \quad (3.36)$$

In case the geometries (outer diameter and center line distance) at both ends of the screw are known, the other geometric parameters for a specific position of x along the screw length could be calculated as:

$$D_a(x) = D_{a,start} - \frac{D_{a,start} - D_{a,end}}{L} \cdot x \quad (3.37)$$

Similarly the center line distance can be given by:

$$a(x) = a_{start} - \frac{a_{start} - a_{end}}{L} \cdot x \quad (3.38)$$

3.7 Areas and Free Volume Calculation of Conical Extruders

The cross sectional area of 8 shaped conical barrel is given as (Himmler, 2010):

$$A_{barrel} = \frac{D(x)^2}{2} \cdot (\pi \cdot \psi(x) + \sin(\psi(x)) \cdot \cos(\psi(x))) \quad (3.39)$$

Integrating the above equation over the screw length gives the volume of the pierced barrel.

$$V_{barrel} = \int_0^L \frac{D(x)^2}{2} \cdot (\pi \cdot \psi(x) + \sin(\psi(x)) \cdot \cos(\psi(x))) \cdot dx \quad (3.40)$$

The conical screw is discretized into many small segments along the length (x axis) and each cross section is considered as a parallel geometry. The free cross sectional area and free volume of the conical screw is determined in the similar way as the parallel twin screw (equations 3.25 - 3.27).

The surface areas of the conical barrel and screws can be determined using the following relation: (Berghaus, 1995) (Hensen, Knappe, & Potente, 1989)

$$S_{barrel} = 2 \cdot \int_0^L \left(\pi - \frac{\psi(x)}{2} \right) \cdot D(x) \cdot dx \quad (3.41)$$

The surface area of the conical screw is determined using the equations 3.29 – 3.31, which are used for the parallel twin screws, considering the change in the cross sectional geometry of the screws along the total length of the screw.

4 Screw Elements

4.1 Introduction

The major application area of co-rotating closely intermeshing twin screw extruders is the compounding of polymers, due to their enormous flexibility and variability of the system through the modular configuration of screw and barrel. One more advantage is, in case of wear, that particular screw or barrel elements can be changed instead of replacing the complete plasticizing unit. This makes the process more economical.

The screw elements configuration is most important for the end product quality, efficiency and performance of the extruder. The development of the screw elements started with the standard Erdmenger self-cleaning geometry. Even now this geometry is mostly used. Based on the Erdmenger screw geometry many new geometry variants are continuously being developed, for improving the compounding and extrusion process.

In practice the screw elements for the left and right screw shafts have the same geometry, in other words they are identical and can be installed to either shaft. Also the elements are congruent when the geometry of an element remains constant along its axis (Kohlgrueber, 2008).

Screw elements can be basically categorized according to their intended function as:

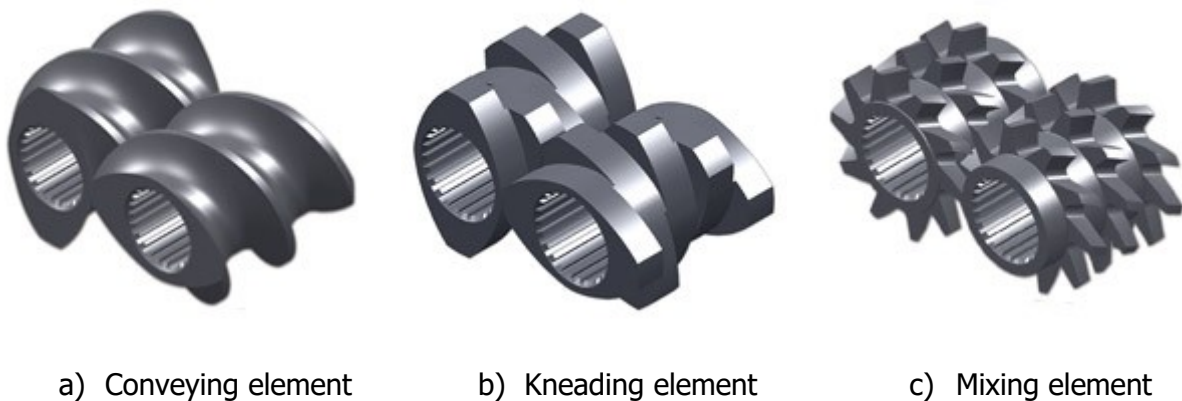


Figure 4.1: Major classification of screw elements (Extricom, 2015)

Conveying and kneading element possess identical cross sectional geometry and they mate perfectly. In case of different cross sections, a transition element is required for connecting the screw elements having either different number of tips or cross sectional geometry. The screw channel is open along the axial direction providing mixing in the lengthwise direction.

The screw channel can be either crosswise closed with screw elements or crosswise open with kneading block elements (Peptflow, 2014). The function and design concept of these screw elements will be elaborated in this chapter. Similar to the parallel twin screw elements, MAS conical extruder has also used the concept of a modular screw, where conveying, mixing and kneading elements can be incorporated according to the area of application.

4.2 Conveying Element

As the name indicates the major function of this element is to convey or meter – granulates, powder, flakes, ground product, melt, etc. – from the feed opening downstream to other processing zone and to built-up pressure. Mostly self-cleaning conveying elements have the standard Erdmenger geometry, which is detailed in chapter 2. The flow of the material inside the conveying element follows a figure 8-path. The polymer in the conveying screw channels are conveyed through the drag force. The polymer is positively transferred from one screw channel to the other screw channel in the intermeshing region by the wiping action (Chung, 2000). No material is exchanged between the channels of the conveying elements, with the exception of some minor exchange due to leakage through the screw clearances. Thus the conveying elements are longitudinally open and transversally closed (Schuler, 1996).

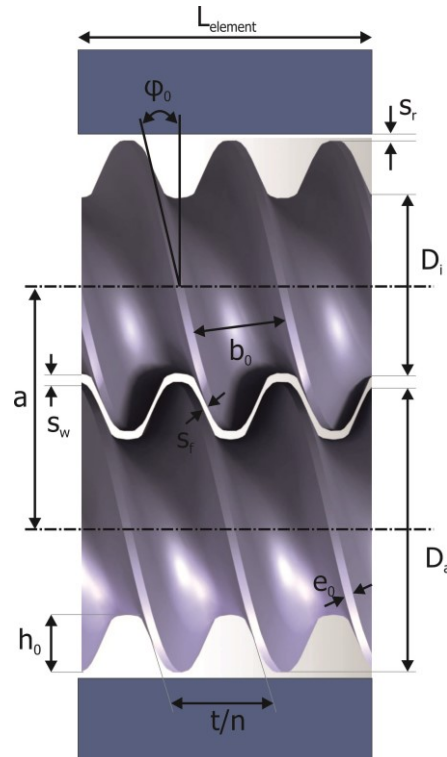


Figure 4.2: Geometry of a convey screw element

The conveying elements can be described by few characteristic parameters, like

- number of flights (single, double or triple flighted) - n
- pitch length (wide and narrow) – t
- pitch direction (positive and negative conveying)
- total length of the element - $L_{element}$

The number of flights is responsible for the available channel free volume. The conveying elements can be single or double or triple flighted (Figure 4.3). The more number of tips, the larger is the available free volume but at the same time the radial clearance is larger and therefore they are not completely self-wiping. Double flighted elements are mostly used in practice.



Figure 4.3: Conveying screw elements with single, double and triple flights (Extricom, 2015)

The conveying elements can have either a wide or narrow pitch according to the position of usage. In the feed section, conveying elements with wide pitch are normally used because of more free volume. Also conveying elements with freely cut profiles (shear edge and box profiles) are used to increase the feed capacity.

The bulk density of the material is an important factor in deciding the pitch length. The optimum screw pitch in the feed section is 1.5 to 2D. A narrow pitch is used to generate pressure and provide melt seal. Mostly a narrow pitch is used in the pressure build-up zone and in the melting zone. A too small pitch leads to less conveying and the screw element act as a flow resistance (Kohlgrueber, 2008). The screw pitch determines the degree of fill of the screw element. The direction of the pitch determines, if the element conveys the melt in positive direction or has a backward pumping effect.

The main characteristics of conveying element are: limited mixing and short residence time. The detailed geometric description of the conveying element is already discussed in chapter 3.

4.3 Backward or Negative Conveying Element

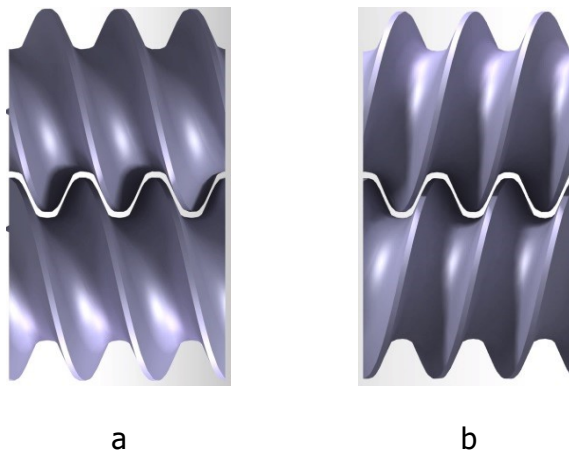


Figure 4.4: a) Positive and b) negative conveying screw elements

The major difference between the normal conveying (Figure 4.4a) and the reverse conveying element (Figure 4.4b) is the direction of the pitch. The backward conveying elements are used as flow restrictions mainly to increase the filling degree of the preceding screw elements. For the melt to flow through the reverse conveying element, a larger pressure is generally required. The pressure flow necessary to overcome the resistance of the backward conveying element results from the sum of the melt conveying and the volume flow (Schuler, 1996). These elements are also axially open when the extruder is not in operation, in operation they fill the upstream elements and help to separate the different processing zones with a melt plug (Kohlgrueber, 2008).

The geometric description of the backward conveying element is the same as the conveying element, except for the pitch angle.

The backward pumping elements can be used in the melting zones and in the mixing zones or in zones where a greater filling degree is required.

4.4 Kneading Element

The kneading elements are basically used for the melting of polymers, mixing and dispersing the fillers and reinforcement into the polymer matrix. The kneading element cross sectional geometry is the same as the conveying element, standard self-cleaning profile. The other important parameters to describe the geometry of kneading block element are:

- number of discs - j_k
- staggering angle - Ω_k
- width of each disc - w_k
- total length of kneading element - L_k

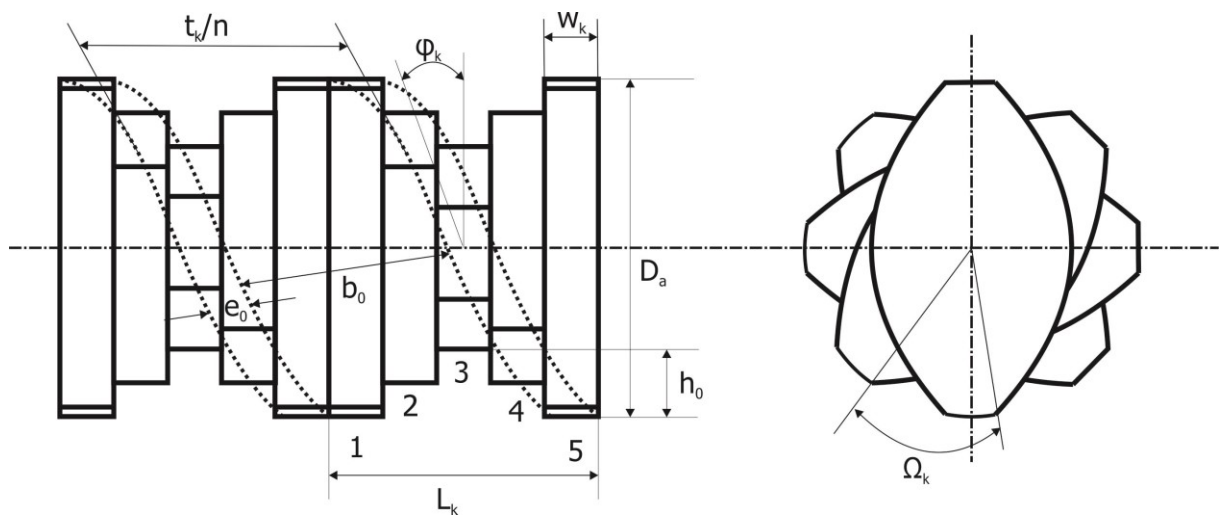


Figure 4.5: Geometry of kneading element (Ansahl, 1993)

Standard kneading elements are arranged symmetrically and the shape and location of the two faces of the element are identical as in the case of conveying elements (Kohlgrueber, 2008). Thus the number of discs and the staggering angle of the discs are dependent on each other. For good dispersive mixing more shearing is required and this is achieved by choosing the right thickness of the kneading disc blocks.

Figure 4.5 shows positive conveying kneading elements with a staggering angle of 45° and 5 kneading discs. The width of each kneading disc (w_k) can be determined by dividing the total length of the kneading element (L_k) by the number of discs (j_k). As defined by Ansahl in his work (1993), the kneading block element could be considered as a standard conveying element. The pitch angle φ_k of the kneading block is given by following relation:

$$\varphi_k = \arctan\left(\frac{t_k}{\pi \cdot D_a}\right) \quad (4.1)$$

where the pitch length t_k is given as:

$$t_k = \frac{2 \cdot \pi \cdot L_k}{\Omega_k \cdot j_k} \quad (4.2)$$

The other geometric parameters, like the channel width b_0 , flight width e_0 and the channel depth h_0 can be determined in the same way as the conveying elements (section 3.2). Also modeling the flow in kneading blocks could be done using the conveying element model, so far the staggering angle is between 0 and α .

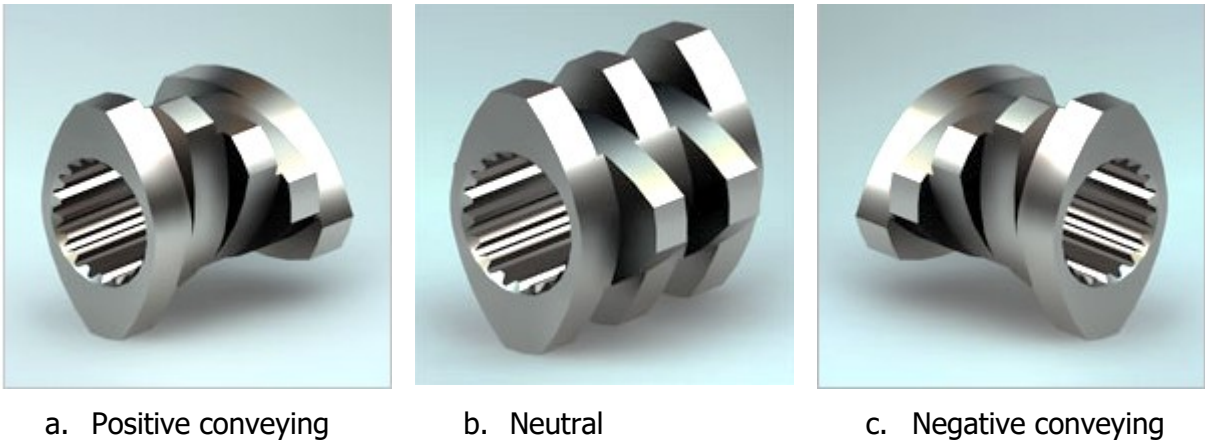


Figure 4.6: Kneading elements with different staggering angle (Extricom, 2015)

The larger the staggering angle, the more axially open is the kneading element and the more mixing in the axial direction. But the drawback of a large staggering angle is the reduced conveying capacity due to more leakage flow. So for larger staggering angle, the leakage flow through the gaps between the discs (A_Δ) as shown in Figure 4.7 should be considered.

The relation to calculate the area of the gap between the discs (A_Δ) is given according to Ansaht (1993) as:

$$A_\Delta = \frac{2}{\Omega_k - \alpha} \cdot I \cdot \left[(\Omega_k - \alpha) \cdot \frac{D_a}{2} - I \right] \quad (4.3)$$

where I is given as:

$$I = \left[(2\psi)^5 - \left(2\psi - \frac{1}{2}(\Omega_k - \alpha) \right)^5 \right] \frac{a_1}{5} + \left[(2\psi)^3 - \left(2\psi - \frac{1}{2}(\Omega_k - \alpha) \right)^3 \right] \frac{a_2}{3} + \frac{1}{2}(\Omega_k - \alpha)(D_a - a) \quad (4.4)$$

In the above equation a_1 and a_2 are constants, which depend on the screw diameter and the centerline distance between the two screws. The constants can be determined as follows:

$$a_1 = - \left[\frac{1}{24} \left(\frac{D_a}{a} \right) - \frac{1}{128} \left(\frac{D_a}{a} \right)^3 - \frac{1}{48} \right] \cdot D_a \quad (4.5)$$

$$a_2 = - \left[\frac{1}{4} - \frac{1}{8} \left(\frac{D_a}{a} \right) \right] \cdot D_a \quad (4.6)$$

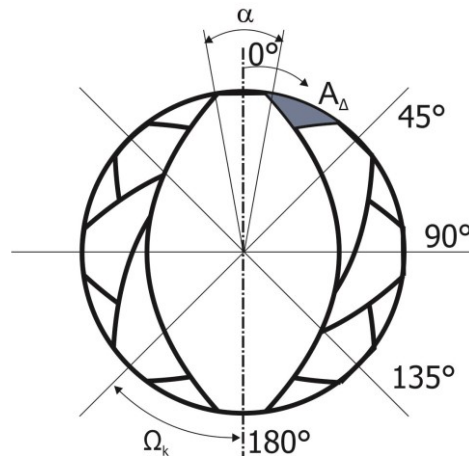


Figure 4.7: Area of leakage gap in kneading block element

A kneading block with 90° staggering angle is neutral conveying (Figure 4.4 b). In this kneading element the conveying of the melt occurs only due to pressure creating a negative pressure gradient. But this element is very good for mixing and homogenizing the melt. Kneading elements with negative staggering angle are also available, which acts as flow restrictor or backward conveying element.

4.5 Mixing Elements

Mixing elements are mainly used for improving the distributive mixing of fillers in the polymer matrix. Mixing elements are generally not self-cleaning. Different mixing elements are available; some of them are detailed in the following section.

4.5.1 Conveying Mixing Element

Screw mixing elements are standard conveying elements which have a self-cleaning profile. The only difference is, here the flights are interspersed with backward or forward conveying slots or gaps parallel to the screw axes (Figure 4.8). The interrupted screw flights enhance the back-mixing and permit communication between adjacent screw channels through

increased leakage flow (Wang Y. , 2000). The degree of opening of the screw flights in the axial direction influences the longitudinal mixing and increases the residence time. These special conveying mixing elements are mostly used in the zones where the degree of fill is 1 (for example before a backward pumping element).

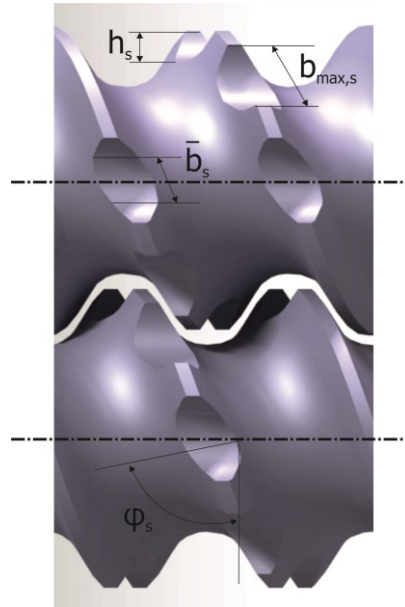


Figure 4.8: Conveying mixing element

The geometry of this special mixing conveying element can be given in the similar way as the standard conveying elements. The extra geometric parameters needed for describing the geometry of the slots are:

- average width of the slot - \bar{b}_s
- height of the slot - h_s
- pitch of the slot - t_s
- pitch angle of the slot - φ_s
- number of tips of the slot - n_s
- number of slots - j_s
- number of screw tips- n
- length of the element - $L_{element}$

In order to make the model simpler and easier, the slots are considered as simple rectangular slot with an average slot width and height.

The total number of slots in an element can be determined by the following relation (Kretschmer, 2004):

$$j_s = n \cdot n_s \cdot \left| \frac{L_{element}}{t} \pm \frac{L_{element}}{t_s} \right| \quad (4.7)$$

Here + is considered when the element and slot have different conveying direction and in other case – is considered.

4.5.2 Gear Tooth Mixing Element

These mixing elements are pitch-less rings having the same outer diameter as the screw outer diameter and have many slots around the circumference. The angle of the slot is responsible for the conveying direction. Elements having a slot angle between 0° and 90° are positive conveying, between 0° and -90° are negative pumping and an angle with 90° is neutral conveying. The toothed ring can be mounted on one shaft and partnered with the rings on the other shaft whose outer diameter corresponds to the core diameter of a screw element.

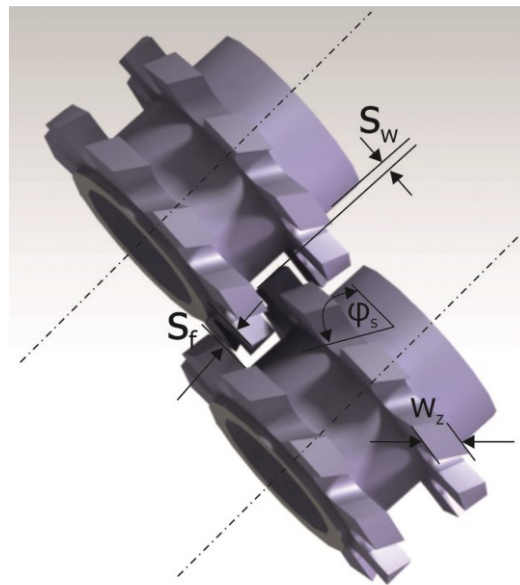


Figure 4.9: Gear tooth mixing element

These elements are not self-cleaning and vary geometrically greatly in the number of teeth, the number of teeth rows, width of the teeth, pitch direction, etc. Similar to the conveying mixing elements, the slots in the gear tooth mixing elements are considered as a simple rectangular geometry.

The geometry of the gear tooth mixing element can be defined (Kretschmer, 2004) as:

- thickness of the disc – w_z

- average width of the slot – \bar{b}_s
- height of the slot – h_s
- pitch angle of the slot – φ_s
- number of slots – j_{zs}
- calendar gap - s_w
- flight gap - s_f
- total length of the element – $L_{element}$

The free channel area in gear tooth mixing element can be determined by the following equations:

$$A_{free,z} = A_{1,z} + n_s \cdot A_{2,z} \quad (4.8)$$

where

$$A_{1,z} = A_{barrel} - \frac{\pi}{4} \cdot D_a^2 - \frac{\pi}{4} \cdot D_i^2 \quad (4.9)$$

$$A_{barrel} = \frac{1}{4} \cdot \left(2 \cdot \pi - \frac{\psi}{2}\right) \cdot D^2 + \frac{1}{2} \cdot a \cdot D \cdot \sin(\psi) \quad (4.10)$$

$$A_{2,z} = \bar{b}_s \cdot h_s \quad (4.11)$$

4.6 Special Shear Element – Blister Ring

The blister rings (Figure 4.10) are used as restrictive element to block the melt flow over the entire cross section and thus increase the degree of fill in the upstream elements. The geometry of the blister ring element is very similar to the tooth mixing element, except for the teeth or slots present in the tooth mixing element. The element is formed by cylinder discs with a specified disc thickness and having a small clearance between the element and the barrel. A ring is fitted to the counter shaft similar to tooth mixing elements.

The melt flow occurs due to pressure difference through the leakage gaps available (Figure 4.11). Moreover the melt experiences high shear while flowing through this element. The geometry of the blister ring can be given by:

- length of the element - $L_{element}$
- radial gap – s_r
- calendar gap - s_w
- width of the ring – w_B

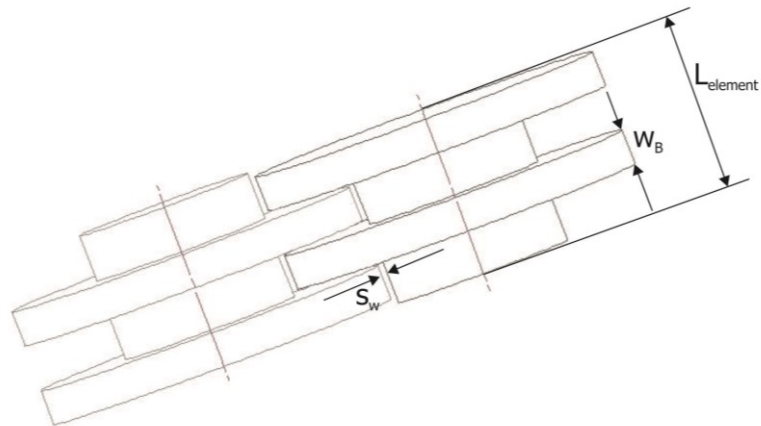


Figure 4.10: Blister ring element

The free channel area of the blister ring element is given as:

$$A_{free,B} = A_{barrel} - \frac{\pi}{4} \cdot D_a^2 - \frac{\pi}{4} \cdot D_i^2 \quad (4.12)$$

The area of the barrel (A_{barrel}) can be calculated using equation (4.10).

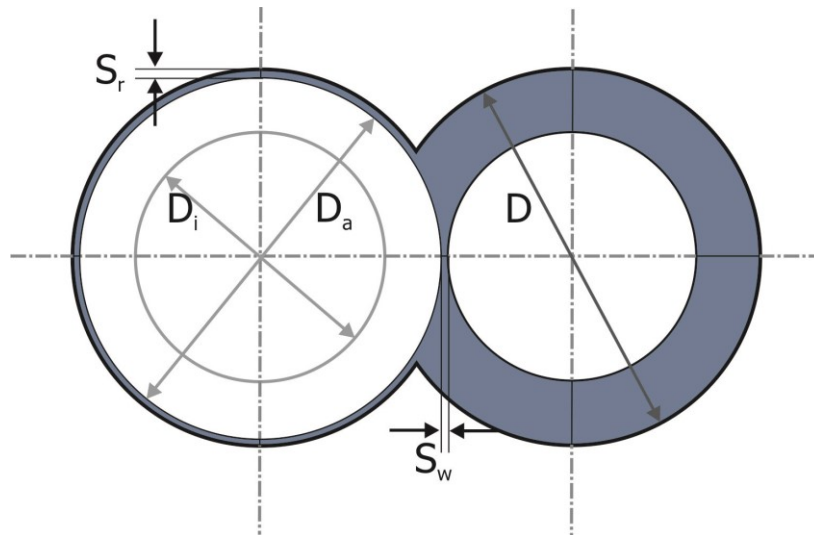
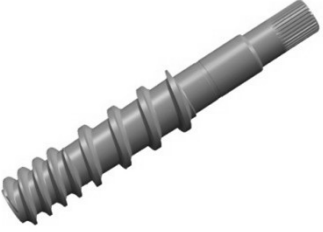

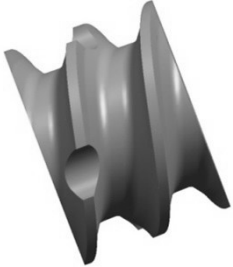




Figure 4.11: Clearances in blister ring element

4.7 Screw Elements Used in MAS Extruder

The different screw elements, which were used in the MAS conical twin screw extruder for this study, are shown below:

Table 4.1: Different screw elements used in MAS NCT55 extruder

<p>Solid Conveying Element</p>		<p>Feed Zone</p>
<p>Single flighted conveying element</p>		<p>Melting zone</p>
<p>Conveying mixing element</p>		<p>Mixing zone</p>
<p>Kneading element</p>		<p>Mixing and melting</p>
<p>Blister ring element</p>		<p>Mixing and flow restriction</p>

Screw Elements

<p>Conveying element</p>		<p>Pressure build-up and venting zone</p>
--------------------------	--	---

5 Solid Conveying

5.1 Introduction

The polymer pellets or material in other shapes or form is fed into the feed zone of the extruder from the hopper through the feed opening. The flow of the solid polymer particles from the hopper is gravitational or by forced feeding. The main function of the solid conveying zone is to compact the bulk material and convey the material through the flow channel into the melting zone. The feed zone geometry is important for achieving the maximum throughput of the extruder.

In contrary to the modeling of melt conveying zone of the co-rotating twin screw extruder, no adequate description or mathematical model exists for the solid conveying zone. The solid conveying zone has so far received less attention than melting and melt conveying zone. Also in case of single screw extruders very less research have been done on the conveying of polymer solid material in the feed zone of an extruder (Tadmor Z., 1970).

In the beginning of the 70's Haering (1974) conducted experimental investigations on the solid conveying mechanism in the co-rotating twin screw extruders using a transparent barrel to study the filling behavior and distribution of the solid materials in the screw channels. His studies showed that the right screw was fully filled and the left screw was partially filled under different feeding conditions.

A mathematical model is important for designing the screw geometry in the feed zone for attaining a maximum throughput. The frictional forces between the solid polymer and barrel and screw surfaces play a decisive role in the solid conveying mechanism. The important parameter that influences the solid conveying are the geometry of the feed opening, geometry of the feed particles and their solid bulk density.

Carrot et al. (1993) described an initial conveyance model for describing the conveying of solid material in the feeding zone of intermeshing co-rotating twin screw extruders. The used model was similar to the approach used in single screw extruders. This model works on the assumption that the solid material accumulates upstream of the leading edge of the flight and that the screw flights are only partially filled over the length of the screw structure. The feedstock is assumed to be subjected to forced conveyance in the intermeshing zone and frictional conveyance in the free channel section.

White et al. (1995) carried out flow visualization experiments to study the flow of solid materials in the feed section under starve fed conditions. Experiments showed two regions of solid conveying, one in the upper nip area in the intermeshing zone which dominated for low screw speeds and flow rates, while the second mechanism occur near the nip on the underside of the screw.

White et al. (1997) developed a composite model for the simulation of the solid conveying, melting and melt conveying in a modular co-rotating twin screw extruders. The solid conveying model was described for starved fed condition, where the pressurization of the bulk particles occurs in the region in front of the kneading block or negative conveying element. The mass balance and energy balance are done to model the solid conveying.

Potente et al. (1996) developed a physico-mathematical model to describe the functioning of the solid conveying zone of a co-rotating twin screw extruder, considering that the feed zone is divided into partially and fully-filled zones. The model permits the calculation of the maximum throughput and the pressure profiles over the length of the solid material zone, considering the force and torque balances. Based on the solid conveying model proposed by Potente et al., the solid conveying of the conical co-rotating twin screw extruders is described mathematically in this work.

5.2 Feed Zone Screw Geometry

The screw geometry in the intermeshing area is important for describing the conveying of the solid materials. The angle of deflection λ – the angle through which the solid is deflected during material transfer and the free length of the screw channel between the two intermeshing zones are the important geometries for the modeling of solid conveying (Melisch, 1997).

As described by Melisch, the angle of deflection (λ) can be determined by considering a cut off a positive pitch or helix angle (φ_0) (which is given by equation 3.10) orthogonally to the axis of the screw, as shown in Figure 5.1.

The angle of deflection is a function of the intermeshing angle and the helix angle and is given by the relation (Melisch, 1997):

$$\lambda_{sc} = \pi - 2 \cdot \arctan\left(\frac{\tan(\psi)}{\cos(\varphi_0)}\right) \quad (5.1)$$

The free length of the screw channel (Z_k) between two intermeshing zones is given as:

$$Z_k = \frac{(\pi - \psi)}{\cos(\varphi_0)} \quad (5.2)$$

The other important screw geometric parameters like intermeshing angle, channel depth, area, free volume etc. for different channel profiles are detailed in Chapter 3 and 4.

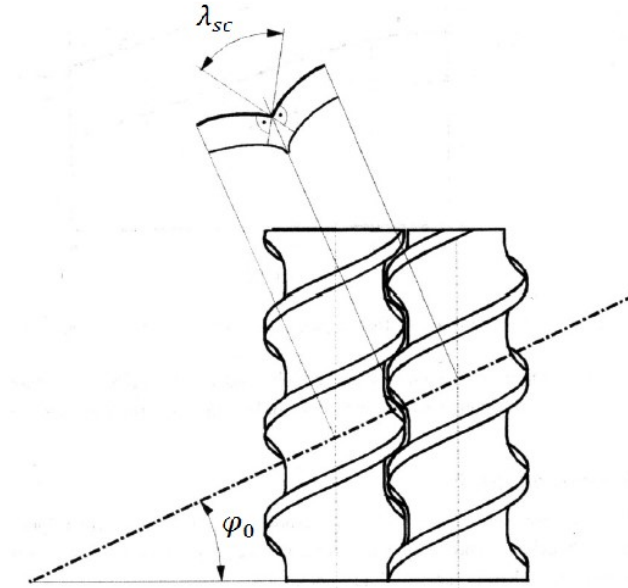


Figure 5.1: Definition of deflection angle

5.3 Maximum Solid Bed

In case of double shear edge channel profile the total channel width (b_0) can be fully filled with the bulk solid material. Due to geometric restrictions, the channel is only partially filled in Erdmenger and shear edge screw channel profile. This unfilled channel volume is dependent on the granulate diameter (d_p) and this can be described using the maximum solid bed width (b_{Fmax}).

The distances x_1 and x_2 are the distance between the channel center and the contact points of granulate with the barrel wall and screw respectively. The angle α_{sc} for calculating the maximum solid bed width is given according to Melish as:

$$\alpha_{sc} = -\arctan\left(\frac{dh(x)}{dx}\right)_{x=x_2} \quad (5.3)$$

The maximum solid bed width for double shear edge channel profile is given by the following equation:

$$b_{Fmax} = b_0 \quad (5.4)$$

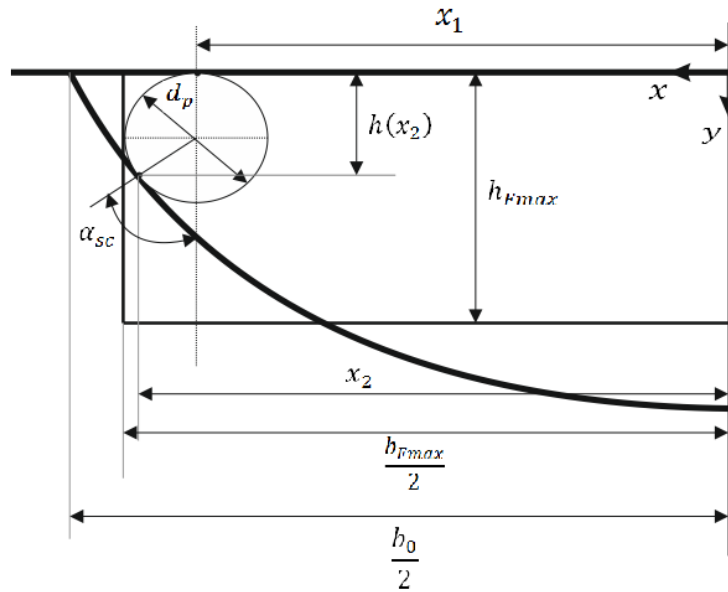


Figure 5.2: Mean solid bed width and solid bed height of Erdmenger channel profile (Melisch, 1997)

In case of standard Erdmenger profile, the maximum solid bed width is determined using the following equations:

$$b_{Fmax} = d_p + 2 \cdot x_1 \quad (5.5)$$

where x_1 is determined iteratively using the following relation

$$\frac{d_p}{2} \cdot (1 + \cos(\alpha_{sc})) = h \left(x_1 + \frac{d_p}{2} \cdot \sin(\alpha_{sc}) \right) \quad (5.6)$$

The maximum solid bed width for shear edge channel profile is given as:

$$b_{Fmax} = \frac{b_0}{2} + x_1 + \frac{d_p}{2} \quad (5.7)$$

The mean solid bed height h_{Fm} is determined by establishing the mean value for the local solid bed height over the width of the solid bed (Potente, Melisch, & Palluch, 1996).

$$h_{Fm} = \frac{2}{b_{Fmax}} \cdot \left[\frac{h_0 \cdot e_0}{2} + \int_{\frac{e_0}{2}}^{\frac{b_{Fmax}}{2}} h(x) \cdot dx \right] \quad (5.8)$$

5.4 Physical Model of Solid Material Feeding Behavior

The solid feed zone of a co-rotating twin screw extruder includes a fully filled compression zone and a partially filled solid feed zone. The maximum throughput of a co-rotating twin screw extruder is mainly influenced by the positioning of the feed opening.

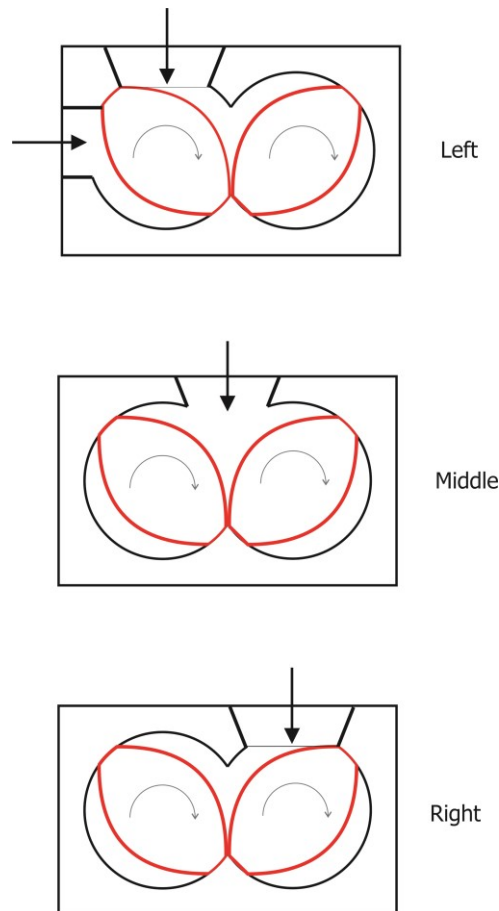


Figure 5.3: Position of the material feeding (Melisch, 1997)

The model is described to explain the feed behavior in which the screws turn to the left when the solid material is metered onto the left hand screw or mid-way between the two screws, as shown in Figure 5.3.

For explaining the solid feed flow, distinguishing three different cases is necessary (Potente, Melisch, & Palluch, 1996).

Case 1: When the extruder is operated with very small amount of metered feedstock, the feedstock is transported at low speed through gravitational conveyance of the loose material in the right hand screw and at high speeds through the circumferential flow of the loose

particles in both screws. The drive power which is induced is converted into solid material friction in the screw channel.

Case 2: If the metered bulk material is increased, the filling level of the right-hand screw will increase. When the first throughput limit is attained, the upper intermeshing zone will fill with loose material, preventing the bulk material from passing to the left-hand screw. In the upstream of the upper intermeshing zone, a tailback of solid material, of length Z_r develops. The deflection resistance and frictional forces will cause a pressure build-up over the tail back length. The remaining channel volume of right-hand screw will be fully filled with solid material without any pressure acting on it, while the left hand screw remains empty. The sudden jump in the drive torque is due to the termination of the gravitational conveyance and the tailback of material upstream of the upper intermeshing zone (Figure 5.4).

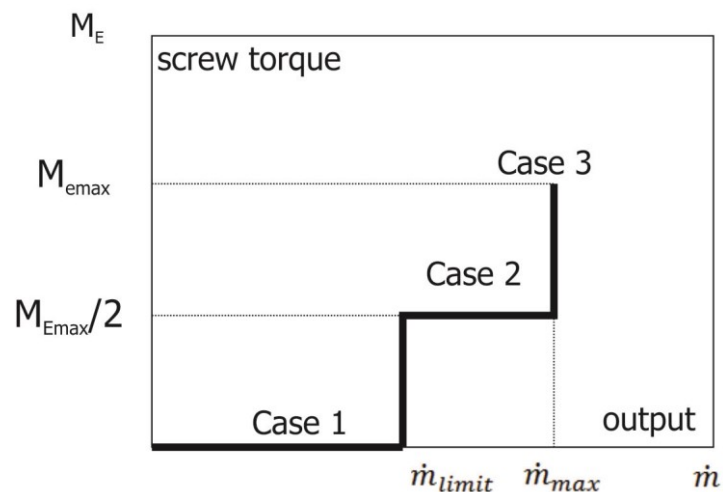


Figure 5.4: Limiting cases of feed behavior (Potente, Melisch, & Palluch, 1996)

Case 3: If the first throughput limit has been attained, the lower half of the left hand screw will fill with loose material as the flow of feedstock metered in is increased further. This process continues until a tailback length has formed upstream of the lower half of the intermeshing zone. The fact is that the upper and lower pressure profiles of the solid material tailbacks are equivalent to each other, that means when two torques undergo a sudden increase, they increase by the same amount. This second limit state is represented in Figure 5.5. and characterizes the maximum throughput that can be fed in.

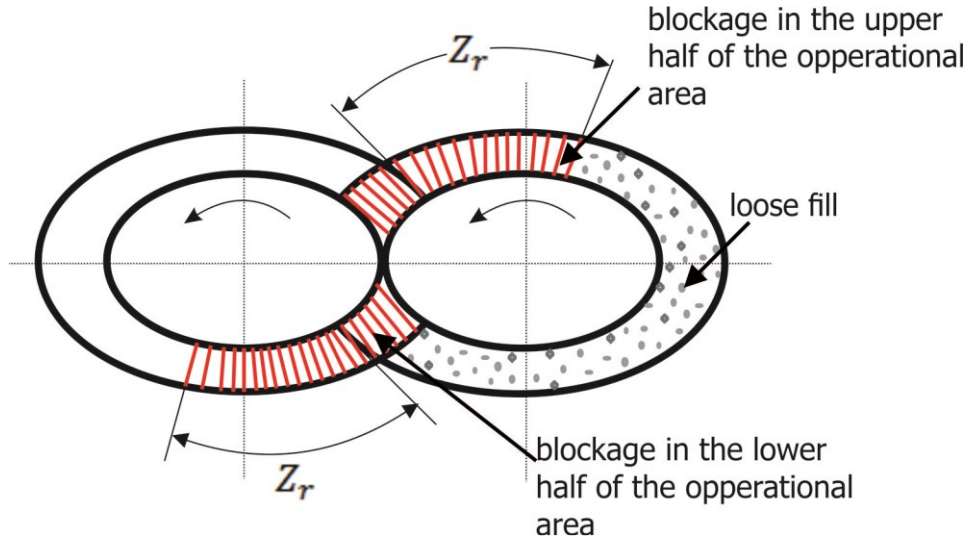


Figure 5.5: Material distribution for third conveying case (Potente, Melisch, & Palluch, 1996)

5.5 Maximum Throughput

The first throughput limit (\dot{m}_{limit}) for the solid feeding zone is characterized by the forced conveyance of loose material in both the upper intermeshing zone and the free volume of the right handed screw. The throughput limit, neglecting the pressure dependence of the bulk density (ρ_{bulk}), is given as:

$$\dot{m}_{limit} = N \cdot \rho_{bulk} \cdot n \cdot \left[\frac{V_{zw}}{2} + Z_k \cdot h_{Fm} \cdot b_{Fmax} \right] \quad (5.9)$$

Where V_{zw} is the free volume of the entire intermeshing zone and it can be determined from the cross sectional area of the intermeshing zone A_{zw} .

$$V_{zw} = A_{zw} \cdot \frac{\psi \cdot t}{\pi} \quad (5.10)$$

where A_{zw} is given by the following equation according to Booy (1980).

$$A_{zw} = m \cdot D_a^2 \quad (5.11)$$

Where m is a geometric parameter which can be derived by Booy's equation

$$m = \frac{1}{2} \cdot \left[\frac{a}{D_a} \cdot \sin(\psi) - \left(1 - \frac{\phi \cdot n}{\pi} \right) \cdot \left[\phi \cdot \left[\left(\frac{a}{D_a} \right)^2 - \frac{a}{D_a} + 0.5 \right] + \psi \cdot \left(\frac{a}{D_a} \right)^2 - \frac{a}{D_a} \cdot \sin(\psi) \right] \right] \quad (5.12)$$

The maximum conveyable throughput according to Potent et al. (1996) in the solid feed zone can be calculated from the forced conveyance of the loose material in the free volume of the right hand screw (which is completely filled with loose material), the loose material in the

intermeshing zone and the loose material in the tailback behind the lower half of the intermeshing zone.

$$\dot{m}_{max} = N \cdot \rho_{bulk} \cdot n \cdot [V_{zw} + (Z_k + Z_r) \cdot h_{Fm} \cdot b_{Fmax}] \quad (5.13)$$

where Z_r is the tail back length, which is not known to start off with.

The internal friction in the loose material and the way the solid particles wedge in the screw channel influence the formation of the tailback. These two influences can be combined to give a resultant internal friction (μ_{ir}) which is described by Koch (Koch, 1987) as:

$$\mu_{ir} = \mu_i^{1-\frac{d_p}{h_0}} \quad (5.14)$$

where μ_i is the internal friction of the material in the powdered state.

5.6 Tailback Length

The tailback length (Z_r) in the intermeshing zone is determined using the force balances for the three volume elements shown in Figure 5.6.

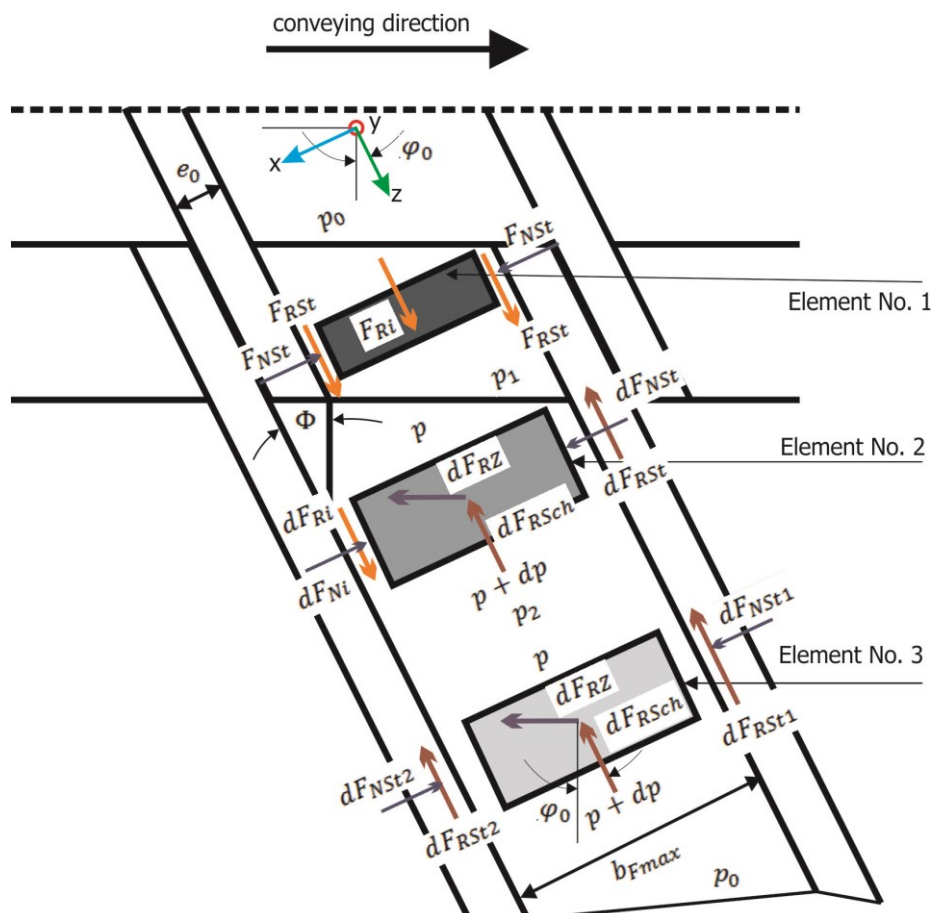


Figure 5.6: Equilibrium forces for three characteristic volume elements in solid feed zone (Potente, Melisch, & Palluch, 1996)

The deflection resistance is made up of two partial resistances – the deflection resistance inside the intermeshing zone (volume element 1) and the flight resistance downstream of the intermeshing zone (volume element 2). Volume element 3 is used to describe the conditions that prevail in the free channel section.

The deflection resistance inside the intermeshing zone is described by the moment balance around the reference point A on the volume element 1 (Figure 5.7), assuming that the material flow is a circular trajectory around point A.

$$(p_1 - p_0) \cdot (b_{Fmax} - e_0) \cdot \frac{h_{Fm}^2}{2} = 2 \cdot F_{Rst} \cdot \frac{h_{Fm}^2}{2} + F_{Ri} \cdot h_{Fm} \quad (5.15)$$

The resultant moment of the compressive forces p_1 and p_0 is maintained in the equilibrium state through the moment of internal friction of the loose material and through the moments of friction on the screw flight.

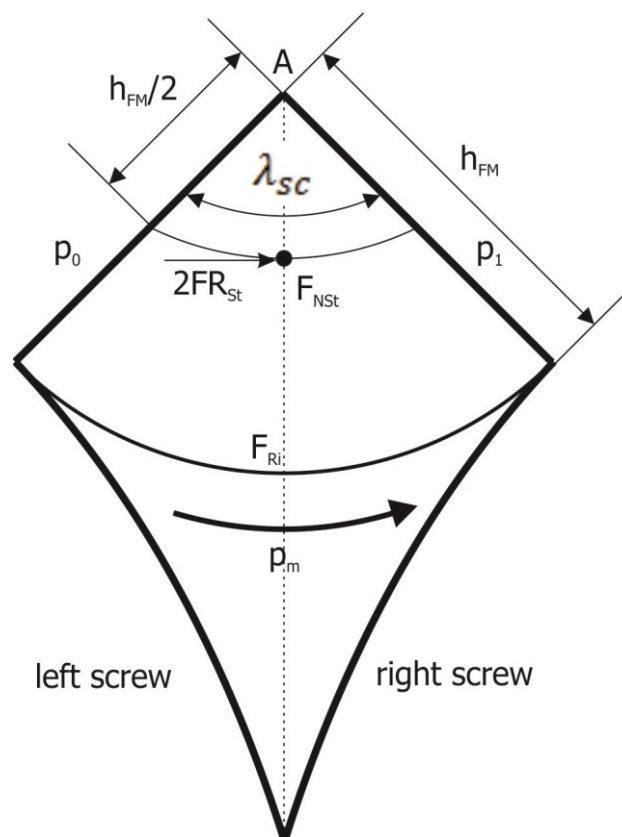


Figure 5.7: Equilibrium of moments for the volume element (Potente, Melisch, & Palluch, 1996)

The pressure distribution in the loose material is assumed to be an exponential fall in the pressure from p_1 to p_0 . $p + dp$.

The internal friction F_{Ri} and the frictional force due to screw flights F_{RSt} are determined using the following relations:

$$F_{Ri} = \mu_{ir} \cdot k_y \cdot p_m \cdot \lambda_{sc} \cdot h_{Fm} \cdot (b_{Fmax} - e_0) \quad (5.16)$$

$$F_{RSt} = \mu_s \cdot k_x \cdot p_m \cdot \lambda_{sc} \cdot h_{Fm}^2 \cdot \frac{1}{2} \quad (5.17)$$

The mean pressure in the intermeshing zone is given as:

$$p_m = \frac{p_1 - p_0}{\ln\left(\frac{p_1}{p_0}\right)} \quad (5.18)$$

This mean pressure is calculated via the logarithmic mean in view of exponential pressure distribution. The anisotropic nature of the pressure propagation in loose material are considered, making allowances with pressure anisotropic coefficients k_x and k_y .

$$k_x = 0.88 \cdot \left[\frac{\mu_s}{\mu_z} \cdot \frac{D_a - 2 \cdot h_{Fm}}{D_a} \right]^{0.7315} ; k_y = 1 \quad (5.19)$$

Substituting the equations 5.19, 5.17 and 5.16 in equation 5.15 gives the pressure upstream of the intermeshing zone

$$p_1 = p_0 \cdot e^{a_z} \quad (5.20)$$

where exponent a_z , which is given by the following relation, can be interpreted as a measure of the deflection resistance inside the intermeshing zone.

$$a_z = \lambda_{sc} \cdot \left(\mu_s \cdot k_x \cdot \frac{h_{Fm}}{b_{Fmax} - e_0} + 2 \cdot \mu_{ir} \cdot k_y \right) \quad (5.21)$$

Upstream of the opposing screw flight there is a volume filled with loose material which is subjected to forced conveyance, which is sheared at an angle of Φ to the direction of channel. For most polymer solids the angle Φ is mentioned in literature with a value of 30° .

The flight tailback length Z_e is calculated from the flight width and angle Φ , as follows

$$Z_e = \frac{e_0}{\tan(\Phi)} \quad (5.22)$$

Force balance is drawn up at infinitesimal volume element 2 to determine the flight resistance. The equilibria of forces in the direction of the screw channel is given as:

$$dF_{Ni} - dF_{NSt} - dF_{RZ} \cdot \cos(\varphi_0) = 0 \quad (5.23)$$

and in orthogonal direction to the screw flight is given as:

$$dF_{Ri} - dF_{RSt} - dF_{Sch} - d_p \cdot b(z_1) \cdot h_{Fm} = 0 \quad (5.24)$$

Other than the compressive forces, there are also normal forces that act on the contact surface of the screw root (F_{NSch}), screw flight (F_{NSt}), barrel wall (F_{FZ}) and frictional forces acting on the screw root (F_{RSch}), screw flight (F_{RSt}), barrel wall (F_{RZ}) and internal friction of loose material (F_{Ri}), which are given by the following relations:

$$dF_{NSt} = k_x \cdot p(z_1) \cdot h_{Fm} \cdot dz \quad (5.25)$$

$$dF_{NZ} = dF_{NSch} = k_y \cdot p(z_1) \cdot b(z_1) \cdot dz \quad (5.26)$$

$$dF_{RSt} = \mu_s \cdot dF_{NSt} \quad (5.27)$$

$$dF_{RSch} = \mu_s \cdot dF_{NSch} \quad (5.28)$$

$$dF_{Ri} = \mu_s \cdot dF_{Ni} \quad (5.29)$$

The local solid bed width is reduced by the local width of the flight tailback.

$$b(z_1) = \frac{e_0}{Z_e} \cdot z_1 + b_{Fmax} - e_0 \quad (5.30)$$

Potent et al. (1996) derived equations to determine the pressure propagation in the intermeshing zone (p_1) and in the flight tailback zone (p_2) as follows:

$$p_1 = p_0 \cdot e^{a_z} \quad (5.31)$$

where a_z is given by equation 5.21.

$$p_2 = p_1 \cdot e^{\Theta_1} \quad (5.32)$$

where exponent Θ_1 is a measure of the flight resistance and this is can be determined by the following equation:

$$\Theta_1 = \left\{ k_x \cdot (\mu_{ir} - \mu_s) \cdot \ln \frac{b_{Fmax}}{b_{Fmax} - e_0} + \frac{e_0 \cdot k_y}{h_{Fm}} \cdot [\mu_{ir} \cdot \mu_s \cdot \cos(\varphi_0) - \mu_s - \mu_z \cdot \sin(\varphi_0)] \right\} \cdot \frac{1}{\tan(\Phi)} \quad (5.33)$$

Similar to volume element 2, forces balances are drawn up at volume element 3 with the exception that the internal frictional force at the interface to the forcibly conveyed volume is replaced by a frictional force due to the flight, which acts in the opposite direction.

The pressure propagation in the screw channel is given as :

$$p_0 = p_2 \cdot e^{\Theta_2} \quad (5.34)$$

where exponent Θ_2 is

$$\Theta_2 = -Z_2 \cdot \left\{ \frac{2 \cdot \mu_s \cdot k_x}{b_{Fmax}} + \frac{k_y}{h_{Fm}} \cdot (\mu_s \cdot \mu_z \cdot \cos(\varphi_0) + \mu_s + \mu_z \cdot \sin(\varphi_0)) \right\} \quad (5.35)$$

The entire loose material trial back length Z_r is given from flight tailback length (Z_e) and intermeshing zone tailback length reduced by the flight tailback length (Z_2) as (Münzer, 2011):

$$Z_r = \frac{e_0}{\tan(\Phi)} + \frac{\ln\left(\frac{p_2}{p_0}\right)}{\left\{ \frac{2 \cdot \mu_s \cdot k_x}{b_{Fmax}} + \frac{k_y}{h_{Fm}} \cdot (\mu_s \cdot \mu_z \cdot \cos(\varphi_0) + \mu_s + \mu_z \cdot \sin(\varphi_0)) \right\}} \quad (5.35)$$

5.7 Bulk Density Correction

The bulk density of loose solid material is generally determined using DIN 53466 under room temperature and ambient pressure. This bulk density cannot be used without correcting in order to consider the wall influences and the conditions in the extruder. The bulk density can be corrected (Schöppner, 1994) using the following relationship:

$$\rho_{bulk,corr} = \rho_{bulk} \cdot \frac{F_0}{F_{0,\infty}} \quad (5.36)$$

Where the dwelling density F_0 is given from the particle volume $V_{P,total}$ to channel volume $V_{channel}$ ratio as:

$$F_0 = \frac{V_{P,total}}{V_{channel}} = \frac{N_{P,total} \cdot \frac{\pi}{6} \cdot d_p^3}{V_{channel}} \quad (5.36)$$

The total number of particles $N_{P,total}$ is given by:

$$N_{P,total} = (n_h \cdot n_b \cdot n_z \cdot N_m + 2 \cdot n_b \cdot n_z \cdot N_A + 4 \cdot n_z \cdot N_k) \cdot f \quad (5.37)$$

Where n_h , n_b and n_z gives the total number of elements along the channel height, channel width and channel length. These can be determined using the following equations:

$$n_h = \frac{d_p}{a_j} \cdot \left(\frac{h_0}{d_p} - 1 \right) \quad (5.38)$$

$$n_b = \frac{d_p}{a_j} \cdot \left(\frac{b_{Fmax}}{d_p} - 1 \right) \quad (5.39)$$

$$n_z = \frac{d_p}{a_j} \cdot \left(\frac{Z}{d_p} - 1 \right) \quad (5.40)$$

The area factor f is given by:

$$f = \frac{e_0 \cdot h_0 + 2 \cdot \int_{\frac{e_0}{2}}^{\frac{b_{Fmax}}{2}} h(x) \cdot dx}{h_0 \cdot (b_{Fmax} - d_p) + d_p^2} \quad (5.41)$$

The parameters N_M , N_A and N_K gives the number of particles per element cell depending on their position (Münzer, 2011) and its numbers are given in Table 5.1.

The edge length a_j for each particle alignment is calculated as follows:

for cubic primitive,

$$a_p = d_p \quad (5.42)$$

for cubic area centered,

$$a_f = \sqrt{2} \cdot d_p \quad (5.43)$$

and for cubic room centered,

$$a_r = \frac{2}{\sqrt{3}} \cdot d_p \quad (5.44)$$

Table 5.1: Number of particles

Position	Parameter	Number of particle		
		Area centered	Room centered	primitive
Middle	N_M	4	2	1
Outer surface	N_A	1	1/2	1/2
Edge	N_K	1/4	1/4	1/4

The dwelling bulk density in an infinite container $F_{0,\infty}$ is given by the ratio of particle volume per unit cell and volume of the unit cell.

$$F_{0,\infty} = \frac{V_{p,z}}{V_z} = \frac{N_m \cdot \frac{\pi}{6} \cdot d_p^3}{a_j^3} \quad (5.44)$$

6 Melting

6.1 Introduction

The melting studies of polymers in screw extruders started in the late 1950s by different authors (Maddock, 1959) (Tadmor, 1970). The developed melting model assumed that the melting occur mainly at the upper solid-melt interface formed due to compaction of solid bed and formation of thin melt film on the barrel surface.

Melting studies in intermeshing modular co-rotating twin screw extruders have been started since 1990. The melting models were simplified formulations based on the single screw extruder melting models. Potent et al. (Potente, Anshal, & Klarholz, 1994) described a composite model to describe the melting profile in the co-rotating twin screw extruders and verified the model experimentally, which showed a good agreement with the theoretical values.

White and Bawiskar (White & Bawiskar, 1995) (White & Bawiskar, 1997) studied experimentally the melting mechanism in twin screw extruders under starve fed conditions, with flow visualization and screw pull out experiments. They reported that the first stage of melting is associated with the heat conduction from the barrel wall heat. Also the melting is generally initiated in the screw region prior to the kneading blocks and the melting gets completed in the kneading disc region. Bawiskar (1998) in his work described melting models for different screw elements (conveying and kneading screw elements). The model considers the formation of two stratified layers of melt in contact with the hot barrel and solid pellets in contact with the relatively colder screw. The kneading block elements act as flow blocking and initiate the melting process. The model predicts the location of melting and the total melting length in a screw configuration.

The melting model described by Anshal (1993), which is a modified Tadmor model, has been considered as basis in this work for developing the melting model for conical co-rotating twin screw extruders. For modeling melting in conical twin screws the groove model has been used considering the geometric changes along the screw axis step wise and the corresponding changes in the shear rate. Also the solid bed width change and the temperature changes of the polymer are performed on the groove model.

In conical co-rotating extruders, the metered polymer material gets compacted due to the conicity and improves the contact of the material with the barrel wall, which initiates the

melting process. This leads to the formation of a thin film on the barrel wall. Due to the formation of the melt film, the frictional flow gets dominated and the material gets conveyed through the intermeshing area, which also induces more mixing. The solid material which does not come in contact with the barrel wall gets heated through thermal conductivity. In the flow channel a melt pool is formed by wiping the melt film from the barrel wall by the screw flights. This melt pool pushes the solid bed to the passive flight side. At the end of the melting the solid bed width completely vanishes.

6.2 Melting Profile Model

The modified Tadmor model by Ansahl (Ansahl, 1993) is shown in Figure 6.1, where the channel geometry is considered as a double edge profile in order to make the model simpler. In Figure 6.1 the melt film thickness as function of the position $\delta_{mf}(X)$ is represented. The average melt film thickness can be determined by the following relation:

$$\overline{\delta_{mf}} = \frac{\delta_{mf}(X)}{1 + c} \quad (6.1)$$

where c is the exponent and its determination is explained later.

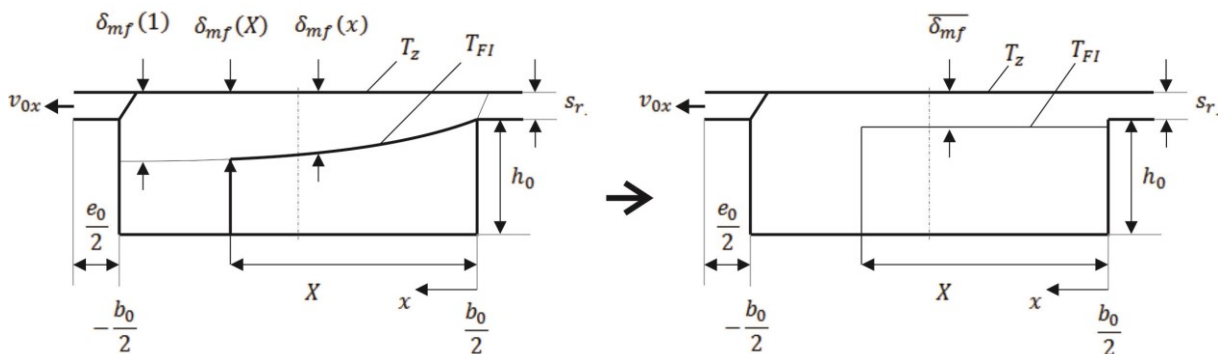


Figure 6.1: Modified Tadmor melting model (Ansahl, 1993)

Figure 6.1b shows the channel with the average melt film thickness $\overline{\delta_{mf}}$. According to Potent et al. (1994) the change in the solid bed profile along the screw channel direction through mass balance is given by the following differential equation, which can no longer be analytically solved:

$$-\frac{\partial}{\partial z}(\rho_{bulk} \cdot v_F \cdot x \cdot h_{Fm}) = \frac{1}{2} \cdot \rho \cdot k_1 \cdot v_{0x} \cdot (\overline{\delta_{mf}} - s_r) \quad (6.2)$$

where v_F is the mean solid bed velocity, v_{0x} is the x component of circumferential velocity. Numerical methods have been implemented to solve the above equation to find the solid bed length.

The solution to the above equation is given by the simple function called Brinkmann number, a dimensionless number, which is the ratio of the heat dissipation to radial thermal conductivity.

$$Br = \frac{K(T_{FI}) \cdot k_2 \cdot v_{rel}^{1+n} \cdot \bar{\delta}_0^{1-n}}{\lambda_s \cdot (T_Z - T_{FI})} \quad (6.3)$$

The approximation solution to equation 6.2 can be described by a simple function:

$$\Psi^* = \frac{\Psi - \Psi_s}{1 - \Psi_s} = y^c \quad (6.4)$$

where

$$\Psi_s = \frac{s_r}{\delta_{0,mf}} \quad (6.5)$$

$$\Psi = \frac{\bar{\delta}_{mf}}{\delta_{0,mf}} = \frac{\delta_{mf}}{\delta_{0,mf}} \quad (6.6)$$

$$y = \frac{x}{b_0} \quad (6.7)$$

Where $\delta_{0,mf}$ is the initial melt film thickness at the barrel wall for $x = b_0$ and the ratio of the solid material with x to the screw channel width b_0 is the standardized solid bed y . The standardized melt film thickness Ψ is formed from the quotient of the melt film thickness δ_{mf} to the starting melt film thickness $\delta_{0,mf}$. The following set of equations is obtained as the solution to the equation 6.2.

The exponent c which is given by the following equation, is determined iteratively.

$$c = \frac{\log\left(\frac{\Psi_1 - \Psi_2}{\Psi_2 - \Psi_s}\right)}{\log\left(\frac{y_1}{y_2}\right)} \quad (6.8)$$

The starting melt film thickness $\delta_{0,mf}$ is given as

$$\delta_{0,mf} = (\delta_{1,mf} - s_r) \cdot y_1^{-c} + s_r \quad (6.9)$$

The constants k_1 and k_2 can be determined by:

$$k_1 = 2 \cdot \left(\frac{1}{1 - e^A} + \frac{1}{A} \right) \quad (6.10)$$

$$k_2 = \frac{2}{A^2} \cdot \left(\frac{A}{e^A - 1} \right)^{1+n} \cdot (e^A - A - 1) \quad (6.11)$$

where A is given by:

$$A = \frac{\beta}{n} (T_z - T_{FI}) \quad (6.12)$$

With these equations y can be given by the following simplified equation

$$y = \frac{x}{b_0} = [1 - (1 - c)(1 - \Psi_s) \cdot \pi_1 \cdot \zeta] \cdot \frac{1}{1 - c} \quad (6.13)$$

$$\pi_1 = \frac{\rho_{bulk} \cdot k_1 \cdot \delta_{0,mf} \cdot v_b \cdot D_a}{2 \cdot \dot{m}} \quad (6.14)$$

$$\zeta = \frac{z}{D_a} = \frac{L}{D_a \cdot \sin(\varphi_0)} \quad (6.15)$$

In order to simplify the calculation procedure, the beginning of the melting (the point of melt pool formation (PMF)) can be equated with the first point of complete filling (Potente, Anshl, & Klarholz, 1994).

The conveying angle Λ is determined using the following equation (Münzer, 2011):

$$\Lambda = \arctan \left(\frac{\tan(\varphi_0)}{\frac{\rho_{bulk,corr} \cdot A_{free} \cdot \pi \cdot D_a \cdot N \cdot \tan(\varphi_0)}{\dot{m}_{feed} - \dot{m}_{fc}}} \right) \quad (6.16)$$

The fed mass flow rate \dot{m}_{feed} is given as:

$$\dot{m}_{feed} = \rho_{bulk,corr} \cdot A_{free} \cdot v_{ax} + \dot{m}_{fc} \quad (6.17)$$

The mass flow rate due to the forced conveyance \dot{m}_{fc} is determined using the following relation:

$$\dot{m}_{fc} = N \cdot \rho_{bulk,corr} \cdot i \cdot (Z_e + e_0 \cdot \tan(\varphi_0)) \cdot e_0 \cdot h_{Fm} \quad (6.18)$$

The axial conveying velocity v_{ax} is determined as:

$$v_{ax} = \frac{\tan(\varphi_s) \cdot \tan(\Lambda)}{\tan(\varphi_s) + \tan(\Lambda)} \cdot \pi \cdot D_a \cdot N \quad (6.19)$$

The solid bed flow velocity v_{Fz} can be calculated using the following relation:

$$v_{Fz} = \frac{v_b \cdot \tan(\Lambda)}{\cos(\varphi_0) \cdot (\tan(\varphi_0) + \tan(\Lambda))} \quad (6.20)$$

6.3 Melt Temperature Profile

One of the major objectives of the melting process in extruders is to achieve the melt temperature of the fed material. The melt temperature profile along the screw axis is an important parameter in configuring the screw. The temperature profile of the polymer material is calculated based on the model described by Ansahl (1993) in his work.

For calculating the temperature changes, the first step is to determine the start temperature. The mean melt film temperature is considered as the average start temperature (\bar{T}_{start}). This start temperature is determined from the energy equation for the melt film at the barrel wall at the first point of melt pool formation. The energy equation is given as:

$$\lambda_s \cdot \frac{\partial^2 T}{\partial y^2} + \tau_{yi} \cdot \frac{\partial v_j}{\partial y} = 0 \quad (6.21)$$

Applying the boundary conditions $T(0) = T_{FI}$; $T(\bar{\delta}_{mf}) = T_z$, the following solution is obtained:

$$T(\xi) = T_{FI} + (T_z - T_{FI}) \cdot \left\{ \xi + Br \cdot \left(\frac{1}{A^2} \cdot \left(\frac{A}{e^A - 1} \right)^{1+n} \cdot [1 - e^{A\xi} - \xi \cdot (1 - e^A)] \right) \right\} \quad (6.22)$$

Where

$$Br = \frac{K(T_{FI}) \cdot v_{rel}^{1+n} \cdot \bar{\delta}_{mf}^{-1+n}}{\lambda_s \cdot (T_z - T_{FI})} \quad (6.23)$$

$$\xi = \frac{y}{\delta} \quad (6.24)$$

and

$$A = \frac{\beta(T_z - T_{FI})}{n} \quad (6.25)$$

The mean temperature for the melt film can be calculated using the following relationship (Potente, Ansahl, & Klarholz, 1994):

$$\bar{T} = \bar{T}_{start} = \frac{\int_0^1 v(\xi) \cdot T(\xi) \cdot d\xi}{\int_0^1 v(\xi) \cdot d\xi} \quad (6.26)$$

with the velocity profile:

$$v(\xi) = v_{rel} \cdot \frac{e^{A\xi} - 1}{e^A - 1} \quad (6.27)$$

and the relative velocity is given as:

$$v_{rel} = \sqrt{(v_{0z} - v_{Fz})^2 + v_{0x}^2} \quad (6.28)$$

The equations to calculate the initial temperature for the calculation of the temperature profile along the screw axis are:

$$\bar{T}_{ini} = [B \cdot \Delta T \cdot (A - 1) \cdot 2 \cdot e^{2A} - (A \cdot B \cdot \Delta T \cdot e^{2A} + A_3 - A_2)] \cdot A_4 \quad (6.29)$$

Where

$$B = Br \cdot \frac{1}{A^2} \cdot \left[\frac{A}{e^A - 1} \right] \quad (6.30)$$

$$\Delta T = T_z - T_{F1} \quad (6.31)$$

$$A = \frac{\beta}{n} \cdot \Delta T \quad (6.32)$$

$$A_1 = A^2 \cdot (B + 1) + 3 \cdot A \cdot B + 2 \cdot (B - 1) \quad (6.33)$$

$$A_2 = [\Delta T \cdot (A \cdot (B + 1) + 2 \cdot B - 1) + A \cdot T_{F1}] \cdot 2 \cdot e^A \quad (6.34)$$

$$A_3 = A^2 \cdot B \cdot \Delta T \cdot e^A + \Delta T \cdot A_1 + 2 \cdot A \cdot T_{F1} \cdot (A + 1) \quad (6.35)$$

$$A_4 = \frac{1}{2 \cdot A \cdot (e^A - A - 1)} \quad (6.36)$$

Assuming $Br = 0$ the simplified equation to find the starting temperature is given as (Potente, Anshl, & Klarholz, 1994):

$$T_{start} = T_{FL} + (T_z - T_{F1}) \cdot \frac{\frac{1}{A} - \frac{A}{2} + e^A \cdot \left(1 - \frac{1}{A}\right)}{e^A - A - 1} \quad (6.37)$$

The groove model is also considered for calculating the material temperature. The following assumptions are made for this temperature calculation (Potente, Anshl, & Klarholz, 1994):

- The screw channel is considered as a flat channel
- No wall slip and melt adheres to the wall
- The flow is laminar and incompressible
- The melt flow behavior is Non-Newtonian (the melt is considered to follow the Power Law)
- Mean values established over individual sections are used for all material values
- Allowances is made for filling degree profile

The differential equation for an individual zone of constant geometry is as follows:

$$\rho \cdot c \cdot \bar{v}_z \cdot \frac{\delta T}{\delta z} = \lambda \cdot \frac{\delta^2 T}{\delta y^2} + (\overline{\tau \cdot \dot{\gamma}})_0 \cdot e^{-\beta \cdot (T - T_0)} \quad (6.38)$$

In the above equation the temperature change in the down channel direction z is given on the left hand side and the right hand side describes the thermal conductivity over the channel depth. The term $(\overline{\tau \cdot \dot{\gamma}})_0$ describes the mean dissipated specific power over the channel cross section. The exponential term describes the temperature dependency of viscosity. The following dimensionless quantities are used to solve the above differential equation.

$$\Theta_0 = \frac{T_0 - T_z}{T_z} \quad (6.39)$$

$$\xi = \frac{y}{h} \quad (6.40)$$

$$\zeta = \frac{z}{Z} \quad (6.41)$$

$$Br = \frac{(\overline{\tau \cdot \dot{\gamma}})_0 \cdot h^2}{\lambda \cdot T_z} \approx \frac{K \cdot v_0^{1+n} \cdot h^{-1-n}}{\lambda \cdot T_z} \quad (6.42)$$

$$Gz = \frac{c_p \cdot \rho \cdot h \cdot \dot{V}}{\lambda \cdot b_0 \cdot Z \cdot i} \quad (6.43)$$

The Graetz number (Gz) is a dimensionless number which describes the ratio of the axial convection to radial thermal conductivity.

The differential equation 6.38 cannot be solved due to the exponential function. The equation can be simplified if it is assumed that the temperature changes along the screw channel direction are small as:

$$\frac{\partial^2 \Theta}{\partial \xi^2} - Gz \cdot \frac{\partial \Theta}{\partial \zeta} = -Br \quad (6.44)$$

This differential equation was solved using the following assumptions (Potente, Ansahl, & Klarholz, 1994) (Carslaw & Jaeger, 1959):

- For the region $\xi > 0$ the mean starting temperature $\Theta(\xi = 0) = \Theta_{start}$ applies
- The heat produced is introduced into the calculation as a mean value per coordinate unit $\Delta \zeta$ and volume unit for $\zeta > 0$
- The barrel wall temperature T_z is constant

The solution for the axial temperature development is given as:

$$\Theta(\zeta, \xi) = \left[\Theta_0 + \frac{Br}{Gz} \cdot \xi^2 \right] \operatorname{erf} \left(\frac{\xi}{\sqrt{\frac{\xi}{Gz}}} \right) + Br \cdot \sqrt{\frac{\zeta}{Gz \cdot \pi}} \cdot e^{\left[\frac{-Gz \cdot \xi^2}{4 \cdot \zeta} \right]} - \frac{Br}{2} \cdot \xi^2 \quad (6.45)$$

$$\bar{\Theta} = \frac{\bar{T} - T_z}{T_z} = \int_0^1 \Theta(\zeta, \xi) \cdot d\xi \quad (6.46)$$

7 Melt Conveying

7.1 Introduction

The conveying or metering of the melt is mainly carried out using the conveying elements, which are described in chapter 4. The geometric description and different types of channel profiles used in conveying elements are briefly described in chapter 3. The melt conveying mechanisms of the conveying elements with different channel profiles will be detailed in this chapter. Modeling of melt conveying in parallel twin screw extruders have been studied by several authors (Michaeli, Grefenstein, & Berghaus, 1995), (Potente, Ansahl, & Wittemeier, 1990), (White, Kim, & Bawiskar, 2001).

Modeling the pressure and throughput characteristics are mainly carried out under isothermal conditions. White et al. (1994) proposed a model for simulating the flow in twin screw extruders under non-isothermal conditions, considering the mean temperature rise in the screw elements. Mours et al.(2000) used computational fluid dynamics (CFD) based on a finite volume method to simulate the three dimensional pressure and velocity field for non-Newtonian fluids in a fully filled screw element in a co-rotating twin screw extruders, considering the non-isothermal conditions which requires a non-steady state calculation.

The usage of pressure consuming screw elements or die leads to accumulation of melt upstream to the pressure consumer. These fully filled zones are important for melting, mixing and homogenization of the melt. The length of fully filled zone upstream to the pressure consuming zones is called the back pressure length. The determination of the back pressure length is very important for designing the pressure build-up zone. This back pressure length and the degree of fill is related to each other.

7.2 Throughput Characteristics under Isothermal Conditions

7.2.1 Groove Model

For analyzing the velocity and the pressure fields in the intermeshing co-rotating twin screw extruder, the groove model (Figure 7.1) is used. This groove or channel model is used in many papers for mathematical-physical description of the flows in axially open screw channels (Potente, Ansahl, & Wittemeier, 1990). The model originates from the theory of the single screw extruder (Wang, White, & Szydowski, 1989). In this groove model (Figure 7.1) the coordinate system is embedded in the screw and the barrel is considered to move relative to it. The melt flow in the co-rotating twin screws can be modeled analogue as single

screw extruders, additionally considering the axial conveying in the intermeshing zone of the twin screw extruders (Schuler, 1996).

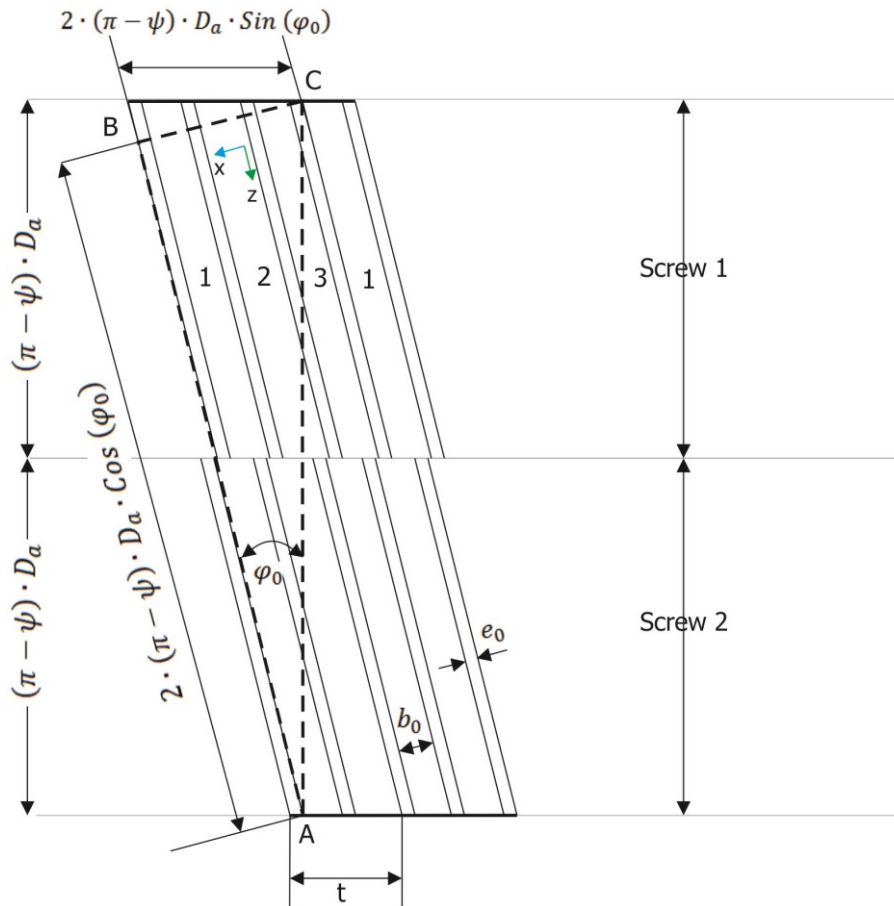


Figure 7.1: Groove model of conveying screw element

The number of available flow channels for conveying elements with n number of flights is given by:

$$i = 2 \cdot n - 1 \quad (7.1)$$

In order to make the model simpler, the wall slip and the gravity forces are not considered and the following assumptions are made:

- the flow is laminar
- the melt is incompressible
- the fluid is non-Newtonian
- the melt is isothermal

In case of conveying elements, the material is not exchanged between the channels except some exchange of material due to leakage through the radial and flight clearances. The melt conveying in the conveying element is longitudinally open and closed transversally.

In case of kneading and other mixing elements, the flow channels are longitudinally and transversally open.

The melt conveying capacity of the intermeshing co-rotating twin screw extruders can be calculated considering the drag (\dot{V}_{drag}), pressure (\dot{V}_{drag}), nip (\dot{V}_{nip}) and the leakage ($\dot{V}_{leakage}$) flows (Figure 7.2).

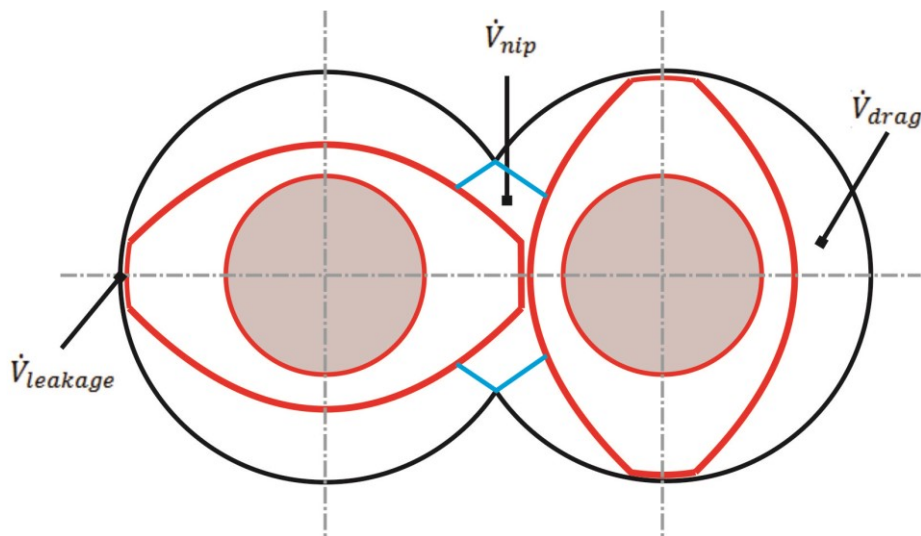


Figure 7.2: Flow in intermeshing co-rotating twin screw conveying element (Schuler, 1996)

7.2.2 Forward Conveying Element - Erdmenger Profile

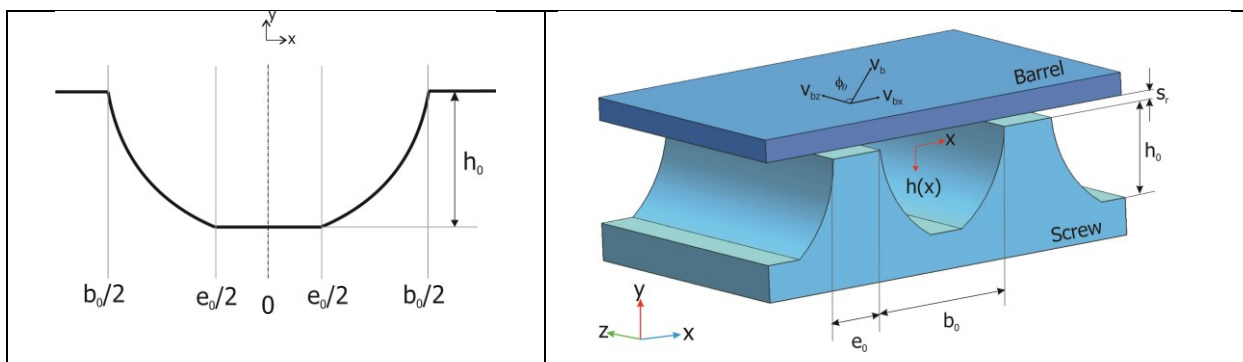


Figure 7.3: Erdmenger (or) standard screw channel geometry

The cross channel geometry and the flat plate model of the Erdmenger profile is shown in Figure 7.3. In the flat plate model the barrel wall is considered to move at a particular velocity (v_b), which is a function of screw diameter and the screw rotation speed.

The basic equation for deriving the velocity profile in the screw flow channels is the simplified Navier-Stokes equation (equation of motion).

$$\frac{\partial p}{\partial z} = \eta \cdot \frac{\partial^2 v_z}{\partial y^2} \quad (7.2)$$

Where p is the pressure and η is the viscosity of the polymer melt.

The viscosity η is dependent on the shear rate $\dot{\gamma}$ and it is defined using the Cross model (7.3) or Power Law model (7.4)

$$\eta(\dot{\gamma}) = \frac{A}{1 + (B \cdot \dot{\gamma})^C} \quad (7.3)$$

Where A is the zero shear viscosity, B is the cross time constant and C is the slope of power law region

$$\eta(\dot{\gamma}) = k \cdot \dot{\gamma}^{n-1} \quad (7.4)$$

Where k is the consistency index and n is the power law index.

The shear rates ($\dot{\gamma}_z$) in the down channel and the cross channel ($\dot{\gamma}_x$) are given by the following relation:

$$\dot{\gamma}_z = 4 \cdot \frac{v_{bz}}{h} - \frac{6 \cdot \dot{V}}{h_0^2 \cdot b_0 \cdot (2 \cdot n - 1)} \quad (7.5)$$

$$\dot{\gamma}_x = \frac{4 \cdot v_{bx}}{h_0}$$

Having the shear rates in the z and x axis, a representative shear rate is calculated:

$$\dot{\gamma}_{rep} = \sqrt{(\dot{\gamma}_z^2 + \dot{\gamma}_x^2)} \quad (7.6)$$

The velocity of the moving barrel is given as:

$$v_b = D_a \cdot N \cdot \pi \quad (7.7)$$

where N is the screw rotation speed.

The down channel velocity (v_{bz}) and the cross channel velocity (v_{bx}) shown in Figure 7.3 are given by the following relations:

$$v_{bz} = v_b \cdot \cos \varphi_0 \quad (7.8)$$

$$v_{bx} = v_b \cdot \sin \varphi_0$$

The velocity profile in the down channel direction is obtained by integrating the partial differential equation (equation of motion 7.2) twice and applying the boundary conditions. The boundary conditions are:

$$v_z(y = 0) = v_{bz} \quad (7.9)$$

$$v_z(y = h(x)) = 0$$

The velocity field in the down channel direction is:

$$v_z(y) = v_{bz} \cdot \left(1 - \frac{y}{h(x)}\right) - \frac{1}{2 \cdot \eta} (h(x) \cdot y - y^2) \cdot \frac{\partial p}{\partial z} \quad (7.10)$$

The net flow rate is obtained by integrating the down channel velocity across the channel cross sectional area (Schuschnigg, 2009).

$$\dot{V} = 2 \cdot \left[\int_0^{\frac{e_0}{2}} \int_0^{h_0} v_z(x, y) \cdot dy \cdot dx + \int_{\frac{e_0}{2}}^{\frac{b_0}{2}} \int_0^{h_0} v_z(x, y) \cdot dy \cdot dx \right] \quad (7.11)$$

Since solving the above integral equation analytically is very complicated, the equation is solved numerically. The first term in the integral equation describes the constant channel depth and the next term describes the change in the channel depth along the screw axis. Also the conicity of the screws, in case of the conical twin screw extruders, is taken into account during solving the equation.

The solution to the above equation is given in equation 7.12. The total net flow is given by the sum of drag flow and pressure flow. In the equation the first term describes the drag flow which is in the positive direction and the second term, the pressure flow which tends to cause the flow in the reverse direction.

$$\dot{V}_{drag,pressure} = (2 \cdot n - 1) \cdot \left\{ 2 \cdot \frac{v_{bz}}{2} \cdot \left[\frac{e_0 \cdot h_0}{2} + \int_{\frac{e_0}{2}}^{\frac{b_0}{2}} h(x) \cdot dx \right] - 2 \cdot \frac{1}{12 \cdot \eta} \cdot \frac{\partial p}{\partial z} \cdot \left[\frac{e_0 \cdot h_0^3}{2} + \int_{\frac{e_0}{2}}^{\frac{b_0}{2}} h(x)^3 \cdot dx \right] \right\} \quad (7.12)$$

As mentioned by Booy (1980) and Tadmor (1970) the shape factors F_d and F_p for drag and pressure back flow can be introduced in the above equation. These shape factors are

dependent only on the channel width (b_0) and channel height (h_0) and they represent the reducing effect of the flights on flow between infinite parallel plates.

The total flow rate \dot{V}_{total} is given considering the drag, pressure and apex flow as:

$$\dot{V}_{total} = \dot{V}_{drag} + \dot{V}_{nip} - \dot{V}_{pressure} \quad (7.13)$$

Booy (1980) derived an equation for computing the flow rate in the nip zone of the co-rotating twin screws, which is given as follows:

$$\dot{V}_{nip} = v_a \cdot A_a = N \cdot t \cdot k_a \cdot \left(\frac{D_a}{2}\right)^2 = \frac{1}{2} \cdot k_a \cdot \frac{t}{D_a} \cdot \left(\frac{D_a}{2}\right)^3 \cdot N \quad (7.14)$$

Here A_a is the area of the nip zone, which changes with the rotation of the screws. So an average value is determined considering a rotation cycle with an angle equal to $\frac{\pi}{2}$. Here k_a is a dimensionless coefficient that is a function of n and ρ_c (Booy, 1980)

$$k_a = \rho_c \cdot \sin(\psi) - \left(1 - \frac{\alpha \cdot n}{\pi}\right) \cdot \left[\frac{1}{2} \cdot \alpha \cdot (\rho_c^2 - 2 \cdot \rho_c + 2) + \psi \cdot \rho_c^2 - \rho_c \cdot \sin(\psi)\right] \quad (7.15)$$

In addition to drag, pressure and nip flows, leakage flow through the clearance between the screw and barrel must be considered. According to Meijer & Elemans (1988) and Schuler (1996), the leakage flow due to simple drag flow is enough to estimate and the pressure flow in the narrow channels is very small and it can be neglected (Jacobi, 1960).

The leakage flow through the radial clearance s_r due to pure drag is given by:

$$\dot{V}_{leakage} = \pi \cdot D_a \cdot N \cdot s_r \quad (7.16)$$

The share of the flows making up the conveying capacity is approximately 91% for drag flow, approximately 16 % for nip flow and approximately -7 % for drag leakage flow (Schuler, 1996).

Considering all these flows, the net flow rate can be defined as:

$$\dot{V}_{total} = \dot{V}_{drag} - \dot{V}_{pressure} + \dot{V}_{nip} - \dot{V}_{leakage} \quad (7.17)$$

Analogous to the single screw extruder, the throttle coefficient a_{coeff} for co-rotating twin screw extruders can be determined from the ratio of the pressure and drag flows.

$$a_{coeff} = \frac{\dot{V}_{pressure}}{\dot{V}_{drag}} \quad (7.18)$$

The value of a_{coeff} is between 0 and 1.

The four operating conditions in the screw elements according to equation 6.16 are (Schuler, 1996):

$a_{coeff} > 1$ – for backward conveying elements, where $\dot{V}_{drag} < 0$ (pressure consumer)

$a_{coeff} < 0$ – for conveying elements, where $\dot{V}_{drag} < \dot{V}_{pressure}$ (pressure consumer)

$a_{coeff} = 0$ – for conveying elements, where $\dot{V}_{drag} = \dot{V}_{total}$ (pressure neutral)

$0 < a_{coeff} < 1$ – for pressure build-up conveying elements, where $\dot{V}_{drag} > \dot{V}_{total}$ (pressure generator)

7.2.3 Forward Conveying Element - Shear Edge Profile

The shear edge profile differs from the standard Erdmenger profile only through the asymmetry of the channel profile. The undercut on one side of the screw channel increases the free channel volume to about 15 % (Kohlgrueber, 2008).

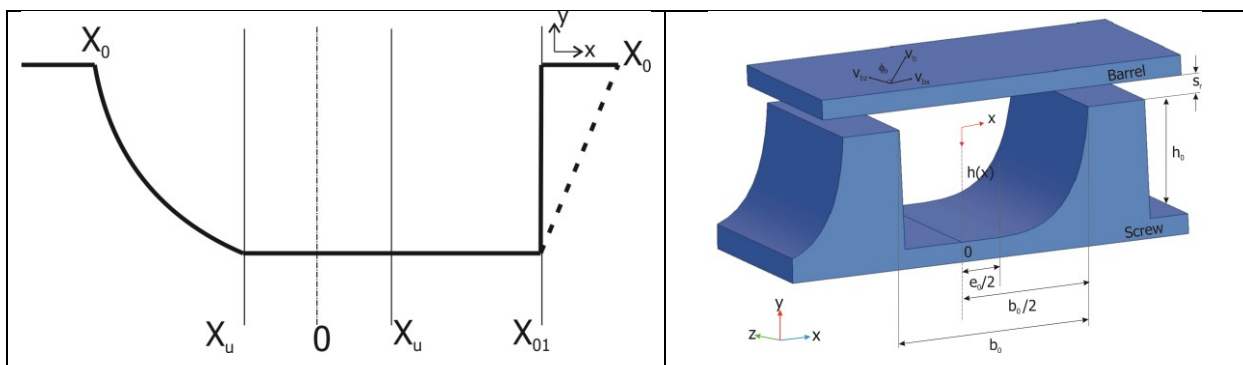


Figure 7.4: Cross sectional view of shear edge screw channel geometry

As shown in Figure 7.4 the shear edge profile can be separated into different segments according to the channel depth variations with respect to the X-axis. The channel depth between 0 and X_u is constant. The channel depth between X_u and X_0 is described using the Erdmenger channel geometry. Between 0 and X_{01} on the other half, the channel depth is constant. The channel depth changes linear between X_{01} and X_0 . The channel depth could also be constant between X_{01} and X_0 in some cases. Here x_0 is the channel width b_0 .

The flow rate of the shear edge profile can be given as:

$$\dot{V}_{drag,pressure} = \iint v_z(x,y) \cdot dx \cdot dy \quad (7.19)$$

$$\begin{aligned}
&= 2 \cdot \int_0^{h_0} \int_0^{xu} v_{bz} \cdot \left(1 - \frac{y}{h_0}\right) - \frac{1}{\eta} \cdot \frac{\partial p}{\partial z} \cdot \left(\frac{h_0}{2} \cdot y - \frac{y^2}{2}\right) \cdot dy \cdot dx \\
&\quad + \int_{xu}^{x_0} \int_0^{h(x)} v_{bz} \cdot \left(1 - \frac{y}{h(x)}\right) - \frac{1}{\eta} \cdot \frac{\partial p}{\partial z} \cdot \left(\frac{h(x)}{2} \cdot y - \frac{y^2}{2}\right) \cdot dy \cdot dx \\
&\quad + \int_{xu}^{x_{01}} \int_0^{h_0} v_{bz} \cdot \left(1 - \frac{y}{h_0}\right) - \frac{1}{\eta} \cdot \frac{\partial p}{\partial z} \cdot \left(\frac{h_0}{2} \cdot y - \frac{y^2}{2}\right) \cdot dy \cdot dx \\
&\quad + \int_{x_{01}}^{x_0} \int_0^{h_1(x)} v_{bz} \cdot \left(1 - \frac{y}{h_1(x)}\right) - \frac{1}{\eta} \cdot \frac{\partial p}{\partial z} \cdot \left(\frac{h_1(x)}{2} \cdot y - \frac{y^2}{2}\right) \cdot dy \cdot dx
\end{aligned}$$

The channel depth $h_1(x)$ can be given by:

$$h_1(x) = \frac{h_0}{x_0 - x_{01}} \cdot (x_0 - x) \quad (7.20)$$

Substituting the value of $h_1(x)$ in equation 6.17, we get

$$\begin{aligned}
\dot{V}_{drag,pressure} &= 2 \cdot \int_0^{xu} v_{bz} \cdot \frac{h_0}{2} - \frac{1}{\eta} \cdot \frac{\partial p}{\partial z} \cdot \frac{h_0^3}{12} \cdot dx + \int_{xu}^{x_0} v_{bz} \cdot \frac{h(x)}{2} - \frac{1}{\eta} \cdot \frac{\partial p}{\partial z} \cdot \frac{h(x)^3}{12} \cdot dx \\
&\quad + \int_{xu}^{x_{01}} v_{bz} \cdot \frac{h_0}{2} - \frac{1}{\eta} \cdot \frac{\partial p}{\partial z} \cdot \frac{h_0^3}{12} \cdot dx + \int_{x_{01}}^{x_0} v_{bz} \cdot \frac{h_1(x)}{2} - \frac{1}{\eta} \cdot \frac{\partial p}{\partial z} \cdot \frac{h_1(x)^3}{12} \cdot dx
\end{aligned} \quad (7.21)$$

$$\begin{aligned}
\dot{V}_{drag,pressure} &= 2 \cdot \frac{v_{bz}}{2} \cdot h_0 \cdot xu - \frac{1}{12 \cdot \eta} \cdot \frac{\partial p}{\partial z} \cdot h_0^3 \cdot xu + \frac{v_{bz}}{2} \cdot \int_{xu}^{x_0} h(x) \cdot dx - \frac{1}{12 \cdot \eta} \cdot \frac{\partial p}{\partial z} \\
&\quad \cdot \int_{xu}^{x_0} h(x)^3 \cdot dx + \frac{v_{bz}}{2} \cdot h_0 \cdot (x_{01} - xu) - \frac{1}{12 \cdot \eta} \cdot \frac{\partial p}{\partial z} \cdot h_0^3 \cdot (x_{01} - xu) \\
&\quad + \frac{v_{bz}}{2} \cdot h_0 \cdot \frac{1}{2} \cdot (x_0 - x_{01}) - \frac{1}{12 \cdot \eta} \cdot \frac{\partial p}{\partial z} \cdot \frac{h_0^3}{4} \cdot (x_0 - x_{01})
\end{aligned} \quad (7.22)$$

Simplifying the above equation gives the total volumetric flow rate including only flow through drag and pressure.

$$\begin{aligned}
\dot{V}_{drag,pressure} &= (2 \cdot n - 1) \left\{ \frac{v_{bz}}{2} \cdot \left[h_0 \left(xu + \frac{x_{01}}{2} + \frac{x_0}{2} \right) + \int_{xu}^{x_0} h(x) \cdot dx \right] - \frac{1}{12 \cdot \eta} \cdot \frac{\partial p}{\partial z} \right. \\
&\quad \left. \cdot \left[\frac{h_0^3}{4} \cdot (3 \cdot x_{01} \cdot x_0) + \int_{xu}^{x_0} h(x)^3 \cdot dx \right] \right\}
\end{aligned} \quad (7.23)$$

Similar to the case of standard Erdmenger profile, the leakage flow and the flow through the nip zone can be calculated in the similar way as mentioned in 7.2.2.

7.2.4 Forward Conveying Element - Double Shear Edge or Box Profile

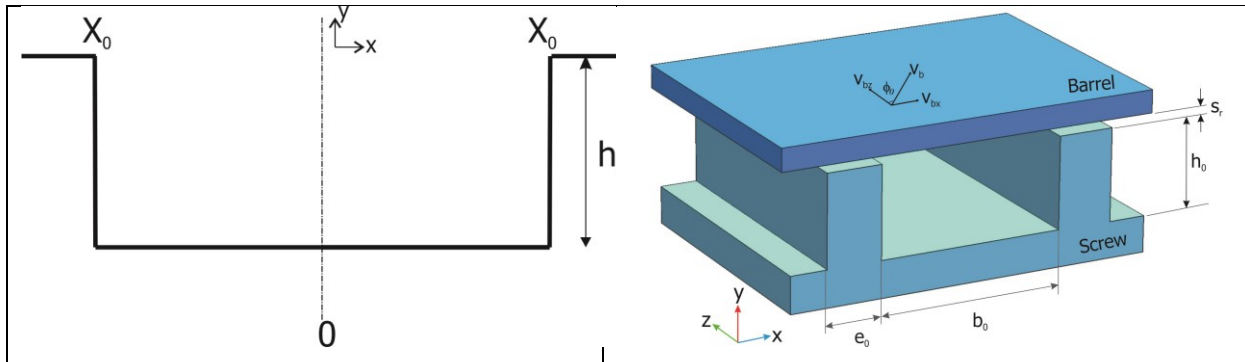


Figure 7.5: Cross sectional view of box (or) double shear edge screw channel geometry

The double shear edge profile or box profile differs from the standard Erdmenger profile in such a way that both sides of the channel have undercuts. The double shear edge channel profile (Figure 7.5) is symmetric as the Erdmenger profile.

The modeling of the double shear edge profile can be done similar to the flow modeling in the single screw extruders, where the flow channel is considered as a box profile with a constant channel depth and channel width.

The volumetric flow rate in a single screw extruder is given by the following equation: (Hensen, Knappe, & Potente, 1989)

$$\dot{V} = \frac{b \cdot h \cdot v_{bz}}{2} - \frac{b \cdot h^3}{12 \cdot \eta} \cdot \frac{\partial p}{\partial z} \quad (7.24)$$

But in contrast to single screws, many channels are filled and the number of flow channels must be considered in calculation the flow rate and the volumetric flow rate can be given as:

$$\dot{V} = (2 \cdot n - 1) \cdot \left(\frac{2 \cdot x_0 \cdot h_0 \cdot v_{bz}}{2} - \frac{2 \cdot x_0 \cdot h_0^3}{12 \cdot \eta} \cdot \frac{\partial p}{\partial z} \right) \quad (7.25)$$

In the above relation the flow through the nip region is not included. In order to derive the flow through the nip region, the free cross-sectional area (Figure 7.6) in the nip area has to be calculated.

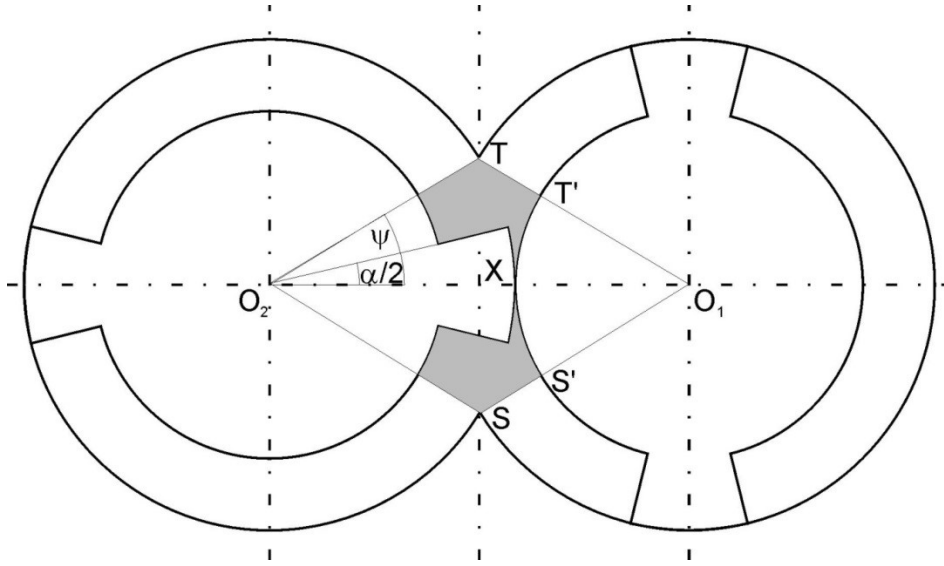


Figure 7.6: Free cross-sectional area in the nip zone of box profile (Himmler, 2010)

The free cross sectional area in the nip area can be determined by subtracting the sector area $A_{O_1S'T'}$, and the cross sectional area of the flight from the cross sectional area of the rhombus $A_{O_1SO_2T}$ (Figure 7.6)

$$A_{O_1SO_2T} = 4 \cdot A_{O_1XT} = \frac{(D_a - h_0)^2}{2} \cdot \tan(\psi) \quad (7.26)$$

The area of the sector is given by:

$$A_{O_1S'T'} = 2 \cdot \frac{\psi}{2} \cdot \left(\frac{D_a}{2} - h_0\right)^2 \quad (7.27)$$

And the area of the flight can be derived as:

$$A_{flight} = h_0 \cdot (D_a - h_0) \cdot \frac{\alpha}{2} \quad (7.28)$$

The free area in the nip region can be given as:

$$\begin{aligned} A_{nip} &= A_{O_1SO_2T} - 2 \cdot A_{O_1S'T'} - A_{flight} \\ &= \frac{(D_a - h_0)^2}{2} \cdot \tan(\psi) - 2 \cdot \psi \cdot \left(\frac{D_a}{2} - h_0\right)^2 - h_0 \cdot (D_a - h_0) \cdot \frac{\alpha}{2} \end{aligned} \quad (7.29)$$

Since both screws rotate, the free cross sectional area in the nip region changes according to the rotation of the screws. The average free cross section can be determined by letting a set of discs rotate through a cycle with an angle equal to $\frac{\pi}{2n}$.

The volumetric flow in the nip area is determined by:

$$\dot{V}_{nip} = N \cdot t \cdot A_{nip} \quad (7.30)$$

The leakage flow through the annular clearance between the screws and barrel can be determined in a similar way as mentioned in 7.2.2.

The total flow rate is given by:

$$\dot{V}_{total} = \dot{V}_{drag} - \dot{V}_{pressure} + \dot{V}_{nip} - \dot{V}_{leakage} \quad (7.31)$$

7.2.5 Dimensionless Screw Characteristic Curves

In order to determine the extruder as well as the screw element's working range the dimensionless characteristics curves are used. As mentioned by Kohlgrueber (2008) dimensional analysis reduces the following seven influencing variables:

- Volume throughput
- Screw rotation speed
- Pressure difference
- Power
- Screw outer diameter
- Screw length
- Viscosity

to three important dimensionless groups:

Pressure number:

$$\Delta p^* = \frac{\Delta p \cdot D_a}{\eta \cdot N \cdot L} \quad (7.32)$$

Power number:

$$P^* = \frac{P}{\eta \cdot N^2 \cdot D_a^2 \cdot L} \quad (7.33)$$

Throughput number:

$$\dot{V}^* = \frac{\dot{V}}{N \cdot D_a^3} \quad (7.34)$$

In the above equations the viscosity η can be determined for shear rate $\dot{\gamma} = 2\pi N$ using the Cross (7.3) or Power Law viscosity model (7.4). The throughput number defines the output of the screw per revolution in dimensionless form.

The dimensionless pressure characteristic curve of a screw element is plotted by linking the pressure and throughput number. The curves are represented dimensionless to remove the influence of the velocity. A typical pressure characteristic curve of a conveying screw element for a Newtonian fluid is shown in Figure 7.7.

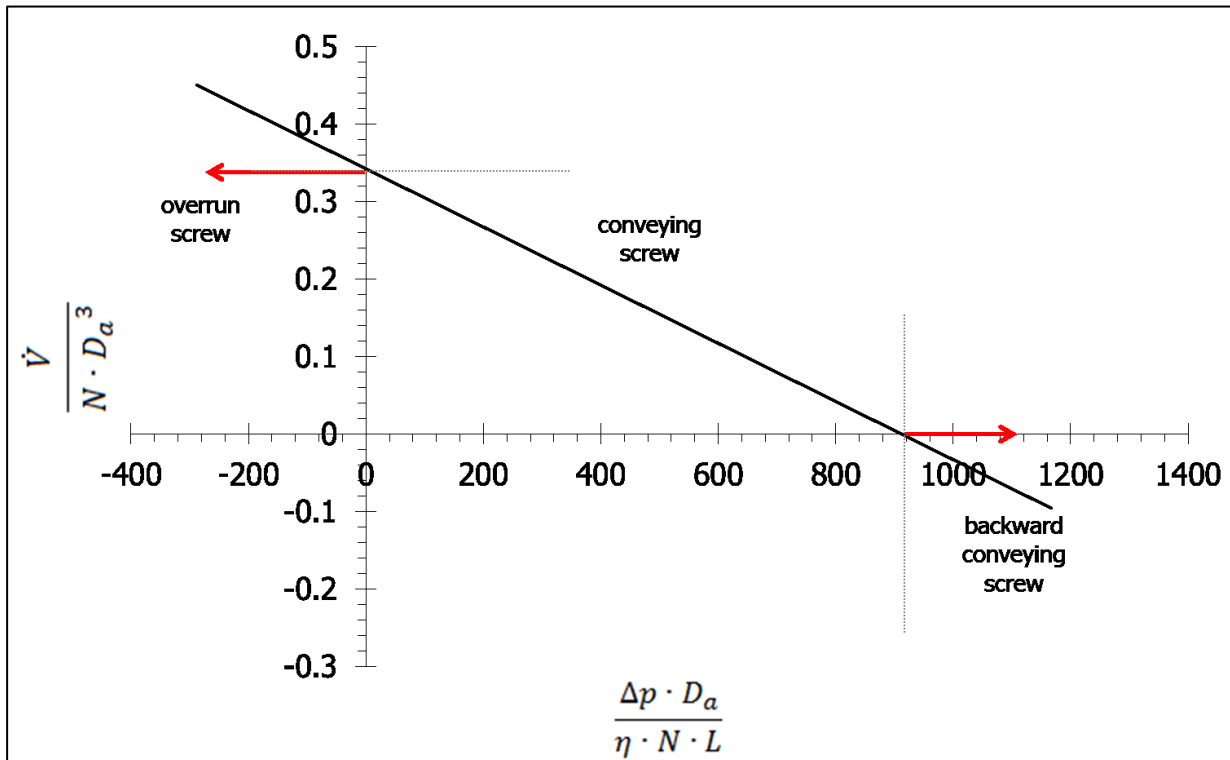


Figure 7.7: Screw characteristic curve for forward conveying element

In Figure 7.7 the screw characteristic curve the intercept on the y-axis (throughput number) indicates the maximum throughput the screw element can achieve if the screw is completely filled and the back-pressure is zero. The intercept on the x-axis (pressure number) indicates the maximum pressure built-up capability of the screw element for a zero throughput. If the throughput per revolution is higher than the maximum throughput, then the screw element is overrun. In case the pressure difference is negative, the screw element is a pressure consuming screw element. The negative throughput shows that the screw element is negative conveying.

7.2.6 Kneading Element

The flow rate in the kneading block elements is determined in the similar way as the conveying element considering the groove model of the kneading element (Figure 7.8). The

only difference is that the shear leakage flow of the melt through the triangular gaps formed by the kneading discs and their staggering angle is considered in calculating the total flow through the kneading elements.

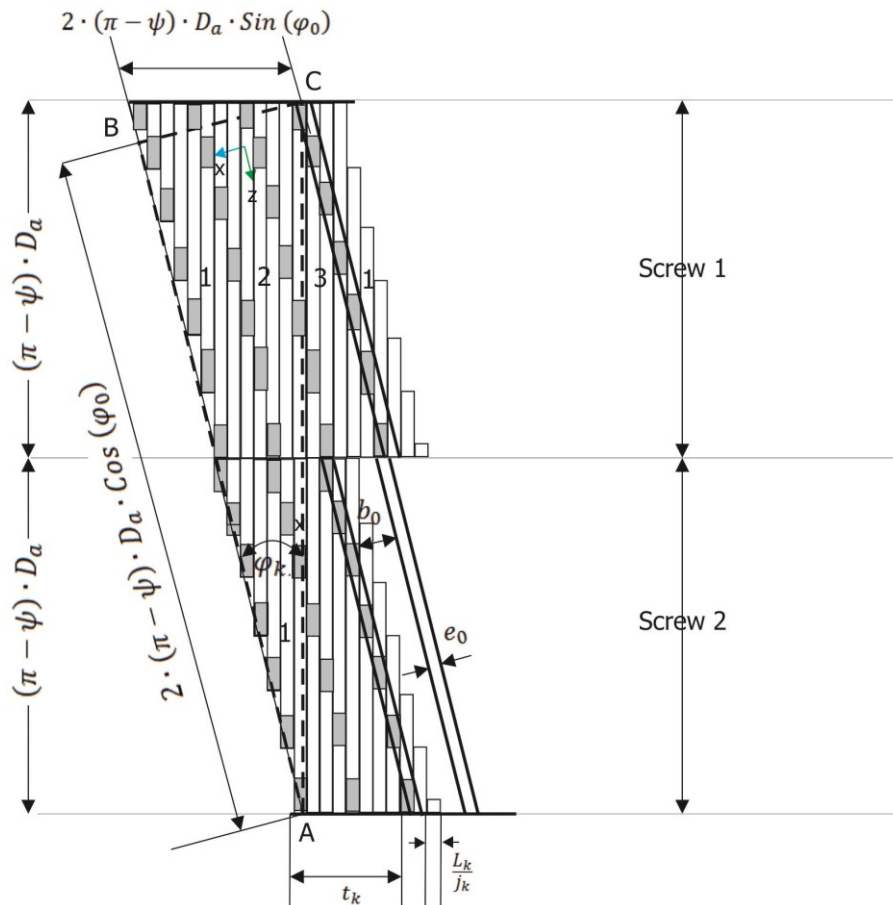


Figure 7.8: Groove model of kneading block element

The number of the triangular gaps J_{Δ} in the kneading block element is given as:

$$J_{\Delta} = b_k \cdot \frac{\sin(\varphi_k)}{\frac{L_k}{J_k}} - 1 \quad (7.35)$$

The length of the flight b_k is given according to Ansaahl as:

$$b_k = (2 \cdot \pi - 2 \cdot \psi) \cdot D_a \cdot \cos(\varphi_k) \quad (7.36)$$

In order to calculate the leakage flow through the radial gap and the triangular gaps, the radial gap has to be corrected including the triangular gaps. The corrected radial gap is given by (Potente, Ansaahl, & Klarholz, 1994) as:

$$s_{r,corrected} = s_r + \frac{J_{\Delta} \cdot A_{\Delta}}{b_k} \quad (7.37)$$

where A_{Δ} is the area of the triangular gap between the kneading discs which is determined using equation 4.3.

The leakage flow through the flights of the kneading element is given as

$$\dot{V}_{k\ leakage} = \frac{1}{2} \cdot v_{bz} \cdot s_r \cdot \pi \cdot D_a \cdot \sin(\varphi_k) \quad (7.38)$$

The total flow rate through a forward conveying kneading block element can be calculated using the relation as follows:

$$\dot{V}_{total} = \dot{V}_{drag} - \dot{V}_{pressure} - \dot{V}_{k\ leakage} \quad (7.39)$$

In case of negative conveying kneading elements, flow takes place mainly due to the pressure flow and the drag flow occurs opposite to the flow direction. The total flow rate of negative conveying kneading element is given as:

$$\dot{V}_{total} = -\dot{V}_{drag} - \dot{V}_{pressure} - \dot{V}_{k\ leakage} \quad (7.40)$$

In case of neutral conveying kneading elements with 90° staggering angle, the flow of the melt occurs only due to the pressure and there is no drag volumetric flow. The total flow rate in a kneading element with 90° staggering angle is:

$$\dot{V}_{total} = -\dot{V}_{pressure} \quad (7.41)$$

The leakage flow through the radial gap can be neglected since it has very little influence on the pressure loss along the down channel direction of the neutral conveying kneading element (Ansahl, 1993).

7.2.7 Conveying Mixing Element

The calculation of the throughput or the pressure generation for a given flow rate is determined using the same equations as for the conveying elements, considering the flow due to drag, pressure, flow through the nip and the leakage flow over the flights. Additionally in this case the leakage flow through the slots $\dot{V}_{slot,leakage}$ of the conveying mixing elements (Figure 7.9) have to be considered.

$$\dot{V}_{total} = \dot{V}_{drag} - \dot{V}_{pressure} + \dot{V}_{nip} - \dot{V}_{leakage} - \dot{V}_{slot,leakage} \quad (7.42)$$

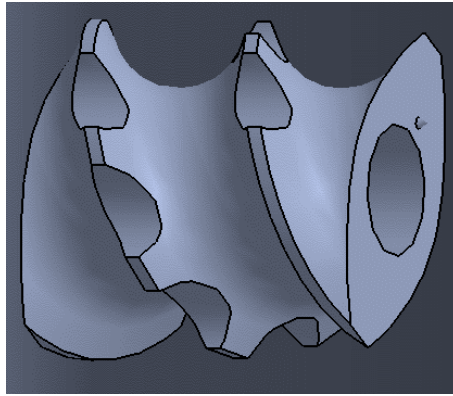


Figure 7.9: conveying mixing elements with mixing slots

The total leakage flow through the slots due to drag is given by the following relationship (Potente, Kretschmer, & Flecke, 2001):

$$\dot{V}_{slot,leakage} = j_s \cdot \left(\frac{1}{2} \cdot v_b \cdot \bar{b}_s \cdot h_s \cdot \cos(\varphi_s) \right) \quad (7.43)$$

7.2.8 Blister Ring

The melt flow in the blister ring element occurs only in the cross channel direction (x-axis) as shown in the Figure 7.10 due to pressure through the radial gap and the gap between the two screws.

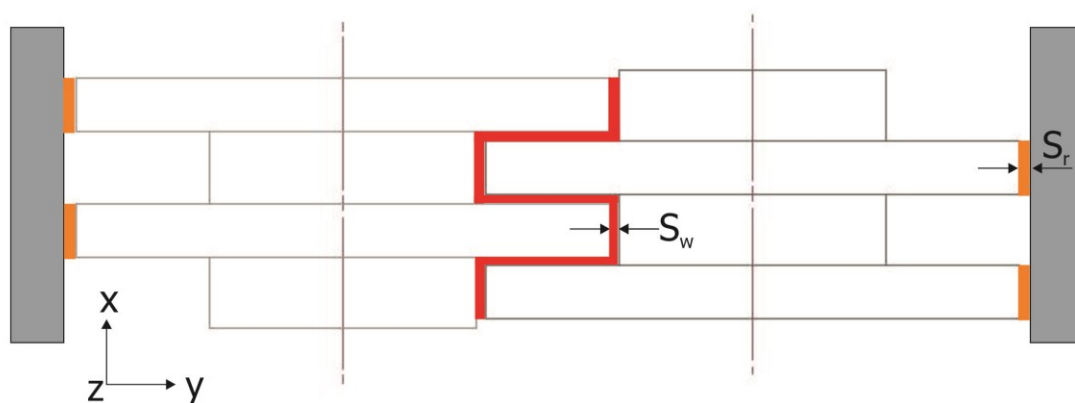


Figure 7.10: Melt flow in the blister ring element

The equation of motion along the cross channel direction is basis for deriving the velocity profile of the melt along the x-axis, which is given by:

$$\frac{\partial p}{\partial x} = \eta \cdot \frac{\partial^2 v_x}{\partial y^2} \quad (7.44)$$

Applying the boundary conditions $y = 0, v_x = 0$; $y = s_w, v_x = 0$ and solving the equation (7.44) the velocity profile is described as:

$$v_x(y) = \frac{1}{\eta} \cdot \left(\frac{y^2}{2} - \frac{y \cdot s_w}{2} \right) \cdot \frac{\partial p}{\partial x} \quad (7.45)$$

Integrating the equation over the area gives the volumetric flow rate through the calendar gap between the two rings.

$$\dot{V}_{s_w, pressure} = - \frac{w_B \cdot s_w^3}{12 \cdot \eta} \cdot \frac{\partial p}{\partial x} \quad (7.46)$$

The flow rate through the radial gap of blister ring due to pressure is:

$$\dot{V}_{s_r, pressure} = - \frac{(D_a + s_w) \cdot (\pi - \psi) \cdot s_w^3}{6 \cdot \eta} \cdot \frac{\partial p}{\partial x} \quad (7.47)$$

The total flow rate is given by the sum of these two flows.

7.2.9 Backward Conveying Element

In the backward conveying element the conveying of the melt is opposite to the flow direction due to negative helix angle, which leads to a negative drag flow and hence a negative pressure gradient is created. The total flow rate in the backward or negative conveying element is given as:

$$\dot{V}_{total} = -\dot{V}_{drag} - \dot{V}_{pressure} - \dot{V}_{nip} - \dot{V}_{leakage} \quad (7.48)$$

7.3 Back Pressure Length

The back pressure length is one of the important design parameters for modeling the pressure build-up zones, for good melting, mixing and homogenizing the melt. If the pressure build-up zone is not long enough, flooding of the polymer melt may occur in the upstream zones (often the venting zone), leading to melt leakage from the vent (Kohlgrueber, 2008).

A totally filled zone is created in the back pressure zone from the pressure consuming elements (screw elements or die).

The back pressure length (L_{BP}) can be determined from the volumetric flow rate equation (7.12) considering only the flow rate due to back pressure. The back pressure length is calculated as follows (Michaeli, Grefenstein, & Berghaus, 1995):

$$L_{BP} = \Delta p \cdot \frac{\partial p}{\partial z} \quad (7.49)$$

In this work an iterative way is used to determine the back pressure length.

The back pressure length is greatly influenced by the material viscosity, the screw pitch, screw rotation speed, throughput and the pressure (Wang, 2000).

7.4 Degree of Fill (DOF)

A totally filled area or zones with a degree of fill "1" is important for melting, mixing, melt homogenizing and pressure generation. The volumetric filling degree (DOF) in the screw elements is given by the ratio of the volumetric flow rate and maximum melt conveying capacity due to drag flow (Michaeli, Grefenstein, & Berghaus, 1995).

$$DOF = \frac{\dot{V}_{total}}{\dot{V}_{drag}} \quad (7.50)$$

If the volume flow is smaller than the melt conveying capacity of the screw element, and no pressure build-up is necessary to overcome the downstream resistance, then the conveying element is partially filled (Schuler, 1996).

In this work the back pressure length and the degree of filling in each screw element are determined in an iterative way. The procedure to determine the back pressure length is represented in Figure 7.11.

The pressure in front of the die or pressure consuming screw elements is initially determined. The back pressure length and the filling degree of the screw elements upstream the pressure consumer are determined iteratively by varying the filling length of the screw elements so that the difference between the pressures developed by the positive conveying screw elements and the pressure consumers is zero.

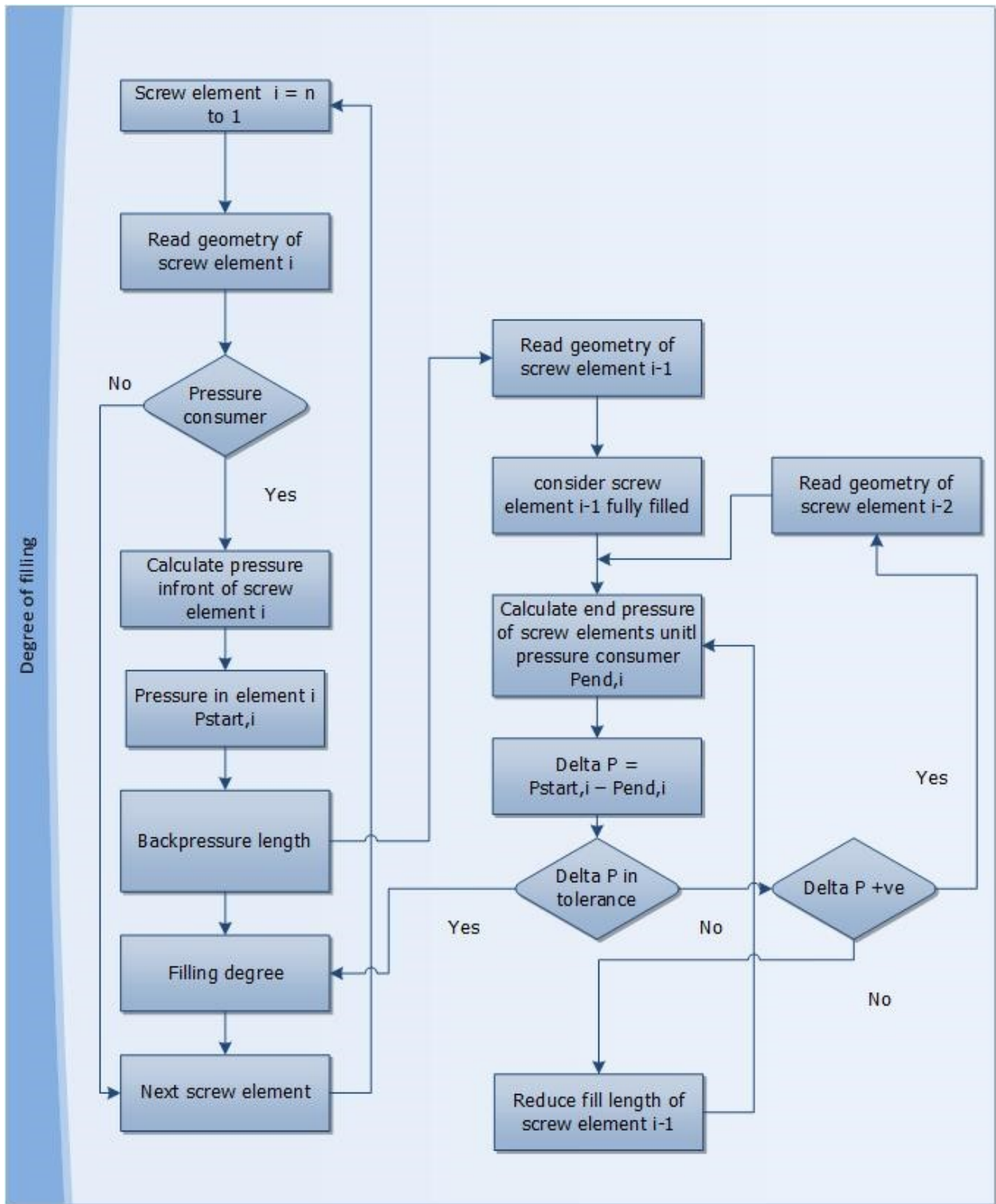


Figure 7.11: Back pressure length calculation algorithm

8 Experimental

8.1 Introduction

Reference practical values, measured on the extruder under different processing settings, are required to verify the accuracy of the mathematical models. Practical trials were made to investigate the process behavior of MAS 55 type extruder provided by Maschinen und Anlagen Schulz GmbH Austria under different process settings. The practical measurements, using a predefined screw configuration and different process settings, were carried out and recorded. This data is compared with later with the theoretically determined values for the same process setting as the practical trials. Similarly practical measured data from Leistritz ZSE 27 MAXX compounder were used to check the accuracy of the parallel twin screw models and the results of the CFD simulation. The details of the measurement of the material data, process behavior of the conical- and parallel co-rotating twin screw extruders are described.

8.2 Conical Co-Rotating Extruder

The NCT 55 extruder used for the measurements is shown in Figure 8.1.

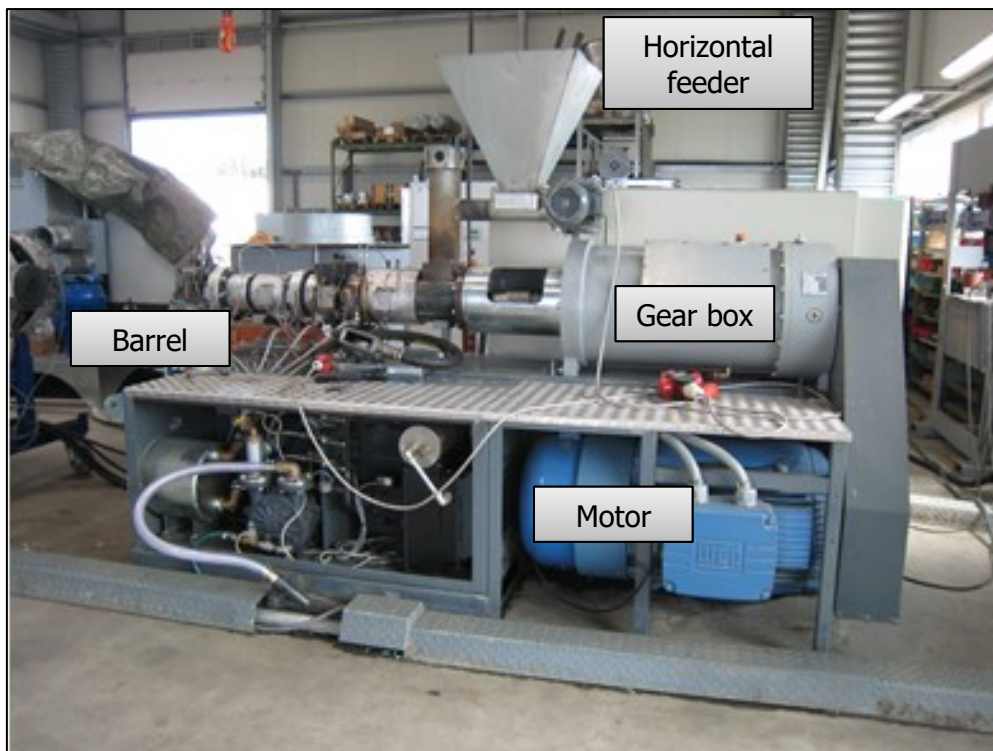


Figure 8.1: MAS NCT55 extruder

The feeding of the material was carried out using a horizontal feeder, with which the dosing of the extruder was controlled. The barrel of the conical extruder has a single vacuum vent and the barrel is composed of two segments. For measuring the pressures along the

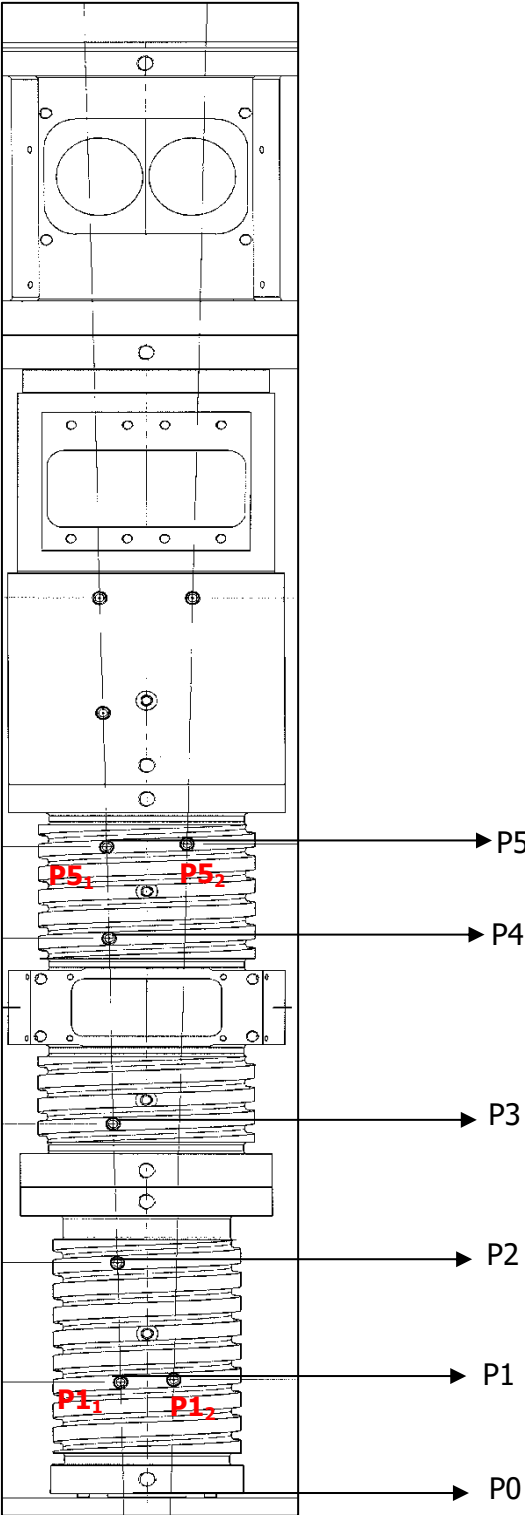


Figure 8.2: Pressure measurement positions along the screw length of NCT55

screw length, provisions were made to mount the pressure transducers at different positions over the entire length of the barrel. The exact positions of the pressure measurements are shown in Figure 8.2. As can be seen in the Figure 8.2, at position P5 and P1 pressures were measured on the left and right screws, in order to verify the filling degrees of the right and the left screws. The data acquisition was carried out using the "Spider 8" data acquisition system from HBM and their "Catman Easy" Software for analyzing the data.

In order to vary the pressure resistance in front of the screw, a special die with adjustable slit height was used. The actual flow rate was measured by weighing the extruded mass per minute. The melt temperature was measured before the melt entering into the die.

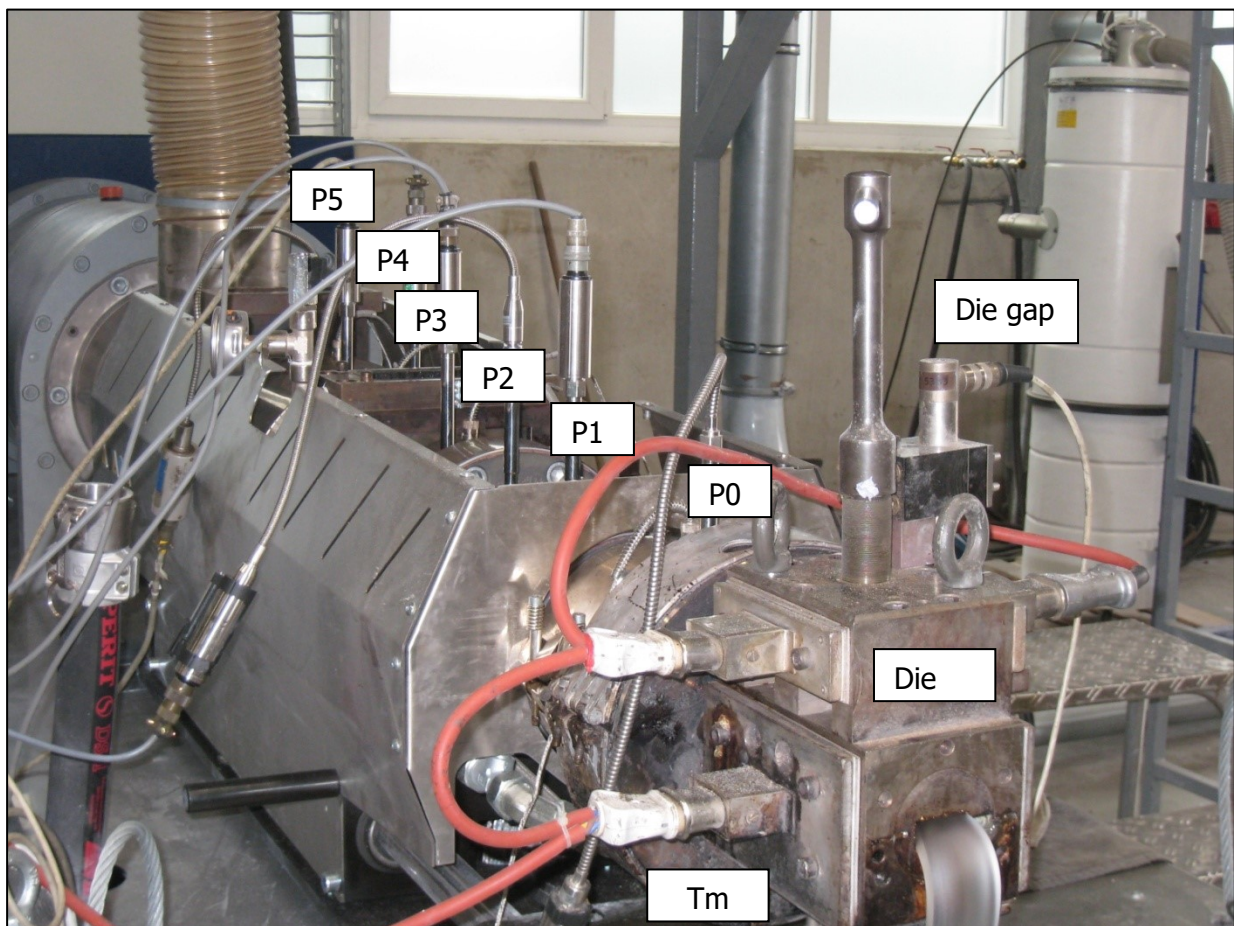


Figure 8.3: Experimental setup of NCT55

In trail I the throughput and the pressure at the end of the screw have been measured for slit heights 2, 2.75 and 3.5 mm and at varying screw speeds 50 % to 90 % of the maximum screw rotation speed of the NCT. The material was plasticized at 250 °C. The temperature settings of the different barrel zones used in both the trails are given in Table 8.2.

The active length of the screw is 1175 mm. The feeding zone and the metering zone screw element have double shear edge screw profile. The geometry of the screw elements used in trail 1 are detailed in Table 8.3. Mainly conveying elements with different pitch are used to meter the material, melt and homogenize.

Table 8.1: Pressure sensors

P0 (Adapter)	Gefran Impact 1000 bar
P1 (End of metering zone)	Gefran 1000 bar
P2 (Middle of metering zone)	Gefran Impact 1000 bar
P3 (Starting of metering zone)	Gefran 700 bar
P4 (Before throttle)	Gefran 500 bar
P5 (In melting zone)	Gefran 350 bar

Table 8.2: Barrel temperature settings

Zone	Temperature (°C)		
	Trial I	Trail II Test 1	Trail II Test 2
Zone E1	235	200	170
Zone E2	240	200	180
Zone E3	240	200	180
Zone E4	240	200	170
Zone E5 Adapter	250	200	210
Die (External heating)	250	210	210

The screw configuration used for the initial measurements (Trial 1) is diagrammatically represented below:

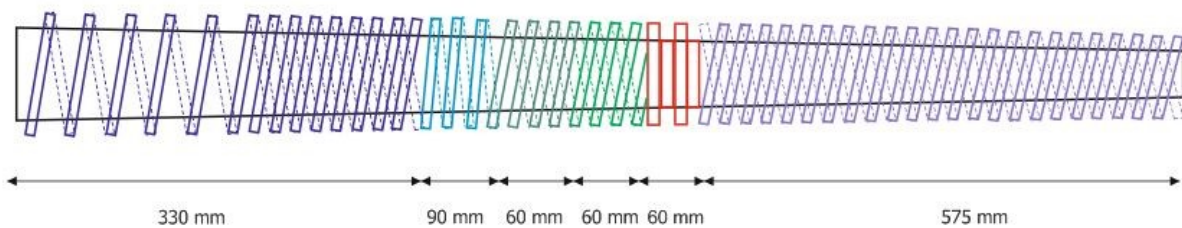


Figure 8.4: Screw configuration with screw element length for Trail 1 (Schuschnigg, 2009)

A pressure consuming element “blister ring” is used before the vacuum venting zone of the extruder. This element increases the back pressure length in the upstream elements (conveying and conveying mixing elements). These conveying elements with narrow pitch induce the melting of the bulk material and the conveying mixing element increases the residence time of the melt and homogenize the melt. The feeding zone with conveying

element with single flight gives the advantage of large free volume. The transition of the flight from single to double reduces the free channel volume. This volume reduction helps in compact the bulk material and initiates the melting of the material. The element used in the metering zone has a constant screw pitch, which helps to generate the pressure.

Table 8.3: Screw elements – Trail 1

Element	Name	Length (mm)	Pitch (mm)
Element 1	Feeding (1& 2 flight)	170 + 160	60
Element 2	Conveying – 1 flight	90	30
Element 3	Conveying – 2 flight	60	60
Element 4	Conveying mixing – 2 flight	60	60
Element 5	Blister ring	60	-
Element 6	Metering – 2 flight	575	60

The pressure and melt temperature were measured at different outputs, screw back pressure and screw rotation speeds. The different process settings of trail 1 are as in Table 8.4.

Table 8.4: Extruder settings – Trail 1

Setting No.	Slit Height (mm)	Screw speed (1/min)	Dosing screw speed (1/min)
1	2	150	38
2	2	180	34
3	2	210	42
4	2	240	50
5	2	270	50
6	2.75	150	30
7	2.75	180	40
8	2.75	210	45
9	2.75	270	75
10	3.5	150	45
11	3.5	180	56
12	3.5	210	60
13	3.5	240	75
14	3.5	270	86

The outputs were chosen in such a way that the metering zone is completely filled and at the same time melt does not flow out of the vacuum vent due to high back pressures. The temperature of the melt was measured before the die entrance.

The screw used for the trial 2 was very similar to the screw configuration used in the trial 1, except for the feed element. The double flighted portion of the feed element flights was reduced by 100 mm, creating a flightless zone between the screw element 1 and 2. The flow in this flightless zone takes place only due to pressure of the bulk material flowing from the feeding element. The screw elements are detailed in Table 8.5.

Table 8.5: Screw elements – Trail 2

Element	Name	Length (mm)	Pitch (mm)
Element 1	Feeding (1& 2 flight)	170 + 60	60
Element 2	Conveying – 1 flight	90	30
Element 3	Conveying – 2 flight	60	60
Element 4	Conveying mixing – 2 flight	60	60
Element 5	Blister ring	60	-
Element 6	Metering– 2 flight	575	60

In trail 2 the process parameters – filling length, die gap and throughput rate were varied, keeping the screw rotation speed constant. The parameters were chosen in such way that the metering zone was fully and partially filled. Additional to the melt temperature measurement in the adapter, the temperature of the melt inside the slit die was measured. The different processing parameters used in trail 2 are listed as in Table 8.6. In trail 2, the initial test (Test 1) was carried out higher barrel temperatures. Due to higher melt temperature the melt viscosity was low and it was not possible to process the material with fully filled metering zone. To avoid material flowing out of the vent, the barrel temperature was reduced (Table 8.2), which led to the reduction of the melt temperature and increase in the melt viscosity respectively.

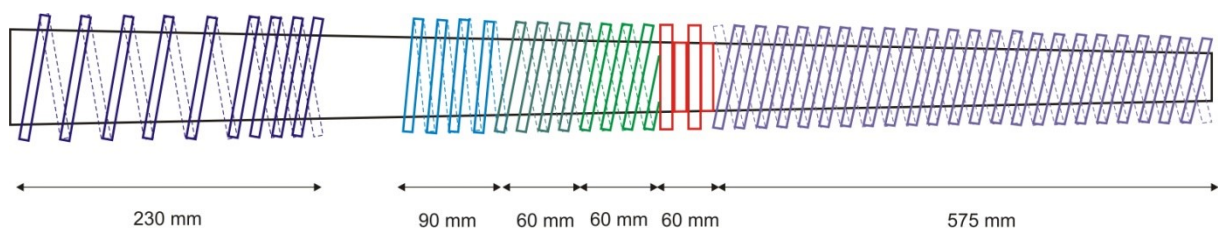


Figure 8.5: Screw configuration with screw element length for Trail 2 (Selvasankar, 2010)

The parameters recorded at the end of the measurement from the machine control are single point values. The die gap, pressure values and the melt temperature were constantly measured and captured using the data acquisition program "Catman Easy" for each setting and the measured data were imported in Microsoft Excel and the measured values are diagrammatically represented as shown in Figure 8.6. An average of the measured values was taken from the range where the measured parameters were constant. These average values were considered as the reference value while verifying the accuracy of the theoretical values.

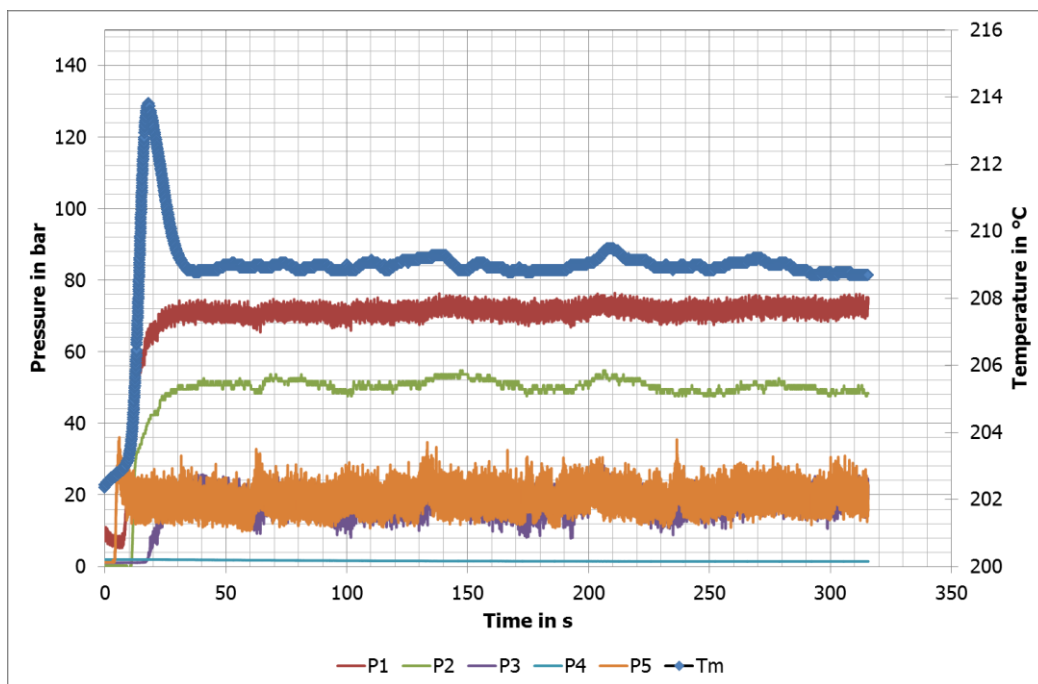


Figure 8.6: Measured pressures and temperature over time

Additional experiments were made to verify the pressure uniformity on the left and right screw at positions P1 and P5, by 200 rpm screw speed, slit height of 4 mm and output.

Table 8.6: Extruder settings – Trail 2

Test	Setting No.	Slit Height (mm)	Screw speed (1/min)	Remarks
1	1	4	200	
	2	4	200	
	3	4	200	Material flow out of vent
	4	3	200	Material flow out of vent
2	5	3	200	
	6	3	200	
	7	3	200	

8	2	200	Material flow out of vent
9	4	200	
10	4	200	
11	4	200	
12	4	200	Material flow out of vent
13	4	150	
14	4	200	P1 left and right screw
15	4	200	P5 left and right screw
16	4	150	

8.3 Parallel Co-Rotating Extruder



Figure 8.7: Leistritz ZSE 27 MAXX Compounder (Kunststofftechnik, 2014)

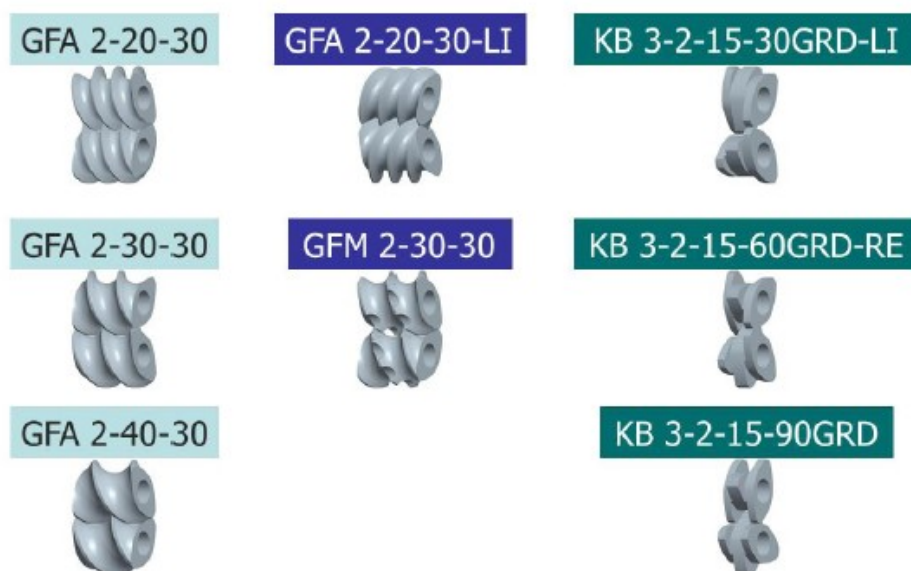
Experiments were performed on the injection molding compounder at the Chair of Injection Moulding of Polymers at Montanuniversitaet Leoben, which combines the ZSE 27 MAXX 44-52D compounder from Leistritz Group (Nuernberg, Germany) and an e-Motion 740/180T injection molding machine from Engel Austria GmbH.

Only the measured and simulated data (Winkler-Ebner, 2014) from the Leistritz compounder has been used in this work. For the experiments the screw length of 44D and with 11 barrel zones has been used. The technical data of the ZSE 27 MAXX compounder is shown in Table 8.7. A gear pump type EXTRU 25.6-3 manufactured by Witte Pumps & Technology GmbH (Uetersen, Germany) has been used in front of the screw tip in order to regulate the back pressure and thus the residence time.

Table 8.7: Technical data of Leistritz compounder (*Kunststofftechnik, 2014*)

Throughput (kg/h)	4 - 40
Screw diameter (mm)	27
Extruder length (L/D)	44 - 52
Max. screw speed (1/min)	600
Max. torque (Nm)	270
Max. temperature (°C)	400

In Winkler's work two different screw geometries were tested. In this work the standard screw geometry and its measured data are used. The used screw elements in this work are given in the Figure 8.8

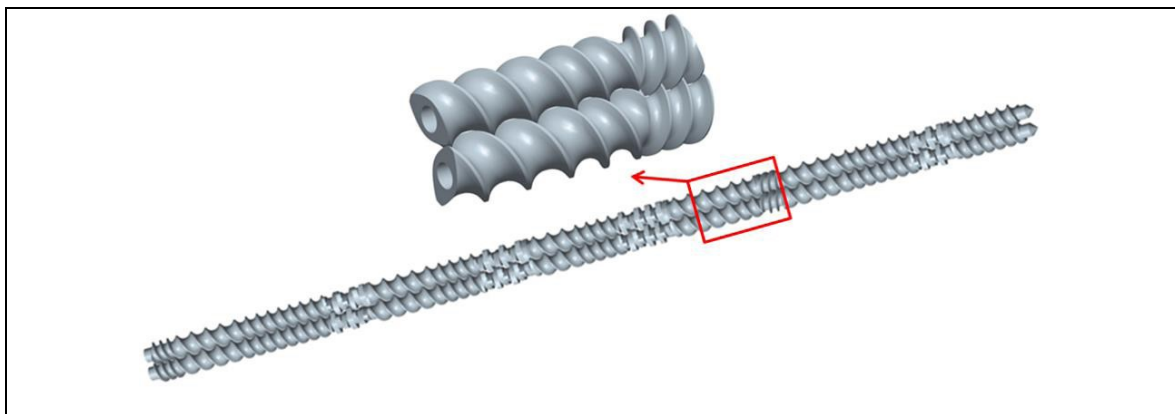
Figure 8.8: Leistritz screw elements used for the trails (*Winkler-Ebner, 2014*)

The main screw elements used in the screw configuration are conveying screw elements (GFA) for metering the bulk and melted polymer material. Also a negative conveying element (GFA-LI) is used to create some back pressure. Special conveying mixing elements (GFM) have been implemented to improve the mixing and homogenization of the melt. Different kneading screw elements (KB) are incorporated for melting and for improving the dispersive mixing of the fillers into the polymer matrix. The constant geometry data of the screw and barrel are shown below:

Table 8.8: Screw and barrel geometry data

Centerline distance (mm)	23
Screw diameter (mm)	28.27
Barrel diameter (mm)	28.40
Clearance (mm)	0.065
Screw length (mm)	1210

The standard screw configuration used for compounding the PP material with the additives before optimizing the screw geometry is shown in Figure 8.9. The screw is configured with four dispersive mixing zones, consisting of kneading elements. Also a negative conveying zone element is included at a cumulative length of 850 mm from the feed section. The detailed description of the used screw elements in the standard screw configuration is diagrammatically represented in Figure 8.11.

*Figure 8.9: Screw configuration – standard screw (Winkler-Ebner, 2014)*

The processing condition for processing the PP Bormed™ DM55pharm unfilled material is given in Table 8.9. The extruder barrel temperature profile was kept the same for the complete trail. The measured material data of PP Bormed™ DM55pharm is given in appendix.

Table 8.9: Processing conditions of Leistritz compounder

Material	PP Bormed™ DM55pharm
Extruder temperature profile (°C)	170-185-200-200-200-200-200-200-200-200-200
Complete Line	Extruder- Gear pump – Filter – slide valve - under water granulation -

Measured pressure values are the only reference value to check validity of the calculation results. In order to record the pressure profile along the screw length, pressure transducers have been mounted at different axial positions (495, 715, 825, 1045 and 1155 mm). The pressure values are measured after the side feeder, which is located at the x-position of 385 mm in the barrel, because the material is in melt state after this position. Pressure transducer in the range 200 bar is mounted at the last barrel zone and the rest of the transducers have measurement range of 100 bar (Winkler-Ebner, 2014). The mounted pressure sensors and its positions are diagrammatically represented in Figure 8.10. All the pressure values were recorded using the data acquisition system as used in the conical extruder experiments.

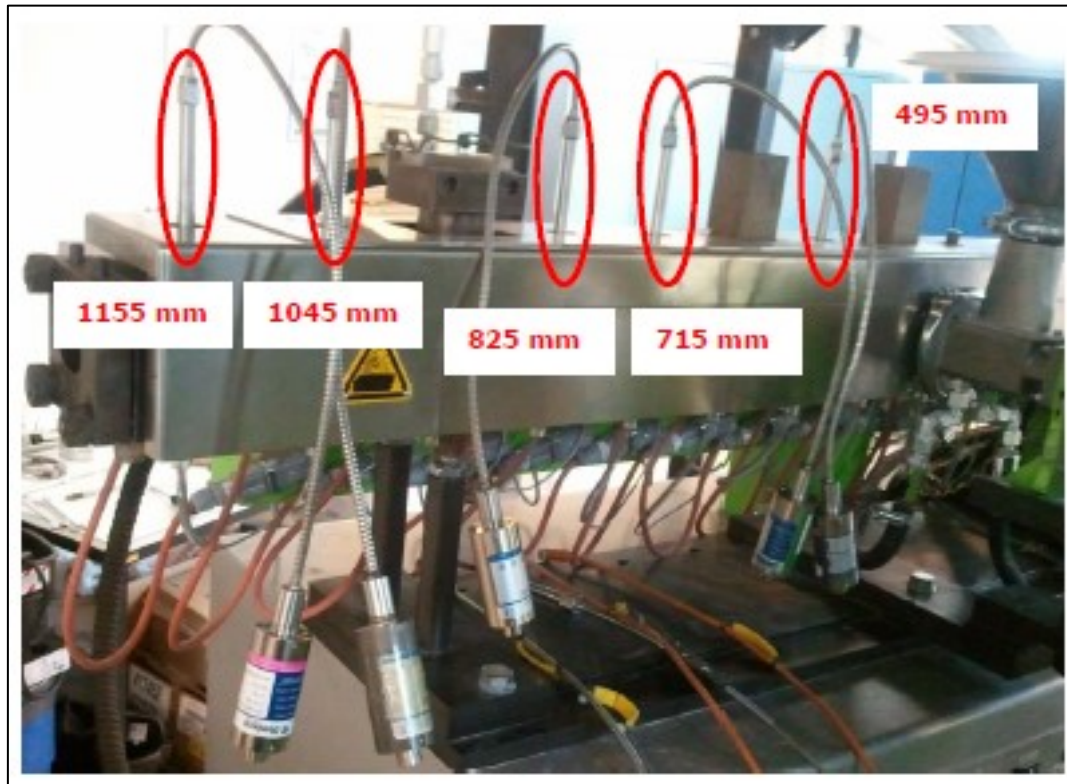
*Figure 8.10: Pressure measurement positions over the screw length (Winkler-Ebner, 2014)*

Table 8.10: Extruder settings for the pressure measurement (Winkler-Ebner, 2014)

Setting No.	Screw Speed (rpm)	Backpressure (bar)	Output (kg/h)
1	55	45	8
2	55	15	8
3	100	30	8
4	145	15	8
5	145	45	8
6	145	15	11
7	145	15	16

The pressure measurement trials were done using the standard screw configuration under different processing conditions (at varying screw speeds, throughputs and backpressures) as shown in Table 8.10.

To check the degree of filling over the complete screw length, screw pulling trials have been carried out on the standard screw configuration at varying screw rotation speeds, backpressure and throughputs (Table 8.11). The screw pulling experiments were done without operating the vacuum vent. After setting the processing parameters on the extruder, the process was allowed to run for 15 min to attain the process stability. After attaining the stability in the compounding process the extruder was stopped and the screw was pulled out of the barrel with material. Each zone of the screw was photographed and the filling condition of each zone was documented (Winkler-Ebner, 2014).

Table 8.11: Extruder settings for the screw pulling experiment (Winkler-Ebner, 2014)

Setting No.	Screw Speed (rpm)	Backpressure (bar)	Output (kg/h)
1	50	15	8
2	55	45	8
3	150	15	8
4	150	45	8
5	150	15	16



GFA 2-30-30
GFA 2-30-30
GFA 2-30-30
KB 3-2-15-30GRD-LI
KB 3-2-15-90GRD
KB 3-2-15-60GRD-RE
KB 3-2-15-60GRD-RE
GFA 2-30-30
GFA 2-30-30
GFA 2-30-30
GFA 2-40-30
GFA 2-40-30
GFA 2-40-30
GFA 2-20-30-LI
GFA 2-30-30
GFA 2-40-30
GFA 2-40-30
GFA 2-40-30
KB 3-2-15-30GRD-LI
KB 3-2-15-90GRD
KB 3-2-15-90GRD
KB 3-2-15-60GRD-RE
KB 3-2-15-60GRD-RE
GFA 2-30-30
GFA 2-30-30
GFA 2-40-30
GFA 2-40-30
KB 3-2-15-30GRD-LI
KB 3-2-15-60GRD-RE
KB 3-2-15-60GRD-RE
KB 3-2-15-60GRD-RE
KB 3-2-15-60GRD-RE
GFA 2-30-30
GFA 2-30-30
GFA 2-30-30
GFA 2-30-30
GFA 2-40-30
GFA 2-40-30
GFA 2-40-30
GFA 2-20-30 A

Figure 8.11: Screw elements of standard configuration

8.4 Materials and Material Data

Different polymers were used in this study. Polypropylene (PP) type Bormed™ DM55pharm is used for the trials with the parallel twin screw extruders, a low density polyethylene (LDPE) was used for the experiments carried out on the conical co-rotating twin screw extruder and a recycled polyethylene terephthalate (PET) was used for the scaling-up of the conical twin screws. The material properties like viscosity, specific volume, thermal conductivity, heat capacity were measured at the Chair of Polymer Processing in Leoben. The material data measurement and the measured values of the LDPE polymer are described here in detail. The material data of the PET material is given in chapter 10.2.3 and the PP material data is given in the appendix.

8.4.1 Material

The experiments on the MAS 55 conical co-rotating extruder were carried out using a Low Density Polyethylene (LDPE), type LD159AC manufactured by ExxonMobil. LD 159AC is a film extrusion grade material, which offers good draw down combined with good mechanical strength.

The material is delivered in granulate form and has a bulk density of 598 kg/m³ and the average diameter of the granule is about 3.71 mm. Some of the resin properties are given in below according to the resin manufacturer.

Table 8.12: Resin properties of LDPE ExxonMobil LD159AC

Density	0.924	g/cm ³
Melt Index (190°C/2.16 kg)	1.2	g/10 min
Peak Melting Temperature	109	°C

8.4.2 Rheological Data

The viscosity measurements were carried out on a high pressure capillary rheometer, type Rheograph 2002, by Göttfert Werkstoff Prüfmaschinen G.m.b.H., Buchen, Germany, according to ISO 11443 at the Chair of Polymer Processing in Leoben. The viscosity of the melt was carried out in the shear rate range between 10 s⁻¹ and 7000 s⁻¹ using a round capillary die with a diameter of D = 1 mm and three different lengths (10, 20 and 30 mm)

for correcting the entrance pressure loss. The viscosities were measured at three different melt temperatures and the curves were fitted using the Cross Arrhenius model. The viscosity master curve for the reference melt temperature (T_{ref}) of 230°C and the Cross Arrhenius model constants are shown Figure 8.12.

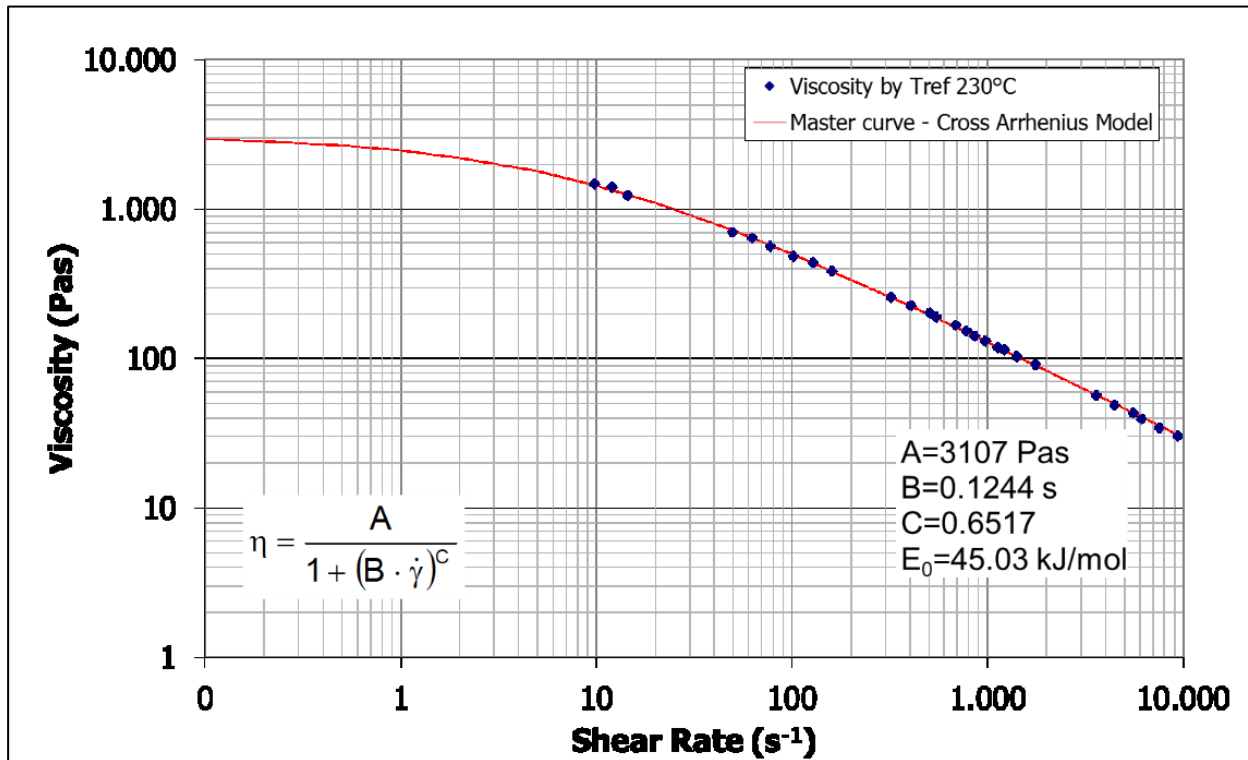


Figure 8.12: Shear viscosity of LDPE ExxonMobil LD159AC

8.4.3 pvT Data

The specific volume dependent on pressure and temperature (pvT diagram) was measured at the Chair of Polymer Processing in Leoben using the pvT Instrument, type PVT100 by Fabrikat SWO Polymertechnik G.m.b.H, Krefeld, Germany.

The pvT data was measured under isobaric cooling with a cooling rate of about 6 °K/min in the pressure range between 200 and 1600 bar.

The curves obtained from the pvT measurement (Figure 8.13) clearly show the semi-crystalline nature of the material. The curves in solid, transition and melt regions are approximated using the Menges Model.

The relation defining the change in the specific volume of the LDPE resin with respect to pressure and temperature in the solid state is given by:

$$V_{solid}(p, T) = \frac{1}{\rho(p, T)} = \frac{K_1}{p + K_4} + \frac{K_2 \cdot T}{p + K_3} + K_5 \cdot e^{(K_6 \cdot T - K_7 \cdot p)} \quad (8.1)$$

The approximation of the specific volume in the melt region is given by:

$$V_{melt}(p, T) = \frac{1}{\rho(p, T)} = \frac{K_1}{p + K_4} + \frac{K_2 \cdot T}{p + K_3} \quad (8.2)$$

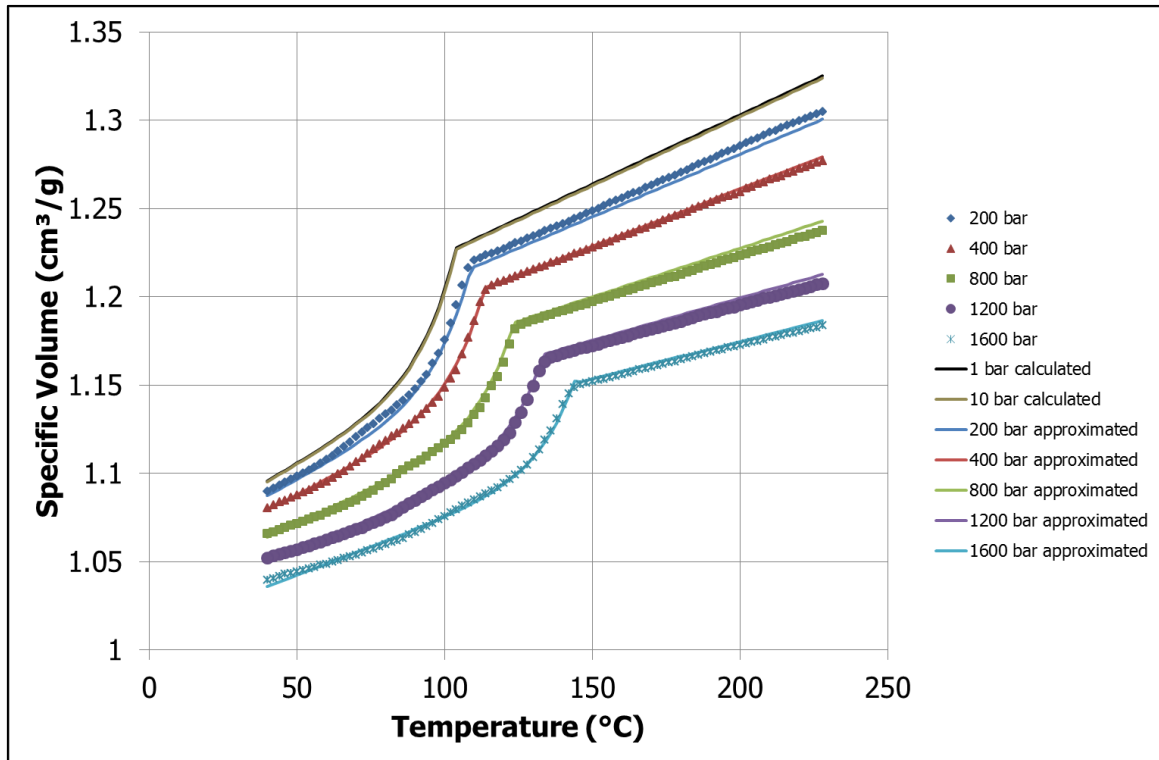


Figure 8.13: *pvT diagram of LDPE ExxonMobil LD159AC*

The transition region between the solid and the melt state of the polymer can be approximated by using the following relation:

$$T(p) = K_8 + K_9 \cdot p \quad (8.3)$$

The coefficients for determining the density of the material at a specified temperature and pressure are given in Table 8.13 and Table 8.14.

Table 8.13: *Coefficients for LPDE LD159AC in solid state*

K1	36357	cm ³ bar/g
K2	3.1125	cm ³ bar/g
K3	3268.7	bar

K4	34386	bar
K5	1.2695 E ⁻⁵	cm ³ /g
K6	0.083	1/°C
K7	0.0023	1/bar

Table 8.14: Coefficients for LPDE LD159AC in melt state and transition region

K1	35378	cm ³ bar/g
K2	1.4776	cm ³ bar/g
K3	1885.2	bar
K4	30861	bar
K8	103.21	°C
K9	0.025648	°C/bar

8.4.4 Thermal Conductivity

The thermal conductivity of the material was measured using the K-System II, manufactured by Advanced CAE Technology Inc., USA. The thermal conductivity dependence on the melt temperature was measured in the temperature range between 30 °C and 250 °C. Figure 8.14 shows the thermal conductivity of LDPE LD159AC. The thermal conductivity of the LPDE is almost constant in the solid phase (25 °C – 100 °C), in the transition region the values gets reduced and in the melt phase the thermal conductivity is almost constant. Since the thermal conductivity value of the LDPE material is almost constant in the melt state (above 150 °C), an average thermal conductivity value of about 0.25 W/mK is used for the calculation.

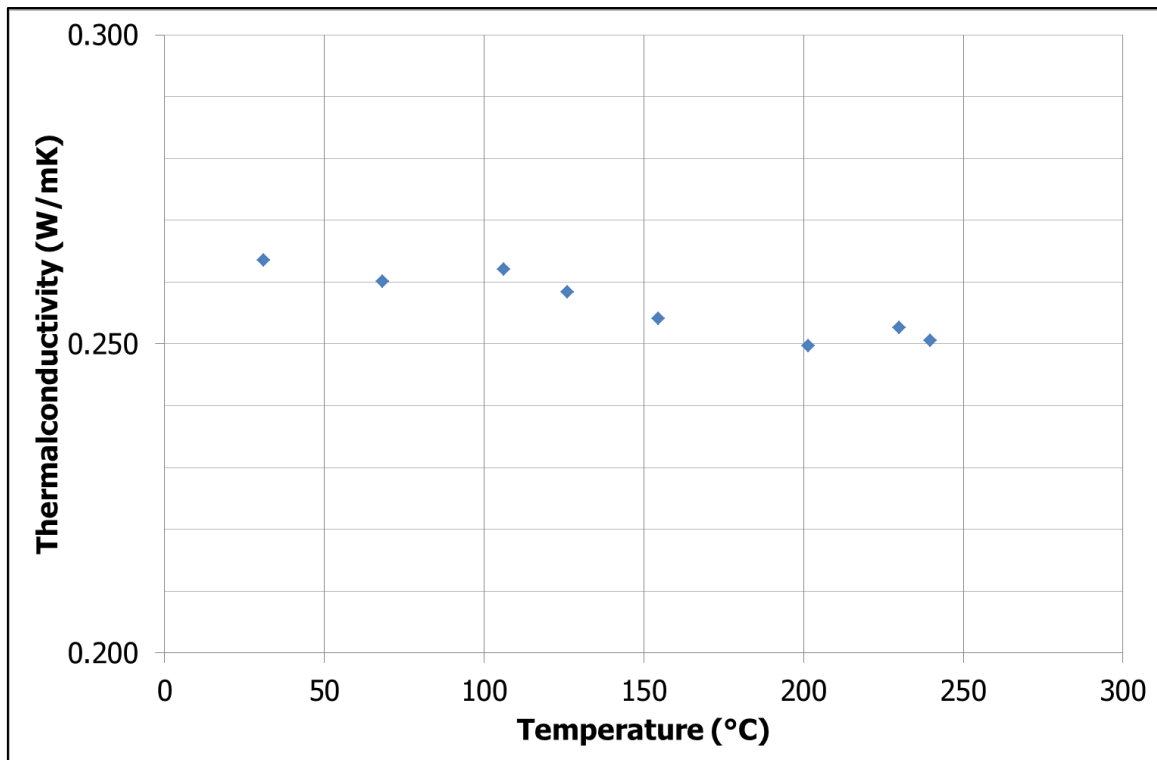


Figure 8.14: Thermal conductivity of LDPE ExxonMobil LD159AC

8.4.5 Specific Heat Capacity

The specific heat capacity c_p of the material is the amount of energy needed to increase the temperature of a unit mass of material. The heat capacity was measured using the differential scanning calorimeter (DSC) 200, by Netsch Gerätebau GmbH, Germany. The specific heat capacity curves as a function of temperature under the heating and cooling modus are shown in Figure 8.15.

The heating curve shows the peak melting point of about 110 °C for the measured LDPE LD159AC material. The specific heat capacity value is constant in the melt state (above 120 °C) and hence an average of 2.2 J/gK heat capacity value in the melt state is used for the calculation.

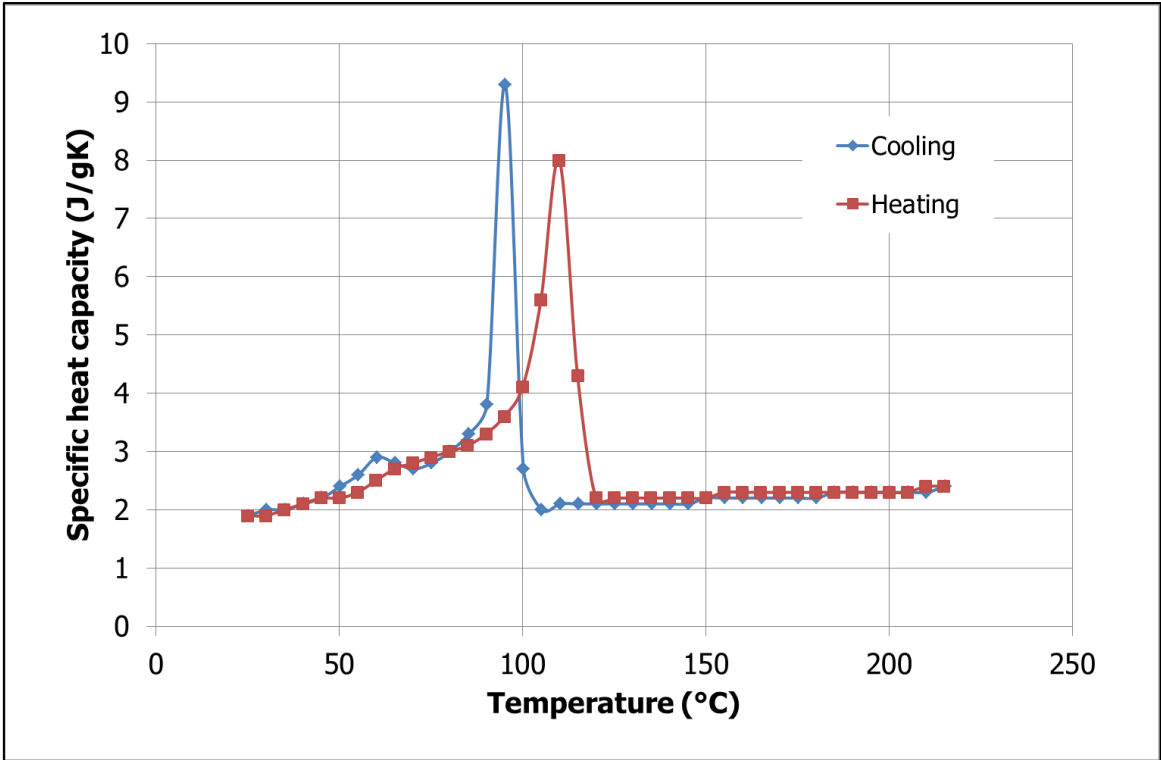


Figure 8.15: Specific heat capacity of LDPE ExxonMobil LD159AC

9 CAE of Co-Rotating Twin Screw Extruders

9.1 Introduction

The heart of the twin screw extruders is the plasticization unit, which is composed of the screw and barrel. Of these two components the most important component is the screw, which determines the quality of the end product. The right screw configuration is mostly defined according to the previously gained experience or by trial and error method. Especially the designing of the screw and the extruder as a whole has more complexities, if the extruder is to be used for some new process, or if the properties of the polymer to be processed are completely different to standard materials (Schuler, 1996). The implementation of new screw elements or screw geometries will be more time and cost consuming, since the functioning of the new element can only be studied using practical test. Similarly different screw configurations and its functionality can be predicted only through practical measurements. In order to predict the working of the screw elements or the screw configuration prior to practical measurements, a software package for computer aided engineering (CAE) of twin screw extruders is required.

The computer programs that simulate processing on twin screw extruders are important tools for compounders, since the simulation software reduces time for testing screw designs and can be used to optimize processing conditions. Moreover this simulation can reduce machine operation time and raw material cost during scaling up process, because only minimum experimental runs are required (Markarian, 2005).

Computational fluid dynamics (CFD) are being used to study the compounding process three dimensionally, to obtain a detailed understanding of the flow process in the extruder (Kohlgrueber, 2008). Even though 3-dimensional simulations have gained more importance and have developed a lot in past few years, still no FEM simulation software, which is available in the market, is able to simulate all the processing zones of a twin screw extruder (from feed zone until the die exit). More over the 3D simulation of a complete screw is more complex and very time consuming.

The Ansys Inc. company offers a wide variety of computer simulation packages for different materials, properties and industries. Polyflow software from Ansys can be used for simulating the extrusion process. The mesh superposition method facilitates the simulation of complex thermal and mechanical interactions in the twin screw extrusion process (Toensmeier, 2015).

The modeling software is not always 100 % accurate, but 80 to 85 % accuracy is attainable (Toensmeier, 2015). This accuracy can help solving most of the problems in the extrusion process saving time and cost.

The simplest way of modeling the twin screw geometry is using a 1D model. In the starting of the 90's two software packages (SIGMA and Akro) for modeling and designing of co-rotating twin screw extruders were developed and commercially sold (Schuler, 1996). In the past years many software were developed for twin screw extrusion simulation. Some commercially available programs for simulating twin screw extrusion are: Polyflow (3D), Sigma, WinTXU, Ludovic and Morex (Markarian, 2005) (Kohlgrueber, 2008).

Since the conical co-rotating twin screw extruders are new to the market, no modeling tools are developed or available until now. So as a part of this thesis a software package for modeling and simulating the conical co-rotating twin screw extruders (NCT V1.0) has been developed. A similar tool has been developed for simulating the parallel co-rotating twin extruders available at the Chair of Polymer Processing.

9.2 Extruder Modeling Dimensions

According to Kohlgrueber (2008), the main purposes of the extruder screw modeling are:

- To aid the screw design
- To observe, control and regulate the processes online
- To improve the process understanding
- Scaling-up or scaling-down
- To reduce the testing time and costs

The modeling approaches of screw extruders can be distinguished according to the model dimensions as (Kohlgrueber, 2008):

- 0 dimensional model (mass balance of the complete screw)
- 1 dimensional model (different processing zones of extruder perceive as single dimension)
- 2 dimensional model (tips of the screw are omitted, "plate-to-plate" model)
- 3 dimensional model (considers x, y and z axis, non-isothermal simulation)

The advantage, disadvantage and the depth or modeling accuracy of the different model dimensions are shown in Figure 9.1.

	Calculations				Measurements
Dimension	0	1	2	3	0-3
Advantage	Simple balances	Process dimensions	Less effort compared with 3D	Real model depth	Real product behavior
Dis-advantage	Low model depth	No gradients in cross-section	Only qualitative results	CPU times, boundary conditions, material properties	Variations expensive, No single effects 1D: averages only 3D: no fields
Model depth Whole extruder	←—————→				

Figure 9.1: Advantages and disadvantages of different model dimensions (Kohlgrueber, 2008)

As could be seen in the Figure 9.1, as the model dimension increases, the depth of modeling the extrusion process increases. But at the same time the description of the different processing zones decreases. Figure 9.2 explains in detail the strengths of the models in describing all or particular processing sections of an extruder.

	Calculations				Measurements
Dimension	0	1	2	3	0-3
Whole extruder	yes	yes	no	no	yes
Extruder section (certain zones)	yes	yes	yes	yes	yes
Extruder cross-section	no	no	yes	yes	no (partly yes, complex)

Figure 9.2: Potential of models in describing the complete extrusion process (Kohlgrueber, 2008)

It can be concluded that 0- and 1-dimensional models can describe the complete extrusion process but not at a great accuracy or depth. The usage of 3-dimensional models are more precise but it is not yet possible to model a complete screw (solid conveying, melting and melt conveying zones) 3-dimensionally. The 3D model can be used to study only certain section, like completely melt filled zones in detail (Kohlgrueber, 2008).

As 1D models have the advantage of being able to describe the whole screw and as they can describe the process more detailed than 0D models, 1D model is used in this work for studying the process of both parallel and conical co-rotating twin screw extruders.

9.3 Calculation Procedure

The calculation steps for modeling the conical and parallel co-rotating twin screws are the same.

Figure 9.3 shows the steps involved in modeling the twin screw configuration. The initial step is to define the extruder and configure the barrel zones and configuring the screw elements.

The next step is to define the material and the material data required for the calculation. The following important step is to define the process parameters like die, barrel zone temperature, screw rotation speed, dosing, output etc.

The final step is to provide the parameters for the calculation, like tolerances, number of iterations and the number of segments etc.

Once all the input parameters are given, the calculation can be done. The main modules of the modeling are calculation of the pressure, degree of filling of the screw and in some cases the melting of the polymer.

Figure 9.4 shows the procedure used for calculating the pressure and the degree of fill in different screw zones, using the screw element geometry, die geometry, material and processing data. The calculation is performed initially by verifying if the feed zone is present. If the feed zone is present the solid conveying and melting calculation is performed. In the absence of feeding barrel element, the pressure calculation is done starting with the pressure determination in the pressure consuming elements and for the respective back pressure lengths are determined. At the end the pressure in the fully filled zones are calculated and the results are graphically and tabular displayed.

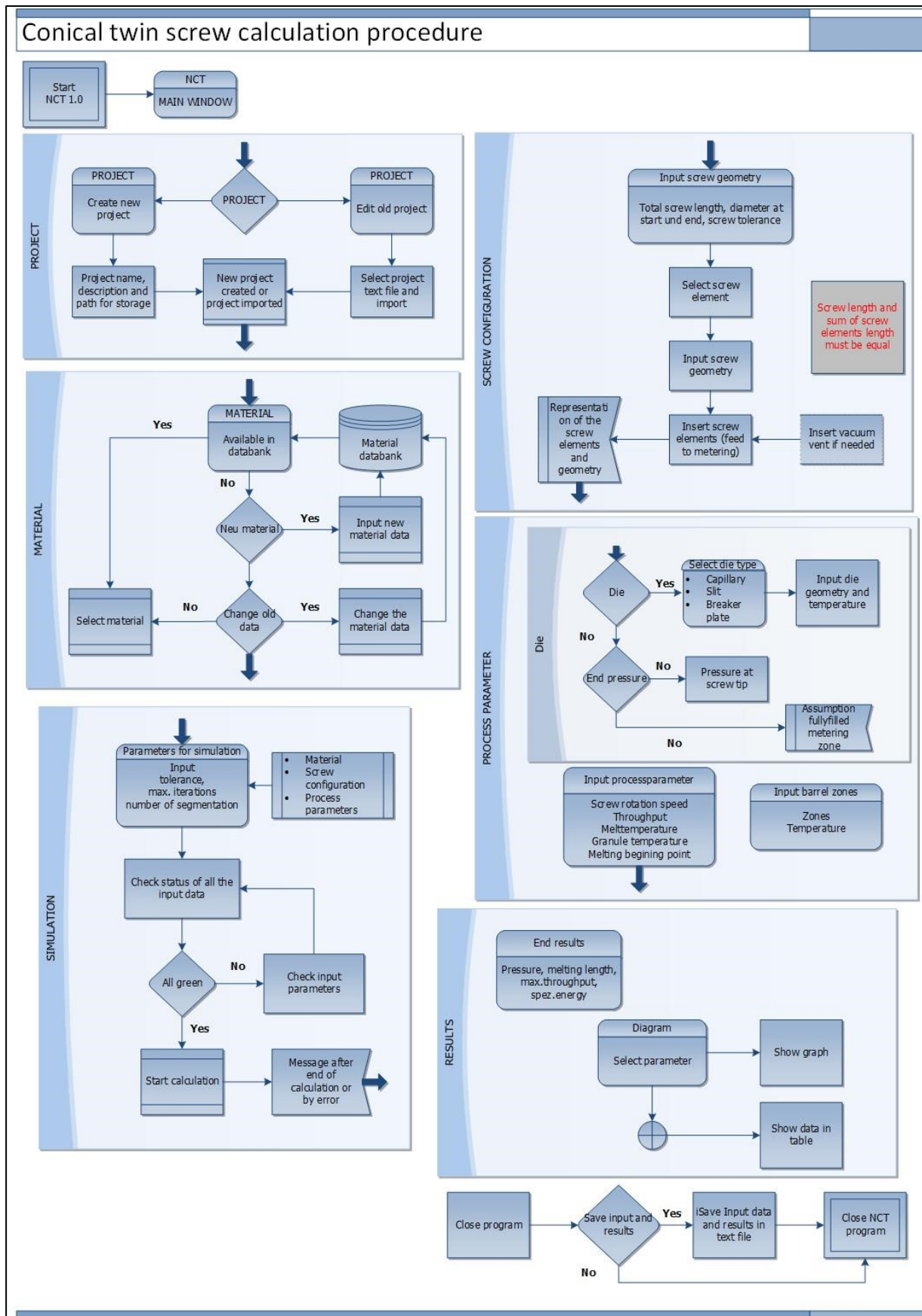


Figure 9.3: General calculation procedure

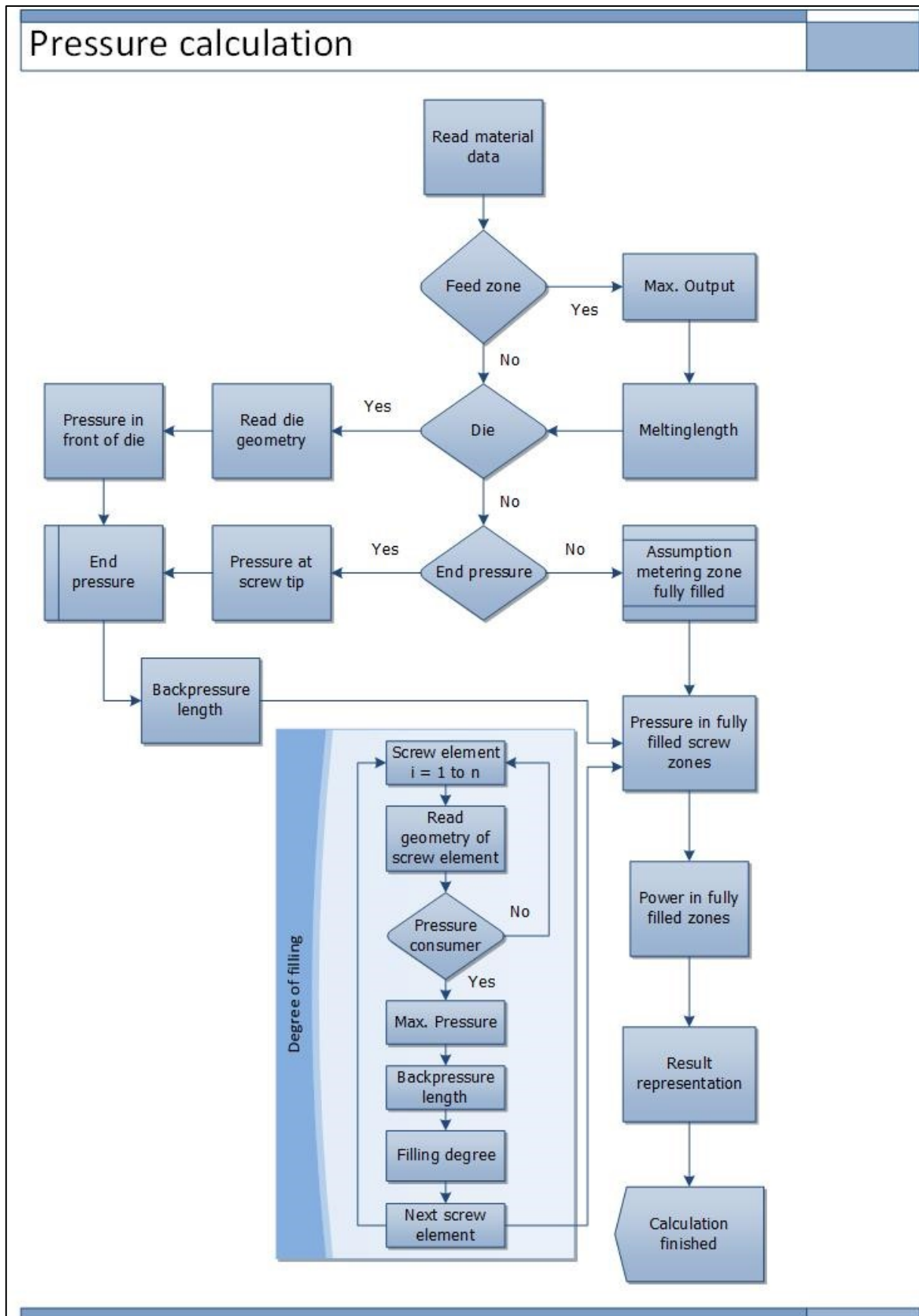


Figure 9.4: Pressure calculation procedure

9.4 Co-rotating Twin Screw Modeling Tool

As a part of this thesis two simple 1-dimensional screw modeling software packages for modeling parallel and conical co-rotating twin screw extruders have been developed using Microsoft Visual Studio 2010 Professional and VB.Net program. The functioning and the accuracy of the software package has been tested and verified by comparing the calculated results with the practical measured values.

9.4.1 NCT – Conical Co-Rotating Twin Screw Modeling Tool

The main window of the NCT Program is shown in Figure 9.5.

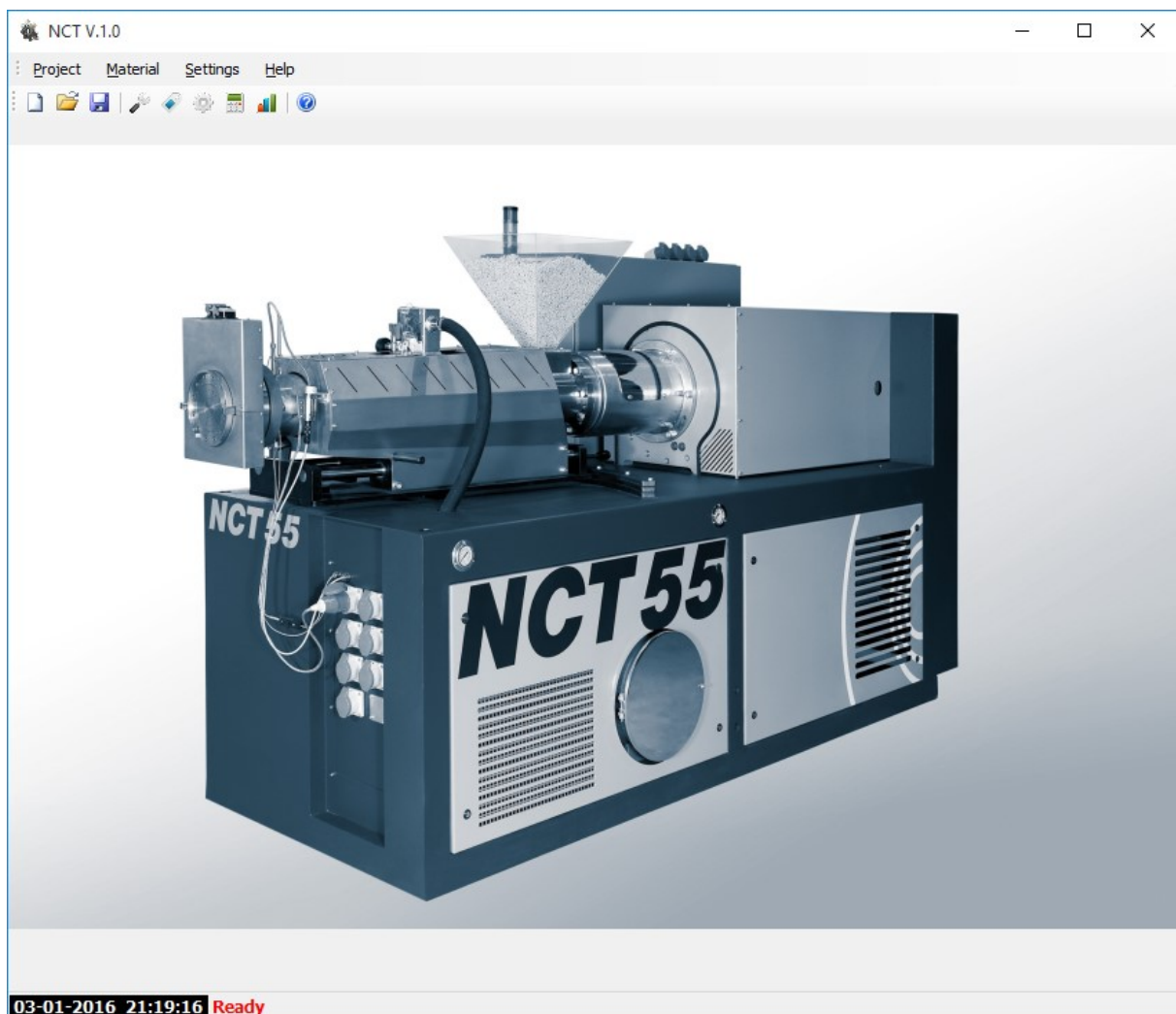


Figure 9.5: NCT main window

Either a new project can be started or an already saved project can be opened, modified and calculated by entering the "Project" menu. The "Project" page () opens on clicking the "Project" menu.

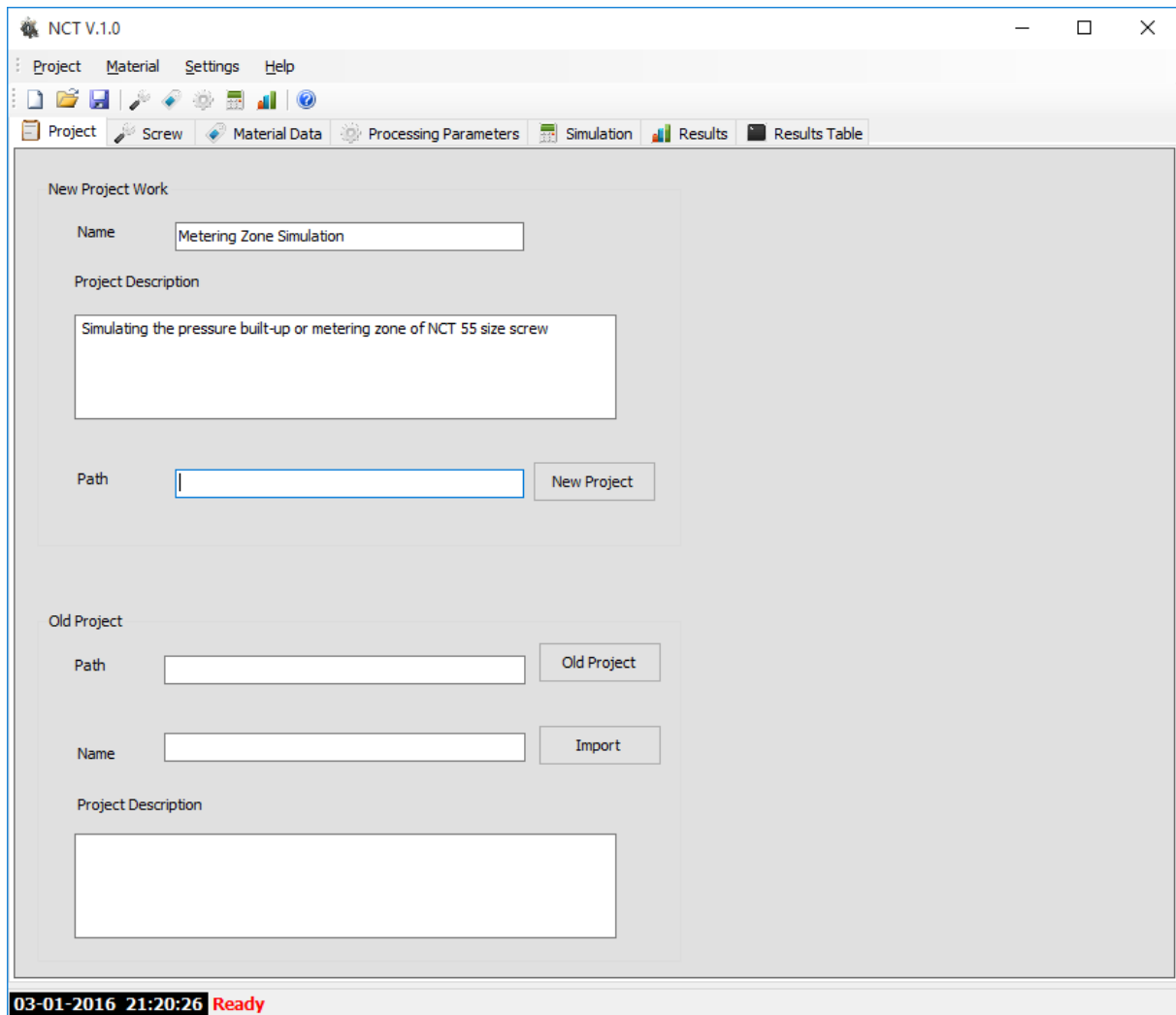


Figure 9.6: Project input page

Before starting a simulation the following parameters have to be defined:

- Project name and path of the project (where the files will be saved)
- Screw configuration
- Material and material data
- Process parameter
- Conditions for iteration in "Simulation" page

The screw can be configured with different screw elements according to the need in the "Screw" page.

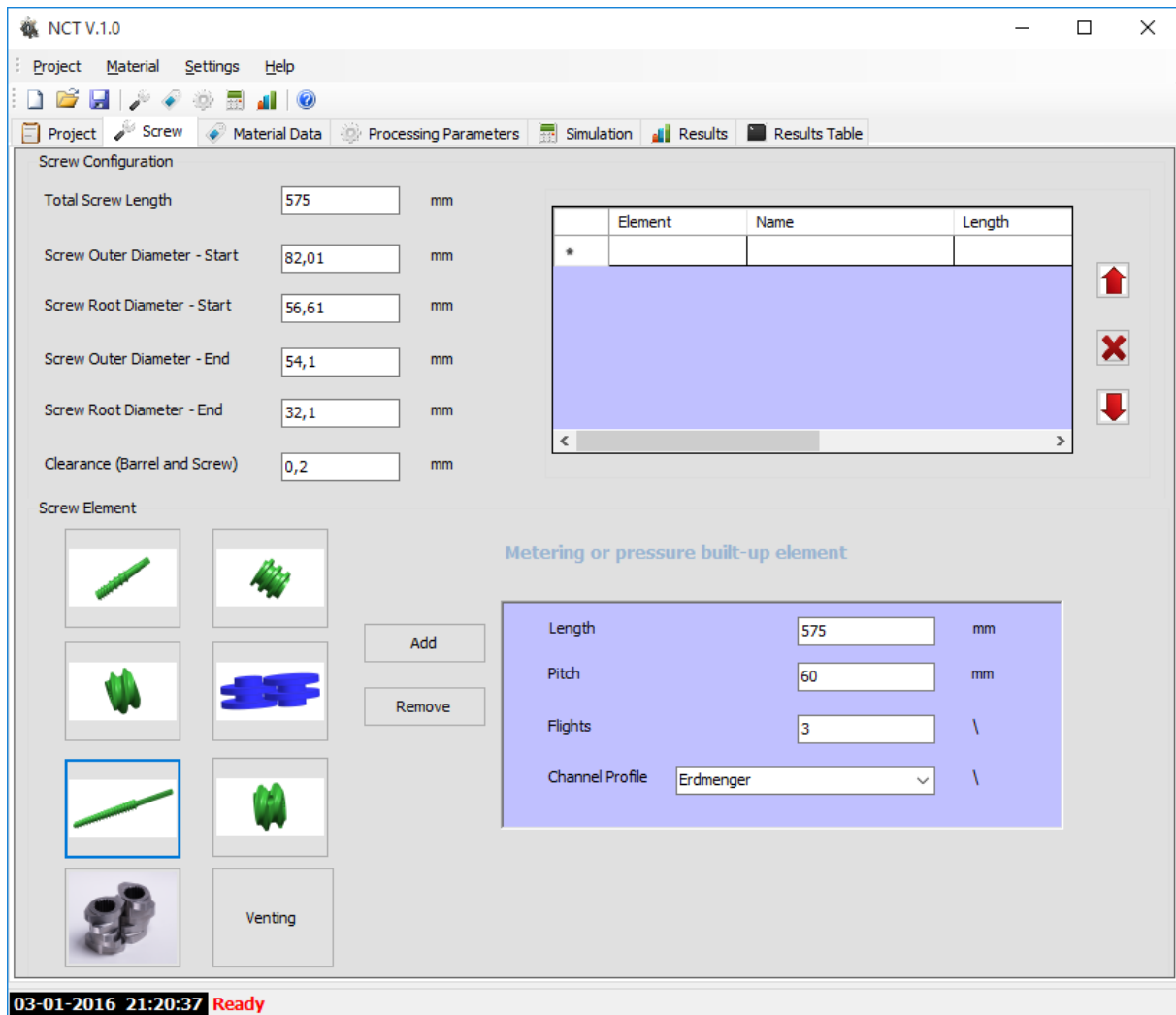


Figure 9.7: Screw configuration page

In this page the total length of the screw, its outside and inside diameters at the screw feeding section and the screw tips are entered. Then the individual screw elements and their respective geometries can be entered and the complete screw can be configured. In this page the position of the vent opening has to be mentioned while configuring the screw.

Once the screw is completely configured the next step is to select the material and its material data, which can be done in the "Material Data" page.

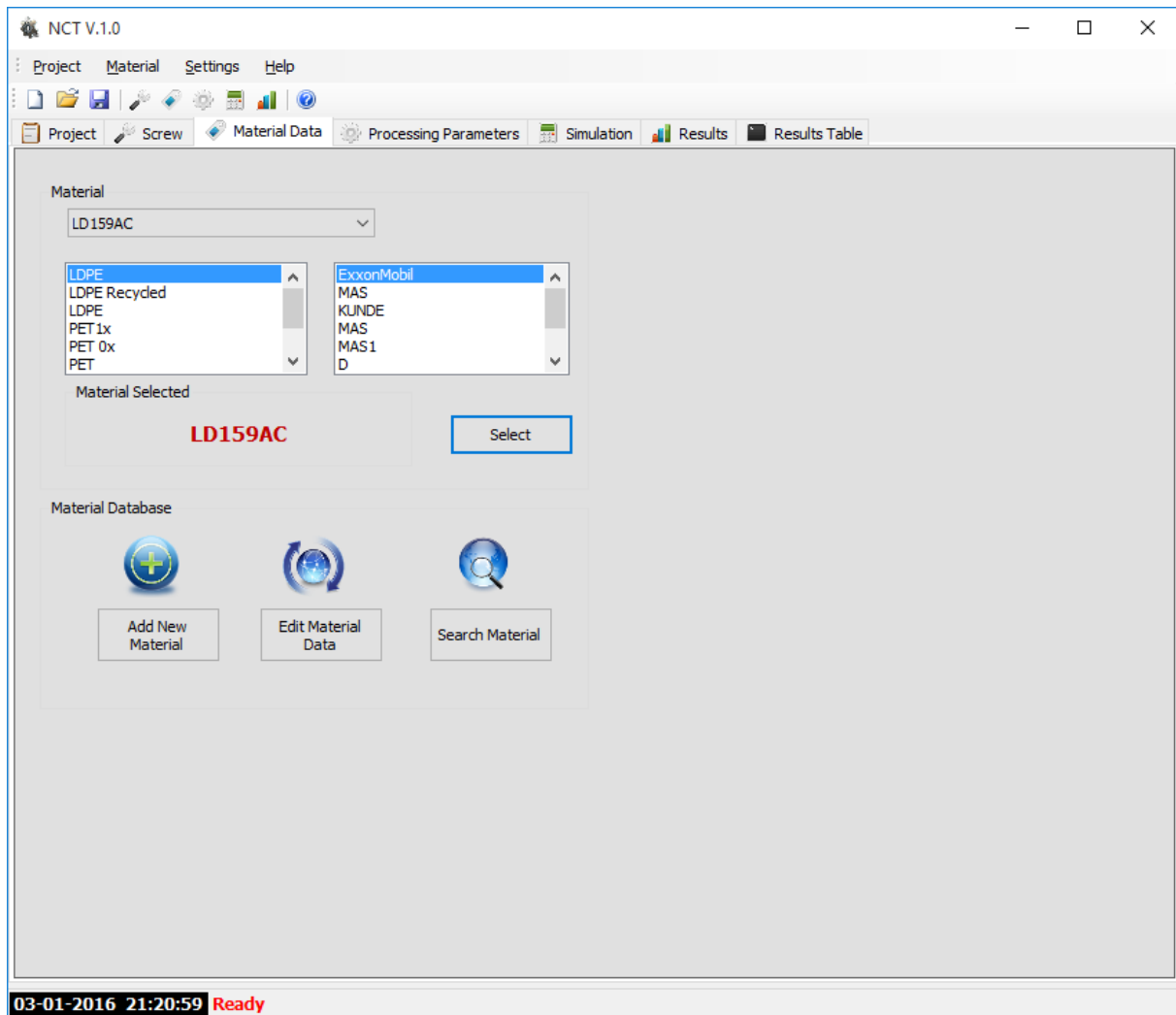


Figure 9.8: Material data window

The available materials and their properties in the databank are listed in the table. In this page the material data for new material can be included to the data bank or the available material data can be viewed and if needed corrections can be done.

The important properties of the material to be entered in the data bank are shown in Figure 9.9.

The next step is to define the process parameters such as:

- Die used
- Screw speed
- Throughput
- Barrel temperature settings
- Melt temperature

- Beginning of the melting
- Raw material temperature

These process settings can be defined in the "Processing Parameters" page Figure 9.10.

Material Database

1 of 9

Material

Reference ID (Materialtype_Charge): LD159AC

Material Name: LDPE

Manufacturer: ExxonMobil

Delete

Update

Properties

Viscosity

$$\eta = \frac{A \cdot aT}{1 + (B \cdot \dot{\gamma} \cdot aT)^c}$$

Power Law

Consistency Index K: 11337,3995 Pa.sⁿ

Power Law Index n: 0,3521 /

Cross Model

Zero Shear Viscosity A: 3106,7375 Pa.s

Cross Time Constant B: 0,12435 s

Slope C: 0,6517 /

Activation Energy E: 45,03 J/kg.K

Reference Temperature Tref: 230 °C

Melt Temperature: 130 °C

Row Material Properties

Granulate Diameter: 3,71 mm

Internal Friction: 0,13 /

Barrel Friction: 0,069 /

Screw Friction: 0,047 /

Deflection Angle : 30 °

Melt State Properties

Melt Density: 755 kg/m³

Heat Capacity: 2,2 J/g.K

Thermal Conductivity: 0,25 W/m.K

Enthalphy: 155 J/g

Solid State Properties

Density: 10 kg/m³

Bulk Density: 598 kg/m³

Heat Capacity: 1,9 J/g.K

Thermal Conductivity: 0,26 W/m.K

Enthalphy: 155 J/g

Figure 9.9: Material properties window

The die option can be selected in case a die is used, or else if the end pressure is known the value can be used for the calculation. If the die and the end pressure are unknown the program considers that the metering zone of the screw is completely filled.

Three different dies are available – round capillary, slit die and breaker plate.

The barrel zones, its function and the temperature can be defined in this page. This temperature is used for the melting calculation.

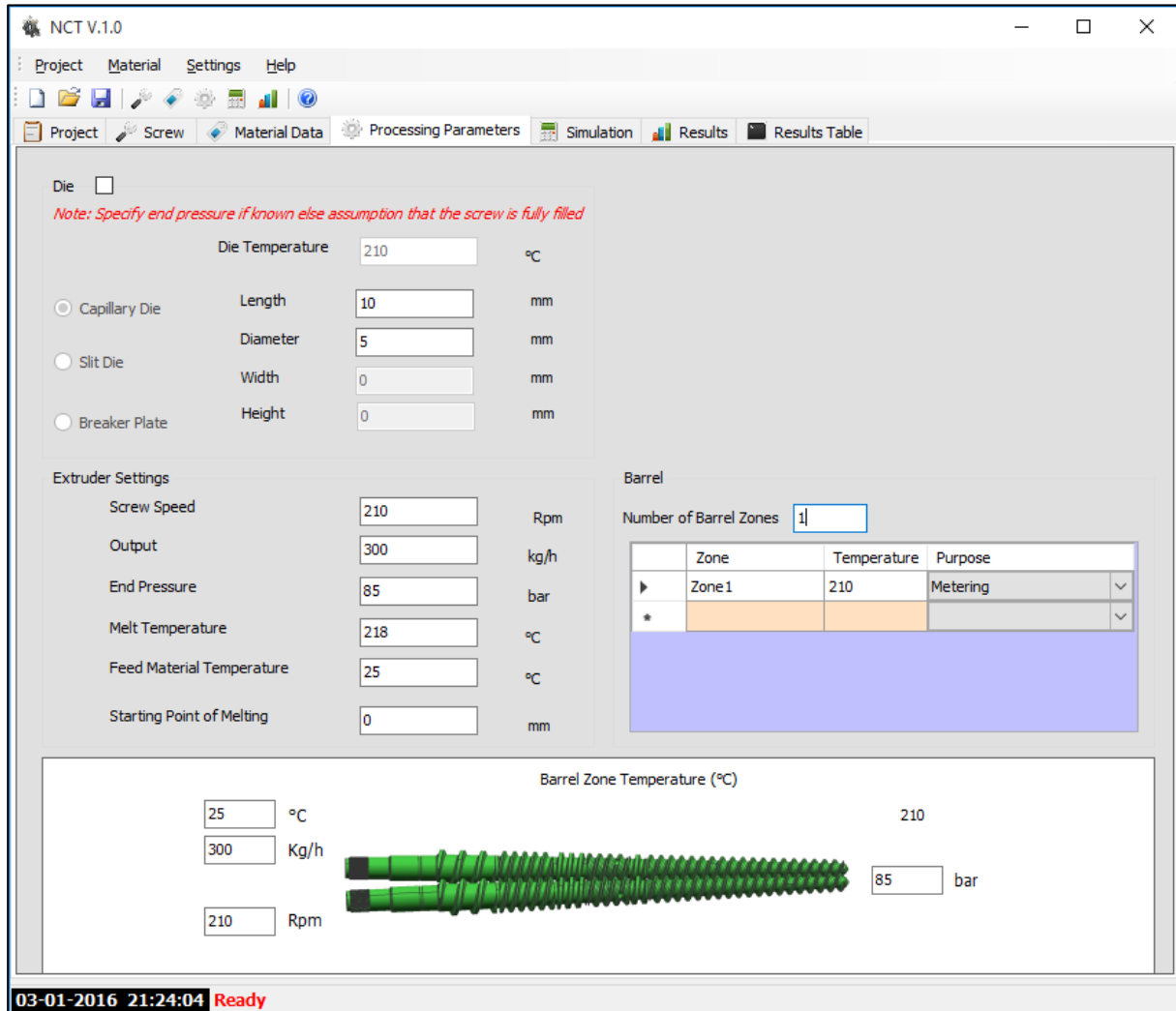


Figure 9.10: Process parameter

The next step is to define the conditions for the iterations, which is done in the "Simulation" page.

Here the number of segments, maximum number of iteration, tolerance and consideration of the form factor (Fp and Fd) are given.

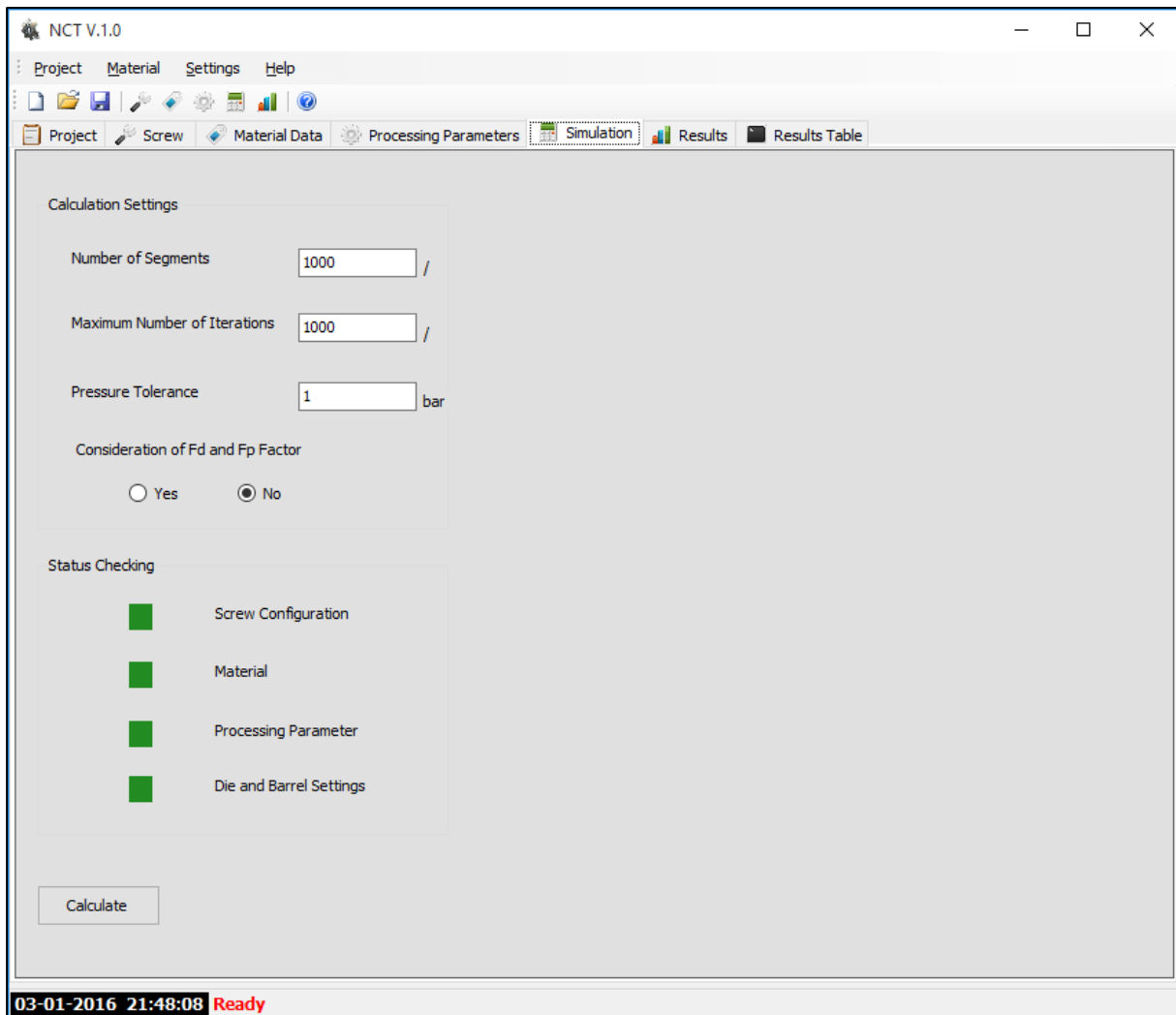


Figure 9.11: Simulation

The status checking shows if all the needed parameters for the calculation are correctly specified. If all the status is green, then the calculation can be started by pressing calculate button. Once the calculation is finished the program gives a message informing the status of the calculation. The results can be seen graphically in the "Results" tabpage (Figure 9.12).

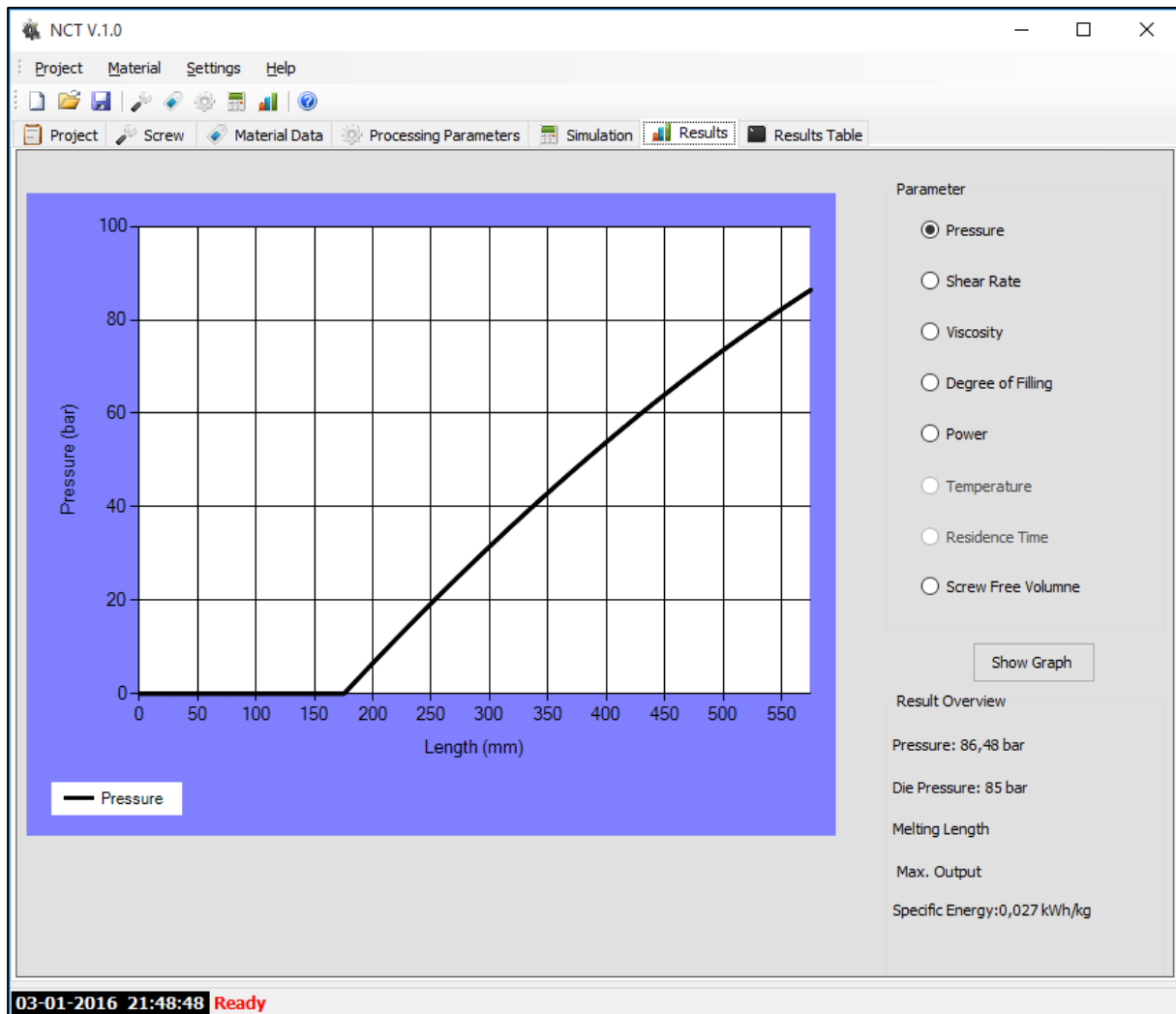


Figure 9.12: Graphical representation of results

9.4.2 2XS – Parallel Co-Rotating Twin Screw Modeling Tool

Similar to the conical twin screw modeling tool, for parallel co-rotating twin screw extruders a screw modeling tool has been developed in Microsoft Visual Studio 2010. The graphical user interface and the program codes are written in Visual Basic .NET language.

The opening window of 2XS program is shown in Figure 10.12:

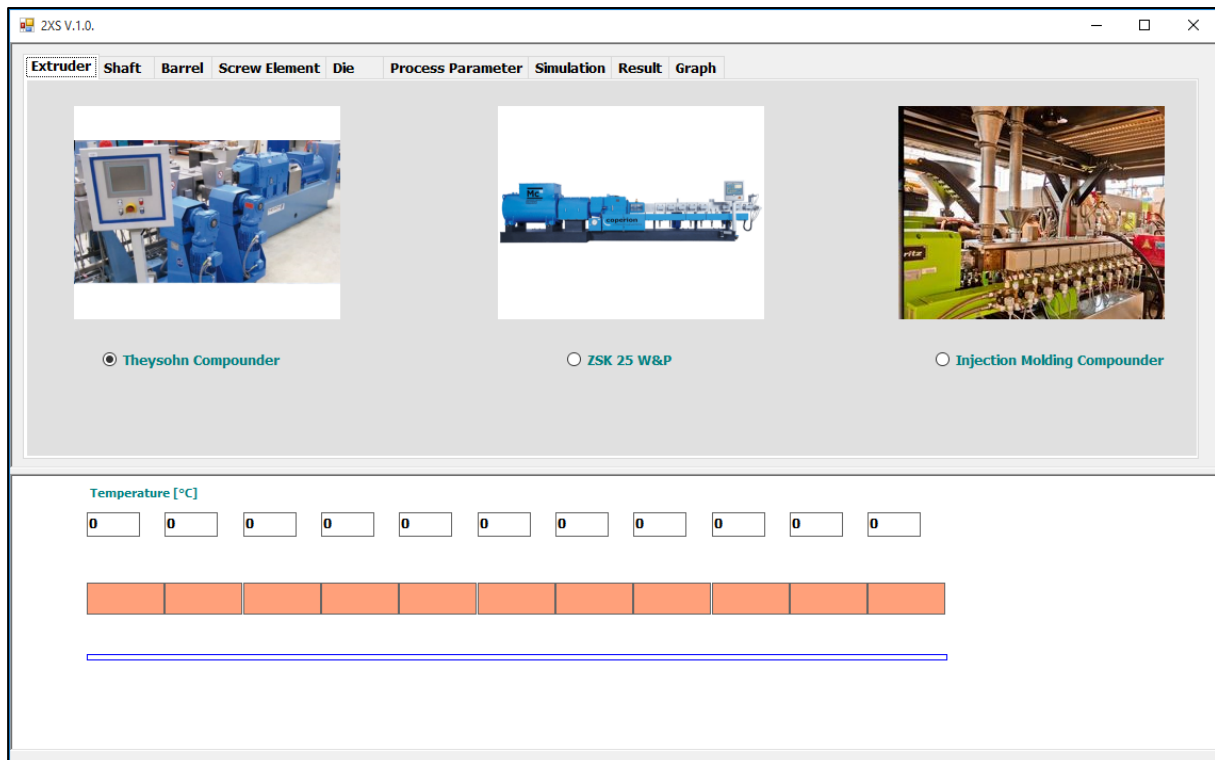


Figure 9.13: Main window of 2XS screw modeling tool

The main window is separated into two areas, the upper area for manually entering the configuration and other parameters for the simulation and the lower part shows the configured screw and barrel graphically.

In the main window the type of compounder to be simulated can be selected. Currently three compounders:

- Theysohn compounder
- ZSK 25 W&P
- Leistritz ZSE 27 MAXX compounder

which are available at the Department of Polymer Engineering and Science in Leoben is included in this program extruder databank. The selection of a particular compounder loads the available barrel elements in the "Barrel" page, screw elements in the "Screw Element" page, dimensions of screw and shaft automatically in the "Shaft" page of the main window Figure 9.14.

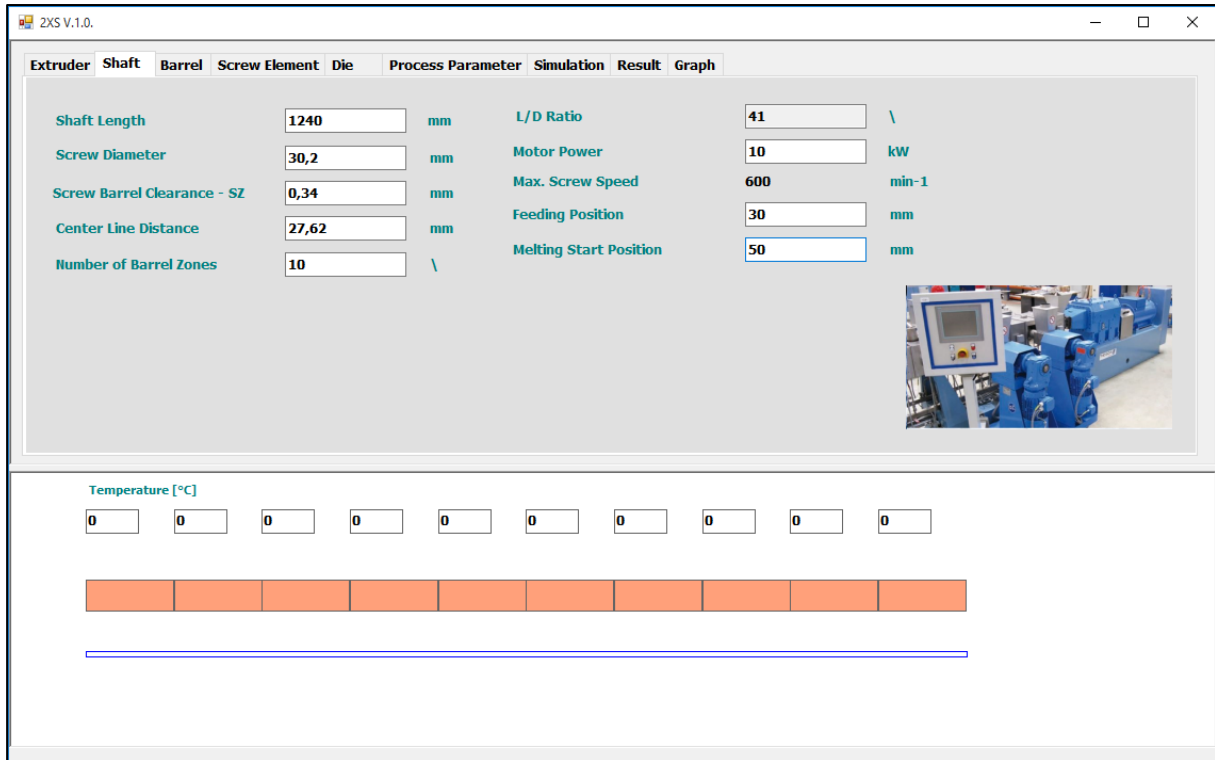
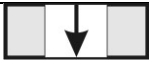






Figure 9.14: Shaft configuration page

This page shows the details about the shaft length, screw outer diameter, screw barrel clearance, centerline distance between the two screws, power and max. screw speed of the extruder. For the melting simulation, the starting point of the melting over the length is manually defined.

The shaft length and the number of barrel zones can be varied according to the needs. The barrel zones can be configured in the "Barrel" page, as shown in Figure 9.15. The different barrel elements included in the tool are listed in Table 9.1.

Table 9.1: Different barrel elements

	Intake element
	Side feeding element
	Atmospheric venting element
	Vacuum venting element
	Standard barrel element with only heating and cooling

Double clicking the barrel elements from the lists or from the picture list, inserts the selected barrel element in the lower part of the configuration window. Also the temperature settings of each barrel zone can be directly entered manually in the input boxes above the elements. The configured barrel zones can be saved and used for other simulation projects too.

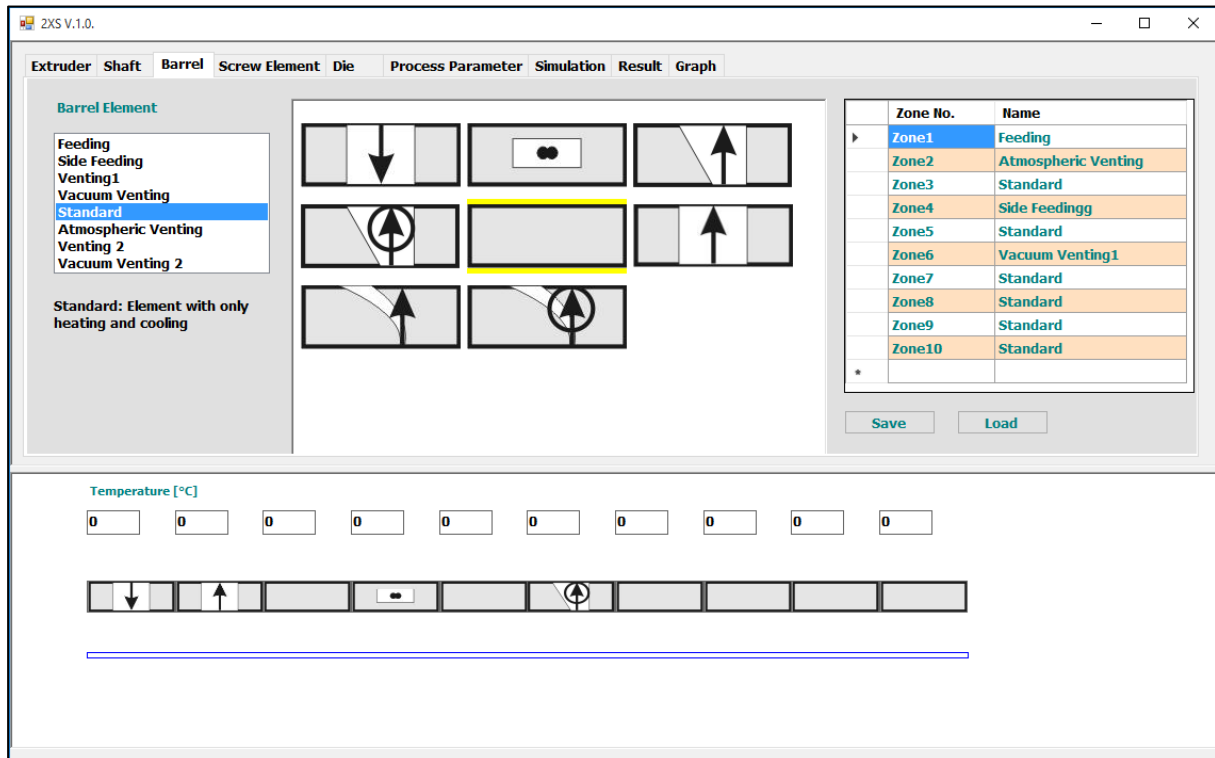


Figure 9.15: Barrel zones configuration

The next and main step is to configure the screw elements, which is done on the "Screw Element" page (Figure 9.16). This page shows the list of screw elements available for the selected compounder. Additionally simple diagrammatic representation of the screw elements will be shown in the picture list. The screw can be configured by double clicking the element from the list, which automatically adds the element to the shaft in the graphic. An overview of the selected screw elements will be shown on the table, which can be stored and retrieved for other simulation projects. The actual configured screw length is denoted by the "Configured Screw Length" value.

In case of entering a wrong screw element, the screw element can be deleted from the configuration by double clicking the element in the graphical configuration area. Removing the complete screw configuration can be easily done by pressing the "Delete" button, so that a new screw configuration can be done from the beginning. A completely configured screw is shown in Figure 9.17

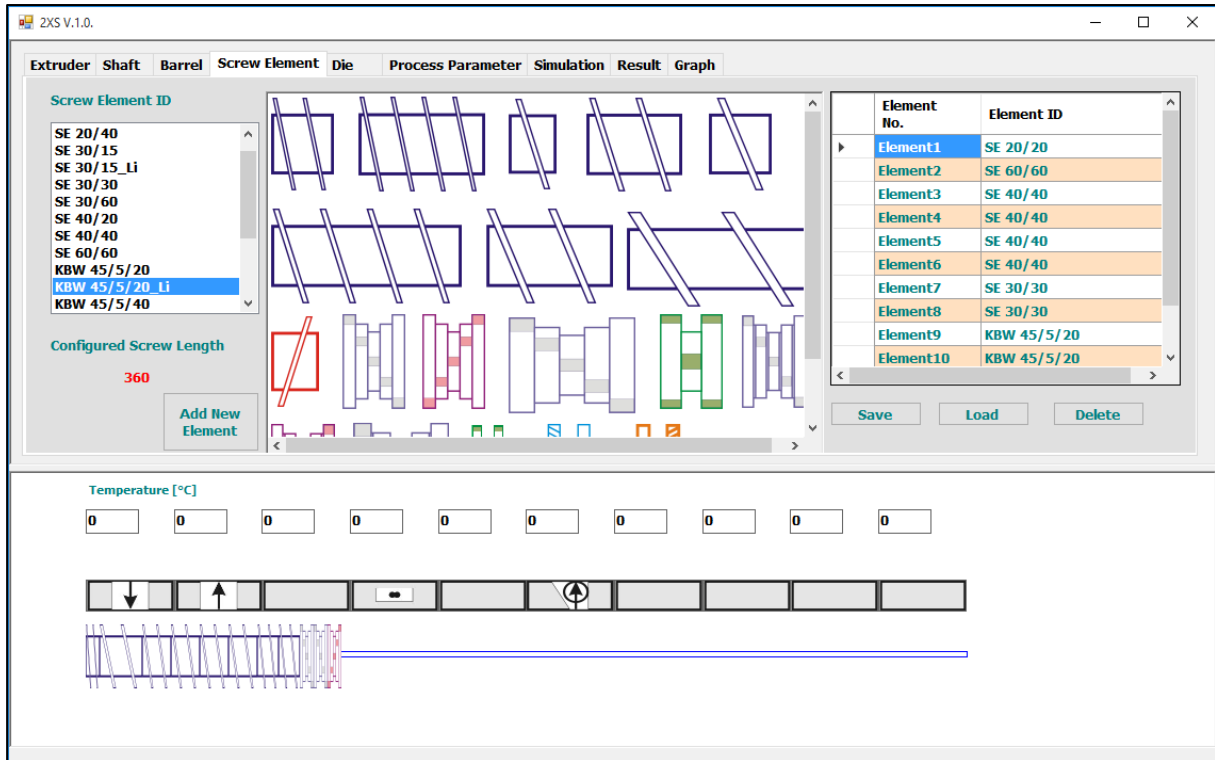


Figure 9.16: Configuration of the screw elements

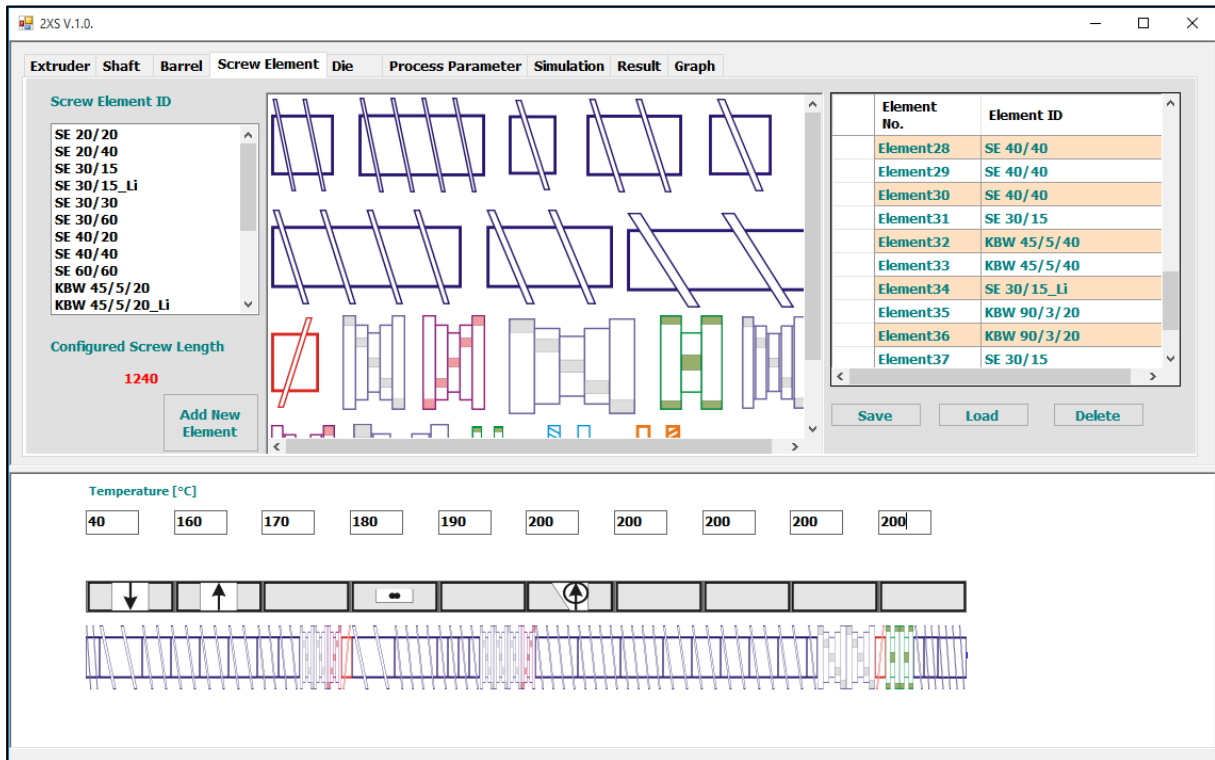


Figure 9.17: A complete configured screw

In case of using a new screw element, which is not available in the data base, there is an option to include a new screw element by clicking the "Add New Element" button. This opens a pop up window showing the list of all available screw elements and their corresponding geometry data. The new screw element can be inserted by pressing the "+" symbol and saving after the geometry data are entered.

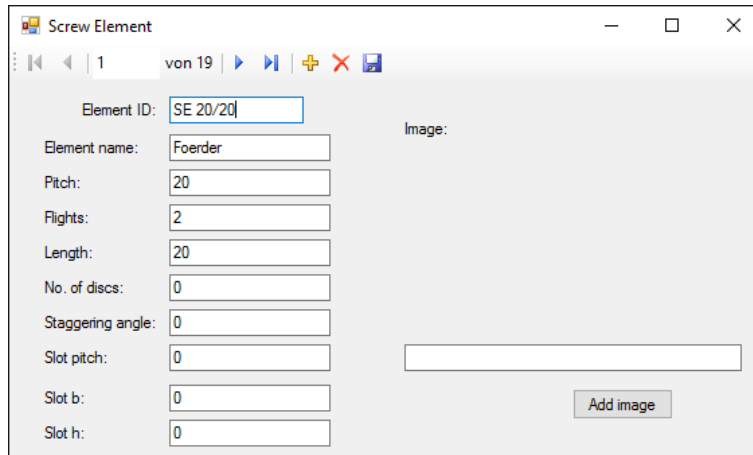


Figure 9.18: Addition of new screw element to the data base

Once the barrel and screw configuration has been done, the die or the flow restriction at the screw tip can be configured in the next page "Die" (Figure 9.19).

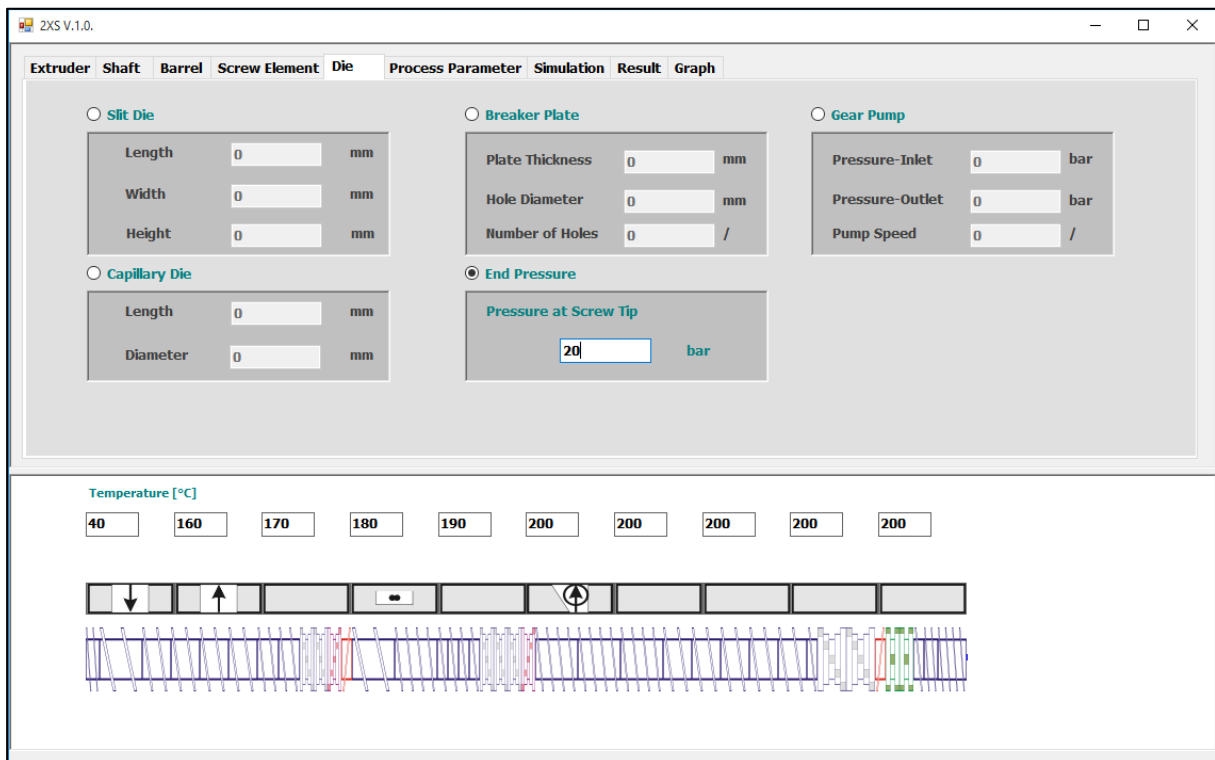


Figure 9.19: Die configuration page

This tool allows the possibility of choosing a die or pressure restricting element at the screw from the below shown list:

- Slit die – with defined length, width and height
- Breaker plate – with defined hole numbers and diameter
- Gear pump – with defined inlet and outlet pressure and the pump rotation speed
- Capillary die – with defined channel diameter and length

In case the die is undefined, the user can define the pressure at the screw tip.

The next step is to define the process parameters and material selection, which can be done on the "Process Parameter" page (Figure 9.20). In the "Polymer" tabpage the material to be used for the simulation can be selected from the available material database. Inclusion or deletion of new material and their respective material data or changing the data of available materials can be performed similar to the NCT tool.

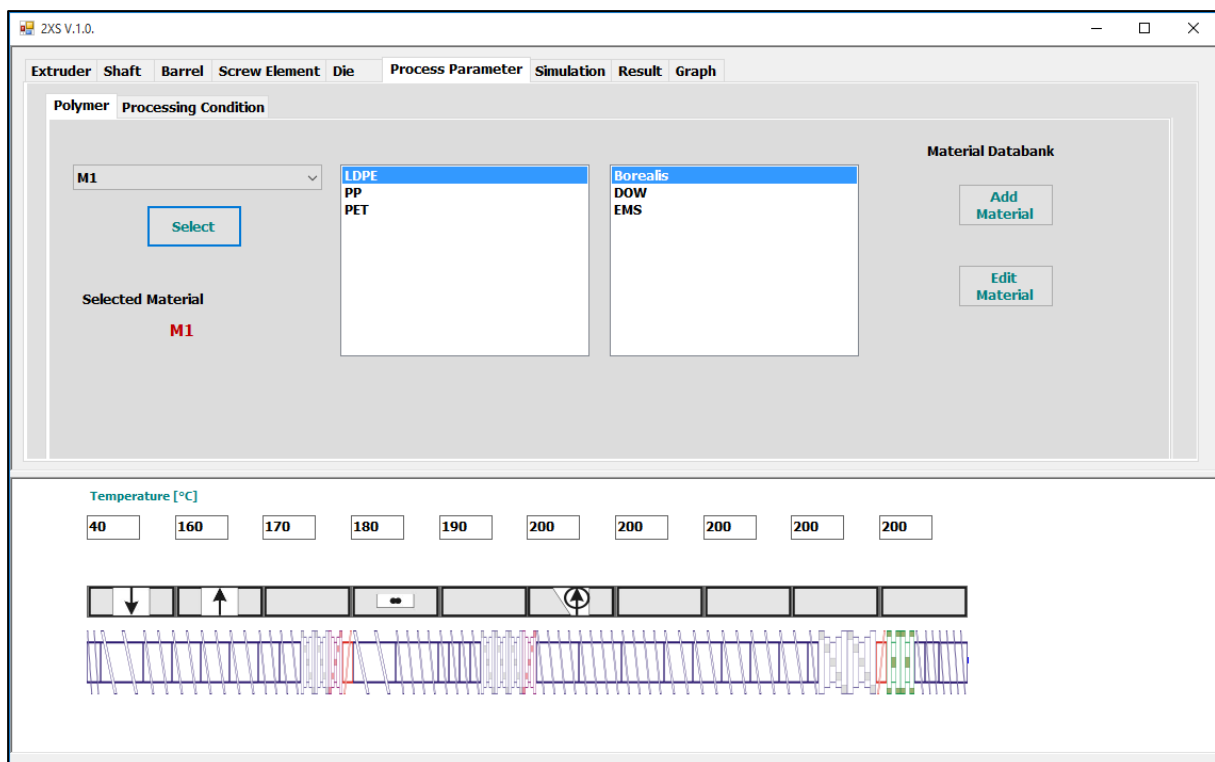


Figure 9.20: Material definition for the simulation

In the tabpage "Processing Condition" the information about the screw speed, dosing, throughput and the temperature of the die, polymer raw material and the polymer melt are defined Figure 9.21. In the 2XS V.1.0 version the option of side feeding of the fillers is deactivated.

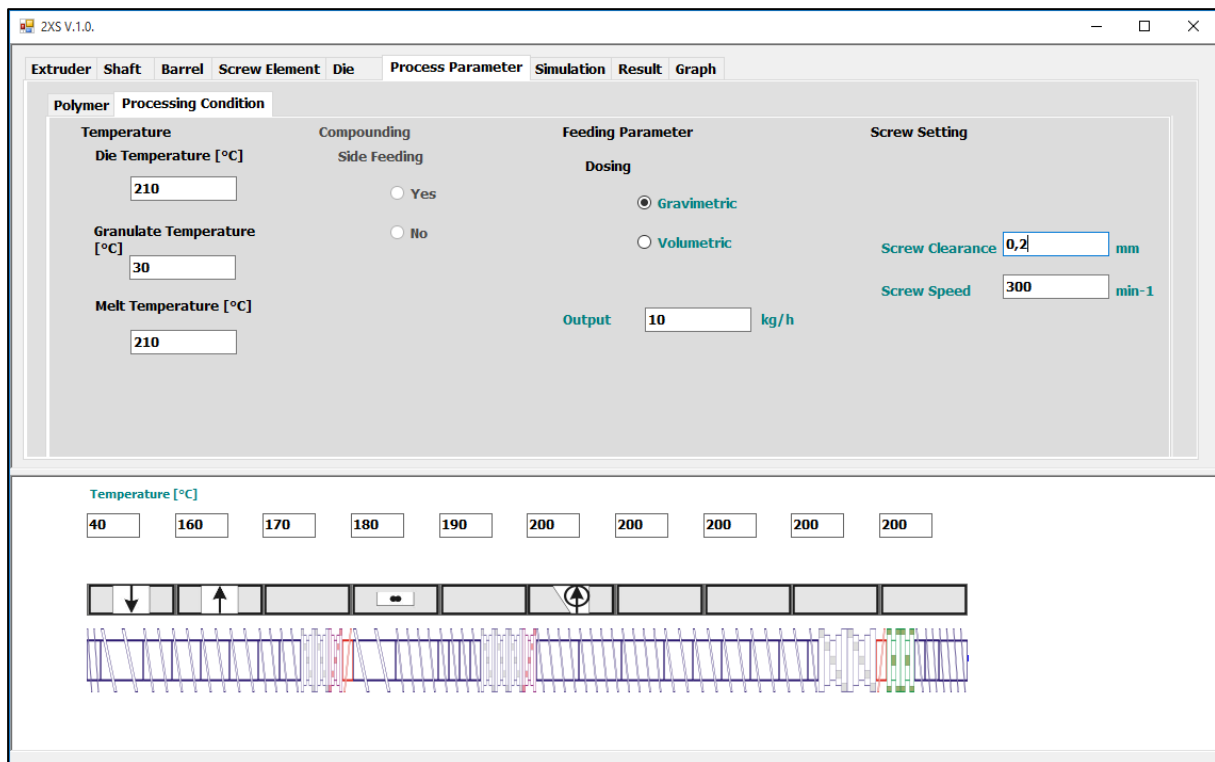


Figure 9.21: Configuring the process settings for the calculation

The simulation can be started, after automatic checking of the input parameters and entering the tolerance and iteration conditions for the convergence in the "Simulation" page Figure 9.22. The number of segments is used for discretizing each screw elements in calculation. For example, if the number of segments is 1000, a screw length with a total length of 60 mm will be divided into 1000 segments each having a length of 0.006 mm.

The consideration of the shape factors (F_d and F_p) for the screw simulation can be specified just by selecting the "Yes" or "No" option.

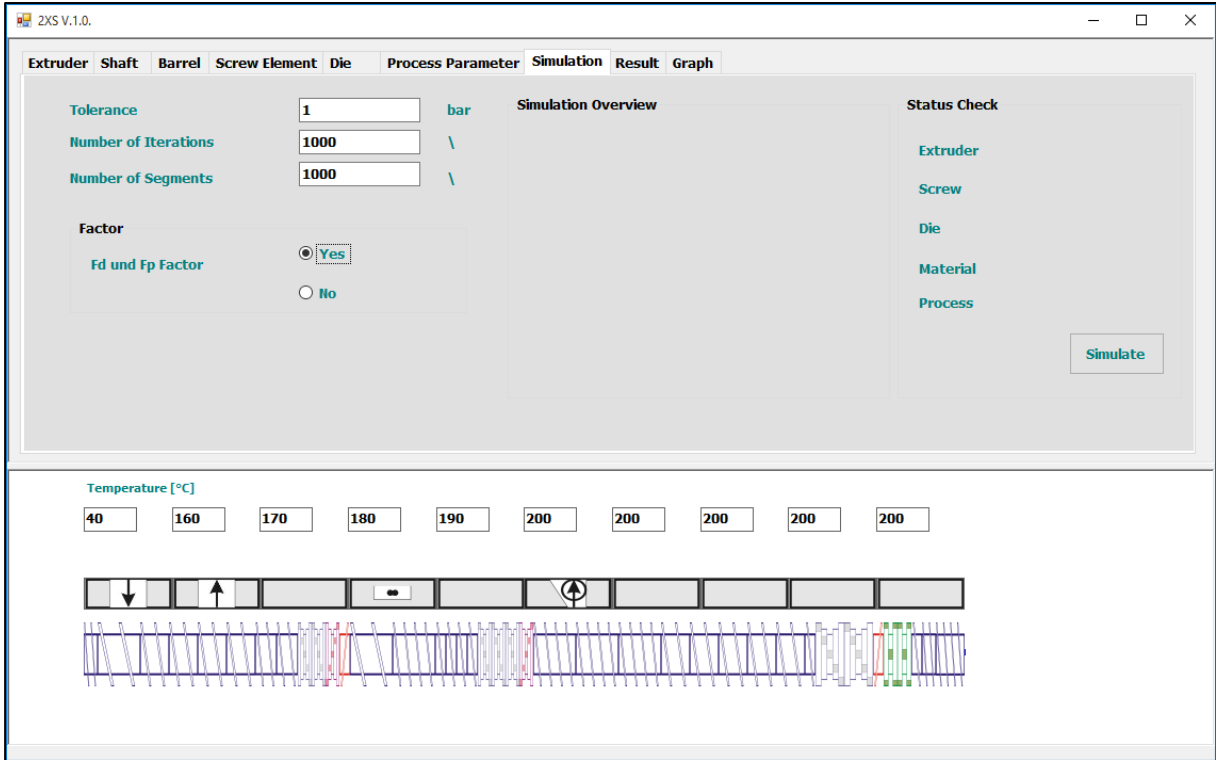


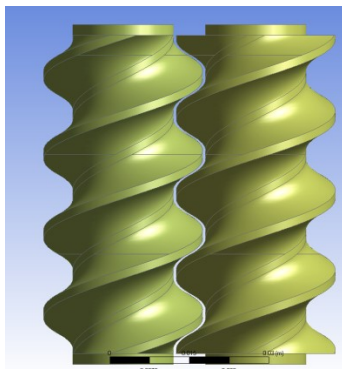
Figure 9.22: Starting the simulation in the simulation window

10 Results and Discussions

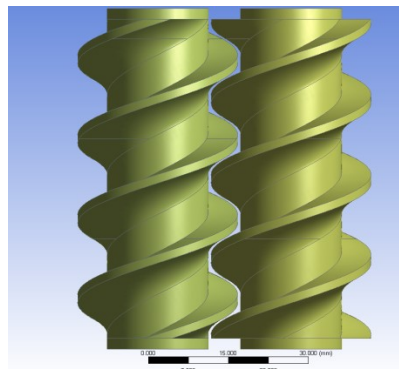
10.1 Comparison of Different Channel Profiles with Flow Simulation

The three different screw profiles - Erdmenger, shear edge and double shear edge profiles as shown in Figure 10.1 were constructed as double flighted conveying elements with the same pitch of 30 mm and the screw element length of 60 mm. The axial distance between the screws is 25 mm and the screw outer diameter of 30 mm. The simulations all the screw elements were done under the following three boundary conditions:

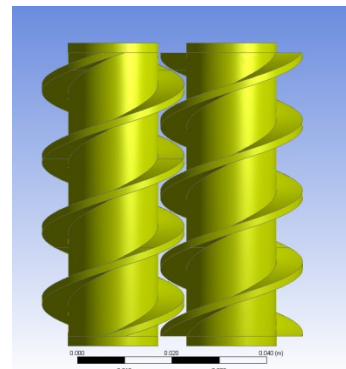
- Maximum flow rate determination with the boundary conditions vanishing normal forces on the inflow and outflow
- Different mass flow rate - 20 and 40 kg/h
- Varying the screw speed - 100, 200 and 300 rpm



Erdmenger profile



Shear edge profile



Double shear edge profile

Figure 10.1: Geometry of conveying elements with different channel profiles for Polyflow simulation

The available free volume of the three channel profiles for the used conveying element is shown in Figure 10.2. Due to the geometric advantage of the double shear edge profile, the free volume of this channel profile is larger compared to the standard Erdmenger profile. For the used screw geometric conditions, the double screw edge profile has 7 % increase in the free volume compared to the Erdmenger profile. This free volume can be increased further more by increasing the clearances between the screw flights and the calendar gap.

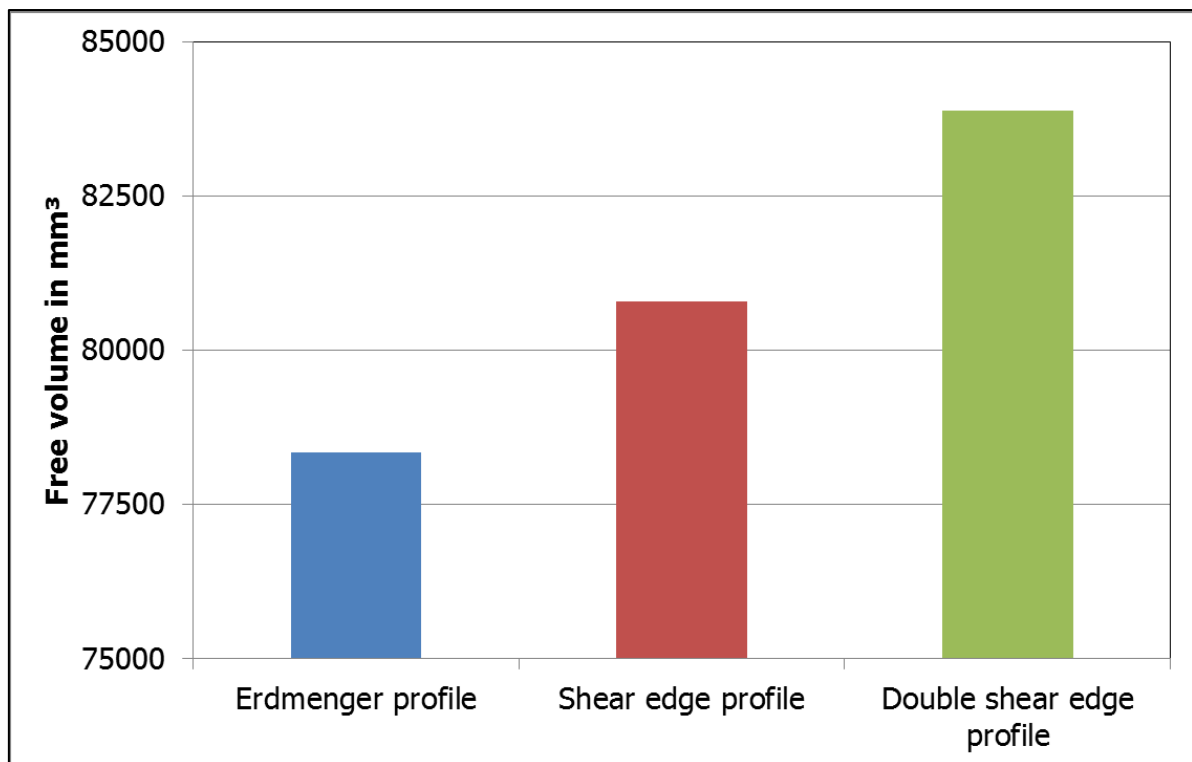


Figure 10.2: Free volume of different channel profiles of screw element

10.1.1 Maximum Flow Rate Comparison

Initially the maximum flow rate of the LDPE material was determined at different screw rotation speeds (100, 200 and 400 rpm), with the boundary conditions vanishing normal forces on the inflow and outflow.

The results (Figure 10.3) show that around 40 % more throughput is achievable with the double shear edge profile screw element compared to the standard Erdmenger profile, due to high free volume available in these channel profile. Due to this positive aspect, the double shear edge screw profile is very suitable for the feeding zone and zones where much free channel volume is required, for example in zones where fillers are dosed.

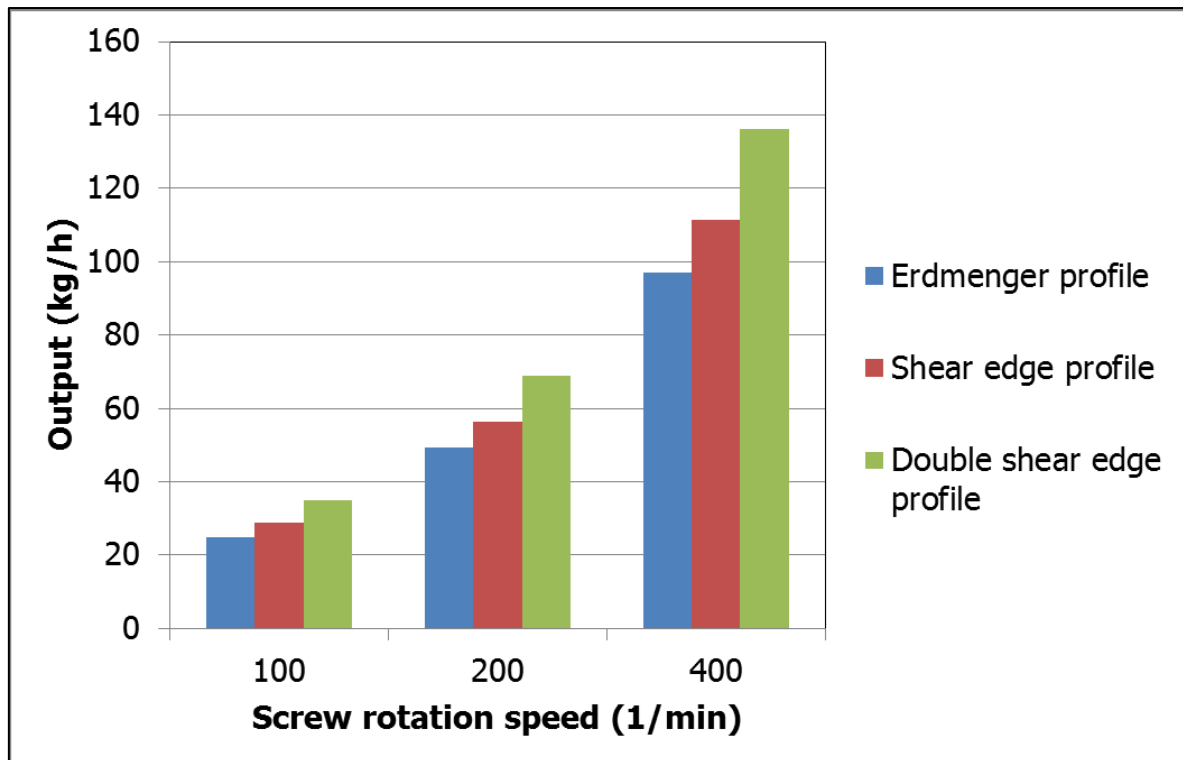


Figure 10.3: Output at different screw speeds for different screw channel profiles

10.1.2 Comparison of Pressure

The maximum pressure built up by the screw elements with different channel profiles were simulated at 20 and 40 kg/h and the comparison of the maximum pressure built up values at different screw speeds are summarized in Figure 10.4 and Figure 10.6.

It could be clearly noticed in Figure 10.4 that the Erdmenger channel profile has good conveying characteristics and hence more pressure generated compared to the other two geometries at low output rates. In this case the output is relatively smaller than the maximum achievable output at the respective screw rotation speeds.

The pressure built up by the screw elements at maximum calculated outputs (Figure 10.4) at different screw rotation speeds shows a different picture (Figure 10.5). In this case the double shear edge profile has a minimum pressure build-up compared to other two profiles. This is due to the higher free volume of the channel and also the lack in the closely intermeshing or self-cleaning property of this screw element. This indicates the poor pressure build-up of the double shear edge screw channel profile.

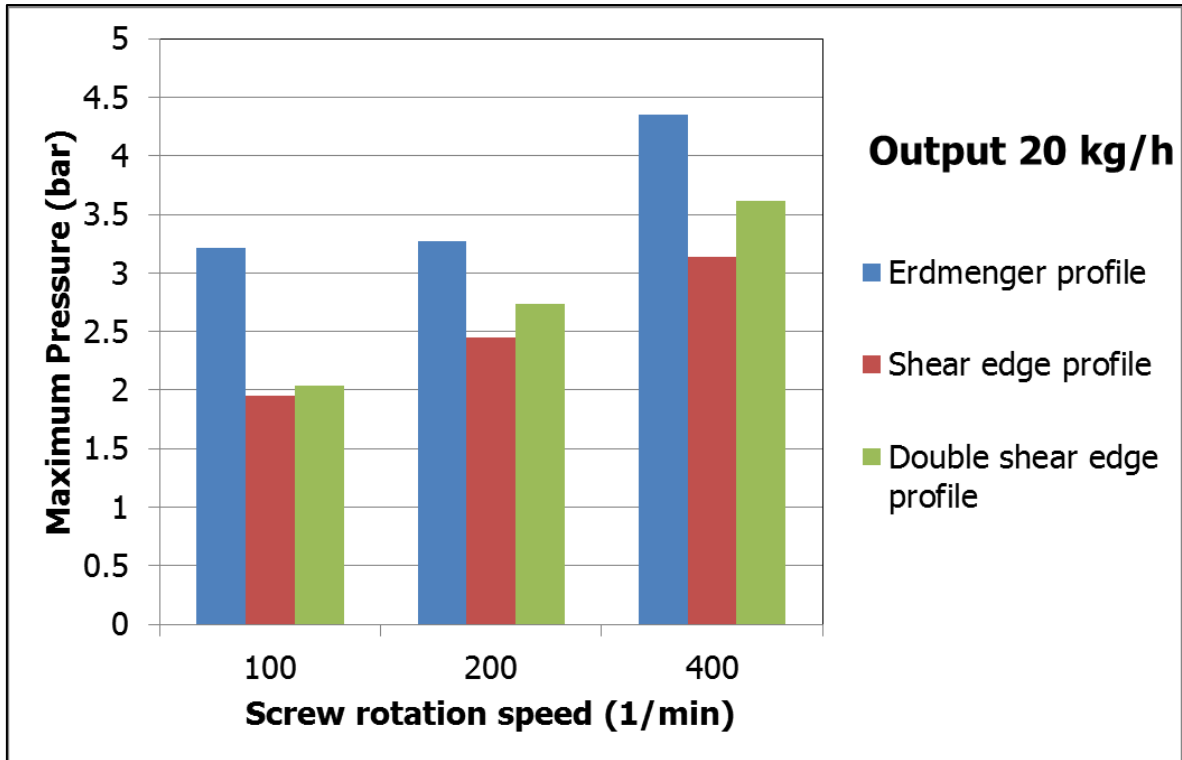


Figure 10.4: Generated max. pressure of different channel profiles at 20 kg/h output and different screw speeds

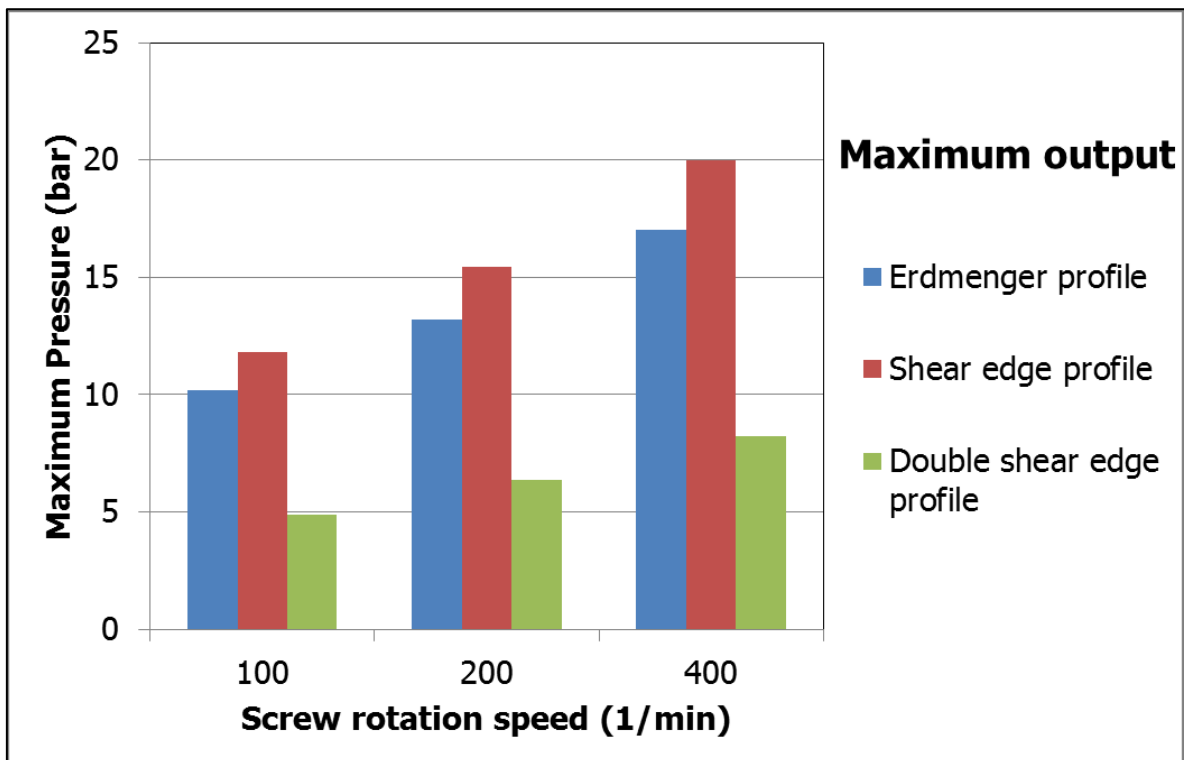


Figure 10.5: Generated max. pressure of different channel profiles at maximum output and different screw speeds

In Figure 10.5 it is clear that the pressure build-up of the shear edge profile is higher than Erdmenger profile and box profile. The geometry of the shear edge profile has advantages of both the Erdmenger (self-cleaning) and double shear edge profile (one undercut for higher free volume). Since the active flight has a Erdmenger channel profile, the conveyance of the melt is good. Moreover the maximum output of shear edge profile is higher than the Erdmenger profile due to the undercut. This is also one of the main reasons for the high pressure generation. Even though the maximum output of the box profile screw element is higher compared to the other two profiles, the pressure generation is less due to poor conveying capacity.

The tendency of pressure build up in case of 40 kg/h at 100 rpm screw speed, is similar to the case of 20 kg/h output (Figure 10.6). The Erdmenger profile generated the highest pressure of 31.27 bar at 40 kg/h compared to the shear edge and double shear edge profile, which generated 19.2 bar and 6.8 bar respectively.

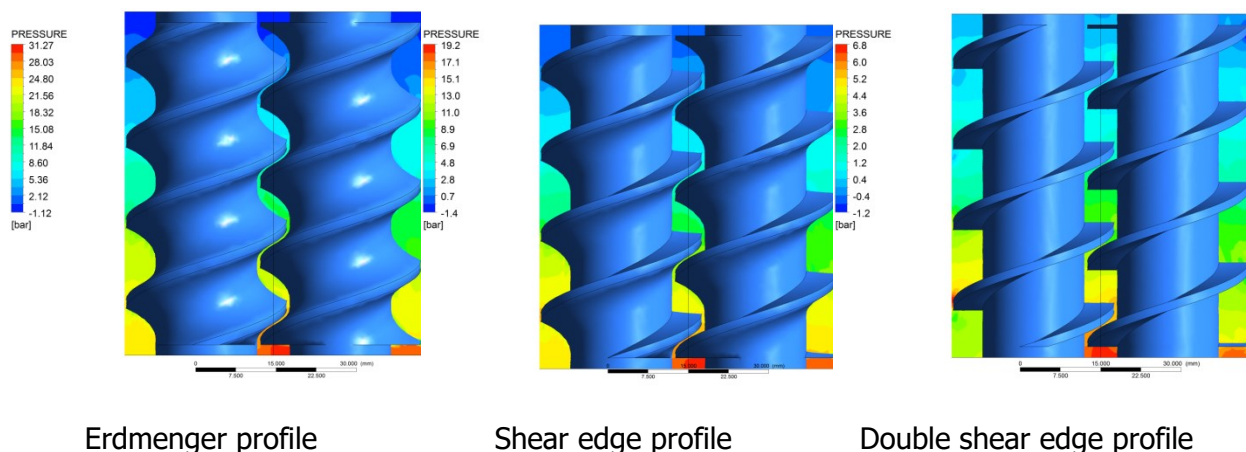


Figure 10.6: Local pressure generation over screw element length for different channel profiles at 40 kg/h and at 100 rpm

The comparison of the pressure build-up of the three channel profiles in the conical co-rotating twin screw extruders were theoretical studied using the MAS 90 screw (Figure 10.7). The metering zone of the MAS 90 screw, with two flights and pitch of 100 mm was numerically calculated for a PET recycled material (material data given in 10.2.3) at 160 rpm screw speed and an output of 600 kg/h. High pressure built-up is obtained with the standard Erdmenger channel profile, similar to the results obtained in the parallel twin screw extruder. At the same screw speed and output the box profile shows minimum pressure generation.

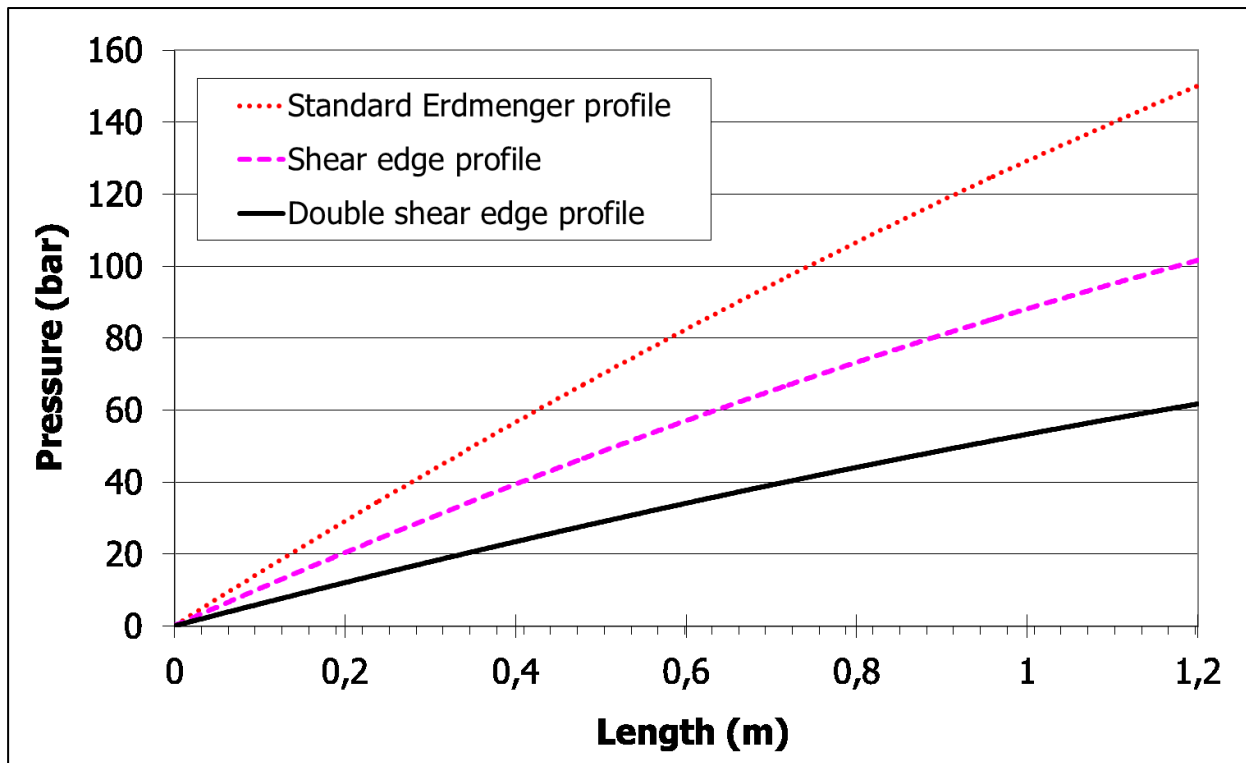


Figure 10.7: Pressure profile over screw length of metering zone of MAS90 extruder at 160 rpm and 600 kg/h for a recycled PET material

10.1.3 Comparison of Shearing and Viscosity

In general the maximum shearing is in the clearance between the screw and barrel or in the intermeshing area of the screws, irrespective of the channel profile.

It can be clearly seen in Figure 10.8 that in general the maximum shearing occurs at the gap between the screw flight and the barrel inner wall. Also high shearing occurs in the intermeshing region of both the screws and the clearance between the flights of the two screws in the intermeshing zone. The LDPE material in the flow channel is subjected to low shearing.

The results (Figure 10.9) show that the maximum shearing of the melt is experienced in case of the Erdmenger channel profile due to the available less free volume. With increase in the screw rotation speed at constant flow rate, the shear rate also increases respectively. In case of volumetric feeding, the shearing decreases with increase in the flow rate at constant screw rotation speed.

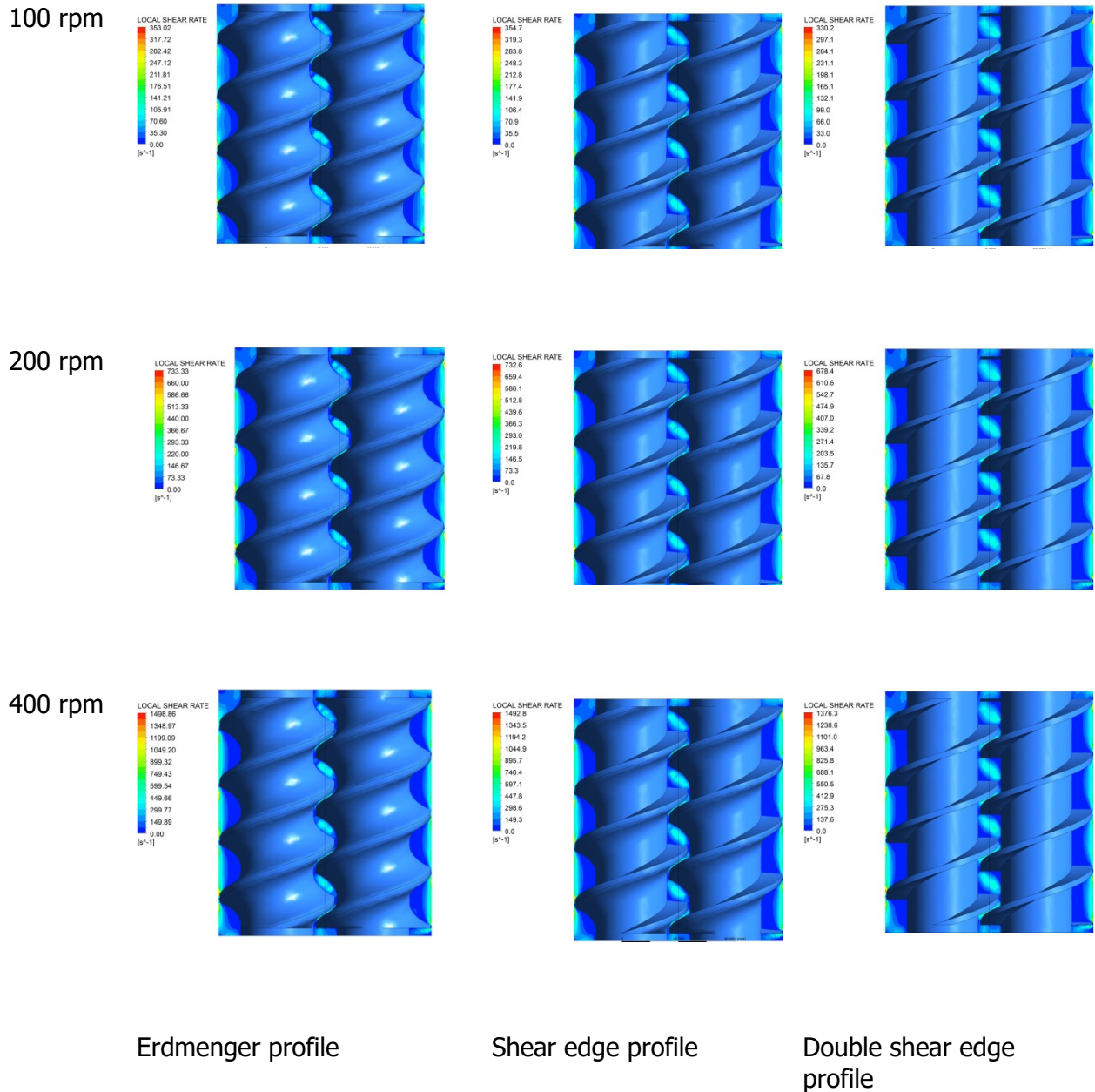


Figure 10.8: Local shear rate at 20 kg/h and at different screw rotation speeds

Figure 10.10 shows that double shear edge profile has very little influence of output on the shearing at constant screw speed. The other two channel profiles show strong reduction in shear rate with increase in output. The box channel profile due to its simple rectangular flow channel show very different shear rates at various screw speed and output compared to Erdmenger and shear edge profile.

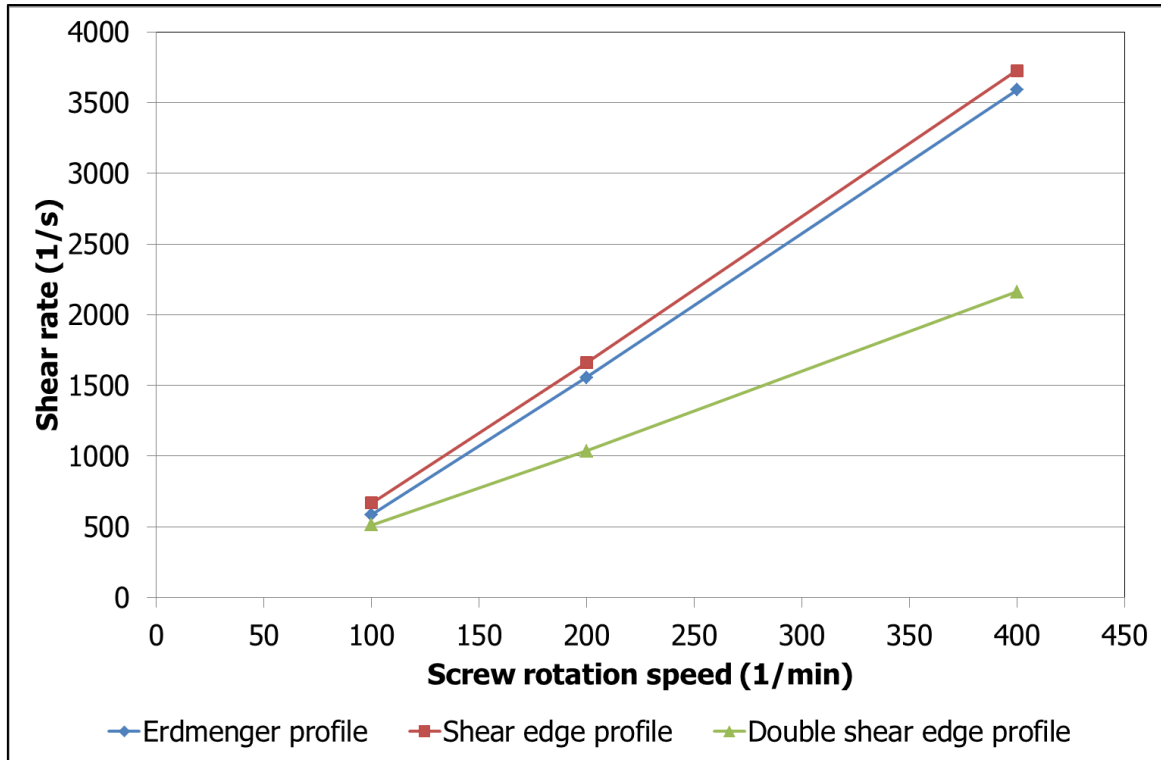


Figure 10.9: Max. shear rate dependence on screw speed at constant flow rate of 20 kg/h

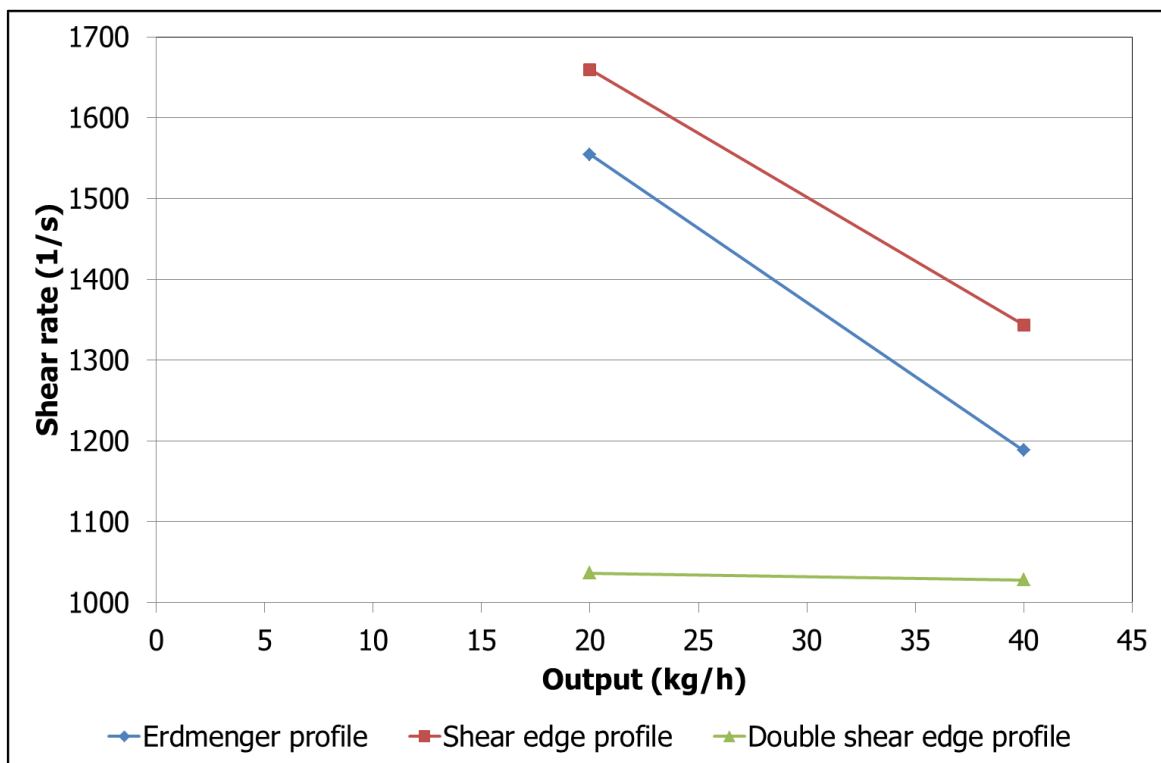


Figure 10.10: Shear rate dependence on flow rate at constant screw speed of 200 rpm

The shearing action has respective effect on the melt viscosity which is shown in following Figure 10.11.

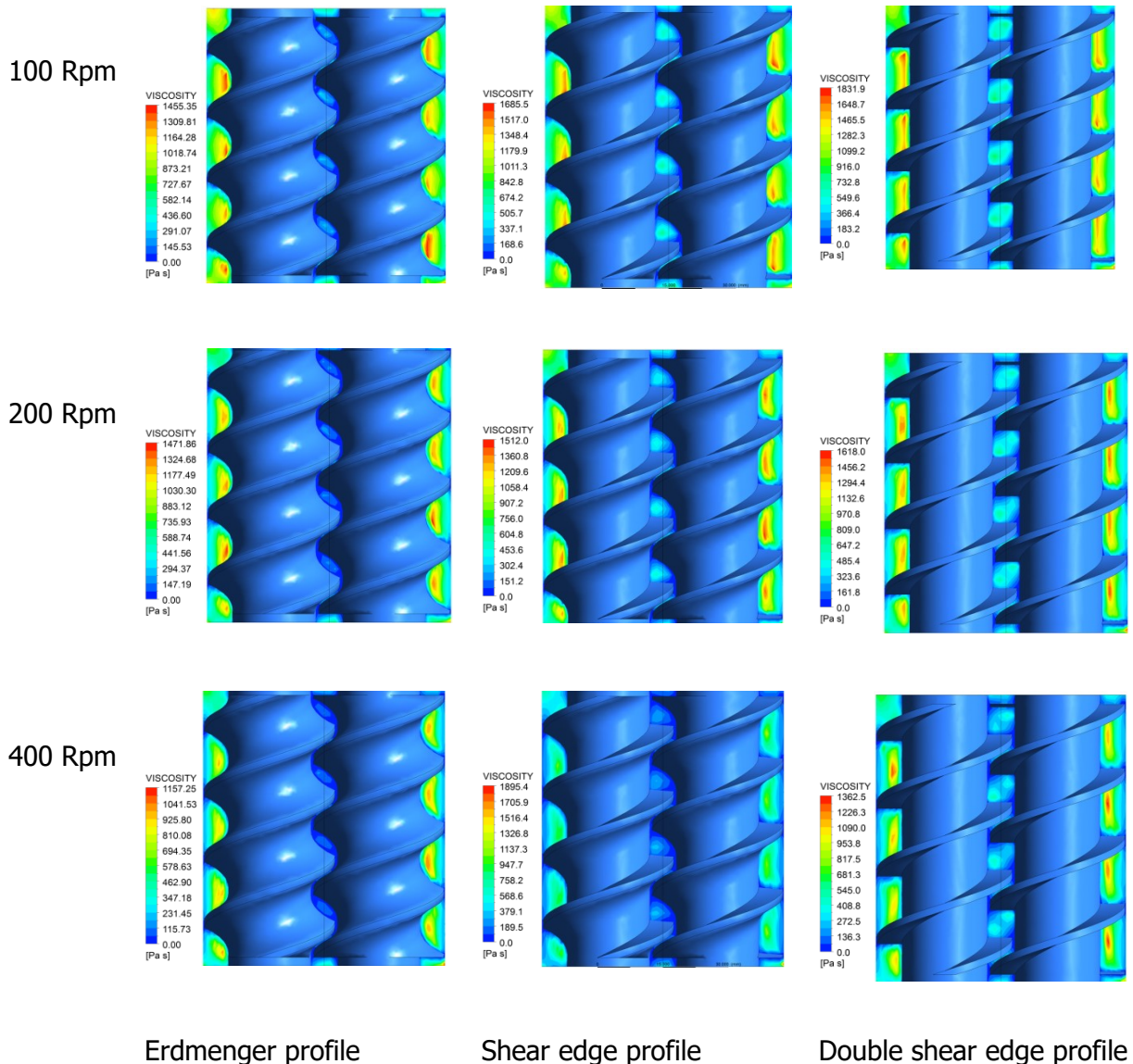


Figure 10.11: Melt viscosity at 20 kg/h and at different screw speeds

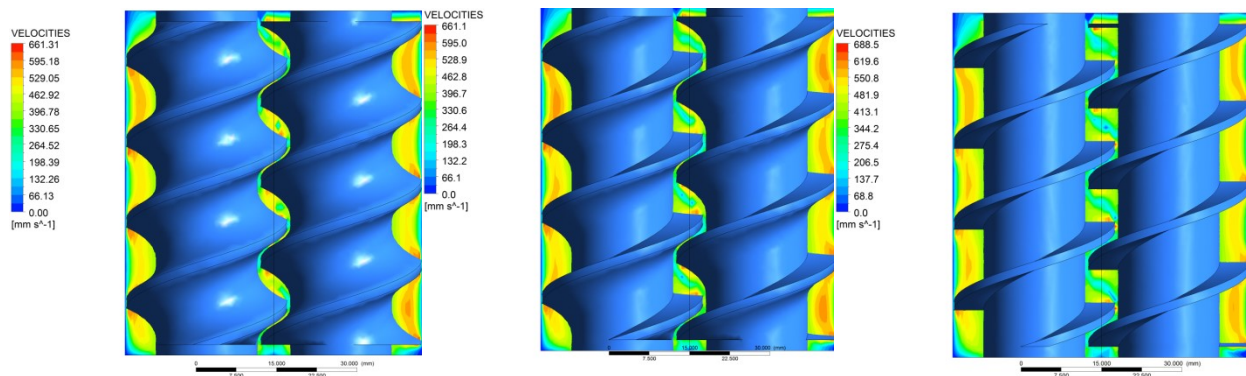
Since the shearing in the middle of the flow channel is low compared to the shearing at the channel walls and in the clearances between the screw flights or screw and barrel, the viscosity is high in the middle of the flow channel. The viscosity is less in the intermeshing area where the shearing is high. The viscosity of the melt is relatively low in the Erdmenger channel profile. In Figure 10.11 it can be clearly seen that the channel profiles influences the viscosity in the nip zones. In case of Erdmenger profile, the viscosity of the melt in nip zone is below 150 Pas at all three screw speeds. This low viscosity is due to high shearing in the screw nip zone. In case of the box profile a high viscosity (>300 Pas at all three screw

rotation speeds) is noticed. The reason is the large flight gap of box channel profile leads to less shearing and thus high viscosity.

10.1.4 Comparison of Flow Velocity

The melt flow velocity is another important parameter which is dependent on the flow channel geometry. An uniform flow profile is very important for the processing and forming of polymer products. In principle the flow velocity near the flow channel wall is minimum and maximum at the middle when considering the thickness of the flow channel.

In the following figure, the melt flow velocities at 400 rpm screw speed and at an output of 40 kg/h for different flow channel profiles are summarized.



Erdmenger profile

Shear edge profile

Double shear edge profile

Figure 10.12: Comparison of flow velocities at 400 rpm and 40 kg/h for different screw channel profiles

More uniform flow velocities can be noticed (Figure 10.12) in Erdmenger channel profile, whereas in the double shear edge and shear edge profile due to the decrease in the self-cleaning efficiency and due to channel geometry the flow velocities in the intermeshing area are slower compared to the melt flow velocity in the flow channel. The double shear edge profile show a maximum local flow velocity of 0.688 m/s, which is higher than the Erdmenger and shear edge profile with a maximum local flow velocity of 0.661 m/s. In Figure 10.12 is can be clearly seen that the flow velocity is maximum at the middle of the channel irrespective of the channel geometry.

10.2 Conical Twin Screw

The outcome of the measurements made on the MAS NCT55 extruder and the theoretical values calculated with help of NCT program are compared and discussed here.

10.2.1 Trail 1 – Comparison of Theoretical and Experimental Results

The measured output and the pressure at the screw tips for trial 1 with varying screw rotation speeds and varying die restrictions are listed in Table 10.1. Since the pressure profile over the screw length was not measured, this trail values were used to model only the metering zone of the NCT55 screw under fully filled condition.

Table 10.1: Experimental results of trail 1

Setting no.	Slit height (mm)	Screw speed (1/min)	Melt temperature (°C)	Output (kg/h)	Pressure P0 (bar)
1	2	150	235	236.9	122
2	2	180	234	219.6	131
3	2	210	231	299	142
4	2	240	235	342	146
5	2	270	235	345	152
6	2.75	150	222	198.6	93
7	2.75	180	223	266.4	104
8	2.75	210	218	297.6	111
9	2.75	270	218	493.8	129
10	3.5	150	209	311.4	88
11	3.5	180	210	373.2	93
12	3.5	210	209	406.5	98
13	3.5	240	205	478	107
14	3.5	270	211	565.2	108

The output as a function of screw speed (Figure 10.13) shows a linear function. Even though the dosing speed was predefined for each process setting to get the metering zone fully filled and to avoid the flow of melt out of the vent, a good linearity in the throughput is achieved with increase in the extrusion screw rotation speed. Higher outputs were achieved with larger slit height due to low flow restriction and low back pressure.

In general the output characteristics dependence on the screw speed for all three die heights should lie parallel to each other (Schuschnigg, 2009). Since the feeding of the material was controlled by the dosing speed, in order to avoid the over flow of the melt out of the vacuum vent, no linear change in output with respect to screw speed was achieved.

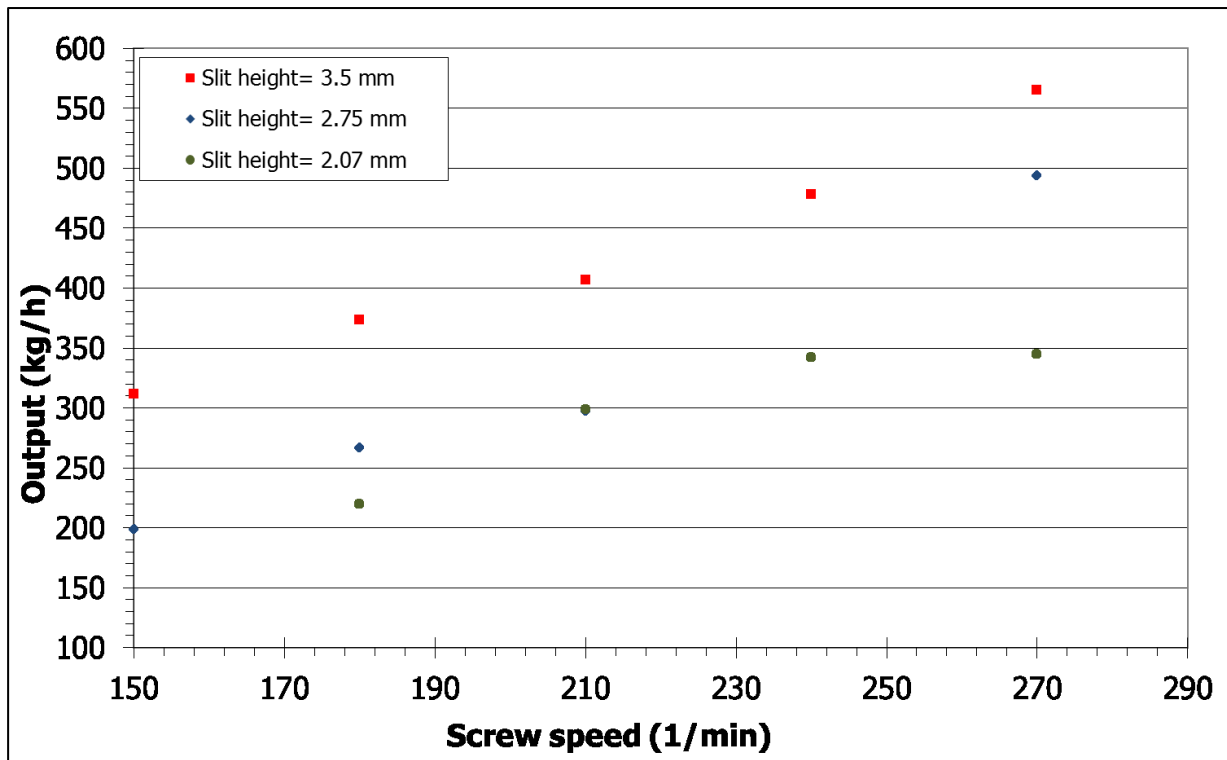


Figure 10.13: Output as a function of screw speed

The melt pressures measured in front of the screw tips and before the filter increases linearly with increase in screw speed and the corresponding output. Higher pressures were measured with the small die gap. From the Figure 10.14 it can be seen that there is no linear change in melt pressure with increase in die height at constant screw speed. The main cause for the non-linear change in melt pressure with respect to the slit die height is the non-linear output and non-isothermal condition. If the feeding hopper is flood fed and the melt temperature is constant, the linear change in the output and pressure with respect to screw rotation speed can be noticed. In case of 2.07 mm slit height the flow resistance is higher compared to the other slit gaps. The higher flow restriction leads to high pressure generation at the die entrance and hence the back pressure length is longer. This leads to longer residence time of the melt in the pressure build-up zone and the melt is sheared more. The high shearing of the melt leads to increase in the melt temperature due to shear heating. The measured melt temperature in front of the screw tip at different screw speeds and slit height is shown in Figure 10.15. The average melt temperature with slit height of 2.07 mm at different screw speeds is 234 °C, which is around 25 °C greater than the average melt temperature measured with 3.5 mm slit height which is due to the high pressure generated by the 2.07 mm slit die, which is around 40 bar more than the pressure generated with 3.5 mm slit die.

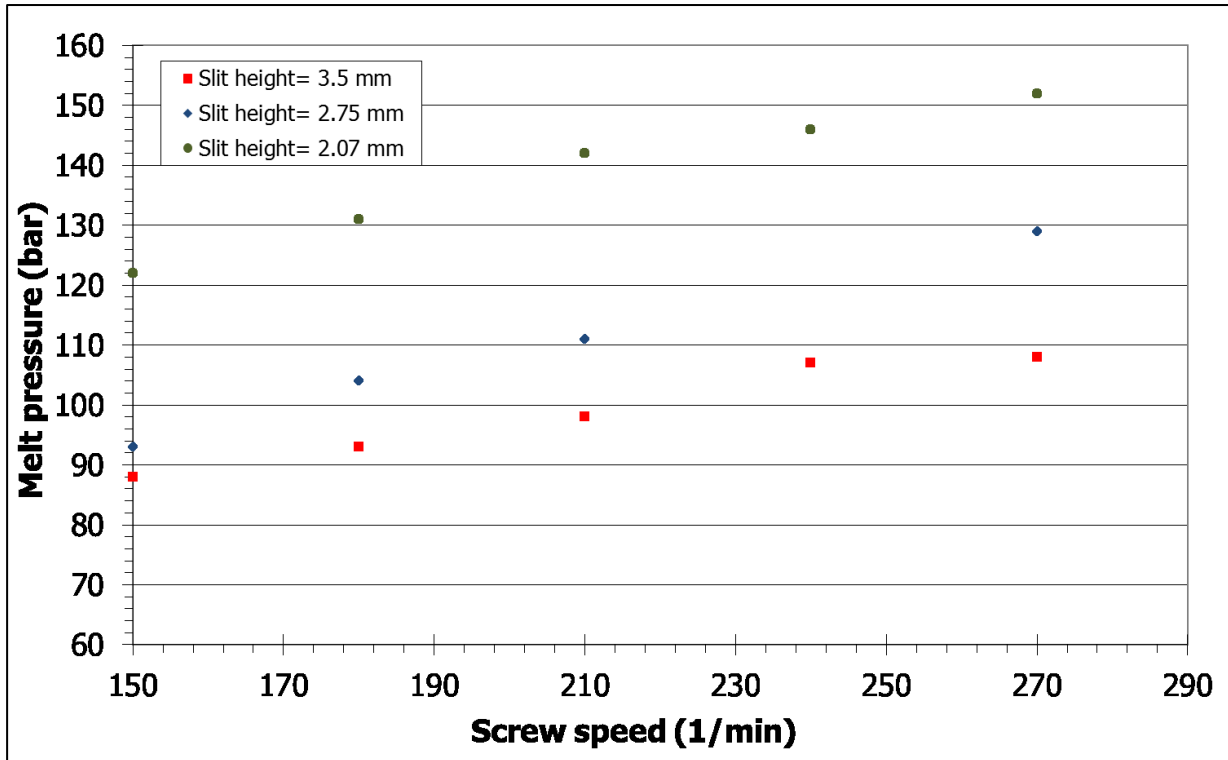


Figure 10.14: Measured melt pressure at different screw speeds and slit heights

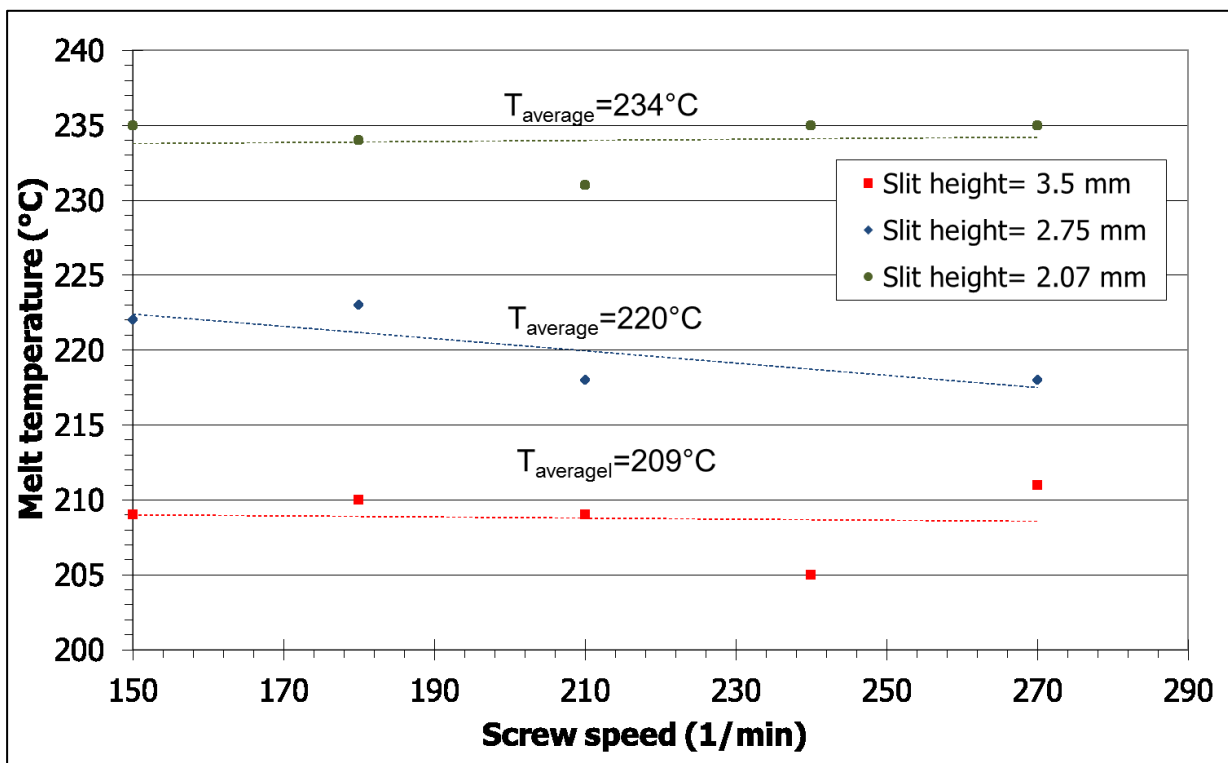


Figure 10.15: Measured melt temperature in front of the die for different screw speed and slit heights

No influence of the increase in the melt due to dissipation in the die occurs in this case, since the temperature is measured before the entrance of the melt into the die.

The pressure characteristics of the conical extruders can be determined by considering the average screw outer diameter over the total screw length. In this calculation the screw end diameter of 55 mm and the metering element length of 575 mm are used for determining the pressure characteristics of the NCT55 extruder. The viscosity of the melt is determined as 736 Pas, using Cross model constants and considering the maximum shearing on the barrel wall at the screw end.

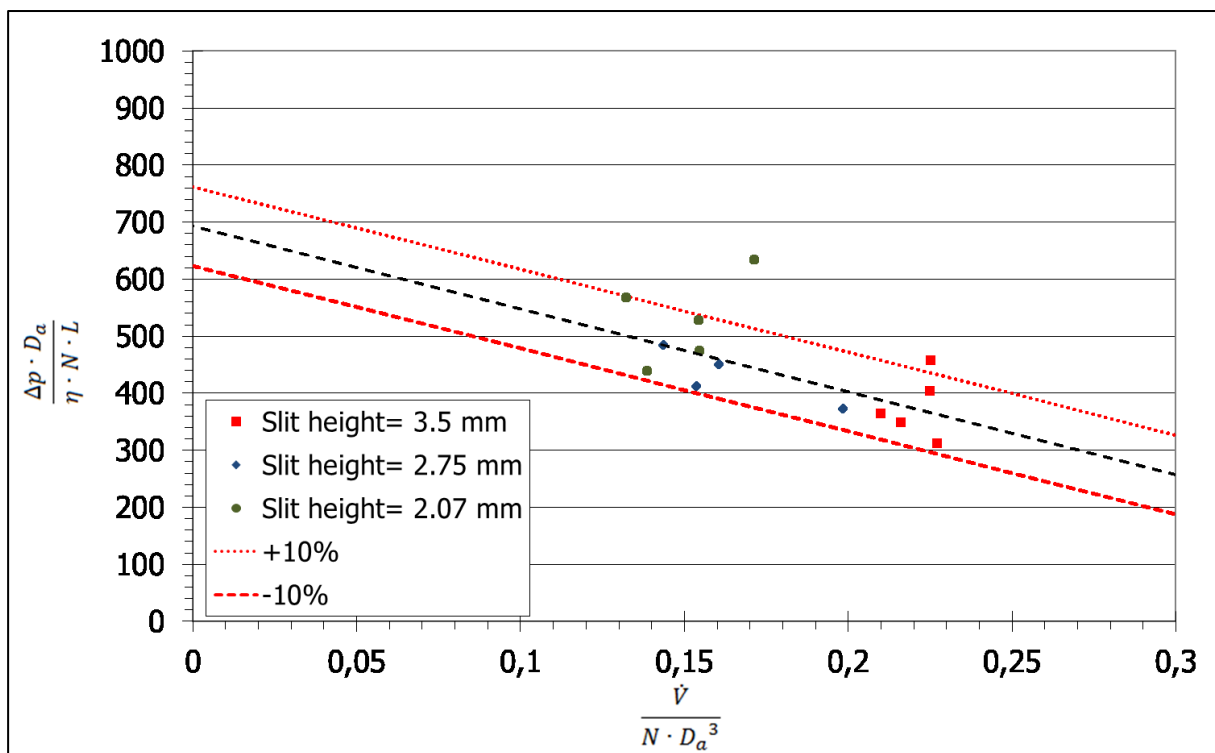


Figure 10.16: Pressure characteristics curve of NCT55

Considering the above pressure characteristics curve, theoretically a maximum of 1300 kg/h output could be achieved when the back pressure is zero and the screw is filled completely. If the throughput per revolution is greater than the inherent throughput, then the screw element is overrun by an element with a larger inherent throughput (Kohlgrueber, 2008). Here in this case the screw is overrun when the throughput is higher than 1300 kg/h and backpressure is zero.

The screw tip pressures are calculated for the settings 1 to 14 (Table 10.1) with NCT V.1.0, considering only the metering screw element of NCT55 under isothermal conditions. The comparison of the calculated and measured pressure values is shown below:

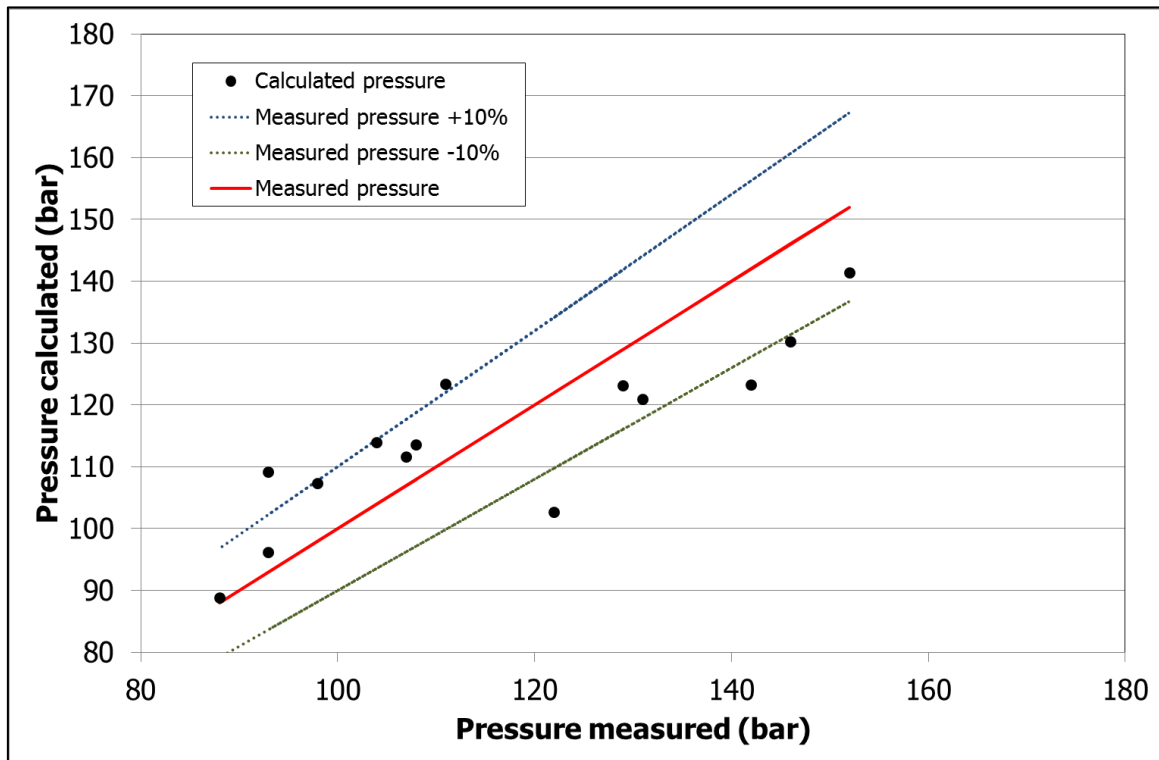


Figure 10.17: Comparison of measured and calculated pressure values – Trail 1

The calculated pressure values lay mostly within the tolerance of +10 % and -10 % of the measured pressure values. The reasons for this deviation could be the non-linearity of the measured pressure values and the die height and the non-linearity of the screw speed to measured output.

10.2.2 Trail 2 – Comparison of Theoretical and Experimental Results

The measured melt pressures at different positions over the screw length for different outputs, die gaps, screw speeds and the corresponding melt temperatures of trail 2 are given in Table 10.2.

The increase in the melt temperature due to shear dissipation in the die is shown in Figure 10.18. Consideration of the melt temperature measured in the die for the simulation can lead to deviation in the modeling of the flow of melt in the screw channels due to the difference in the melt viscosity. The melt viscosity decreases with increase in the melt temperature and can lead to less pressure generation.

Table 10.2: Experimental results of trail 2

Setting no.	Slit height (mm)	Screw speed (1/min)	Output (kg/h)	Melt temperature (°C)	Pressure (bar)					
					P0	P1	P2	P3	P4	P5
1	4	200	300	209	85	71	51	18	2	18
2	4	200	350	209	91	80	60	40	2	32
3	4	200	400	209	93	83	62	45	2	43
4	3	200	300	218	110	95	72	46	2	20
5	3	200	300	216	110	97	60	46	1	20
6	3	200	250	214	106	88	55	27	1	9
7	3	200	200	213	96	75	35	1	0	3
8	2	200	200	228	132	113	76	52	1	3
9	4	200	300	204	93	74	48	15	1	21
10	4	200	350	206	97	82	61	37	1	33
11	4	200	250	205	86	64	34	0	0	10
12	4	200	400	207	98	85	65	45	0	48
13	4	150	300	202	91	77	57	41	0	46
14	4	200	300	205	93	74	46	14	77	20
15	4	200	300	205	93	73	45	12	44	20
16	4	150	300	203	91	77	46	40	77	45

For this reason the measured melt temperature in the adapter is considered for determining the melt viscosity and other flow characteristics in the screw channels respectively.

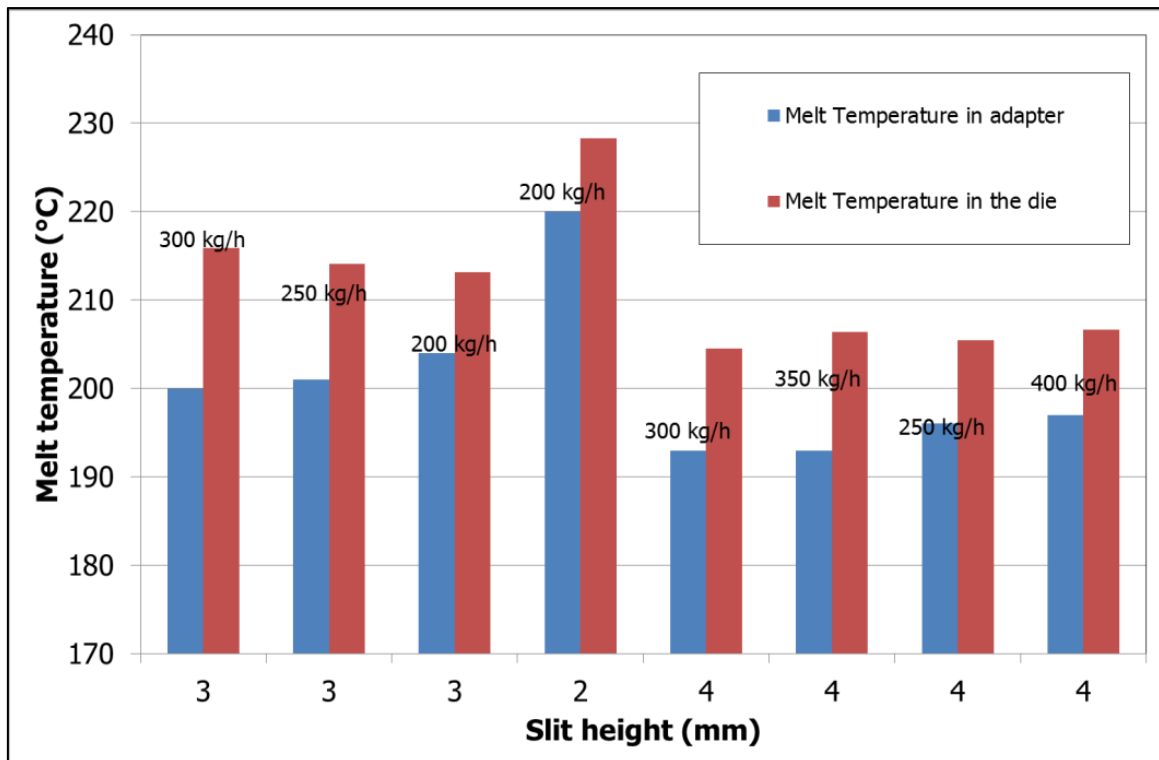


Figure 10.18: Melt temperature in the die and adapter at different flow rates and slit heights

For the measured pressures at different slit heights and at a constant screw speed of 200 rpm, the theoretical throughput was determined iteratively under isothermal condition. The screw characteristic curve shows a linear function (Figure 10.19). The throughput decreases with increase in the screw end pressure. The decrease in the die slit height leads to a high pressure development at low output range. Whereas high throughput can be achieved with larger slit height due to low back pressures. This phenomenon can be clearly seen in the die characteristic curve (Figure 10.19).

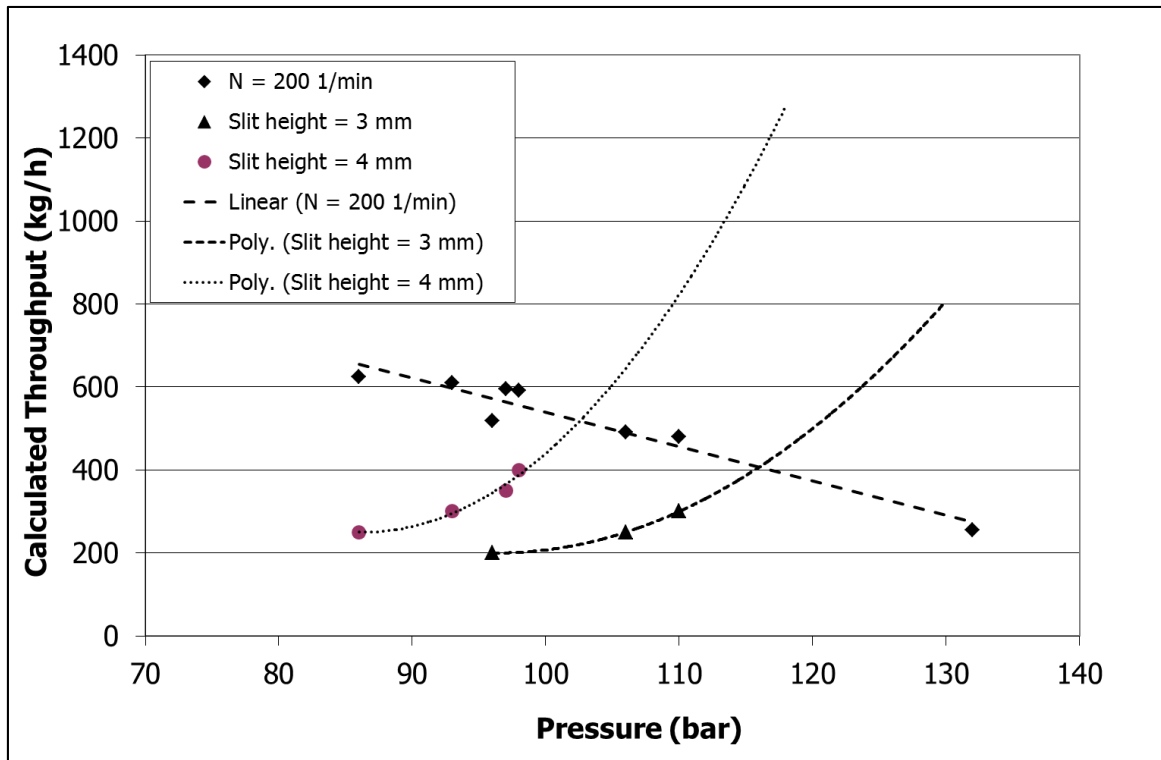


Figure 10.19: Screw and die characteristics curve of NCT 55 extruder

In contrary to trail 1, the melt pressures were measured over the screw length in trail 2. These measured pressures at different axial position serve as reference values to validate the simulated results. The pressure measurement positions over the screw length are shown in Figure 10.20.

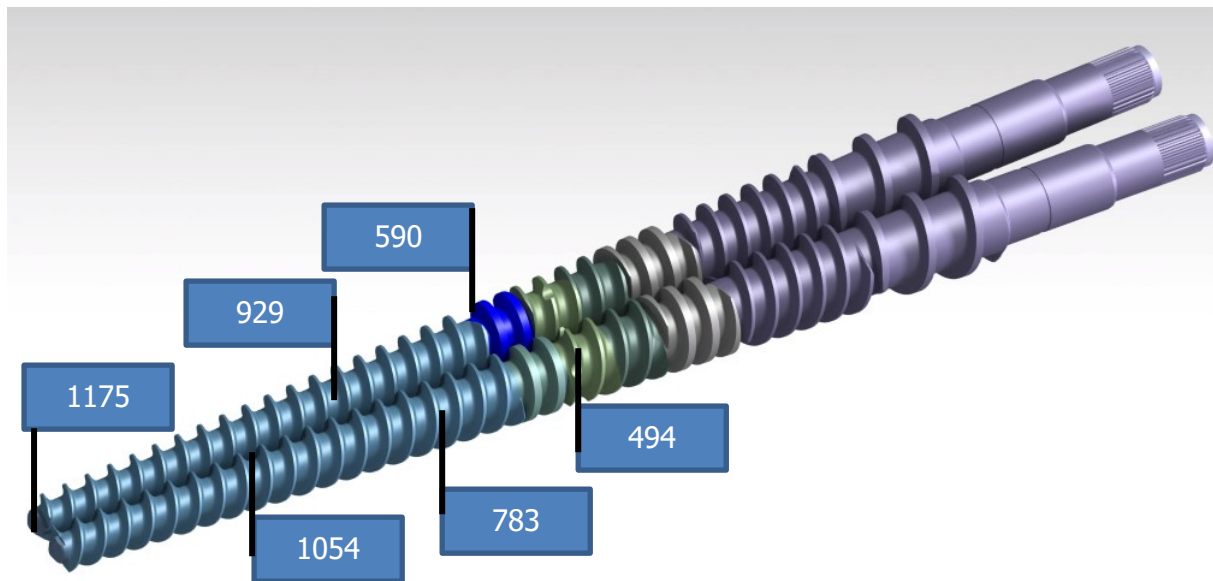


Figure 10.20: Position of pressure sensor over the screw length

Four pressure values were measured from the starting of the metering element until the screw tip. In the metering zone, the pressure sensor at position 783 mm showed 0 bar pressure in case of partial filling or if the back pressure length was not long enough until this position. The maximum pressure was noted at the screw tip (position 1175 mm). Also two pressure transducers were mounted before and after the pressure consuming element (494 mm and 590 mm), blister ring. These measured values and the calculated values were compared, to check the accuracy of the developed model.

Figure 10.21 shows the pressure profile of the pressure built-up zone alone at a slit height of 2 mm, output of 200 kg/h and screw speed of 200 rpm. Under this processing condition the metering zone was completely filled during the practical trial. All the pressure transducers in the metering zone showed pressure values greater than 0 bar. Considering the melt temperature of 228 °C, the pressure profile along the screw length is determined for the given output and the end pressure of 132 bar under isothermal conditions using the developed NCT V.1.0 tool considering F_d and F_p factor and also the leakage and apex flows. The numerical calculation shows that the metering zone is completely filled under this processing condition. Also the measured pressure values and the calculated pressure values show a very good agreement.

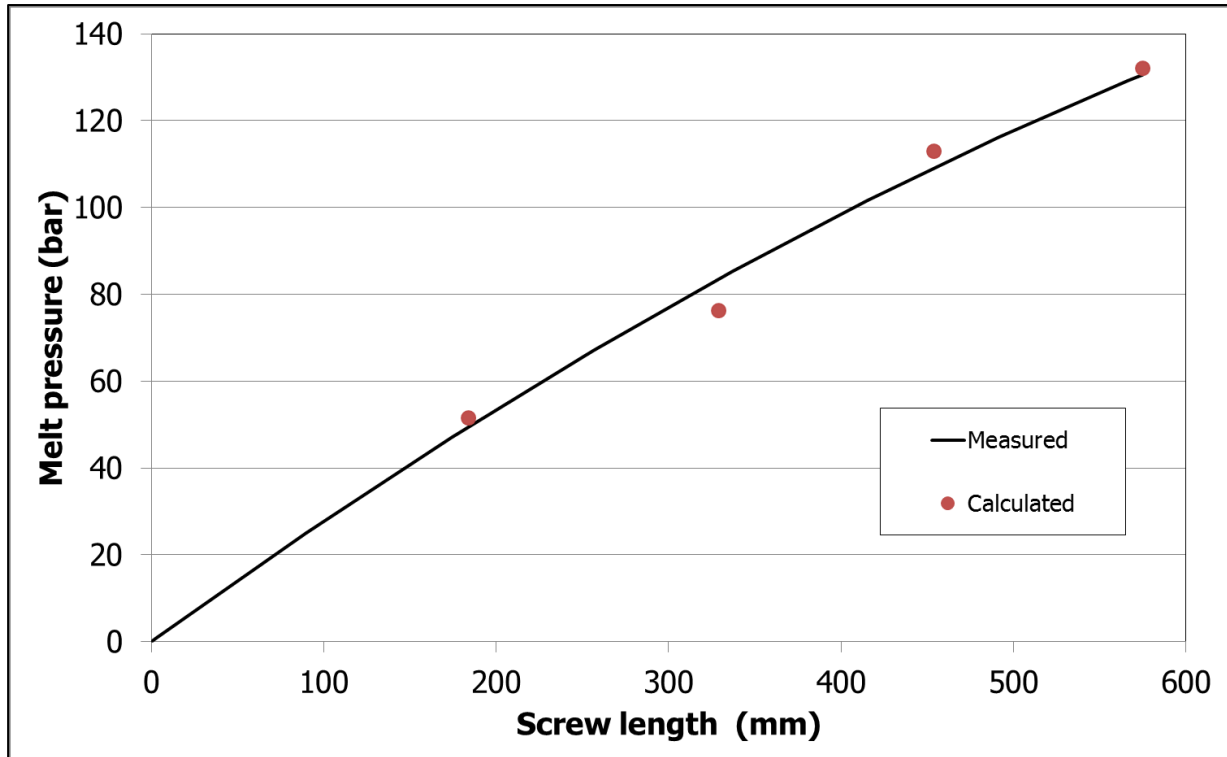


Figure 10.21: Measured and calculated pressure values over the metering zone at 200 kg/h output; 2 mm slit height; 200 rpm screw speed

In case of the 3 and 4 mm slit height different outputs were achieved at same extruder screw speed and varying the dosing speed. These varying throughputs lead to different filling degree in the metering zone. The measured and calculated pressure values at different outputs with 4 mm slit die height are shown in Figure 10.22. A very good agreement between measured and calculated values can be seen. At same slit height at 4 mm and constant screw rotation speed at 200 rpm, changes in the throughput lead to change in the back pressure length. This is effect can be clearly seen in Figure 10.22. At an output of 250 kg/h the generated pressure at the screw tip was 86 bar and the pressure sensor at position p3 showed 0 bar. This indicates that the metering zone is not completely filled under this process setting. The calculated pressure profile show that the back pressure length was 373.2 mm from the screw tip and the rest of the metering zone is only partially filled. As the throughput increases the back pressure and the back pressure length increases respectively. At an output of 400 kg/h the generated pressure is 98 bar and the metering zone is completely filled.

The back pressure length is linearly dependent on the output at constant screw speed. This phenomenon can be clearly seen in the Figure 10.23 showing the calculated back pressure length at different outputs at constant screw speed of 200 rpm and different slit die heights.

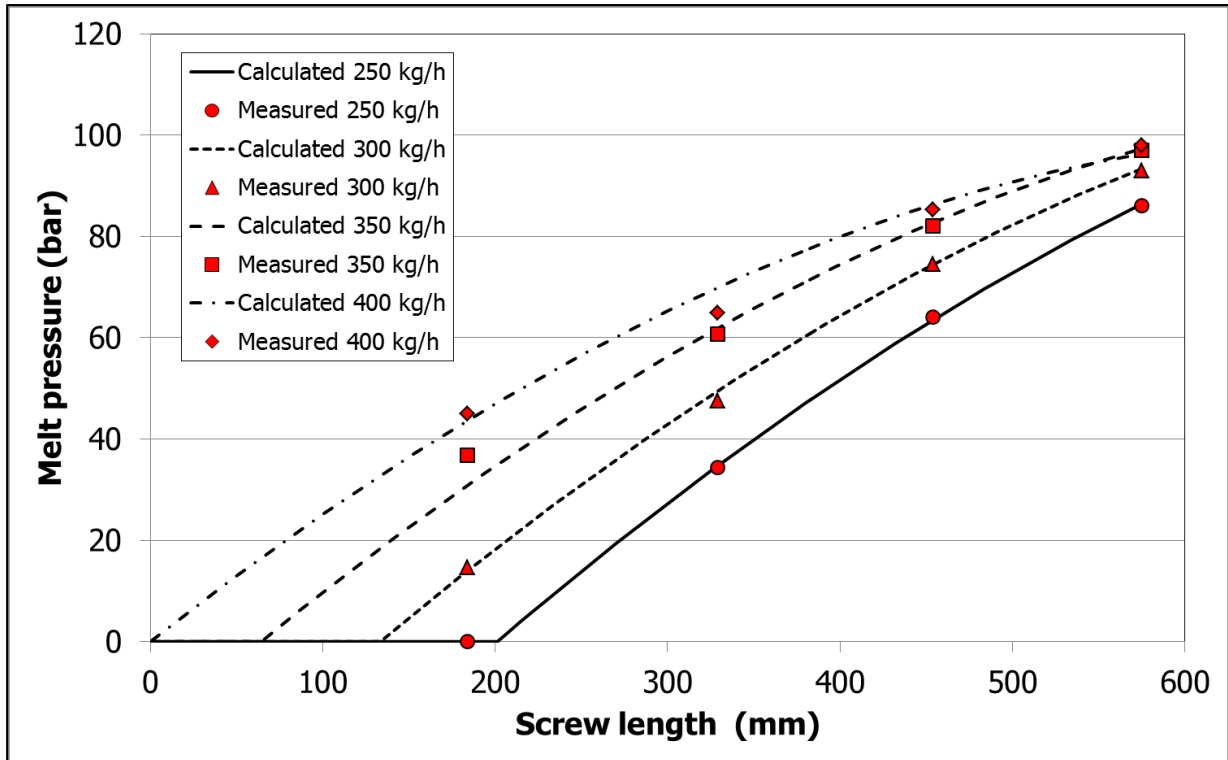


Figure 10.22: Measured and calculated pressure values over metering zone at 200 rpm and 4 mm slit height for different throughputs

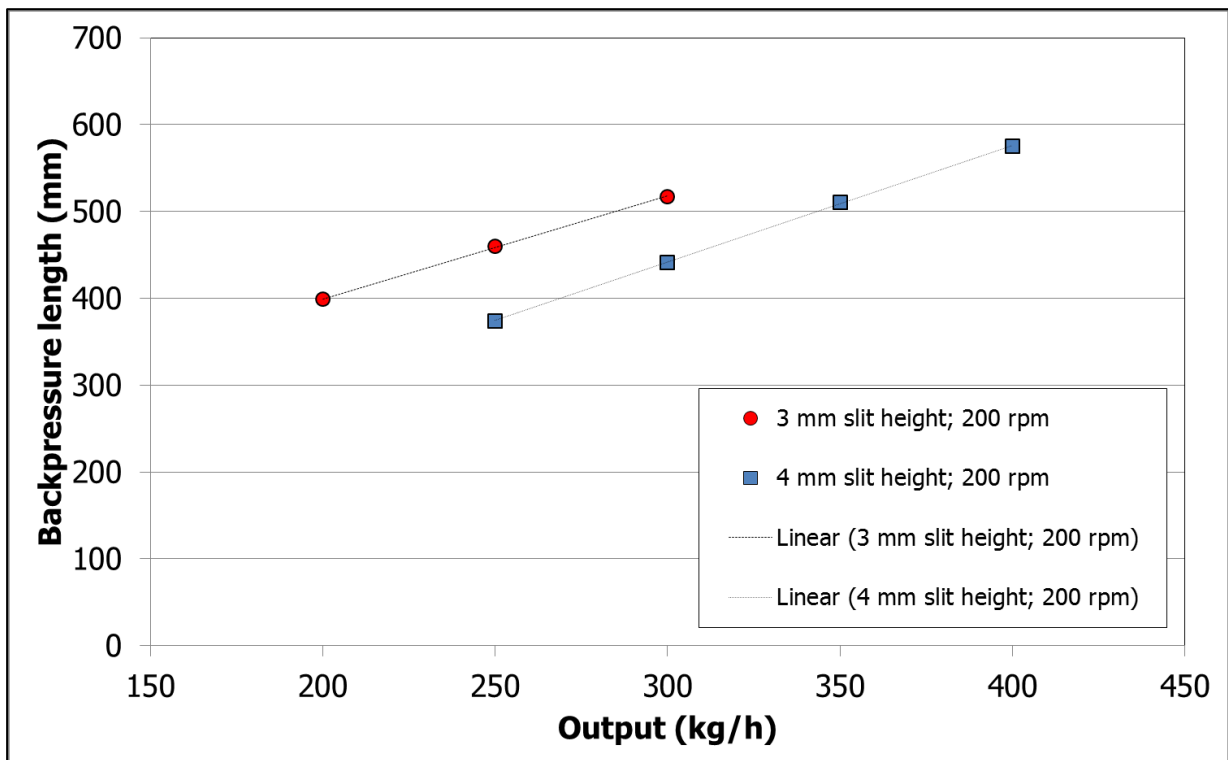


Figure 10.23: Dependence of back pressure length on output at constant screw speed of 200 rpm and slit height of 4 mm

The back pressure length is also dependent on the die geometry. In case of high die resistance the generated pressure is high which leads to a long back pressure length. In Figure 10.23 at an output of 250 kg/h, the back pressure length is 460 mm while using 3 mm slit height due to more pressure generation compared to the backpressure length of 373 mm with the 4 mm die gap.

The calculation of the zones preceding the metering zone and the vacuum vent are also done using the NCT V.1.0. considering the melt temperature in these zones is the same as the melt temperature at the screw tip. The pressure in the blister ring element is initially calculated and the back pressure length for the calculated pressure is estimated in an iterative way. The comparison of the calculated and the measured pressures for the complete screw length at 200 kg/h output, 200 rpm screw speed and using 2 mm slit height is shown in Figure 10.24.

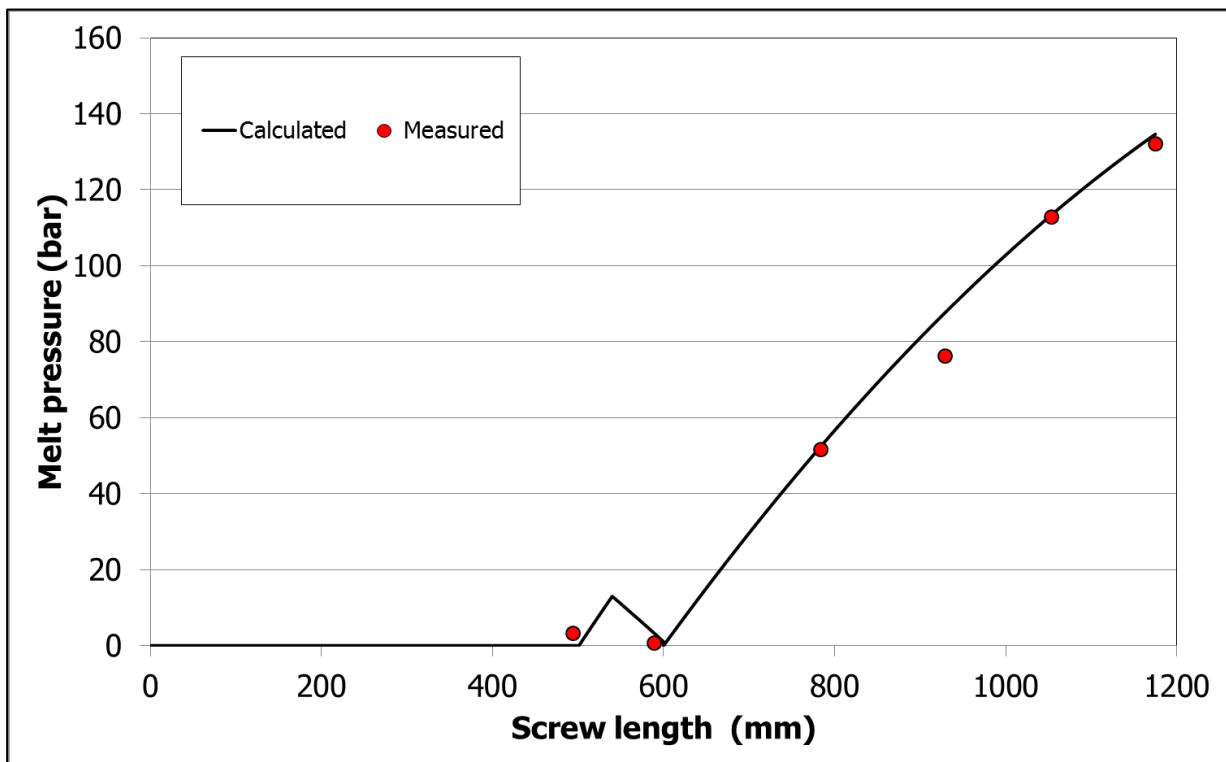


Figure 10.24: Measured and calculated pressure values over complete screw length at 200 rpm, 200 kg/h and 2 mm slit height

The pressures generation at position P4 and P5 (positions 590 mm and 494 mm), before the vacuum vent, is irrespective of the die characteristics. The pressure position P5 is dependent on the back pressure generated by the pressure consuming element (blister ring in this case). The pressure measured at the position P4 was very low or 0 bar, since the generated

pressure is consumed by the blister ring element and at the end of this zone the pressure is zero. More over the vent opening is located next to this pressure sensor position, so the pressure should be zero at this position to avoid the flowing of melt out of the vent.

In case of 200 kg/h output and 200 rpm screw the pressure at P5 was around 3 bar (Figure 10.24). Good correlation between the measured and calculated values can be seen from the graph.

The pressure in the conveying mixing element increased with increase in the output, independent of the slit height used. The degree of fill and the pressure generation in the conveying mixing element is mainly due to the pressure consuming element (in this case a single flighted screw element with narrow pitch). A linear increase in the pressure at position P5 with increase in the output at constant screw speed can be seen in Figure 10.25, irrespective of the slit height.

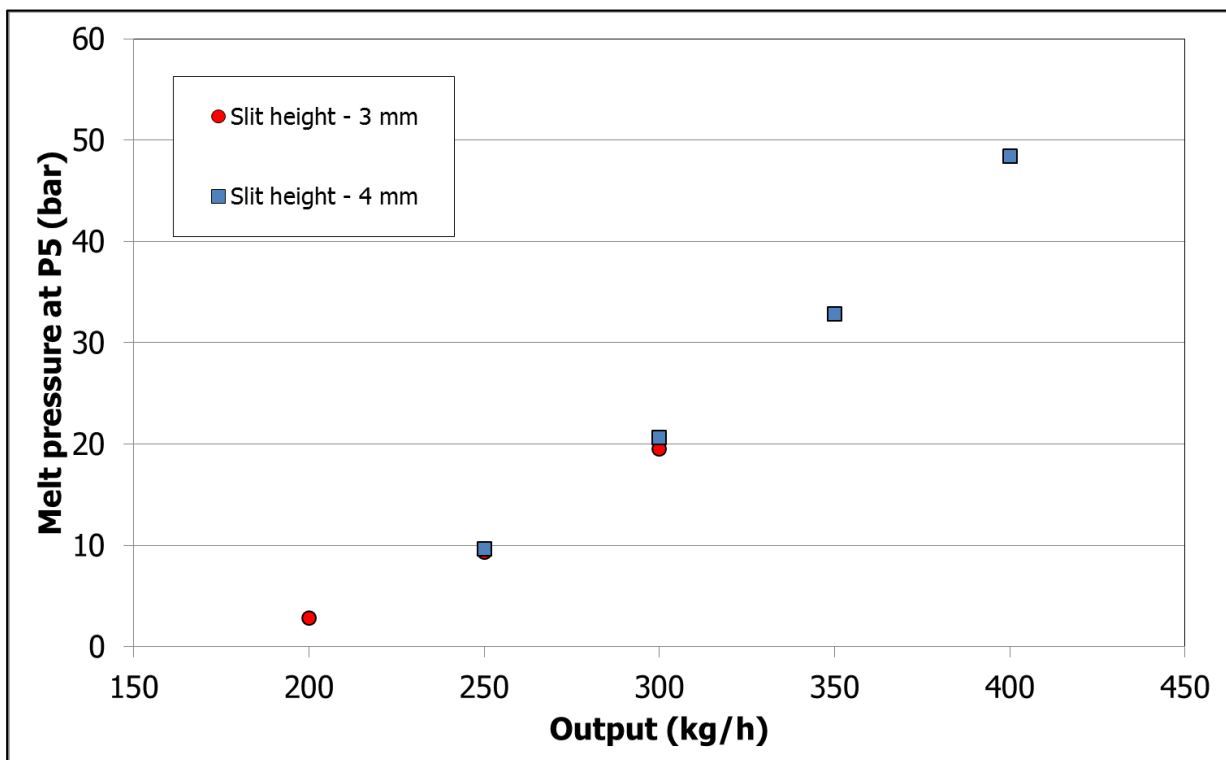


Figure 10.25: Pressure vs. output in the conveying mixing zone

While calculating the pressure in the mixing conveying elements the back flow through the slots in the flights are considered. Good correlation is achieved between the measured and calculated values (Figure 10.26). The measured pressure value at position P5 was 9.31 bar and the calculated value was 8.04 bar. The difference between the measured and calculated is 14%. This deviation in the pressure could be due to the difference in the viscosity of the

melt. In the praxis the melt temperature in the conveying mixing zone is less than the melt temperature at the screw tip, which is 201 °C for this extruder setting. Due to the consideration of higher melt temperature than the actual melt temperature, the viscosity of the melt is reduced and leads to lower pressure values. This deviation can be minimized by calculating the temperature changes of the melt over the screw length and performing the calculations under non-isothermal conditions.

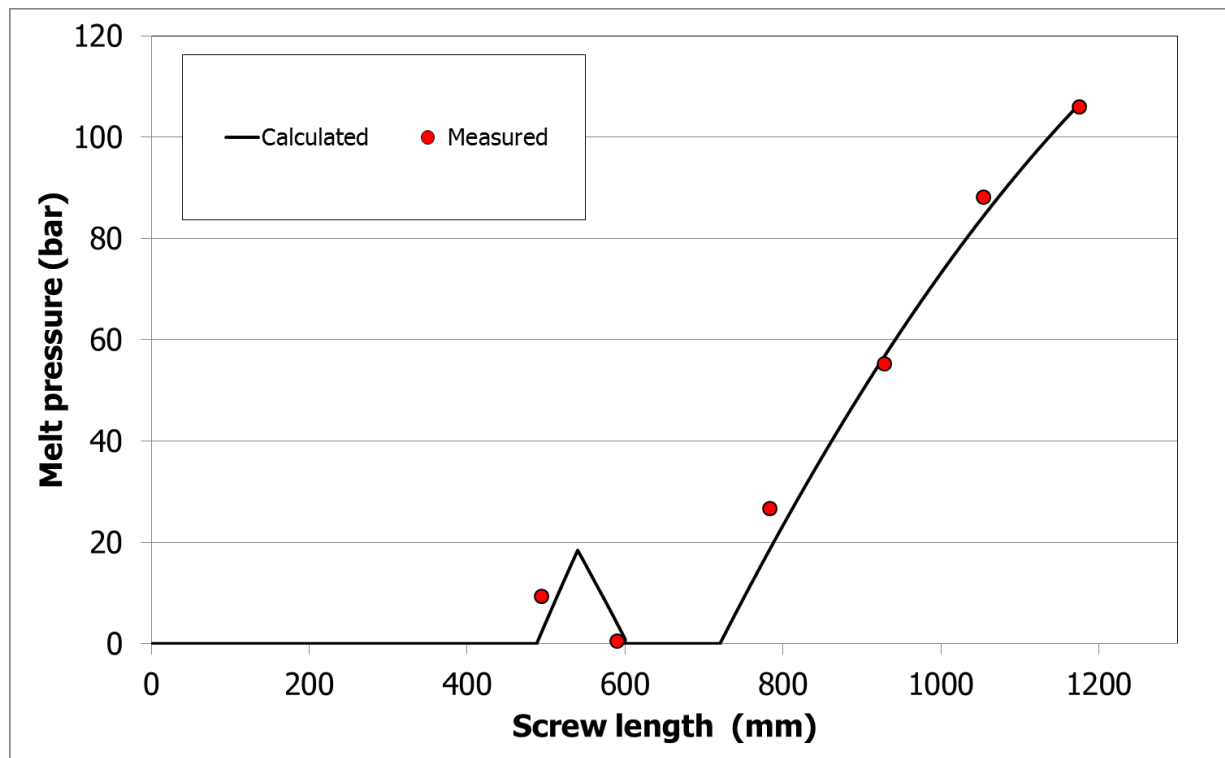


Figure 10.26: Measured and calculated pressure value over complete screw length at 200 rpm, 250 kg/h output and 3 mm slit height

10.2.3 Scale Up NCT 90 – Metering Zone

Since the results of the melt conveying model for the metering zone of the NCT 55 extruder had a good correlation with the experimental data, a scale up of the NCT 90 extruder metering zone was done to analyze the maximum pressure built-up capacity of the zone and to optimize the geometry.

The influence of different screw geometric and processing parameters on the pressure built-up of NCT 90 metering zone was theoretically determined, considering that the zone is completely filled. The scaled up values of the NCT 90 pressure built-up zone are compared with the NCT 55 in Table 10.3.

Table 10.3: Scale up geometry of NCT 90 pressure built-up zone

Geometric Parameters	NCT 55	NCT 90	Unit
$D_{a,start}$	82.01	128.89	mm
$D_{i,start}$	56.61	88.36	mm
$D_{a,end}$	54.1	87	mm
$D_{i,end}$	32	54.3	mm
$\frac{D_a}{D_i}$	1.45	1.46	-
$L_{element}$	575	1200	mm
t	60	100	mm
n	2	2	-
s_r	0.2	0.5	mm

The material used for this calculation is a recycled PET material (from the PET bottle waste), which was processed and granulated on the NCT 55 extruder. The melt density of the recycled PET is 1179 kg/m³ and the Cross Arrhenius model viscosity constants for the recycled material at 285 °C melt temperature are shown below:

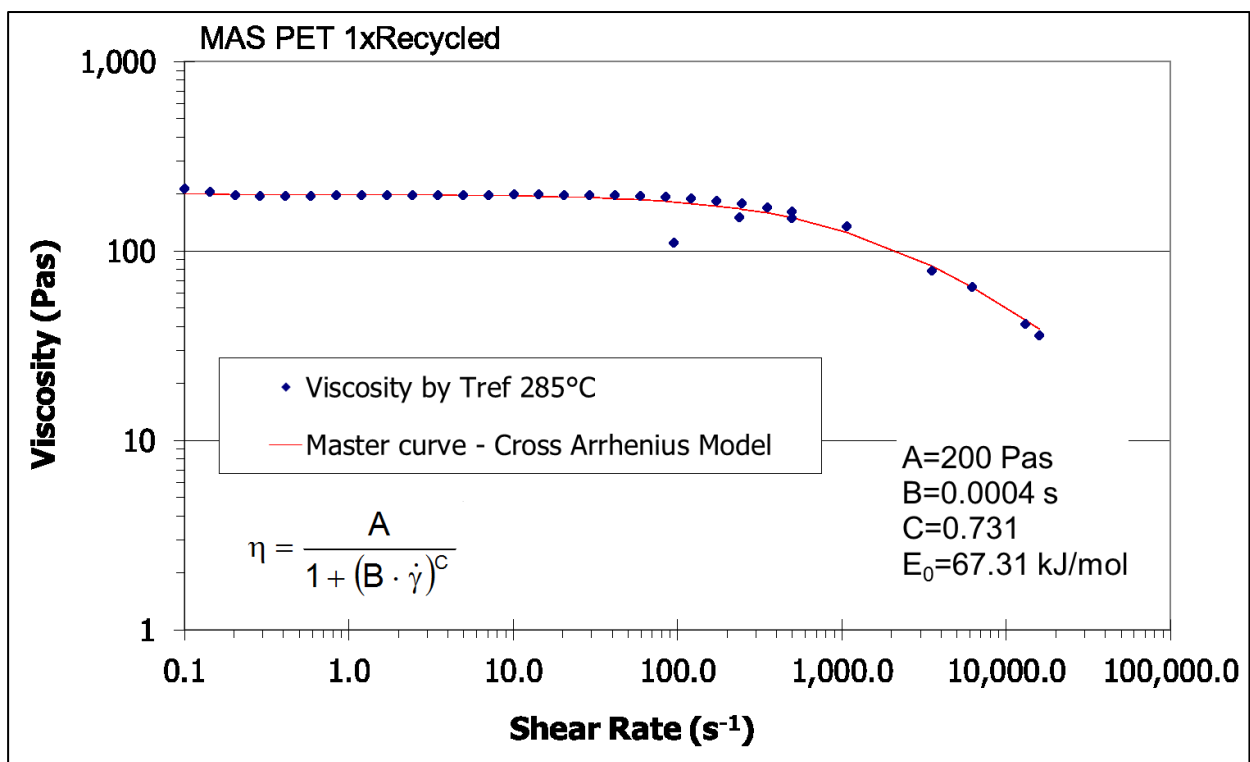


Figure 10.27: Shear viscosity of recycled PET (Arbeiter, 2011)

Initially the dependence of the throughput on the pressure built-up of the metering zone of the NCT 90 extruder was theoretically determined for the geometry given in Table 10.3 at constant screw speed using NCT V.1.0. At constant screw speed and varying throughputs, under fully filled condition the pressure at the screw tip decreases with increase in the output (Figure 10.28). The theoretical results show a typical screw characteristic curve of the screw extruder. A linear relationship can be seen between the throughput and the pressure. The maximum conveying efficiency of the screw is achievable when the back pressure is lower. At a constant output, an increase in the screw speed leads to increase in the pressure.

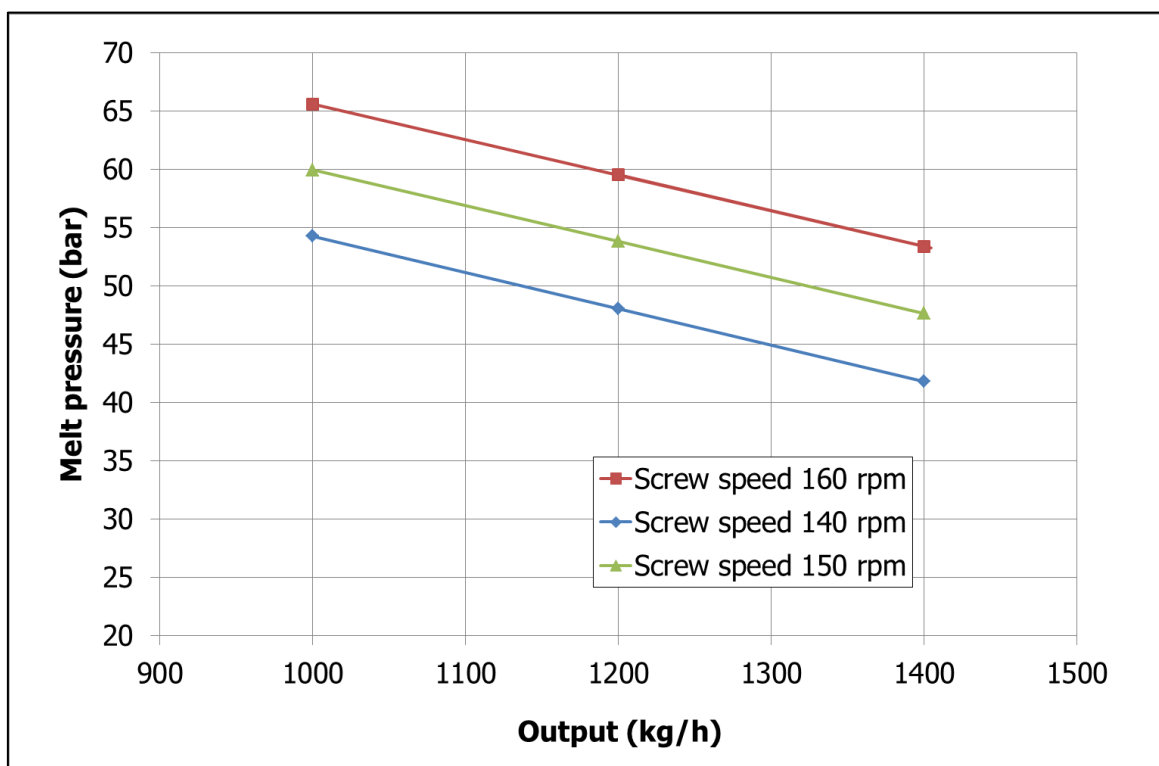


Figure 10.28: Effect of extruder output on the pressure of the NCT 90 pressure built-up zone at constant screw speed

Figure 10.29 shows the influence of the change in the screw pitch of the double flighted pressure built-up zone of the NCT 90 extruder. As could be seen in the figure the pressure built-up increases with decrease in the pitch. As mentioned by Kohlgrueber (2008) the pitch of the screw does not affect the cross sectional area but influences the free volume of a screw channel. The larger the screw pitch, the greater the free volume in the screw element. There is an optimal pitch for a certain throughput and screw speed (Schuler, 1996). When considering the pressure built-up element with different pitch lengths at a constant output

rate, increase in the pitch generates more pressure up to a certain extent and then the pressure drops over the optimal pitch. Using the optimal pitch will lead to optimal throttle coefficient (a_{coeff}) and the maximum pressure built-up.

The number of flights has a huge influence on the pressure built-up of the metering zone (Figure 10.30). Usually the metering zone is designed with a maximum possible number of flights in order to have low energy dissipation in the clearances and also to achieve a small flight width.

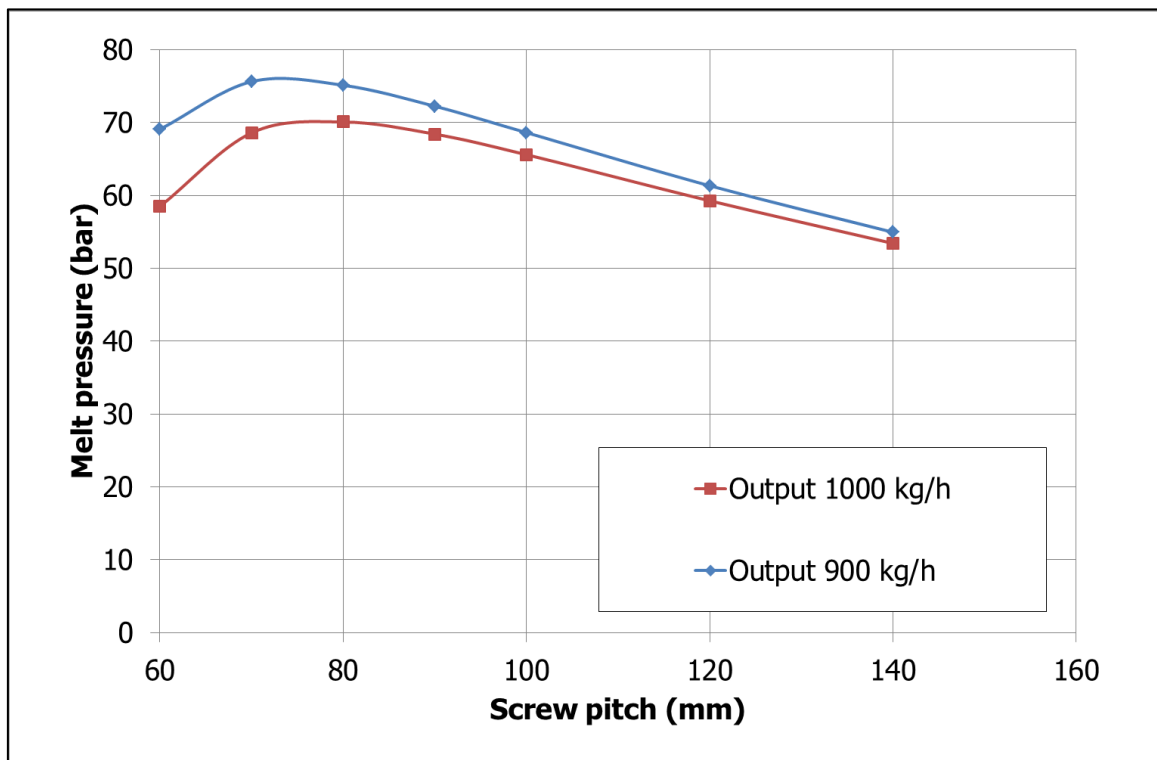


Figure 10.29: Effect of screw pitch on the pressure of the NCT 90 pressure built-up zone at screw speed of 160 rpm

According to Kohlgrueber (2008) the single- and double-flighted elements with closely intermeshing profiles can be used in large volume screw elements. Also elements having more flights have larger radial clearances and are therefore not completely self-wiping. As can be seen in the Figure 10.30 the number of flights has no linear change in the pressure built-up due to the increase in the leakage flow through the clearances with increase in number of flights. Moreover the free volume of the pressure built-up element depends mainly on the number of flights. The free volume of the element is higher with double flight than single flight. The optimal number of flights for the pressure built-up element is two.

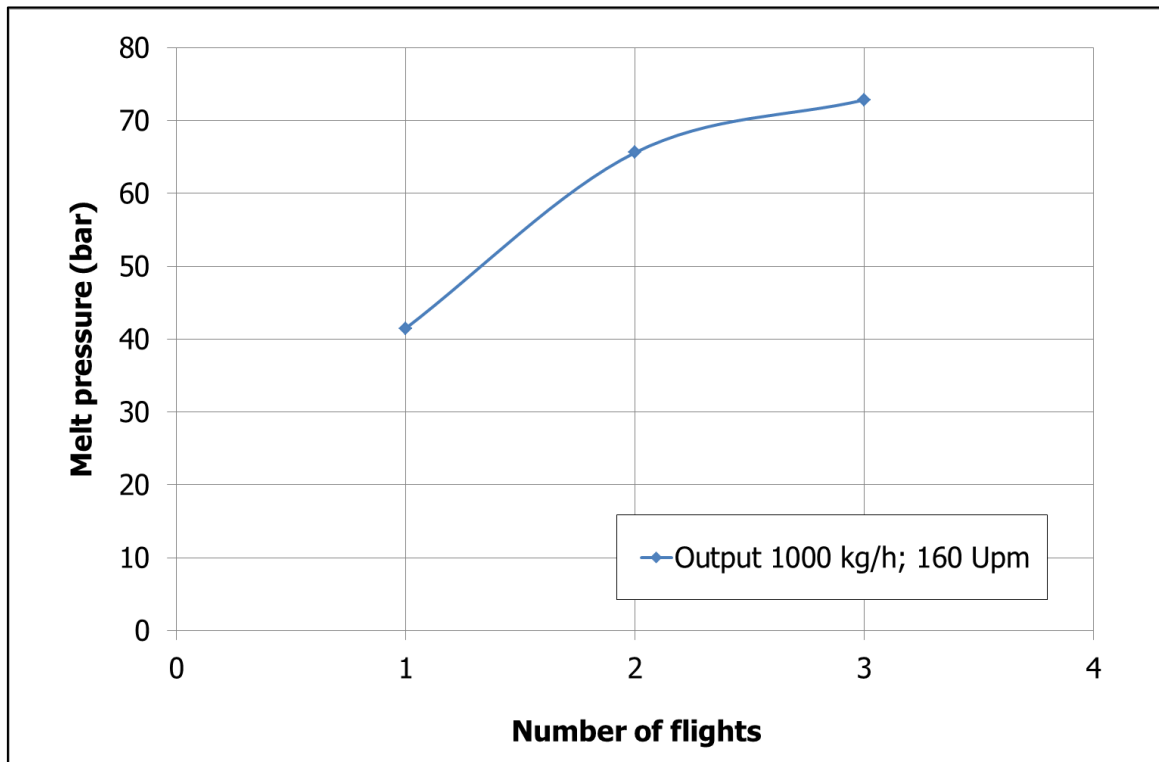


Figure 10.30: Effect of number of flights on the melt pressure generation of the NCT 90 pressure built-up zone at screw speed of 160 rpm and 1000 kg/h output

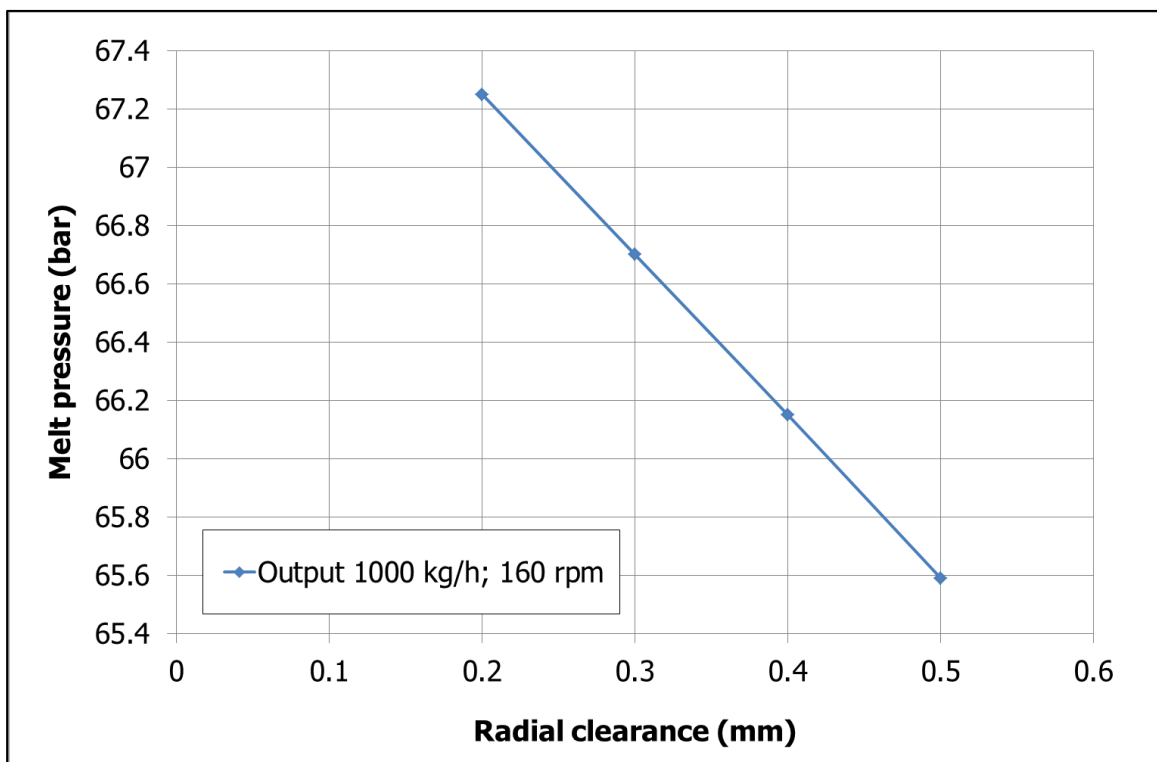


Figure 10.31: Effect of radial clearance on the pressure of the NCT 90 pressure built-up zone at screw speed of 160 rpm and 1000 kg/h output

The radial clearance has a very little influence on the pressure built-up, which can be seen in the Figure 10.31. The increase in the radial clearance leads to more leakage flow through the gap, which reduces the pressure generation. Moreover as mentioned already, the increase in the radial clearance also reduces the self-wiping effect of the screw element. But a minimum clearance between the screws and the screw and barrel is very important in order to avoid the mechanical contact between the elements and hence avoid the wear of screw and barrel.

The increase in the screw rotation speed leads to a linear increase in the pressure built-up at a constant flow rate and constant melt temperature. The screw speed has influences on the melt viscosity and the drag flow rate.

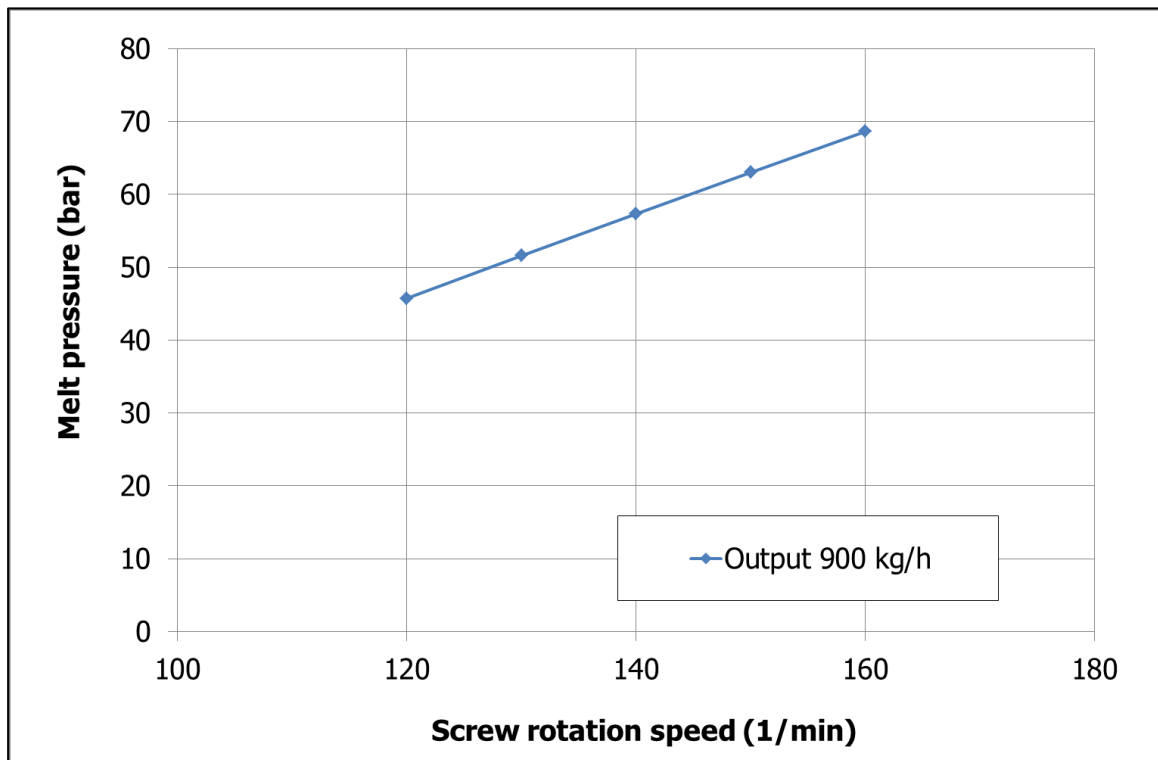


Figure 10.32: Effect of screw rotation speed on the pressure of the NCT 90 pressure built-up zone at a constant output of 900 kg/h and melt temperature of 285 °C

10.2.4 Solid Conveying and Melting

The total number of particles of LDPE with an average diameter of 3.7 mm, which can occupy the channel volume in the feed zone calculated with a maximum channel depth $h_0 = 13.65$ mm, screw diameter $D_a = 109.4$ mm, pitch $t = 60$ mm and number of flights $n = 2$ calculated using the equation 5.37 for different particle alignment is shown in Figure 10.33.

Table 10.4: Material data of PE-LD 159AC for solid conveying and melting

Parameter	PE-LD 159AC	Unit
Bulk density	598	kg/m ³
Diameter of particle	3.75	mm
Internal friction in powder state	0.13	-
Coefficient of friction of screw surface	0.047	-
Coefficient of friction of barrel surface	0.069	-
Angle of steady shear flow of loose material	30	°

The area centered particle alignment gives the maximum packing density and this alignment is used for the solid conveying and melting calculation in this work. The packing density is only dependent on the mean particle diameter. Due to this the calculation can be implemented for granulates with different bulk densities.

For calculating the solid conveying and the melting the material data of LDPE LD159AC given in the Table 10.4 is used. The friction co-efficient values for the LDPE material were taken from the literature (Potente, Melisch, & Palluch, 1996), due to unavailability of respective instruments to measure the friction co-efficient of the polymers used in this work.

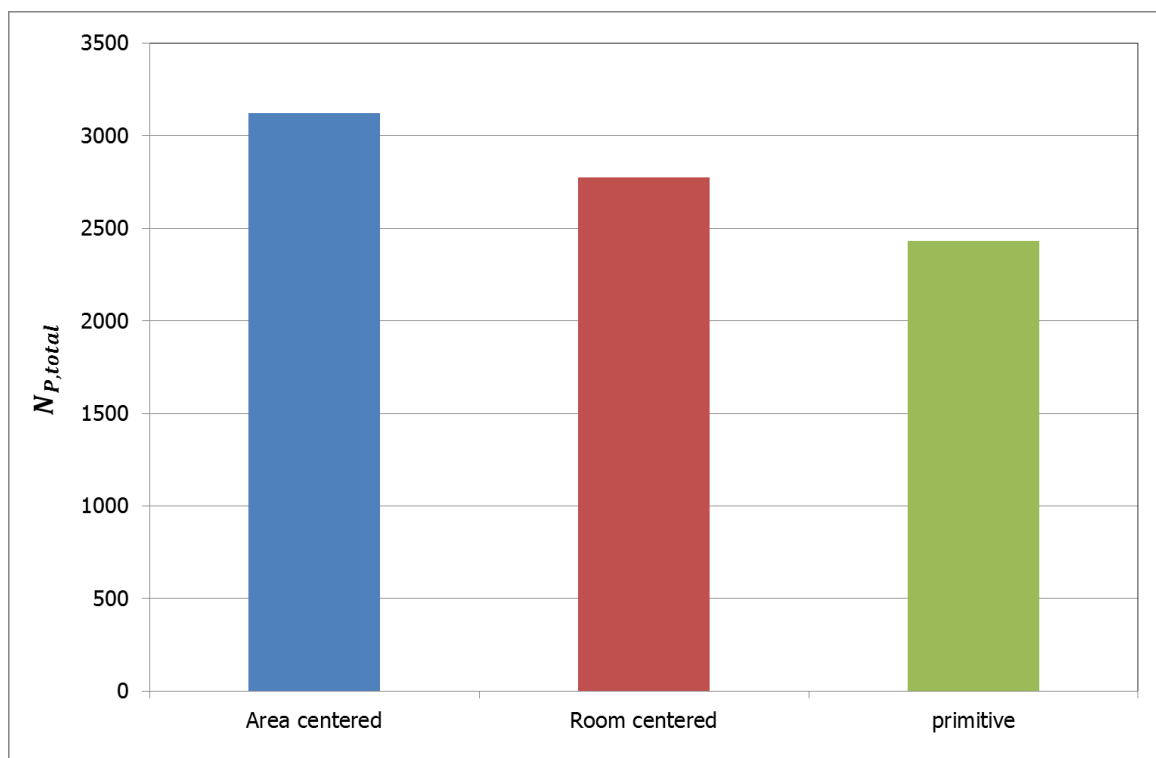


Figure 10.33: Total number of particles dependent on the particle alignment for LDPE

The geometry of the solid conveying or the feeding zone of NCT 55 is given in Table 10.5. The feeding element has a total length of 330 mm. The initial 170 mm is single flighted with a pitch of 60 mm and the following 160 mm is double flighted and has a pitch of 60 mm. Even though the single flighted element has less free volume, this element is used in the feed section due to its good conveying effect. This is especially good when extruding material with low bulk density (for example regrinded PET flakes or regrinded sheets or films). The second half of the feed element with the two flights provide more free volume and also compress the loose feedstock within the flow channel and this removes the entrapped air between the loose material.

Table 10.5: Feedzone element geometry of NCT 55

Geometric Parameters	NCT 55	Unit
$D_{a,start}$	109.4	mm
h_0	13.65	mm
$L_{element}$	170/160	mm
t	60/60	mm
n	1/2	-

The influence of the pellet diameter on the maximum solid bed width for different channel geometries of double flighted elements are calculated according to equation 5.5 - 5.7 is shown in Figure 10.34. The maximum pellet diameter, which can fit the flow channel, is the maximum channel depth. For screw elements with Erdmenger profile, the maximum solid bed reduces drastically with increase in the particle diameter. In case of box profile the solid bed width is independent of the particle diameter and it is equal to the maximum channel width.

Comparing Figure 10.34 with Figure 10.35 shows that the influence of the number of flights has a big influence on the change in maximum solid bed width with change in the particle diameter.

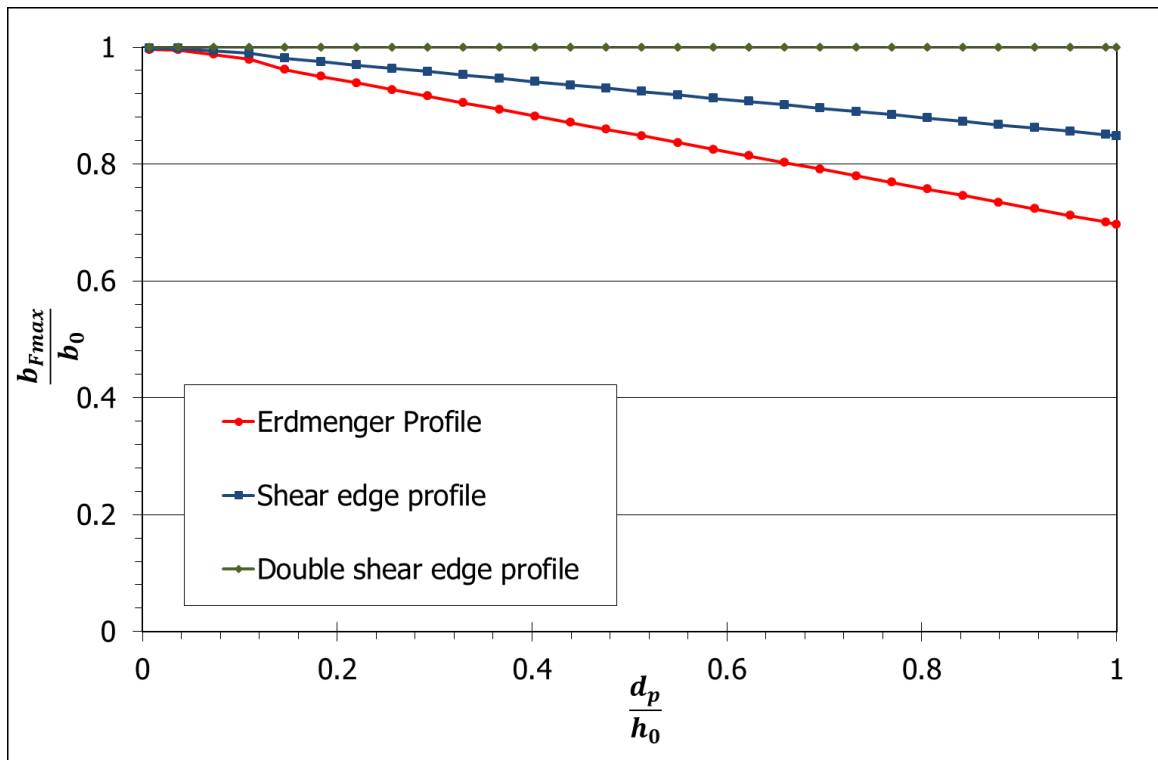


Figure 10.34: Solid bed width as a function of particle diameter for double flighted solid conveying zone

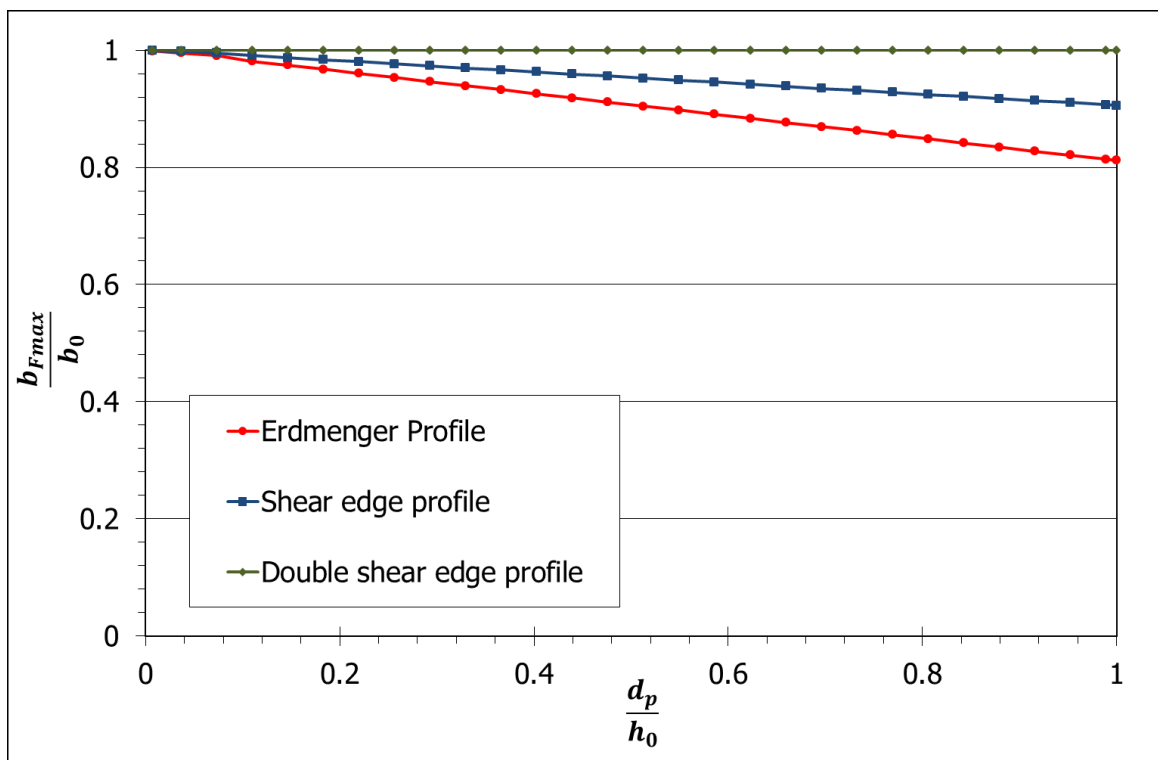


Figure 10.35: Solid bed width as a function of particle diameter for single flighted solid conveying zone

The maximum throughput of the NCT55 feeding element with different channel profiles, calculated theoretically according to equation 5.13, is shown in Figure 10.36. The maximum output is calculated considering the flood fed condition. A linear increase in the output with increase in screw speed can be seen, as measured in the trail 1 (Figure 10.13). Figure 10.36 shows clearly, as explained already, that the channel profile influence the output. The increase in the channel cross sectional area from Erdmenger to double shear edge profile through shear edge profile leads to higher throughput. The results show that the double shear edge profile is ideal for the maximum solid conveying.

The theoretical output values of the feeding zone are not comparable with the experimental results (Table 10.1) because the measured output values have the influence of the die back pressure and moreover the experiments were not carried out under flood fed conditions. The huge free volume available in the feed zone, compared to the pressure built-up zone, of the conical screws, leads to higher theoretical solid throughput. This theoretical output is a function of the bulk density of the polymer, the free channel volume in the intake zone and the screw rotation speed. Further experiments are needed to verify the maximum theoretical output calculation of the feeding or solid conveying zone.

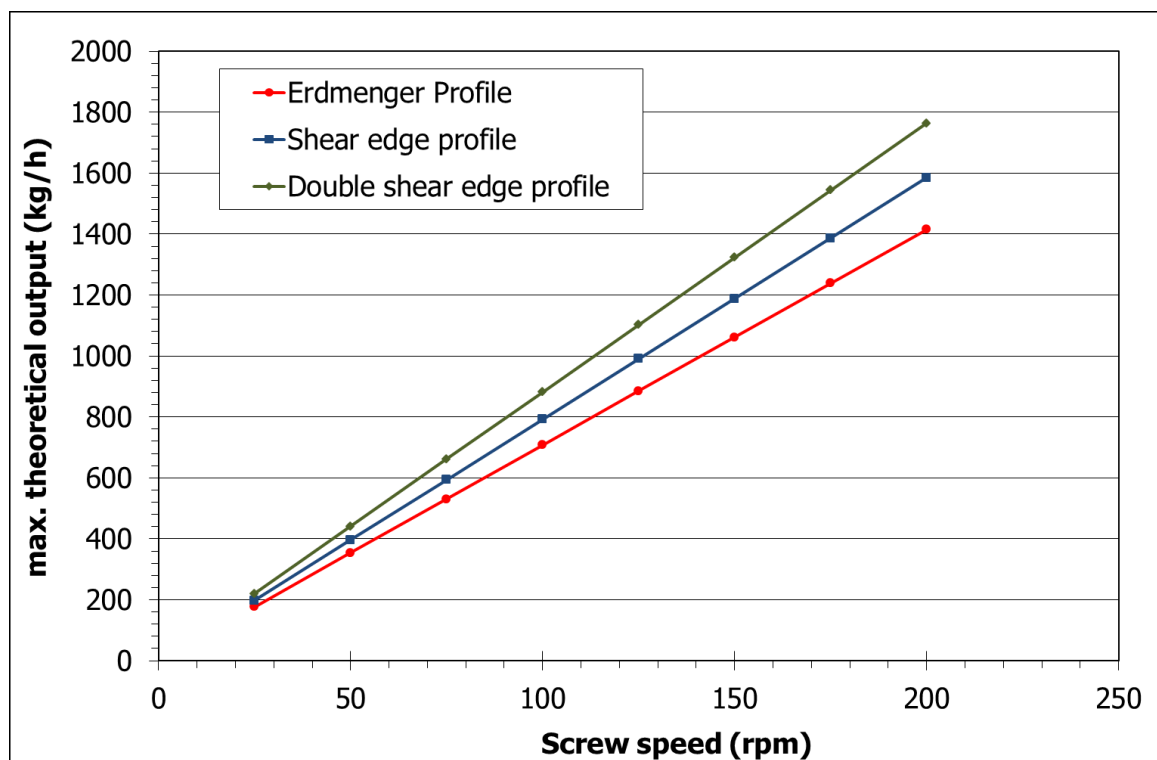


Figure 10.36: Theoretical maximum output of NCT 55 feeding element for PE-LD 159AC under flood fed condition

According to Schuler (1996) the maximum solid conveying capacity of the twin screws are dependent on the optimal pitch of the feeding zone and the conveying factor. Also the bulk density of the material can affect the solid conveying, if the air is not adequately removed.

The melting profile calculation for the NCT55 screw configuration (Figure 8.4) at a screw rotation speed of 270 rpm, barrel temperature of feed zone 170 °C and throughput of 550 kg/h is shown in Figure 10.37. The calculation was performed considering that the screw was completely filled (flood fed) and the melting starts after the end of the feed opening. The dimensionless solid bed width reduces from 1 from the melting start point. After the screw position 170 mm, the value increases due to the change in the screw geometry (from single to double flight). The end of the melting process is achieved, when the dimensionless solid bed width reaches the 0 value. In practice, under starve fed condition the start of melting is at the first fully filled position after the feeding zone.

Figure 10.37 also shows the change in the melt temperature over the screw length in the melting zone. The temperature of the material rises from 155 °C from the start of melting point and reaches a maximum of 176 °C at the end of melting process. The melt temperature and the melting length can be highly influenced by the barrel temperature.

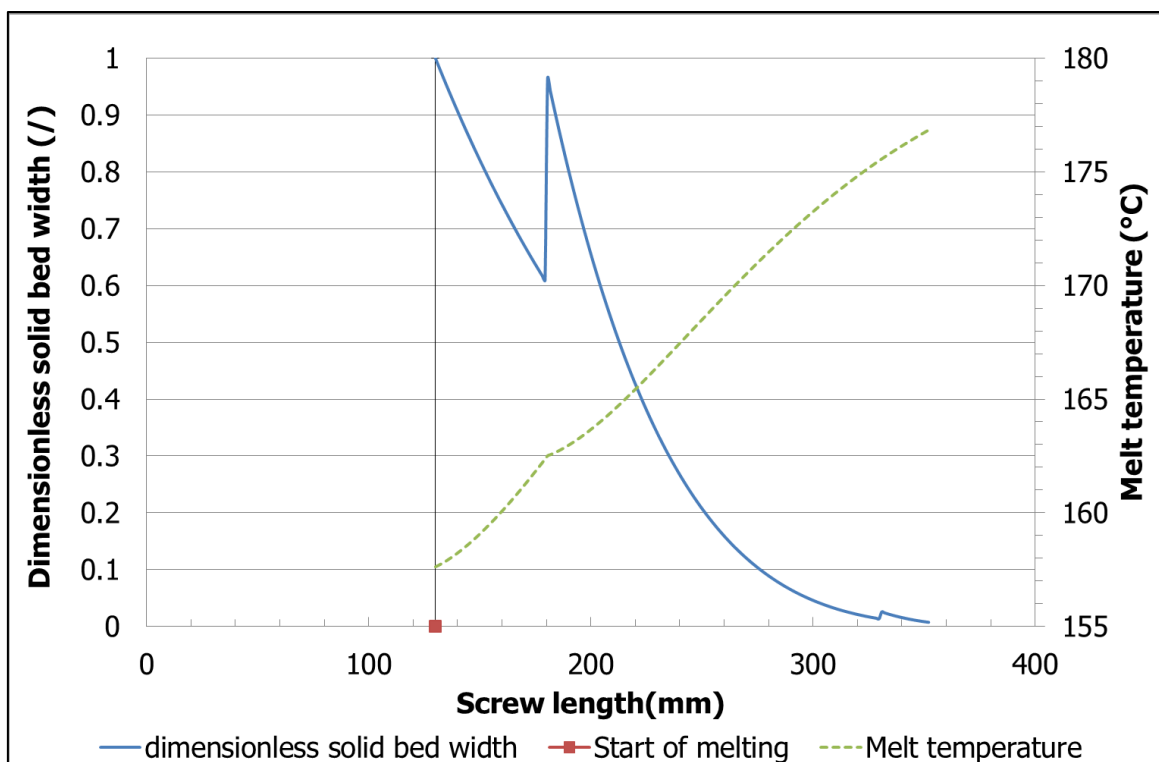


Figure 10.37: Dimensionless solid bed width and melt temperature as a function of screw length

The best practice to study the melting behavior is the screw pulling out experiment. In this method the extruder is stopped once the process stability is attained, the material is cooled below the flow temperature and the screws are pulled out of the barrel with the material and melt in the screw channels. Since the practical measurements were done on a production scale extruder, there was no possibility to carry out these trials. The measurement of the melt temperature in the melting zone of screw is also one of the tough jobs, since the thermocouple has to come in contact only with the melt pool or material without colliding with the screw. The only possibility to measure the temperature in the barrel or the screw channel is to use an infra-red melt temperature sensor. Due to unavailability of a laboratory size conical MAS extruder, the melting and solid conveying experimental analysis was not considered for this work. Since no practical measurements on solid conveying and melting (screw pulling out analysis or melt temperature measurement in the melting region) were carried out on the NCT 55 extruder, the theoretically calculated results of solid conveying and melting model could not be verified.

10.3 Parallel Twin Screw

With the help of the developed software the screw characteristics curves for individual screw elements of the Leistritz twin screw were determined initially for PP DM55pharm. The calculation results of the individual screw elements and the complete configured screw were compared with the experimental values and FEM simulation and the outcome of the comparison are discussed in this chapter.

10.3.1 Screw Element Pressure Characteristics

Initially the maximum volumetric flow rate of the individual conveying screw elements was determined using the equation 6.11 for the PP Bormed DM55Pharm material at a screw speed of 55 and 145 rpm, neglecting the flow due to pressure because the maximum flow rate is achieved when the volumetric flow due to pressure is zero. Also the leakage flow and flow in the nip zone were neglected in determining the maximum flow rate of the screw elements.

The comparison of the maximum flow rate, determined using the program 2XS calculation and Polyflow simulation, for different screw conveying elements at a screw rotation speed of 55 rpm is shown in Figure 10.38.

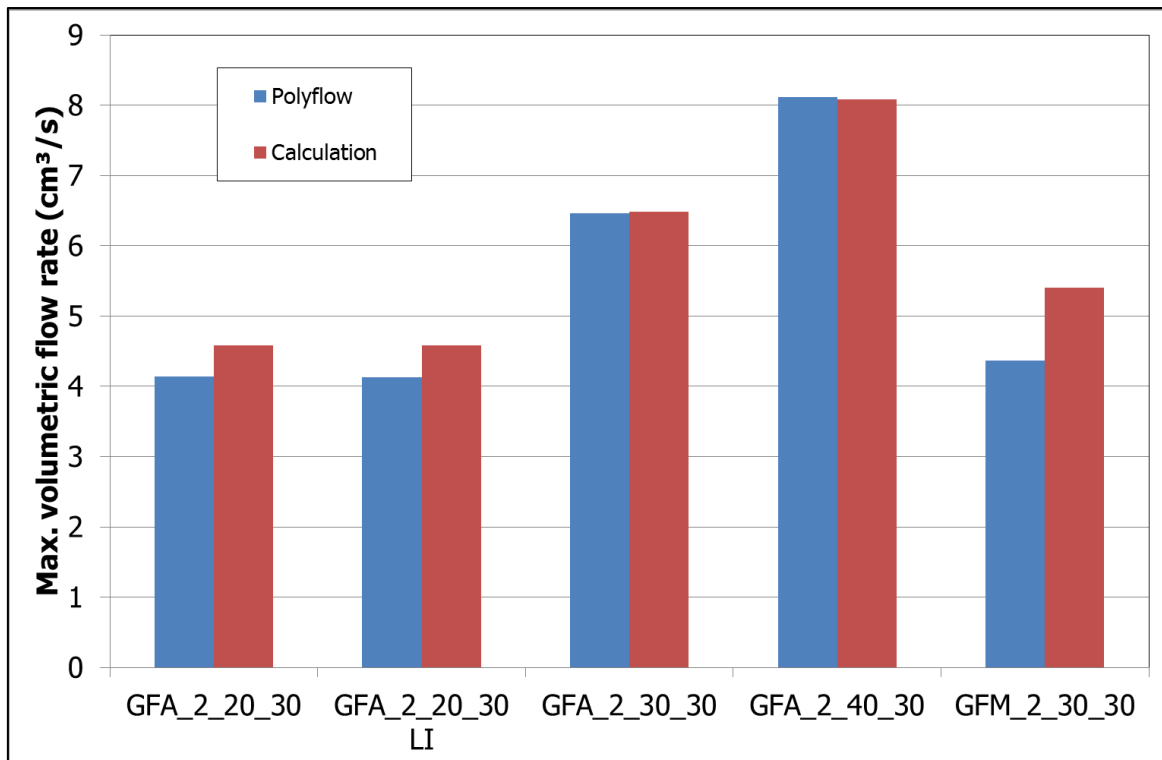


Figure 10.38: Maximum flow rate of conveying elements with different pitch for PP DM55 at 55 rpm screw speed and 200 °C melt temperature

The maximum flow rate is depended only on the drag flow and thus the viscosity and pressure effects on the flow rate of the screw elements are neglected. The comparison of the maximum flow rate of the 2 flighted GFA screw elements with 20, 30 and 40 mm pitch clearly shows that with the increase in screw pitch, the maximum flow rate increases.

In case of the negative conveying element (GFA_2_20_30_LI), the drag flow is in the backward direction. The maximum flow rate of the conveying mixing element (GFM_2_30_30) is lower than the conveying element (GFA_2_30_30), with the same pitch and flight numbers, due to the interruptions in the flights caused by the slots and leakage flow caused by drag flow through the slots.

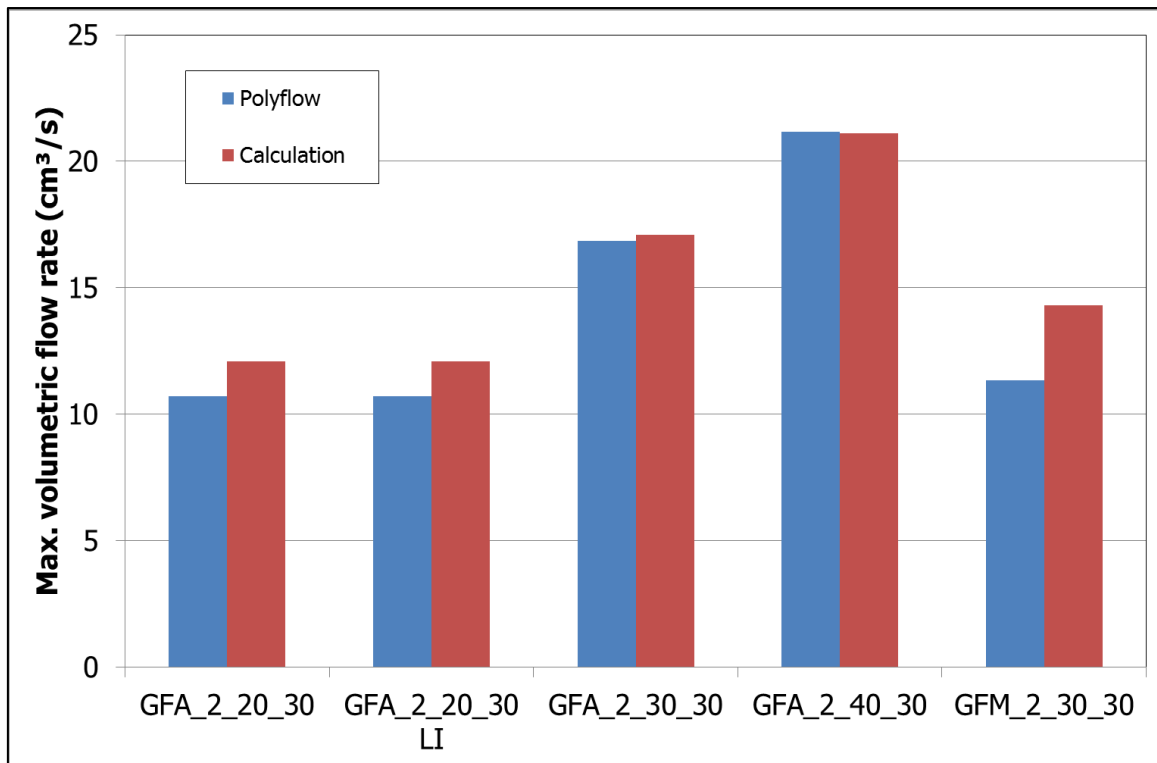


Figure 10.39: Maximum flow rate of conveying elements with different pitch for PP DM55 at 145 rpm screw speed and 200 °C melt temperature

Similar results are shown in Figure 10.39 for different conveying elements at 145 rpm screw speed. As the screw speed increases the drag flow rate increases. The comparison between the calculated and simulated values shows very good agreement except in case of the conveying mixing element (GFM_2_30_30). The cause is the approximation of the slot geometry to a simple rectangular channel profile with the average breadth and height in the calculation, which leads to some deviations in calculating the leakage flow due to drag forces through the slots.

This maximum achievable flow rate at a specified screw speed for a screw element provides the information about the pressure generation and the pressure consumption capability of the screw element. Also this helps in determining the backpressure length and the filling degree of the screw elements.

Before determining the screw elements pressure characteristics curves, the maximum pressure generation or pressure reduction capability of different screws elements at predefined screw rotation speeds (55 and 145 rpm) and throughput (8 kg/h) for PP Bormed DM55Pharm material at 200 °C were determined using flow simulation (Polyflow) and using the developed calculation software (2XS).

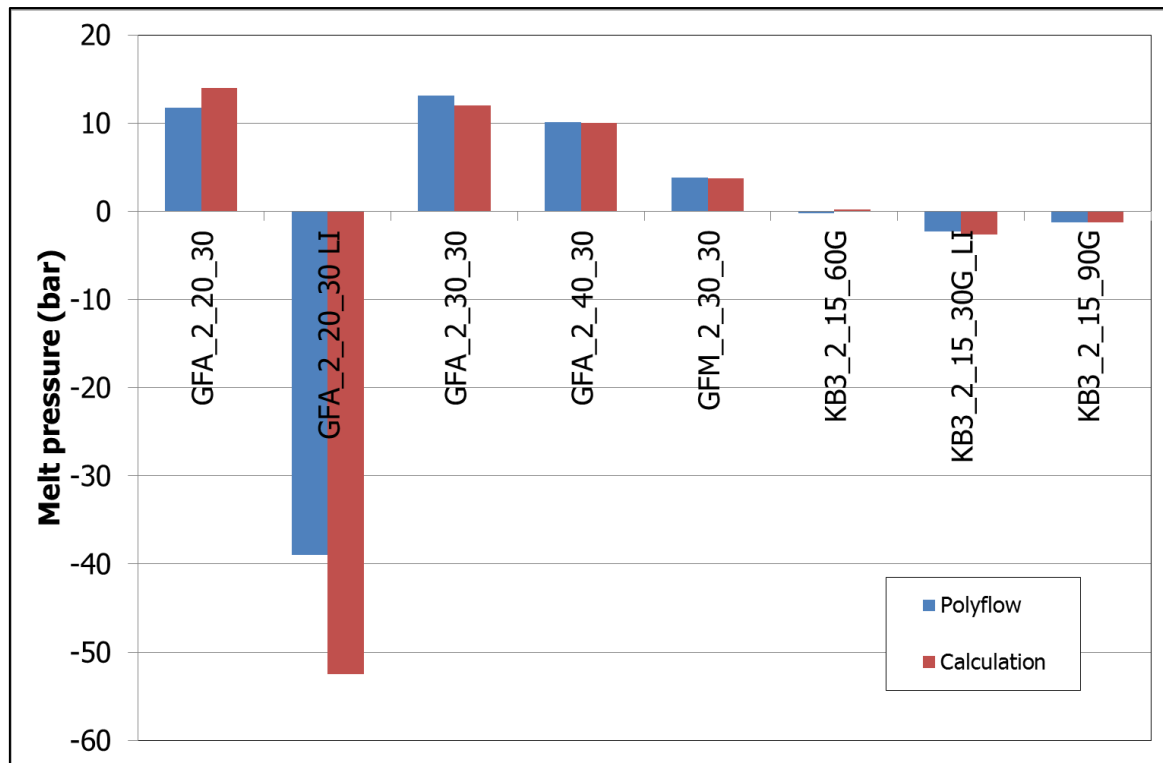


Figure 10.40: Pressure generation of different screw elements for PP DM55 at 8 kg/h output; 55 rpm screw speed and 200 °C melt temperature

In Figure 10.40 the negative pressure represents the pressure consuming element. The conveying screw elements GFA with different pitches (20, 30 and 40 mm), show a linear decrease in the pressure built-up with increase in screw pitch, at constant screw rotation speed and output. The calculated pressure and the 3D simulated pressure values for different screw elements are very close, except in case of the negative conveying element GFA_2_20_30_LI. There the deviation between the calculated and the simulated value is 35 %. But in case of melt pressure calculation at 145 rpm screw speed for DM 55 at 8 kg/h (Figure 10.41), the deviation is only 5 %. The main cause for this inaccuracy in the melt pressure calculation of the negative conveying element is the non-Newtonian viscosity effect of the material. At 55 rpm the representative shear rate determined, according to the equations 6.4 and 6.5, is 39.5 s^{-1} and at 145 rpm the shear rate is 141.5 s^{-1} . The respective shear viscosities at 55 and 145 rpm are 1140 Pa.s and 474 Pa.s. The high melt viscosity at lower screw speed leads to higher pressure built-up than the melt pressure generated at same output but at higher screw speed.

The dimensioned screw characteristics curves, representing flow rate as a function of pressure, of different screw elements are initially determined using the non-Newtonian Cross

viscosity model for PP Bormed DM55 Pharm at a melt temperature of 200 °C and screw rotation speeds of 55 and 145 rpm at different flow rates.

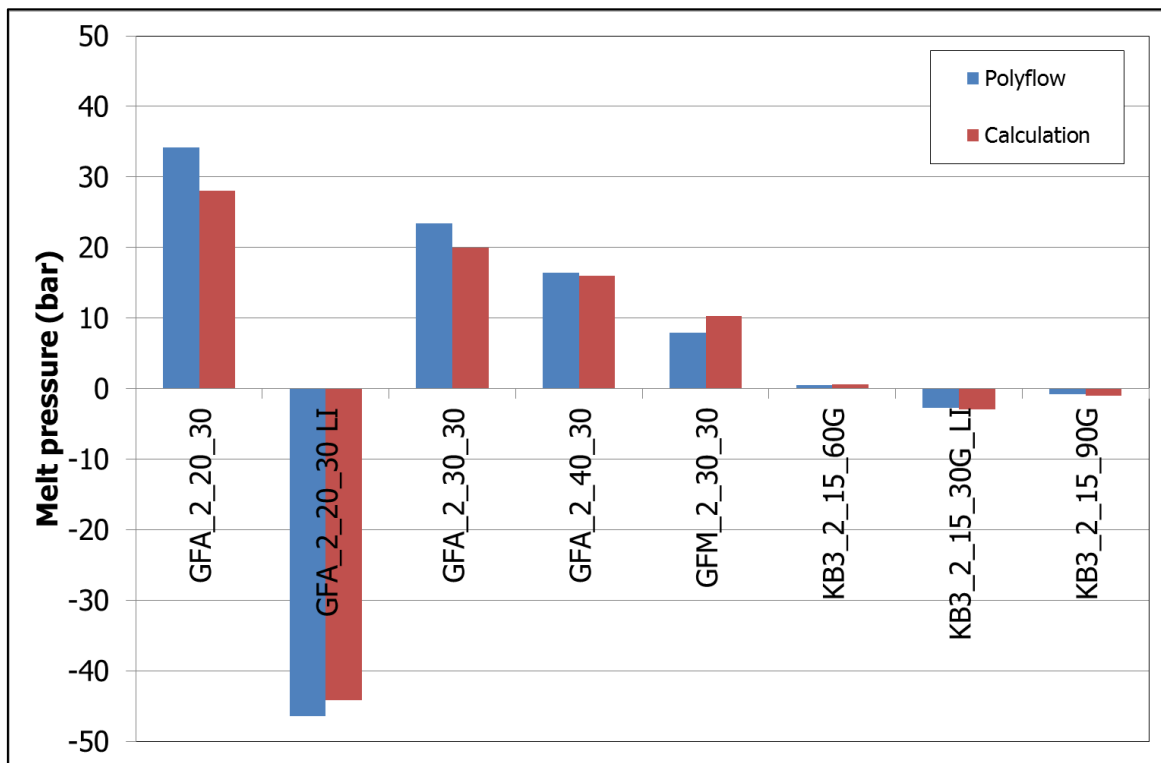


Figure 10.41: Pressure generation of different screw elements for PP DM55 at 8 kg/h output; 145 rpm screw speed and 200 °C melt temperature

Figure 10.42 describes the screw characteristics curves of positive and negative conveying elements and conveying mixing elements. The backward conveying element (GFA_2_30 LI)

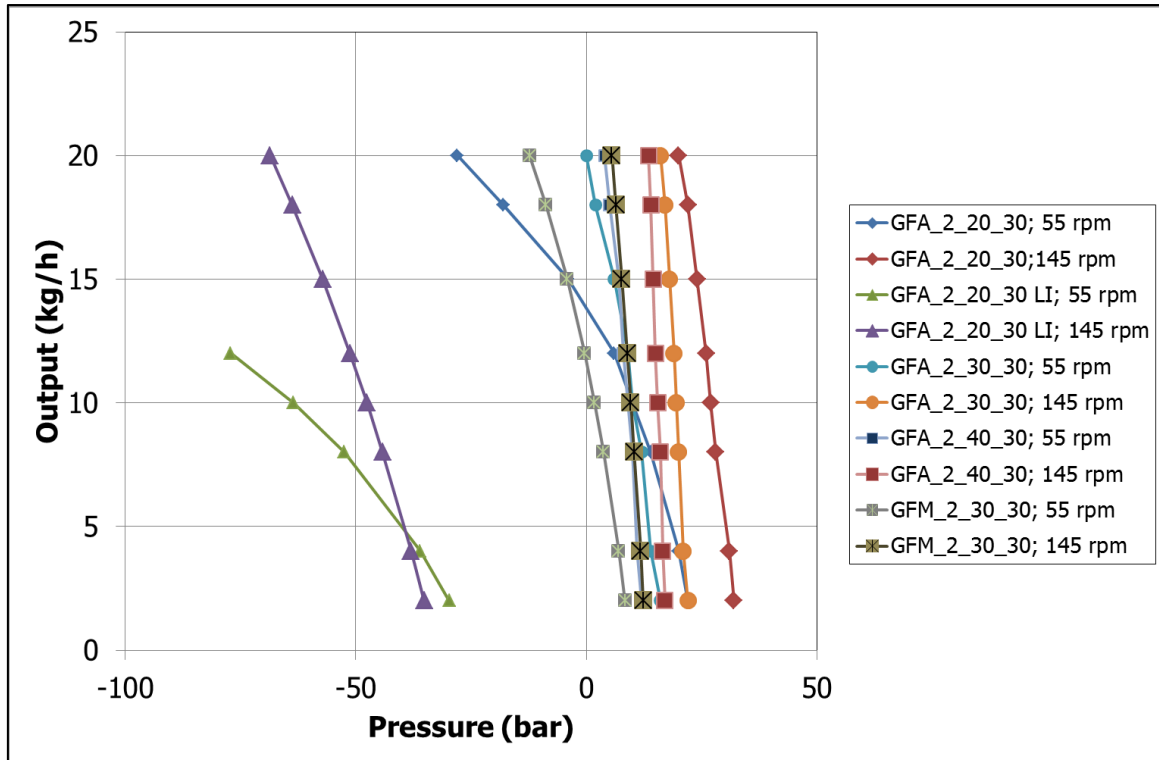


Figure 10.42: Screw characteristic curve of conveying (positive, negative and mixing) elements for PP Bormed™ DM55Pharm at 200 °C melt temperature

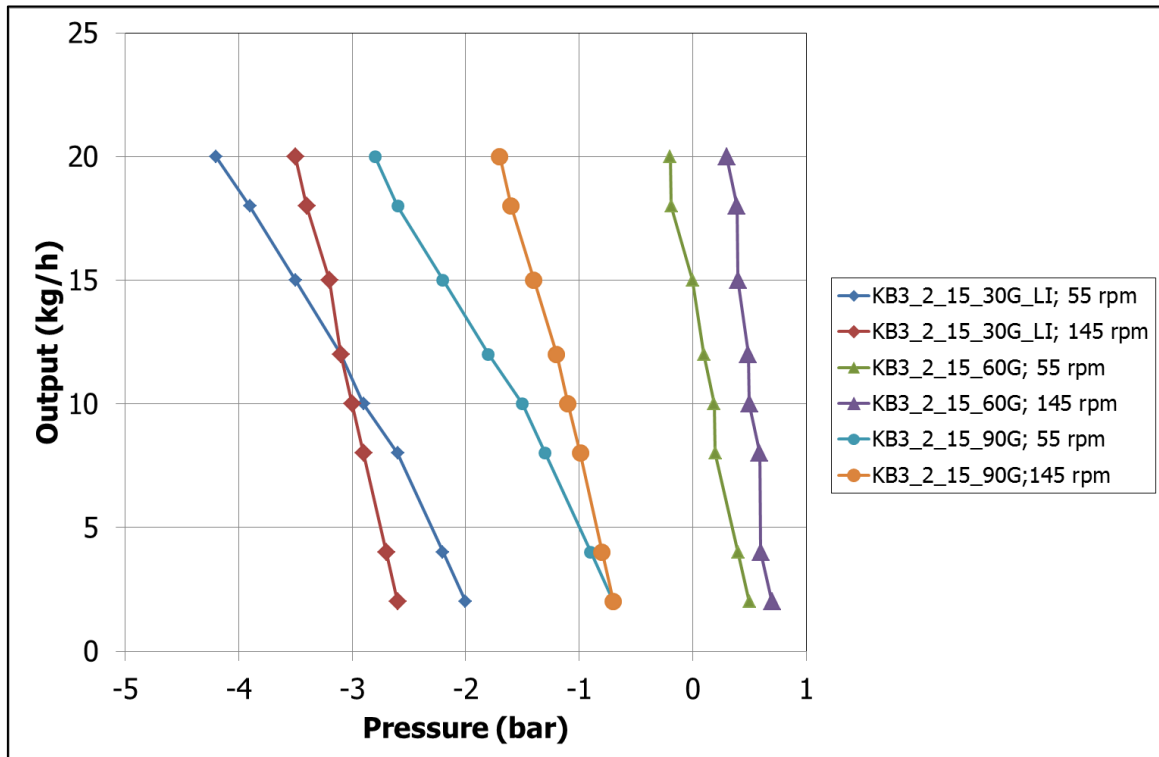


Figure 10.43: Screw characteristic curve of kneading elements (positive, negative and neutral conveying) for PP Bormed™ DM55Pharm at 200 °C melt temperature

always operates by consuming the pressure, which leads to negative pressure values and the pressure drop increases with the increase in the flow rate and screw rotation speed.

The positive conveying elements usually generate pressure and the pressure generation increases with the increase in screw speed. The negative pressure gradient of positive conveying elements (GFA_2_20_30 and GFM_2_30_30) at high output by a screw rotation speed of 55 rpm indicates that the screw elements are overrun.

Similar to the conveying elements characteristic curves, the pressure characteristic curves for the kneading elements are determined and are shown in Figure 10.43. From the figures it is very clear that the kneading elements generate very low pressure compared to the conveying elements.

As could be seen the negative conveying kneading element (KB3_2_15_30G_LI) has only negative pressure gradient. The neutral conveying element (KB3_2_15_90G) with 90° staggering angle operates at low pressure drop. Similar to the positive conveying screw elements, the positive conveying kneading elements generates pressure, which increases with the screw rotation.

With the pressure characteristic curves, the dimensionless pressure and volume number for the screw elements are determined using equations 7.32 and 7.34. The dimensionless screw characteristic curves for the forward conveying elements with different pitch and back conveying element are represented using linear approximation in Figure 10.44.

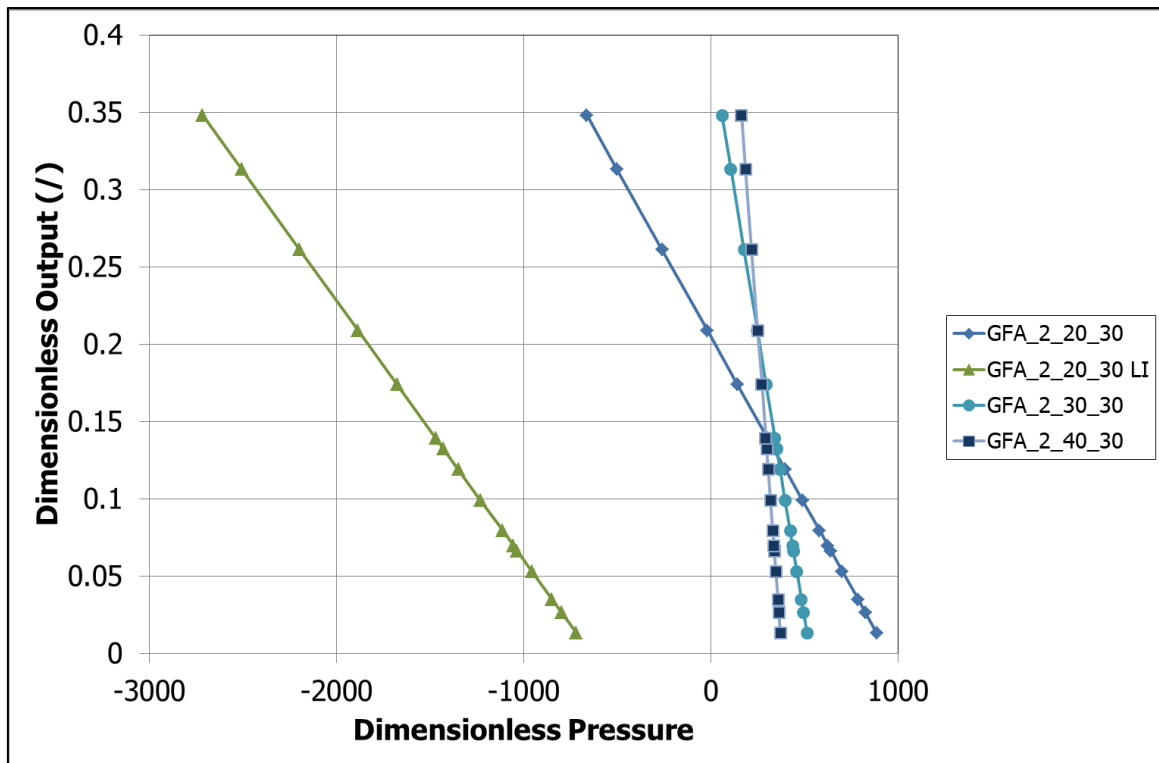


Figure 10.44: Dimensionless screw characteristic forward and backward conveying elements for PP Bormed™ DM55Pharm at 200 °C melt temperature

10.3.2 Screw Pull Out Study and Degree of Fill

The screw pull out experiment was performed to analyze the degree of filling of the screw elements under different processing conditions. These experimental results were visually quantified and the results were compared with the theoretically determined values.

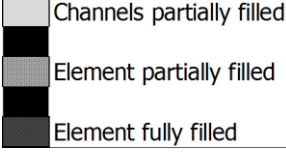

The results of the practical screw pull out measurement values using PP DM55Pharm under varying outputs, screw rotation speeds and back pressures at the screw tip are tabulated in Table 10.6. The result does not accurately show the length fully filled region of each screw element, rather it gives picture if the screw element is fully or partially filled.

For the same experimental extruder settings, the degree of fill for the configured standard screw geometry was calculated using the 2XS software. The results of the theoretically determined degree of fill values are shown in Table 10.7. The theoretical results, in contrary to the experimental results, show the accurate length of completely filled length of a screw element. The inaccuracy in the experimental values is due to the complexity in visual interpretation of the filling degree of the screw channels and the corresponding filling length of the screw elements.

Table 10.6: Experimental degree of fill at different processing setting (Winkler-Ebner, 2014)

Channels partially filled	Element partially filled	Element fully filled	Screw Element	Screw Element Length (mm)	Screw cumulativ length (mm)	8	8	8	8	16	
						kg/h 50 rpm 15 bar	kg/h 55 rpm 45 bar	kg/h 150 rpm 15 bar	kg/h 150 rpm 45 bar	kg/h 150 rpm 15 bar	
					0						
			Shaft End	10	10						
			GFA 2-20-30 A	30	40						
			GFA 2-40-30	30	70						
			GFA 2-40-30	30	100						
			GFA 2-40-30	30	130						
			GFA 2-30-30	30	160						
			GFA 2-30-30	30	190						
			GFA 2-30-30	30	220						
			GFA 2-30-30	30	250						
	Block 1			KB 3-2-15-60GRD-RE	15	265					
				KB 3-2-15-60GRD-RE	15	280					
				KB 3-2-15-60GRD-RE	15	295					
				KB 3-2-15-30GRD-LI	15	310					
	Block 2			GFA 2-40-30	30	340					
				GFA 2-40-30	30	370					
				GFA 2-40-30	30	400					
				GFA 2-30-30	30	430					
				GFA 2-30-30	30	460					
				KB 3-2-15-60GRD-RE	15	475					
				KB 3-2-15-60GRD-RE	15	490					
				KB 3-2-15-60GRD-RE	15	505					
	Block 3			KB 3-2-15-60GRD-RE	15	520					
				KB 3-2-15-30GRD-LI	15	535					
				GFA 2-40-30	30	565					
				GFA 2-40-30	30	595					
				GFA 2-30-30	30	625					
				GFA 2-30-30	30	655					
				KB 3-2-15-60GRD-RE	15	670					
				KB 3-2-15-60GRD-RE	15	685					
	Block 4			KB 3-2-15-90GRD	15	700					
				KB 3-2-15-90GRD	15	715					
				KB 3-2-15-30GRD-LI	15	730					
				GFA 2-40-30	30	760					
				GFA 2-40-30	30	790					
				GFA 2-40-30	30	820					
				GFA 2-30-30	30	850					
			GFA 2-20-30-LI	30	880						
Block 5			GFA 2-40-30	30	910						
			GFA 2-40-30	30	940						
			GFA 2-40-30	30	970						
			GFA 2-30-30	30	1000						
			GFA 2-30-30	30	1030						
			GFA 2-30-30	30	1060						
			KB 3-2-15-60GRD-RE	15	1075						
			KB 3-2-15-60GRD-RE	15	1090						
Block 6			KB 3-2-15-90GRD	15	1105						
			KB 3-2-15-30GRD-LI	15	1120						
			GFA 2-30-30	30	1150						
		GFA 2-30-30	30	1180							
		GFA 2-30-30	30	1210							

Table 10.7: Calculated degree of fill at different processing settings

		Screw Element	Screw Element Length (mm)	Screw cumulativ length (mm)	8 kg/h 50 rpm 15 bar	8 kg/h 55 rpm 45 bar	8 kg/h 150 rpm 15 bar	8 kg/h 150 rpm 45 bar	16 kg/h 150 rpm 15 bar
				0					
	Block 1	Shaft End	10	10					
		GFA 2-20-30 A	30	40					
		GFA 2-40-30	30	70					
		GFA 2-40-30	30	100					
		GFA 2-40-30	30	130					
		GFA 2-30-30	30	160					
		GFA 2-30-30	30	190					
		GFA 2-30-30	30	220					
		GFA 2-30-30	30	250					
		KB 3-2-15-60GRD-RE	15	265					
	KB 3-2-15-60GRD-RE	15	280						
	KB 3-2-15-60GRD-RE	15	295						
	KB 3-2-15-30GRD-LI	15	310						
	Block 2	GFA 2-40-30	30	340					
		GFA 2-40-30	30	370					
		GFA 2-40-30	30	400					
		GFA 2-30-30	30	430					
		GFA 2-30-30	30	460					
		KB 3-2-15-60GRD-RE	15	475					
		KB 3-2-15-60GRD-RE	15	490					
		KB 3-2-15-60GRD-RE	15	505					
	Block 3	KB 3-2-15-60GRD-RE	15	520					
		KB 3-2-15-30GRD-LI	15	535					
		GFA 2-40-30	30	565					
		GFA 2-40-30	30	595					
		GFA 2-30-30	30	625					
		GFA 2-30-30	30	655					
		KB 3-2-15-60GRD-RE	15	670					
		KB 3-2-15-60GRD-RE	15	685					
	Block 4	KB 3-2-15-90GRD	15	700					
KB 3-2-15-90GRD		15	715						
KB 3-2-15-30GRD-LI		15	730						
GFA 2-40-30		30	760						
GFA 2-40-30		30	790						
Block 5	GFA 2-40-30	30	820						
	GFA 2-30-30	30	850						
	GFA 2-20-30-LI	30	880						
	GFA 2-40-30	30	910						
	GFA 2-40-30	30	940						
	GFA 2-40-30	30	970						
	GFA 2-30-30	30	1000						
	GFA 2-30-30	30	1030						
	GFA 2-30-30	30	1060						
	KB 3-2-15-60GRD-RE	15	1075						
Block 6	KB 3-2-15-60GRD-RE	15	1090						
	KB 3-2-15-90GRD	15	1105						
	KB 3-2-15-30GRD-LI	15	1120						
Block 6	GFA 2-30-30	30	1150						
	GFA 2-30-30	30	1180						
	GFA 2-30-30	30	1210						

The back pressure generated by the gear pump at the screw tip influences the filling degree on the screw channels in the block 6. At constant output (8 kg/h) and back pressure (15 bar), increasing the screw rotation speed (50 and 150 rpm) lead to a decrease in the filling length. At a screw speed of 50 rpm, the back pressure of 15 bar lead to a completely filled length of 41.4 mm from the screw tip, which is more than one screw element length. At 150 rpm screw speed and 15 bar back pressure, the filled length of the screw from the screw tip is only 21.6 mm, which means the screw element GFA 2-30-30 element with length of 30 mm is partially filled. Increasing the output from 8 kg/h to 16 kg/h at constant back pressure (15 bar) and constant screw rotation speed (150 rpm) leads to increase in axial filling length from 21.6 mm to 24.6 mm.

The comparison of experimental (Table 10.6) and theoretically calculated (Table 10.7) degree of fill values shows that the developed model predicts the DOF accurately and very precisely. The exception is the correlation of the DOF results of block 4 with forward and backward conveying elements. The reason for this deviation is the inaccurate pressure characteristic of the negative conveying element, which generates high back pressure leading to high filling length in elements prior to the negative conveying element.

Figure 10.45 shows the direct comparison of the measured and calculated DOF values for PP Bormed™ DM55Pharm by 8 kg/h output at a screw speed of 50 rpm, 15 bar back pressure and 200 °C melt temperature. If the screw channel is completely filled the DOF is represented as 1; and 0 if the channels are partially filled. The agreement between the predicted and measured DOF is very good expect in the screw region between 640 mm and 880 mm. The measured value shows that the screw region between 730 mm and 790 mm is partially filled. In the rest of the zones the calculated DOF show the accurate filling length.

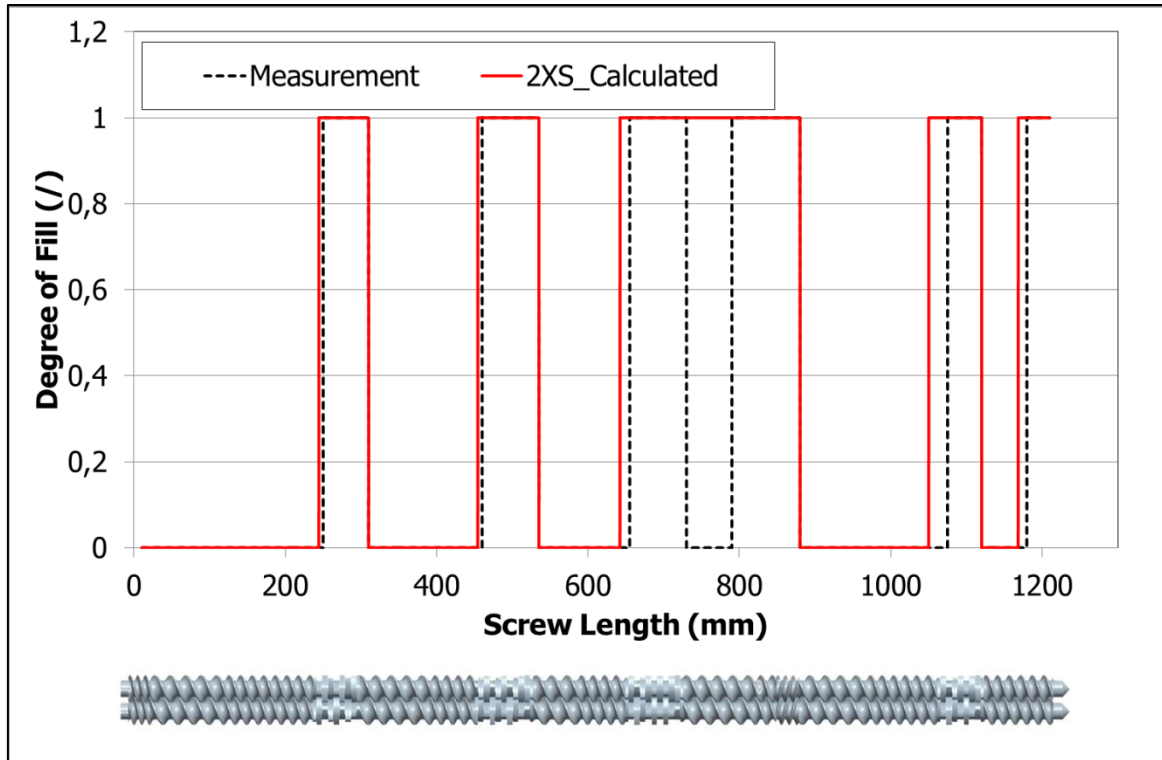


Figure 10.45: Comparison of DOF measured and calculated for 8 kg/h of PP DM55 at 50 rpm, 200 °C melt temperature and 15 bar back pressure at screw tip

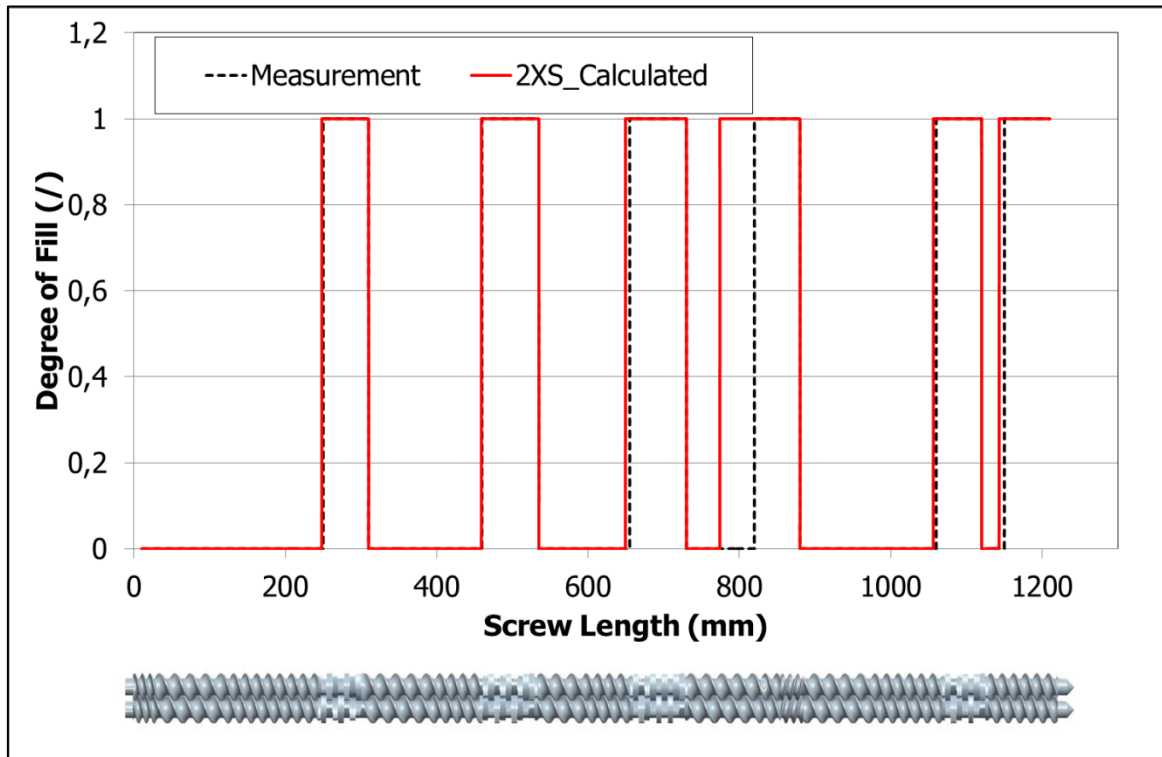


Figure 10.46: Comparison of DOF measured and calculated for 8 kg/h of PP DM55 at 150 rpm, 200°C melt temperature and 45 bar back pressure at screw tip

A similar comparison with good agreement of DOF values is shown in Figure 10.46 for 8 kg/h output at a screw speed of 150 rpm, 45 bar back pressure and 200 °C melt temperature. In this case the agreement between the measured and the calculated DOF in block 4 is good. The measurement result shows that the negative conveying element (GFA-2-30-30 LI) and the preceding two elements (GFA-2-30-30 and GFA-2-40-30) are completely filled. But the calculated result shows that not only the two preceding elements are completely filled, rather a partial length of one more conveying element (GFA-2-40-30) is completely filled.

10.3.3 Pressure Profile over Screw Length

With the help of the developed screw calculation program (2XS), the pressure profile along the configured complete screw geometry was determined for the PP Bormed™ DM55Pharm material for different extruder settings. The calculated values are compared with the measurement and Polyflow simulation results and discussed in detail in this section. The pressures measured over the screw length axis at different positions for different screw rotation speed and output is shown in Table 10.8.

Table 10.8: Measured pressure values over screw axis and melt temperature at screw tip at different extruder settings

No.	Screw speed (1/min)	Back-pressure (bar)	Output (kg/h)	Melt temperature (°C)	Pressure (bar)					
					495 mm	715 mm	825 mm	1045 mm	1155 mm	1210 mm
1	55	45	8	210	3.1	2.3	26.8	2.8	19.3	45
2	55	15	8	208	3.1	2.3	26.5	0.8	0	15
3	100	30	8	210	1.9	2.3	23.4	0	0	30
4	145	15	8	210	0.6	2.3	21.0	0	0	15
5	145	45	8	218	0.7	2.1	21.5	0	3.3	45
6	145	15	11	212	1.7	2.7	24.1	0.02	0	15
7	145	15	16	213	3.6	3.4	29.9	0.1	0.1	15

The maximum pressure was measured at the position 825 mm, short before the backward conveying element, for all the extruder settings irrespective of the back pressure set at the screw tip. Even though the barrel temperature settings were made in such a way to achieve a melt temperature of about 200 °C, the back pressure and the screw rotation speed influenced the melt temperature, measured at the screw tip. A maximum melt temperature of 218 °C was attained at a back pressure of 45 bar and 145 rpm. The minimum melt temperature was 208 °C at low screw rotation speed (55 rpm) and low back pressure of 15 bar. The high screw rotation speed generates high shear energy and the back pressure induces longer residence time due to back flow of the melt in the metering zone, which leads

to an increase in the melt temperature. The 0 bar measured at the positions 1045 mm and 1155 mm show that the screw channels were not completely filled.

The CFD simulation of the complete screw was performed block by block, starting from the screw tip towards the material feeding side. The simulation of the screw element blocks were carried out only for the fully filled elements. The fully filled zone was determined theoretically using the pressure characteristic curve of the screw elements. From the simulation results, the average pressure over the screw cross section was determined for the whole screw length. The pressure in the partially filled blocks are considered zero (Winkler-Ebner, 2014).

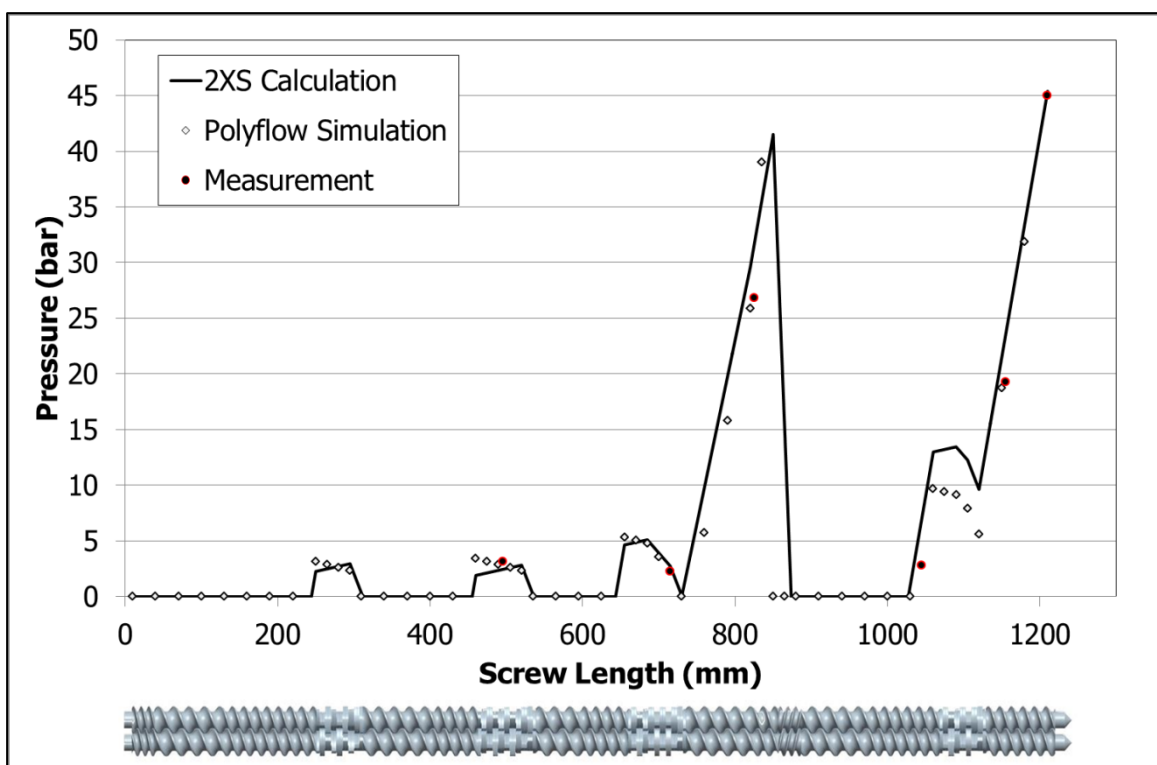


Figure 10.47: Pressure profile along screw length at 8 kg/h; 55 rpm; 200 °C and 45 bar back pressure

Similar to the Polyflow simulation, the complete screw geometry was configured and the pressure generation in each screw zones was determined using the 2XS software from the screw tip towards the feeding side of the screw. The pressure results from the calculation are compared with the simulation and the measured values. Such a comparison of the pressure profile over the screw length for PP DM55Pharm material at 8 kg/h output, 55 rpm screw rotation speed, 200 °C melt temperature and 45 bar back pressure at the screw end is shown in Figure 10.47. As explained already the pressure generates downstream the pressure consuming elements. The backward conveying element GFA 2-20-30 LI and

negative conveying kneading elements restrict the flow of melt in the forward direction leading to fully filled channels in the downstream screw elements, which helps in generating the pressure.

Overall an excellent match between the calculated, simulated and measured pressure values can be seen, except for the deviation of the pressure in the block 5 kneading zones. The calculation shows higher pressure value than the simulation in block 5 due to the difference in pressure generation capability of the GFA 2-30-30 conveying screw elements (Figure 10.40) in the block 6. According to simulation the GFA 2-30-30 element generates 13 bar at 8 kg/h and 55 rpm and 12 bar according to the calculation. With totally three GFA 2-30-30 elements in the block 6, simulation shows a maximum pressure of 39 bar generation whereas calculation gives 36 bar. Therefore for 45 bar backpressure, the pressure at the end of block 5 is 9 bar and 6 bar according to simulation and calculation respectively. This leads to different pressure profile between the simulation and calculation in block 5.

For pressure determination, it is very important to determine the shear rate and the respective viscosity of the melt over the complete screw length. The calculated shear rate and viscosity over the screw length for DM55Pharm material at 8 kg/h output at 55 rpm screw speed and 200 °C melt temperature is shown in Figure 10.48.

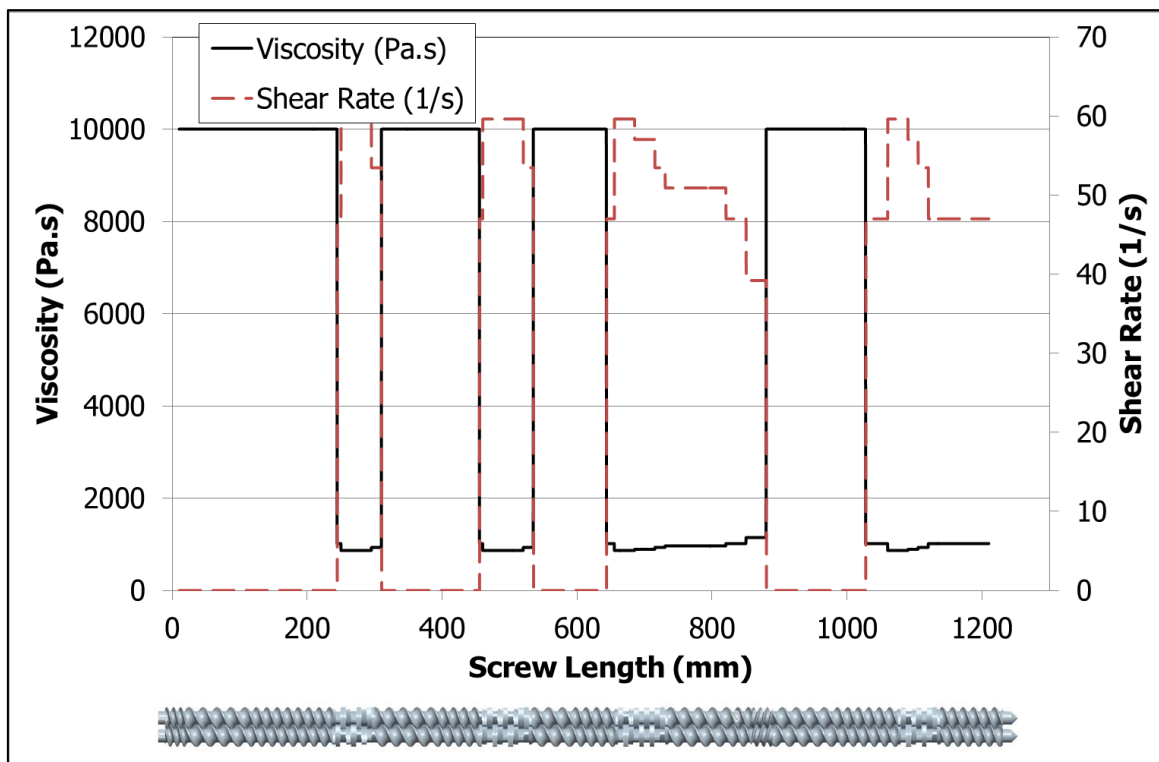


Figure 10.48: Viscosity and shear rate profile along screw length at 8 kg/h; 55 rpm; 210 °C and 45 bar back pressure

In the partially filled screw elements, the channels are not completely filled and hence the shear rate is considered to be zero and zero shear viscosity is given in these partially filled screw zones. Figure 10.48 shows clearly that the maximum shearing occurs in the kneading block elements. Due to high shear rate the viscosity of the melt is lower in the kneading zones, compared to the melt viscosity in the conveying element channels. The viscosity and shear rate considered here for the calculation is an average value over the complete channel depth. Generally the shear rate will be high in the screw and barrel clearances, where the flow channel is very narrow. Also the viscosity of the melt will not be constant in the screw channels. The viscosity of the melt will be high in the middle of the flow channel and lower at walls of the channel, due to high wall shear rate.

The pressure profile over the screw length for different back pressures at the screw tip (15 bar and 45 bar) at a constant flow rate and screw rotation speed is compared in Figure 10.49. The back pressure at the screw tip induced by the gear pump has no influence on the pressure generation in all other zones prior to the venting zone which is located between 910 mm and 1100 mm. The back pressure length in the metering zone (block 5 and 6) at 45 bar pressure is higher compared to the 15 bar back pressure.

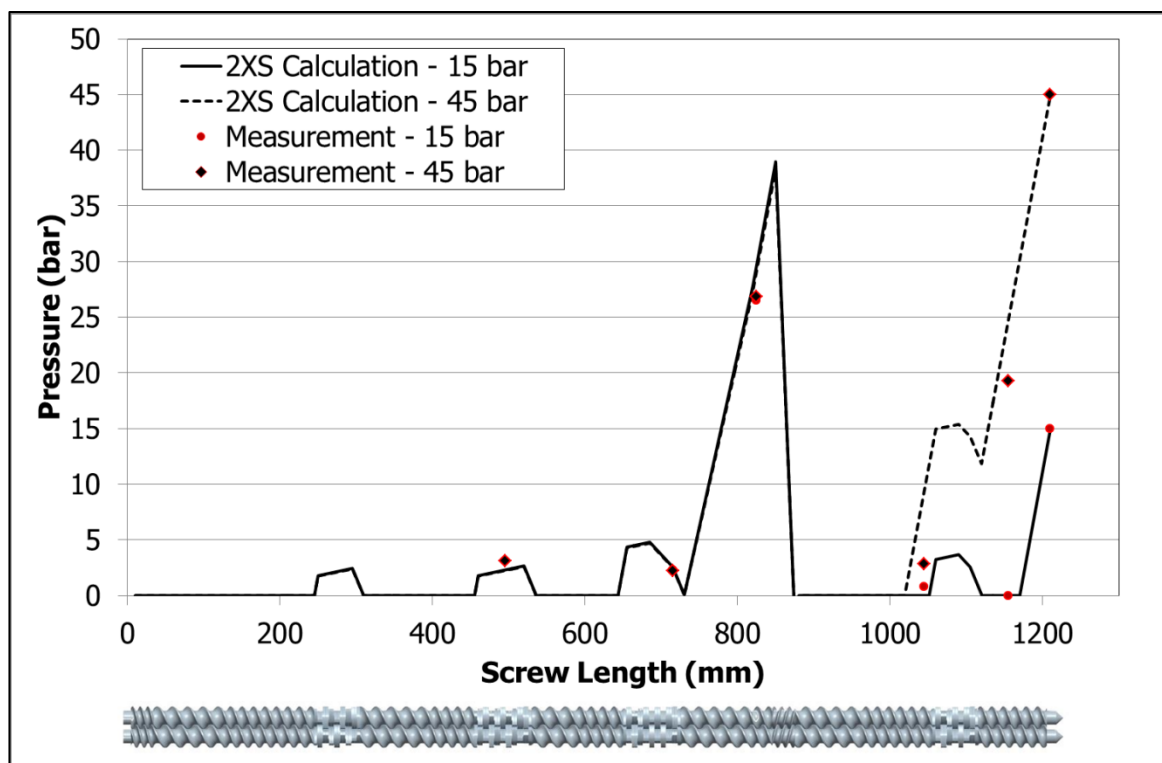


Figure 10.49: Pressure profile along screw axis at 8 kg/h; 55 rpm; 210 °C for 45 bar and 15 bar back pressure

The 15 bar pressure at the screw tip leads to a back pressure length of 40 mm axial screw length and the rest of the 50 mm screw length is partially filled and no pressure is generated in this zone. This is confirmed by the 0 bar pressure measured at position 1155 mm. In case of 45 bar back pressure the three conveying elements in the block 6 are completely filled and reduce the pressure from 45 bar to 12 bar at the end of block 5. This 12 bar leads to a back pressure length of 90 mm. All together the 45 bar back pressure leads to 180 mm back pressure length. Figure 10.49 shows a very good agreement between the measured and the calculated values.

The pressure distribution over the screw axial length for different throughputs at a constant screw speed of 145 rpm and constant back pressure of 15 bar is compared in Figure 10.50. With the increase in the output the pressure built-up in front of the negative conveying element increases. The agreement between the pressure measured at position 825 mm (pressure before the backward conveying element) and the simulation shows significant deviations. This difference is mainly due to the inaccuracy in determining the pressure characteristics of the backward conveying element using the model.

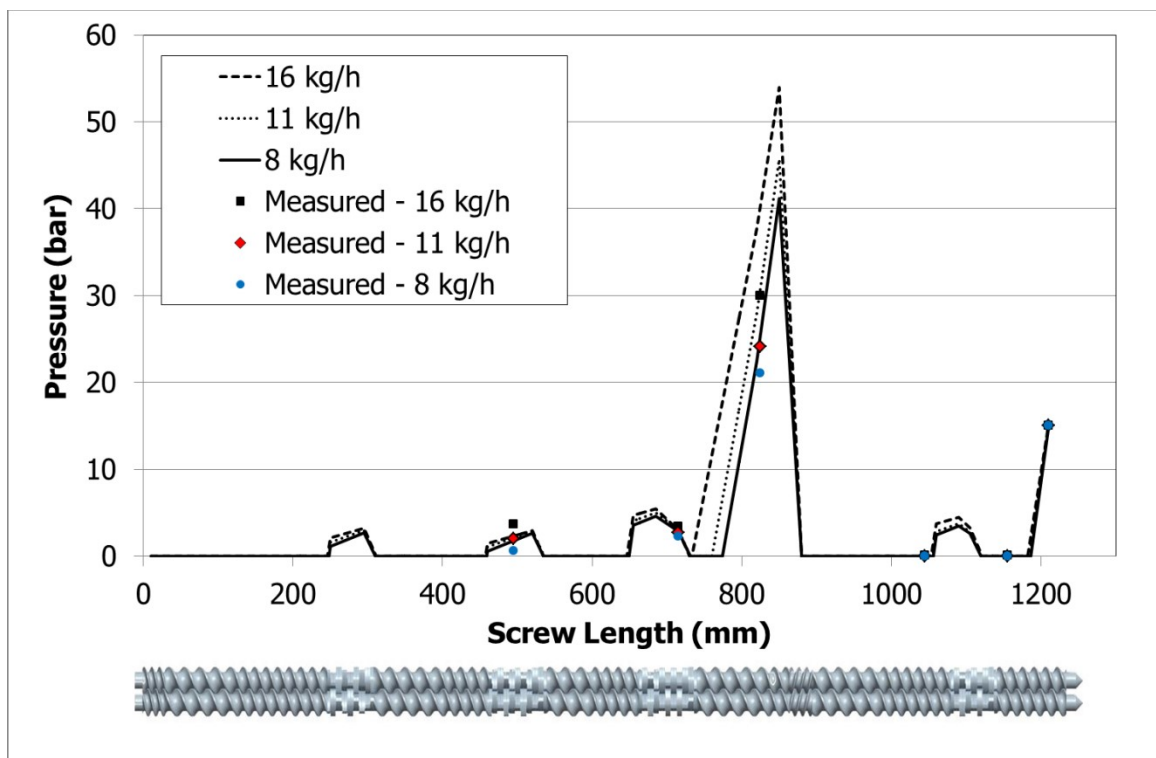


Figure 10.50: Pressure profile along screw length at a constant screw speed of 145 rpm, 15 bar back pressure, 210 °C melt temperature and different output

The reasons for the deviation of the measured and calculated pressure at position 495 mm is mainly due to the melt temperature and melt viscosity. The temperature, which is considered

for the pressure determination over the screw length, is the melt temperature measured at the screw tip. For the calculation a constant melt temperature is considered but in reality the material temperature over the screw length is not the same and this induces differences in the melt viscosity over the screw length. At position 495 mm the melt temperature would be considerably lower than 210 °C and the lower melt temperature leads to a higher viscosity. Hence the pressure built-up will be higher. Overall the comparison of the calculated and measured pressure values shows a good agreement.

11 Conclusions

This work was concerned mainly with the modeling of co-rotating tightly intermeshing twin screw extruders and specifically on the conical co-rotating twin screw extruders NCT developed by MAS Austria GmbH and developing a screw simulation program using the developed models. The processing zones of the MAS conical extruder are similar to the parallel compounders with possibility for side feeding the fillers, devolatilization etc. The conical extruders combine the advantages of the parallel co-rotating and conical geometry concept of the counter rotating extruders. One of the main advantages of the conical extruders is the large intake volume of the feeding zone, due to the conical design, which allows easy processing of very low bulk density materials. Moreover the reduction in the screw free channel volume over the screw length improves the pressure generation efficiency and leads to less shearing of the melt. The screw and barrel maintenance and cleaning is also a big advantage since the screws can be easily pulled out from backside after swelling the barrel.

Based on the available physical mathematical models for the parallel twin screws, models have been developed to characterize the solid conveying, melting and melt conveying of the conical twin screw extruders MAS55 and this models have been transferred into a simulation program. The mathematical geometric description of different screw elements, like conveying, mixing and kneading elements, for both conical and parallel extruders has been detailed. Since the conical screws have no constant screw geometry over the screw length, the conical screw element geometry was discretized into many small segments and each segment was considered as parallel screw geometry. The free cross sectional area was determined for each segment and the free volume calculations was determined considering the screw element length. In order to analyze the influence of the channel profile geometry on the flow characteristics of the screw elements, FEM (finite element method) was used. Using Ansys Polyflow screw conveying elements with Erdmenger profile, shear edge profile and double shear edge profiles have been simulated. The results showed that the Erdmenger channel profile has the minimum free channel volume and can generate a maximum pressure compared to other channel profiles. The double shear edge profile has the maximum free volume which is more advantageous in the intake zone of the extruder. The major drawback of the shear edge and double shear edge profile is the reduced or no self-wiping capability. With this result the new conical screw series pressure build-up screw element was implemented with the Erdmenger channel geometry. For the mathematical

description of the different processing zones of the twin screw extruder, flat plate models were used in this study.

The feeding zone and melting zone of the MAS55 extruder were theoretically characterized considering the models available for the parallel twin screw extruder. Initially the three different channel profiles were considered to determine the theoretical maximum throughput of the MAS55 extruder for the used LDPE material. The results, considering the area centered particle alignment and including the bulk density correction and maximum solid bed width, showed that the maximum output can be achieved when using a double shear edge channel profile followed by shear edge and Erdmenger profile. The geometric advantage of the box profile allows the possibility to pack more bulk material in the feeding zone. The verification of the throughput calculation was not possible due to two main reasons. Firstly the friction coefficient values have a major influence on the throughput calculation and there was no possibility to determine the friction values for the used materials. Secondly the back pressure at the screw tip influences the throughput. Moreover all the trials were done under starve fed conditions and no experimental data was available under flood fed condition to verify the model accuracy.

The melting model for the conical twin screw extruder was described based on the Tadmor model, which considers the location dependent melt film thickness. The melt viscosity changes were assumed to follow the Power law viscosity models and the temperature dependency of the viscosity considered using an exponential model. The melting length was determined considering a user defined start of the melting position. In the starve fed condition the start of the melting point was equated with the first point of fully filled screw. The computation showed that start of melting point and the barrel temperature highly influenced the melting length. Due to measurement complexity and unavailability of the instruments to measure the melt temperature in the screw channels, no practical data were available to verify the melt temperature calculations in the melting model. The screw pulling studies were not done due to unavailability of the resources. Further works are recommended to study the melting and solid conveying zone.

The melt conveying models of the different screw elements and for different channel profiles were developed considering the drag, pressure, apex and leakage flows. The shear viscosity of the melt was determined using the Power Law or Cross viscosity model. In order to make the model simpler the melt was considered to be isotherm and no changes of the melt temperature due to shear dissipation or due to barrel heat along the screw length was incorporated in the models. The back pressure length or the degree of fill in front of the

pressure consuming elements, like die head or gear pump or negative conveying elements, were determined iteratively. The comparison of the experimental and theoretical results showed a very good level of agreement in modeling the melt conveying and the DOF for both conical and parallel twin screw extruders.

The developed mathematical models and algorithms for characterizing all the processing zones of the conical and parallel twin screw extruders were implemented in software packages (NCT and 2XS), which are available as prototypes. Using the screw modeling software it is possible to characterize the individual processing zones or individual screw elements or the complete configured screw easily and fast. The graphical user interface of the software makes it easier for the user to configure different screw geometries and compute the screw characteristics under different processing conditions (throughputs, screw speeds, dies, materials etc.).

The NCT modeling software is developed considering only the MAS55 screw elements. The melting and solid conveying calculations have to be verified by screw pull out experiments. The melt conveying of different MAS55 screw elements, DOF and back pressure length calculations showed a very good correlation with the MAS55 experimental results. Similar experiments have to be done on the other screw sizes (MAS24, MAS45, MAS75, MAS90 and MAS93) and the accuracy of the calculation models have to be verified. In the current version of the NCT the melt is considered to be isothermal, to make the first step simpler and uncomplicated. Further work can be done to extend the models considering the melt temperature changes along the screw axis, while calculating the pressure profile.

Similarly the calculation accuracy of the 2XS software is verified only for the Leistritz ZSE 27 MAXX compounder. Since the program has the screw elements database of the other compounders, Theysohn and ZSK 25 W&P, it is possible to simulate the screw configurations of these compounders and at the same time the accuracy of the 2XS software can be checked. 2XS software can currently simulate the flow in the screws under isothermal metal conditions. Here also some additional works can be done, to improve the software by adding the models to simulate the flow under non-isothermal conditions.

Both the developed software can be upgraded by including new screw elements, including models for filler addition (side feeding), mixing of the filler in the polymer melt and residence time calculation.

This work is the initial step to simulate the conical co-rotating twin screw extruders and it is recommended to do further research in developing the models further.

12 Nomenclature

12.1 Symbols

Symbol	Description
a	centerline distance
$a(L)$	centerline distance as a function of screw length
$a(x)$	centerline distance as function of axial position
a_1	constant
a_2	constant
a_{coeff}	throttle coefficient
a_{end}	final centerline distance of conical screws
a_f	edge length for cubic area centered
a_j	edge length
a_p	edge length for cubic primitive
a_r	edge length for cubic room centered
a_{start}	initial centerline distance of conical screws
a_z	pressure transfer exponent
b	solid bed width reduced by the local width of the flight tailback
b_0	maximum channel width
b_{Fmax}	maximum solid bed width
b_k	Length of the flight in kneading element
\bar{b}_s	average width of the slot
c	exponent
d_p	granulate diameter
e_0	maximum flight width
f	area factor
h	channel depth
$h(L)$	channel depth as a function of screw length
$h(x)$	channel depth a function of the Cartesian coordinates
$h(\theta)$	channel depth a function of the angular coordinate
h_0	maximum channel depth
h_{Fm}	mean solid bed height

h_s	height of the slot
i	number of flows channels
j_k	number of discs in kneading element
j_s	number of slots
j_{zs}	number of slots in gear tooth mixing element
J_{zs}	Number of slots in gear tooth mixing elements
k	consistency index
k_1 and k_2	constants for melt film thickness calculation
k_a	dimensionless coefficient
k_x and k_y	pressure anisotropy coefficients
m	geometric parameter for throughput calculation
\dot{m}_{fc}	mass flow rate due to the forced conveyance
\dot{m}_{feed}	fed mass throughput
\dot{m}_{limit}	first throughput limit
\dot{m}_{max}	maximum throughput in feed zone
n	number of screw tips
n	power law index
n_h	number of elements along the channel height
n_b	number of elements along the channel width
n_s	number of tips of the slot
n_z	number of elements along the channel length
p	local pressure
p_0	ambient pressure
p_1	pressure behind intermeshing zone
p_2	pressure behind flight tailback
p_3	pressure in front of intermeshing zonw
p_m	mean pressure
Δp^*	Pressure number
Δp	Pressure difference
S_f	flight clearances
S_f	flight gap of gear teeth mixing discs
S_r	radial clearance
$S_{r,corrected}$	radial clearance corrected for kneading disc element
S_w	calendar gap
S_w	calendar gap of gear tooth mixing elements

t	pitch length
t_k	pitch length of kneading element
t_s	pitch of the slot
v_{0x}	x component of circumferential velocity
v_{0x}	x component of circumferential velocity
v_F	mean solid bed velocity
v_F	mean solid bed velocity
v_{Fz}	solid bed flow velocity
v_{ax}	axial conveying velocity
v_b	barrel velocity
v_{bx}	velocity in cross channel direction
v_{bz}	velocity in down channel direction
v_{rel}	relative velocity
w_B	width of the blister ring
w_k	width of each kneading disc
w_z	thickness of the disc of gear tooth mixing element
x_1	distance between channel center point and contact point of granulate with barrel wall
x_2	distance between channel center point and contact point of granulate with screw
x, y, z	Cartesian co-ordinates
A	zero shear viscosity
A_Δ	area of the gap between the discs
$A_{1,z}$	area of the channel
A_1	flight tip area
$A_{2,z}$	area of the slots
A_2	screw root area
A_3	flight flank area
A_4	triangular section area
A_a	free area in the nip zone
A_{barrel}	cross sectional area of the 8 shaped barrel
$A_{free,B}$	free area in blister ring element
$A_{free,z}$	free area in gear tooth mixing element
A_{free}	free cross-sectional area of the screw
A_{nip}	free area in the nip zone
$A_{profile}$	area of screw profile

A_{zw}	free area in intermeshing zone
B	cross time constant
Br	Brinkmann number
C	slope of power law region
D	barrel diameter
$D(L)$	diameter as a function of screw length
$D_{a,end}$	final screw outer diameter of conical screw
$D_{a,start}$	initial screw outer diameter of conical screw
D_a	outer screw diameter
$D_a(x)$	screw outer diameter as function of axial position
$D_{i,end}$	final screw inner diameter of conical screw
$D_{i,start}$	initial screw inner diameter of conical screw
D_i	inner screw diameter
$F_{0,\infty}$	dwelling bulk density in infinite container
F_0	dwelling bulk density
F_N	normal force acting on screws in intermeshing zone
F_{NSch}	normal force acting on screw root
F_{NSt}	normal force acting on flight
F_{NZ}	normal force acting on barrel
F_{RSch}	force of friction of screw root
F_{RSt}	force of friction of flight
F_{RZ}	force of friction of barrel
F_{Ri}	force of internal friction of loose material
F_d	shape factor – drag flow
F_p	shape factor – pressure flow
Gz	Graetz number
I	dimensionless constant
J_{Δ}	number of triangular gaps in kneading element
$K_1 - K_9$	Menges model constants
L	length of the screw
L_{BP}	backpressure length
$L_{element}$	total length of the element
L_k	total length of kneading element
N	screw rotation speed
N_A	number of particles - Outer

N_K	number of particles - edge
N_M	number of particles - Middle
$N_{P,total}$	number of particles
P^*	Power number
S_{barrel}	surface area of the barrel
S_{flank}	flight flank surface area
S_{nip}	flight tip surface area
$S_{profile}$	surface area of the screw profile
S_{root}	root surface area
T	temperature
\bar{T}	mean melt temperature
\bar{T}_{ini}	initial temperature
\bar{T}_{start}	average start temperature
T_{FI}	bulk material temperature
T_z	barrel temperature
\dot{V}	volumetric flow rate
$V_{P,total}$	total volume of the particle
V_{barrel}	volume of the barrel
$V_{channel}$	channel volume
V_{free}	free channel volume
$V_{p,z}$	particle volume
V_z	volume of unit cell
$\dot{V}_{sr,pressure}$	pressure flow through the radial gap of blister ring element
$\dot{V}_{sw,pressure}$	pressure flow through the calendar gap of blister ring element
\dot{V}^*	volume number
\dot{V}_C	flow in the C-channel of gear tooth mixing elements
\dot{V}_{drag}	volumetric flow rate though drag force
$\dot{V}_{k\ leakage}$	leakage flow over the flights in kneading element
$\dot{V}_{leakage}$	volumetric leakage flow rate
\dot{V}_{nip}	volumetric flow rate though nip area
$\dot{V}_{pressure}$	volumetric flow rate though pressure
$\dot{V}_{slot,leakage}$	leakage flow through slots of the conveying mixing element
\dot{V}_{total}	total volumetric flow rate

V_{zw}	free volume in intermeshing zone
Z_1	tailback length in partially filled channel section of compression zone for the first compression case
Z_2	intermeshing zone tailback length reduced by the flight tailback length
Z_3	tailback length in partially filled channel section of the compression zone for the third compression case
Z_e	flight tailback length
Z_k	free length of the screw channel between two intermeshing zones
Z_r	tailback length

12.2 Greek Symbols

Symbol	Description
$\dot{\gamma}_{rep}$	representative shear rate
$\dot{\gamma}_x$	shear rate in the cross channel direction
$\dot{\gamma}_z$	shear rate in the down channel direction
$\overline{\delta_{mf}}$	average melt film thickness
Θ_1	pressure transfer exponent of flight tailback
Θ_2	pressure transfer exponent of channel section downstream of flight tailback
Ω_k	staggering angle
α_{sc}	angle for calculating max. solid bed width
$\dot{\gamma}$	shear rate
$\delta_{0,mf}$	starting melt film thickness
$\delta_{mf}(x)$	melt film thickness as a function of position
λ_s, λ	thermal conductivity
λ_{sc}	deflection angle
μ_i	internal friction in powder state
μ_{ir}	resultant internal friction
μ_s	coefficient of friction of screw surface
μ_z	coefficient of friction of barrel surface
π_0 and π_1	dimensionless characteristics value
$\rho_{bulk,corr}$	corrected bulk density
ρ_{bulk}	bulk density of loose material
ρ_c	centerline distance ratio
φ_0	pitch angle
φ_k	pitch angle of kneading element
φ_s	pitch angle of the slot
Λ	conveying angle
Φ	angle of steady shear flow of loose material
Ψ	standardized melt film thickness
α	tip and root angle
γ	cone angle of barrel
γ	deflection angle of loose material in intermeshing zone
δ	cone angle of centerline distance

Nomenclature

ζ	dimensionless coordinate in z direction
η	shear viscosity
θ	angular coordinate
ξ	dimensionless coordinate in y direction
ρ	density
χ	angle of substitute circle section
ψ	intermeshing angle

12.3 Acronyms

Symbol	Description
0D	Zero Dimension
1D	One Dimension
2D	Two Dimension
3D	Three Dimension
CAE	Computer aided engineering
CFD	Computational fluid dynamics
DOG	Degree of fill
DSC	Differential scanning calorimeter
FEM	Finite element method
LDPE	Low density poly ethylene
MAS	Maschinen und Anlagen Schulz
NCT	New Conical Technology
NFC	Natural Fiber Composites
PA	Polyamide
PC	Polycarbonate
PET	Polyethylenetherephthalate
PMF	Point of melt pool formation
PPC	Polymer Plastics Composites
PVC	Polyvinylchloride
WPC	Wood Plastics Composites

13 List of Tables

Table 2.1: MAS Extruder series and throughput (MAS Maschinen und Anlagenbau Schulz GmbH, 2016)	15
Table 3.1: Nodes, elements and free volume of different channel profiles	27
Table 4.1: Different screw elements used in MAS NCT55 extruder	44
Table 5.1: Number of particles	58
Table 8.1: Pressure sensors	88
Table 8.2: Barrel temperature settings	88
Table 8.3: Screw elements – Trail 1	89
Table 8.4: Extruder settings – Trail 1	89
Table 8.5: Screw elements – Trail 2	90
Table 8.6: Extruder settings – Trail 2	91
Table 8.7: Technical data of Leistritz compounder (Kunststofftechnik, 2014)	93
Table 8.8: Screw and barrel geometry data	94
Table 8.9: Processing conditions of Leistritz compounder	95
Table 8.10: Extruder settings for the pressure measurement (Winkler-Ebner, 2014)	96
Table 8.11: Extruder settings for the screw pulling experiment (Winkler-Ebner, 2014).....	96
Table 8.12: Resin properties of LDPE ExxonMobil LD159AC.....	98
Table 8.13: Coefficients for LPDE LD159AC in solid state	100
Table 8.14: Coefficients for LPDE LD159AC in melt state and transition region.....	101
Table 9.1: Different barrel elements.....	119
Table 10.1: Experimental results of trail 1	136
Table 10.2: Experimental results of trail 2	141
Table 10.3: Scale up geometry of NCT 90 pressure built-up zone	149
Table 10.4: Materidata of PE-LD 159AC for solid conveying and melting.....	154
Table 10.5: Feedzone element geometry of NCT 55	155
Table 10.6: Experimental degree of fill at different processing setting (Winkler-Ebner, 2014)..	167
Table 10.7: Calculated degree of fill at different processing settings	168
Table 10.8: Measured pressure values over screw axis and melt temperature at screw tip at different extruder settings.....	171

14 List of Figures

Figure 1.1: Classification of extruders.....	1
Figure 1.2: New classification of extruders.....	3
Figure 2.1: a) Construction of segmented screw elements assembled on splined shafts and modular barrel elements (Martin, 2011) b) Main components of a compounder (Harold F.G., 2005)	6
Figure 2.2: Processing zones of parallel twin screw extruder (Kohlgrueber, 2008)	7
Figure 2.3: Types of mixing in polymer compounding	9
Figure 2.4: Types of venting in twin screw extruders (Kohlgrueber, 2008).....	10
Figure 2.5: MAS 55 conical co-rotating twin screw extruder (MAS Maschinen und Anlagenbau Schulz GmbH, 2016).....	11
Figure 2.6: Concept of NCT extruder (Klammer G. , 2009)	12
Figure 2.7: MAS 90 extruder with double vent (MAS Maschinen und Anlagenbau Schulz GmbH, 2016)	13
Figure 2.8: Applications of MAS extruder (MAS Maschinen und Anlagenbau Schulz GmbH, 2016).....	14
Figure 2.9: Processing zones of MAS extruder (MAS Maschinen und Anlagenbau Schulz GmbH, 2016)	16
Figure 2.10: Modular screw concept of MAS conical extruder	17
Figure 3.1: Self-cleaning screw element geometry.....	19
Figure 3.2: Number of flow channels and free volume in single and multiple-flighted screw elements (Kohlgrueber, 2008)	20
Figure 3.3: Major three angles of intermeshing twin screw element (Rauwendaal C. , 1996)...	21
Figure 3.4: Channel depth as a function of angle (θ)	21
Figure 3.5: Screw cross section view perpendicular to screw axis	22
Figure 3.6: Conveying elements with different channel geometries (Kohlgrueber, 2008).....	23
Figure 3.7: Flat plate model of Erdmenger channel profile	24
Figure 3.8: Flat plate model of double edge or box profile	24
Figure 3.9: Geometry of a shear edge profile.....	25
Figure 3.10: Meshing of the Erdmenger screw element and barrel.....	26
Figure 3.11: Free cross-sectional area of self-wiping twin screw geometry (Ansahl, 1993)	28
Figure 3.12: Concept of conical extruders (Seifert, 2005).....	30
Figure 3.13: Conical extruder screw geometry (Hensen, Knappe, & Potente, 1989).....	31
Figure 4.1: Major classification of screw elements (Extricom, 2015).....	33
Figure 4.2: Geometry of a convey screw element	34
Figure 4.3: Conveying screw elements with single, double and triple flights (Extricom, 2015) .	35
Figure 4.4: a) Positive and b) negative conveying screw elements	36

Figure 4.5: Geometry of kneading element (Ansahl, 1993).....	37
Figure 4.6: Kneading elements with different staggering angle (Extricom, 2015).....	38
Figure 4.7: Area of leakage gap in kneading block element.....	39
Figure 4.8: Conveying mixing element.....	40
Figure 4.9: Gear tooth mixing element.....	41
Figure 4.10: Blister ring element.....	43
Figure 4.11: Clearances in blister ring element.....	43
Figure 5.1: Definition of deflection angle.....	48
Figure 5.2: Mean solid bed width and solid bed height of Erdmenger channel profile (Melisch, 1997).....	49
Figure 5.3: Position of the material feeding (Melisch, 1997).....	50
Figure 5.4: Limiting cases of feed behavior (Potente, Melisch, & Palluch, 1996).....	51
Figure 5.5: Material distribution for third conveying case (Potente, Melisch, & Palluch, 1996)..	52
Figure 5.6: Equilibrium forces for three characteristic volume elements in solid feed zone (Potente, Melisch, & Palluch, 1996).....	53
Figure 5.7: Equilibrium of moments for the volume element (Potente, Melisch, & Palluch, 1996).....	54
Figure 6.1: Modified Tadmor melting model (Ansahl, 1993).....	60
Figure 7.1: Groove model of conveying screw element.....	68
Figure 7.2: Flow in intermeshing co-rotating twin screw conveying element (Schuler, 1996)...	69
Figure 7.3: Erdmender (or) standard screw channel geometry.....	69
Figure 7.4: Cross sectional view of shear edge screw channel geometry.....	73
Figure 7.5: Cross sectional view of box (or) double shear edge screw channel geometry.....	75
Figure 7.6: Free cross-sectional area in the nip zone of box profile (Himmler, 2010).....	76
Figure 7.7: Screw characteristic curve for forward conveying element.....	78
Figure 7.8: Groove model of kneading block element.....	79
Figure 7.9: conveying mixing elements with mixing slots.....	81
Figure 7.10: Melt flow in the blister ring element.....	81
Figure 7.11: Back pressure length calculation algorithm.....	84
Figure 8.1: MAS NCT55 extruder.....	85
Figure 8.2: Pressure measurement positions along the screw length of NCT55.....	86
Figure 8.3: Experimental setup of NCT55.....	87
Figure 8.4: Screw configuration with screw element length for Trail 1 (Schuschnigg, 2009)....	88
Figure 8.5: Screw configuration with screw element length for Trail 2 (Selvasankar, 2010)....	90
Figure 8.6: Measured pressures and temperature over time.....	91
Figure 8.7: Leistritz ZSE 27 MAXX Compounder (Kunststofftechnik, 2014).....	92
Figure 8.8: Leistritz screw elements used for the trails (Winkler-Ebner, 2014).....	93

Figure 8.9: Screw configuration – standard screw (Winkler-Ebner, 2014)	94
Figure 8.10: Pressure measurement positions over the screw length (Winkler-Ebner, 2014)....	95
Figure 8.11: Screw elements of standard configuration.....	97
Figure 8.12: Shear viscosity of LDPE ExxonMobil LD159AC.....	99
Figure 8.13: pvT diagram of LDPE ExxonMobil LD159AC.....	100
Figure 8.14: Thermal conductivity of LDPE ExxonMobil LD159AC.....	102
Figure 8.15: Specific heat capacity of LDPE ExxonMobil LD159AC.....	103
Figure 9.1: Advantages and disadvantages of different model dimensions (Kohlgrueber, 2008).....	106
Figure 9.2: Potential of models in describing the complete extrusion process (Kohlgrueber, 2008).....	106
Figure 9.3: General calculation procedure.....	108
Figure 9.4: Pressure calculation procedure	109
Figure 9.5: NCT main window	110
Figure 9.6: Project input page	111
Figure 9.7: Screw configuration page.....	112
Figure 9.8: Material data window.....	113
Figure 9.9: Material properties window.....	114
Figure 9.10: Process paramter.....	115
Figure 9.11: Simulation.....	116
Figure 9.12: Graphical representation of results	117
Figure 9.13: Main window of 2XS screw modeling tool.....	118
Figure 9.14: Shaft configuration page	119
Figure 9.15: Barrel zones configuration	120
Figure 9.16: Configuration of the screw elements.....	121
Figure 9.17: A complete configured screw	121
Figure 9.18: Addition of new screw element to the data base.....	122
Figure 9.19: Die configuration page	122
Figure 9.20: Material definition for the simulation.....	123
Figure 9.21: Configuring the process settings for the calculation.....	124
Figure 9.22: Starting the simulation in the simulation window	125
Figure 10.1: Geometry of conveying elements with different channel profiles for Polyflow simulation.....	126
Figure 10.2: Free volume of different channel profiles of screw element	127
Figure 10.3: Output at different screw speeds for different screw channel profiles	128
Figure 10.4: Generated max. pressure of different channel profiles at 20 kg/h output and different screw speeds.....	129

Figure 10.5: Generated max. pressure of different channel profiles at maximum output and different screw speeds.....	129
Figure 10.6: Local pressure generation over screw element length for different channel profiles at 40 kg/h and at 100 rpm.....	130
Figure 10.7: Pressure profile over screw length of metering zone of MAS90 extruder at 160 rpm and 600 kg/h for a recycled PET material	131
Figure 10.8: Local shear rate at 20 kg/h and at different screw rotation speeds.....	132
Figure 10.9: Max. shear rate dependence on screw speed at constant flow rate of 20 kg/h	133
Figure 10.10: Shear rate dependence on flow rate at constant screw speed of 200 rpm	133
Figure 10.11: Melt viscosity at 20 kg/h and at different screw speeds	134
Figure 10.12: Comparison of flow velocities at 400 rpm and 40 kg/h for different screw channel profiles.....	135
Figure 10.13: Output as a function of screw speed.....	137
Figure 10.14: Measured melt pressure at different screw speeds and slit heights	138
Figure 10.15: Measured melt temperature in front of the die for different screw speed and slit heights.....	138
Figure 10.16: Pressure characteristics curve of NCT55.....	139
Figure 10.17: Comparison of measured and calculated pressure values – Trail 1.....	140
Figure 10.18: Melt temperature in the die and adapter at different flow rates and slit heights .	141
Figure 10.19: Screw and die characteristics curve of NCT 55 extruder.....	142
Figure 10.20: Position of pressure sensor over the screw length.....	143
Figure 10.21: Measured and calculated pressure values over the metering zone at 200 kg/h output; 2 mm slit height; 200 rpm screw speed	144
Figure 10.22: Measured and calculated pressure values over metering zone at 200 rpm and 4 mm slit height for different throughputs	145
Figure 10.23: Dependence of back pressure length on output at constant screw speed of 200 rpm and slit height of 4 mm.....	145
Figure 10.24: Measured and calculated pressure values over complete screw length at 200 rpm, 200 kg/h and 2 mm slit height.....	146
Figure 10.25: Pressure vs. output in the conveying mixing zone	147
Figure 10.26: Measured and calculated pressure value over complete screw length at 200 rpm, 250 kg/h output and 3 mm slit height	148
Figure 10.27: Shear viscosity of recycled PET (Arbeiter, 2011)	149
Figure 10.28: Effect of extruder output on the pressure of the NCT 90 pressure built-up zone at constant screw speed	150
Figure 10.29: Effect of screw pitch on the pressure of the NCT 90 pressure built-up zone at screw speed of 160 rpm.....	151
Figure 10.30: Effect of number of flights on the melt pressure generation of the NCT 90 pressure built-up zone at screw speed of 160 rpm and 1000 kg/h output.....	152

Figure 10.31: Effect of radial clearance on the pressure of the NCT 90 pressure built-up zone at screw speed of 160 rpm and 1000 kg/h output	152
Figure 10.32: Effect of screw rotation speed on the pressure of the NCT 90 pressure built-up zone at a constant output of 900 kg/h and melt temperature of 285 °C	153
Figure 10.33: Total number of particles dependent on the particle alignment for LDPE	154
Figure 10.34: Solid bed width as a function of particle diameter for double flighted solid conveying zone	156
Figure 10.35: Solid bed width as a function of particle diameter for single flighted solid conveying zone	156
Figure 10.36: Theoretical maximum output of NCT 55 feeding element for PE-LD 159AC under flood fed condition	157
Figure 10.37: Dimensionless solid bed width and melt temperature as a function of screw length	158
Figure 10.38: Maximum flow rate of conveying elements with different pitch for PP DM55 at 55 rpm screw speed and 200 °C melt temperature.....	160
Figure 10.39: Maximum flow rate of conveying elements with different pitch for PP DM55 at 145 rpm screw speed and 200 °C melt temperature	161
Figure 10.40: Pressure generation of different screw elements for PP DM55 at 8 kg/h output; 55 rpm screw speed and 200 °C melt temperature.....	162
Figure 10.41: Pressure generation of different screw elements for PP DM55 at 8 kg/h output; 145 rpm screw speed and 200 °C melt temperature	163
Figure 10.42: Screw characteristic curve of conveying (positive, negative and mixing) elements for PP Bormed™ DM55Pharm at 200 °C melt temperature	164
Figure 10.43: Screw characteristic curve of kneading elements (positive, negative and neutral conveying) for PP Bormed™ DM55Pharm at 200 °C melt temperature	164
Figure 10.44: Dimensionless screw characteristic forward and backward conveying elements for PP Bormed™ DM55Pharm at 200 °C melt temperature	166
Figure 10.45: Comparison of DOF measured and calculated for 8 kg/h of PP DM55 at 50 rpm, 200 °C melt temperature and 15 bar back pressure at screw tip.....	170
Figure 10.46: Comparison of DOF measured and calculated for 8 kg/h of PP DM55 at 150 rpm, 200°C melt temperature and 45 bar back pressure at screw tip.....	170
Figure 10.47: Pressure profile along screw length at 8 kg/h; 55 rpm; 200 °C and 45 bar back pressure	172
Figure 10.48: Viscosity and shear rate profile along screw length at 8 kg/h; 55 rpm; 210 °C and 45 bar back pressure.....	173
Figure 10.49: Pressure profile along screw axis at 8 kg/h; 55 rpm; 210 °C for 45 bar and 15 bar back pressure	174
Figure 10.50: Pressure profile along screw length at a constant screw speed of 145 rpm, 15 bar back pressure, 210 °C melt temperature and different output.....	175

15 Bibliography

- Ansahl, J. (1993). *Grundlagen zur Auslegung dichtkämmender Gleichdrall-Doppelschneckenextruder*. Dissertation, Universität Paderborn.
- Arbeiter, F. (2011). *Vergleichende Messungen von MFR, IV-Werten und Viskositätskurven von PET aus dem Recycling*. Bachelor Thesis - Institut für Kunststoffverarbeitung, Montanuniversität Leoben.
- Barrera, M., Vega, J., & Martinez-Salazar, J. (2008). Three-dimensional modelling of flow curves in co-rotating twin-screw extruder elements. *Journal of Materials Processing Technology*, 197(1-3), 221-224.
- Bawiskar, S., & White, J. (1998). Melting model for modular self-wiping co-rotating twin screw extruders. *Polymer engineering and science*, 38 (5).
- Berghaus, U. (1995). Aufbau der Verfahrenszonen und Betriebsverhalten. In *Der Doppelschneckenextruder Grundlagen- und Anwendungsgebiete*. Duesseldorf: VDI Verlag GmbH.
- Bittermann, R., & Sykacek, E. (2007). From tetra pack to raw material. *Kunststoffe International*, 10.
- Booy, M. (1978). Geometry of fully wiped twin screw equipment. *Polymer Engineering and Science*, 18 (12).
- Booy, M. (1980). Isothermal flow of viscous liquid in co-rotating twin screw devices. *Polymer Engineering and Science*, 20 (18).
- Bravo, V., Hrymak, A., & Wright, J. (2000, February). Numerical simulation of pressure and velocity profiles in kneading elements of a co-rotating twin screw extruder. *Polymer Engineering & Science*, 40 (2), 525-541.
- Carrot, C., Guillet, J. M., & Puaux, J. (1993). Modeling of the conveying of solid polymer in the feeding zone of intermeshing co-rotating twin screw extruders. *Polymer Engineering and Science*, 33 (11), pp. 700-708.
- Carlsaw, H., & Jaeger, J. (1959). *Conduction of heat in solids*. London: Oxford University Press.
- Chung, C. (2000). *Extrusion of Polymers: Theory and Practice*. Hanser Publishers.
- Coperion. (2013). *ZSK MEGAcoumponder*. Retrieved December 31, 2013, from <http://www.coperion.com/compounding-extrusion/maschinen-anlagen/zsk-baureihe/zsk-megacomponder/>
- Elsay, J. R. (2002). *Dynamic modelling, measurement and control of co-rotating twin screw extruders*. University of Sydney. Australia: Doctor Thesis, University of Sydney.
- Erdmenger, R., Meskat, W., Dormagen, & Gladbach, B. (1954). *Patent No. 2,670,188*.
- Extricom. (2015). Retrieved February 09, 2015, from <http://www.extricom.de/>
- Gotsis, A., Ji, Z., & Kalyon, D. (1990). 3D Analysis of the flow in Co-rotating twin screw extruders. *ANTEC*, (pp. 139-142).
- Häring, E. (1974). *Feststoffförderverhalten einer Doppelschneckenpresse*. University of Stuttgart.

- Harold F.G., W. J. (2005). *Extrusion: The Definitive Processing Guide and Handbook*. New York: William Andrew, Inc.
- Hauck B.W., W. L. (2002). *Patent No. US 6688217 B2*. US.
- Hensen, F., Knappe, W., & Potente, H. (1989). *Handbuch der Kunststoff-Extrusionstechnik I Grundlagen*. München Wien: Carl Hanser.
- Himmler, G. (2010). *Verfahrenstechnische Auslegung der Ausstoßzone eines konischen gleichlaufenden Doppelschneckenextruders*. Master Thesis - Institut für Kunststoffverarbeitung, Montanuniversität Leoben.
- Jäcker, M. (2000). The conical concept of the future. *Kunststoffe Plast Europe*, 90 (12).
- Jacobi, H. (1960). *Grundlagen der Extrudertechnik*. München: Carl Hanser Publishers.
- Janssen, L., Goffart, D., Van Der Wal, D., Klomp, E., Hoogstraten, H., Breyse, L., & Trolez, Y. (1996). Three-dimensional flow modeling of a self-wiping corotating twin-screw extruder. Part I: The transporting section. *Polymer Engineering & Science*, 36 (7), 901-911.
- John Wood & Associates Ltd. (2009). *MAS*. Retrieved January 2, 2014, from NCt Extruder: <http://www.johnwoodassociates.com/MAS%20NCT.htm>
- Klammer, G. (2009). Conical co-rotation. *Kunststoffe International*, 10.
- Klammer, G. (2010). A conical co-rotating machine puts on the pressure. *Kunststoffe International*, 8.
- Koch, M. (1987). *Berechnung und Auslegung von Nutbuchsenextrudern*. University of Paderborn.
- Kohlgrueber, K. (2008). *Co-Rotating Twin-Screw Extruders - Fundamentals, Technology and Applications*. Munich: Carl Hanser Verlag.
- Kretschmer, K. (2004). *Untersuchung und Beschreibung des Prozess- und Mischverhaltens von Mischelement für Glieddrall-Doppelschneckenextruder*. Dissertation, Universität Paderborn.
- Kunststofftechnik. (2014). *Department of Injection Moulding of Polymers*. Retrieved 11 30, 2015, from <http://www.kunststofftechnik.at/sgk-injection-moulding-machines/>
- Kunststofftechnik-Leoben. (2015). *Kunststofftechnik Leoben*. Retrieved February 12, 2016, from http://www.kunststofftechnik.at/files/attachments/7432/539796_Equipment_KT_Leoben.pdf
- Maddock, B. (1959). A visual analysis of flow and mixing in extruder screws. *SPE ANTEC Tech. Papers*, 15, pp. 382-389.
- Markarian, J. (2005, March/April). Compounder look to simulation software for savings in time and costs. *Plastics Additives & Compounding*, pp. 34-36.
- Martin, C. (2011, July). Look Before You Leap: When Direct Extrusion Makes Sense. 57(7), pp. 22-25.
- MAS. (2014). *eFACTOR THRee*. Retrieved January 3, 2014, from Product Literature: http://efactor3.com/wp-content/uploads/mas_wpc-E-mail.pdf
- MAS Maschinen und Anlagenbau Schulz GmbH. (2016). *MAS Extruder*. Retrieved February 04, 2016, from <http://www.mas-austria.com/en/Products/MAS-extruder>
- Meijer, H., & Elemans, P. (1988). The modeling of continuous mixers Part 1: The co-rotating twin screw extruder. *Polymer Engineering and Science*, 28 (5).

- Melisch, U. (1997). *Grundlagen zur Simulation der Förder- und Plastifizierprozesses dichtkämmernder Gleichdrall-Doppelschneckenextruder*. Universität-GH Paderborn.
- Michaeli, W., Grefenstein, A., & Berghaus, U. (1995). Twin-Screw Extruders for Reactive Extrusion. *Polymer Engineering and Science*, 35 (19).
- Mours, M., Reinelt, D., Wagner, H.-G., Gilbert, N., & Hofmann, J. (2000). Melt conveying in co-rotating twin screw extruders. *International Polymer Processing*, 14.
- Münzer, M. (2011). *Berechnung der Einzugszone und der Aufschmelzzone eines konisch gleichlaufenden Doppelschneckenextruders*. Master Thesis, Lehrstuhl für Kunststoffverarbeitung.
- Padmanabhan, B. (2008). Understanding the extruder processing zone: the heart of a screw extruder. *Plastic Additives & Compounding*.
- Peptflow. (2014). *Sciences Computers Consultants*. Retrieved February 09, 2014, from <http://www.sccconsultants.com/docs/PEPTFlowMachineDesignHandbook.pdf>
- Potente, H., Ansahl, J., & Klarholz, B. (1994). Design of tightly intermeshing co-rotating twin screw extruder. *International Polymer Processing*, IX, 11-25.
- Potente, H., Ansahl, J., & Wittemeier, R. (1990). Throughput characteristics of tightly intermeshing co-rotating twin screw extruders. *International Polymer Processing*, V(3).
- Potente, H., Kretschmer, K., & Flecke, J. (2001). A physical-mathematical model for the description of the process behavior of mixing elements. *SPE ANTEC*. Dalla, Texas.
- Potente, H., Melisch, U., & Palluch, K. (1996). A physico-mathematical model for solid conveying in co-rotating twin screw extruders. *International Polymer Processing*, XI.
- Rauwendaal, C. (2001). *Polymer Extrusion* (Vol. IV). Munich: Carl Hanser Verlag.
- Rauwendaal, C. (1996). The geometry of self-cleaning twin screw extruders. *Advances in Polymer Technology*, 15(2), pp. 127-133.
- Schneider, H. P. (2005, 5). The historical development of the counter-rotating twin screw extruder. *Kunststoffe*, pp. 1-6.
- Schöppner, V. (1994). *Simulation der Plastifiziereinheit von Einschneckenextrudern*. Universität-GH Paderborn.
- Schuler, W. (1996). *Process engineering design of co-rotating twin screw extruders*. Doctor Thesis, University of Wales Swansea.
- Schulz, H. (2006). *Patent No. US 2009/0040867 A1*. AT.
- Schuschnigg, S. (2009). *Untersuchungsbericht - Geometrie*.
- Schuschnigg, S. (2009). *Untersuchungsbericht - Versuch I*.
- Schuschnigg, S. (2014). *Simulation twin screw elements*.
- Schuschnigg, S., Klammer, G., & Holzer, C. (2010). Introduction of the conical co-rotating twin screw extruder. *PPS 26 Conference Proceedings*.
- Seifert, S. (2005). Comparison of parallel and conical twin screw extruders from the processing point of view. *Plastics, Rubbers and Composites*, 34 (3), pp. 134-142.
- Selvasankar, R. (2010). *Untersuchungsbericht - Versuch II*.
- Tadmor Z., K. I. (1970). *Engineering Principles of Plasticating Extrusion*. New York: Van Nostrand Reinhold Company.

- Tadmor, Z., & Klein, I. (1970). *Engineering principles of plasticating extrusion*. New York: Van Nostrand Reinhold Company.
- Tayeb, J., Vergnes, B., & Della Valle, D. (1988). Theoretical computation of the isothermal flow through the reverse screw element of a twin screw extrusion cooker. *Journal of Food Science*, *53* (2), pp. 616-625.
- Thermo Scientific. (2013). *HAAKE™ MiniCTW Micro-Conical Twin Screw Compounder*. Retrieved December 31, 2013, from <http://www.thermoscientific.com/en/product/haake-minictw-micro-conical-twin-screw-compounder.html>
- Theysohn Extrusion. (2013). *Compounder TSK*. Retrieved December 31, 2013, from <http://www.ht-extrusion.com/de/produkte/compounder-tsk/>
- Todd, D. (1998). *Plastics compounding, equipment and processing*. Munich: Hanser Publishers.
- Toensmeier, P. (2015, February). This year's model: advances in computer simulation. *Compounding World*, pp. 33-40.
- Unipetrol. (2016). *Mosten TB 003*. Abgerufen am 13. February 2016 von Unipetrol Deutschland:
http://www.unipetrol.de/de/produktuebersicht/thermoplaste/Seiten//product_details_M.aspx?product=Mosten%20TB%20003
- Vergnes, B., Della Valle, G., & Delamare, L. (1998). A global computer software for polymer flows in corotating twin screw extruders. *Polymer Engineering & Science*, *38* (11), pp. 1781-1792.
- Wang, Y. (2000). *Compounding in Co-rotating twin screw extruders* (Vol. 10). Rapra Technology Ltd.
- Wang, Y., White, J., & Szydowski, W. (1989). Flow in a modular intermeshing co-rotating twin screw extruder. *International Polymer Processing*, *4* (4).
- White, & Szydowski. (1987). Composite models of modular intermeshing co-rotating and tagential counter-rotating twin screw extruders. *Advances in Polymer Technology*, *7* (4).
- White, J. L., & Bawiskar, S. (1997). A composite model for solid conveying, melting, pressure and fill factor profiles in modular co-rotating twin screw extruders. *International Polymer Processing*, *4*, pp. 331-340.
- White, J. L., & Chen, Z. (1994). Simulation of non-isothermal flow in modular co-rotating twin screw extrusion. *Polymer Engineering and Science*, *34* (3).
- White, J. L., & Kim, E. K. (2010). *Twin Screw Extrusion Technology and Principles* (Vol. II). Hanser Gardner Publications.
- White, J., & Bawiskar, S. (1995). Solids conveying and melting in a starve fed self-wiping co-rotating twin screw extruder. *International Polymer Processing*, *2*, pp. 105-110.
- White, J., & Jung, H. (2003). Investigation of melting phenomena in modular co-rotating twin screw extrusion. *Intern.Polymer Processing*, *XVIII*.
- White, J., Byong-Jun, K., Santosh, B., & Jong, K. (2001). Development of a Global Computer Software for Modular Self-Wiping Corotating Twin Screw Extruders. *Polym.-Plast. Technol. Eng.*, *40* (4), pp. 385-405.
- White, J., Kim, B., & Bawiskar, S. (2001). Development of a global computer software for the modular self-wiping corotating twin screw extruders. *Polym.-Plast. Technol. Eng.*

Winkler-Ebner, J. (2014). *Simulationgestützte Schneckengeometrieoptimierung für die Herstellung von nanoverstärkten Polypropylenecompounds*. Leoben: Master Thesis, Department of Injection Moulding of Polymers, Montanuniversity.

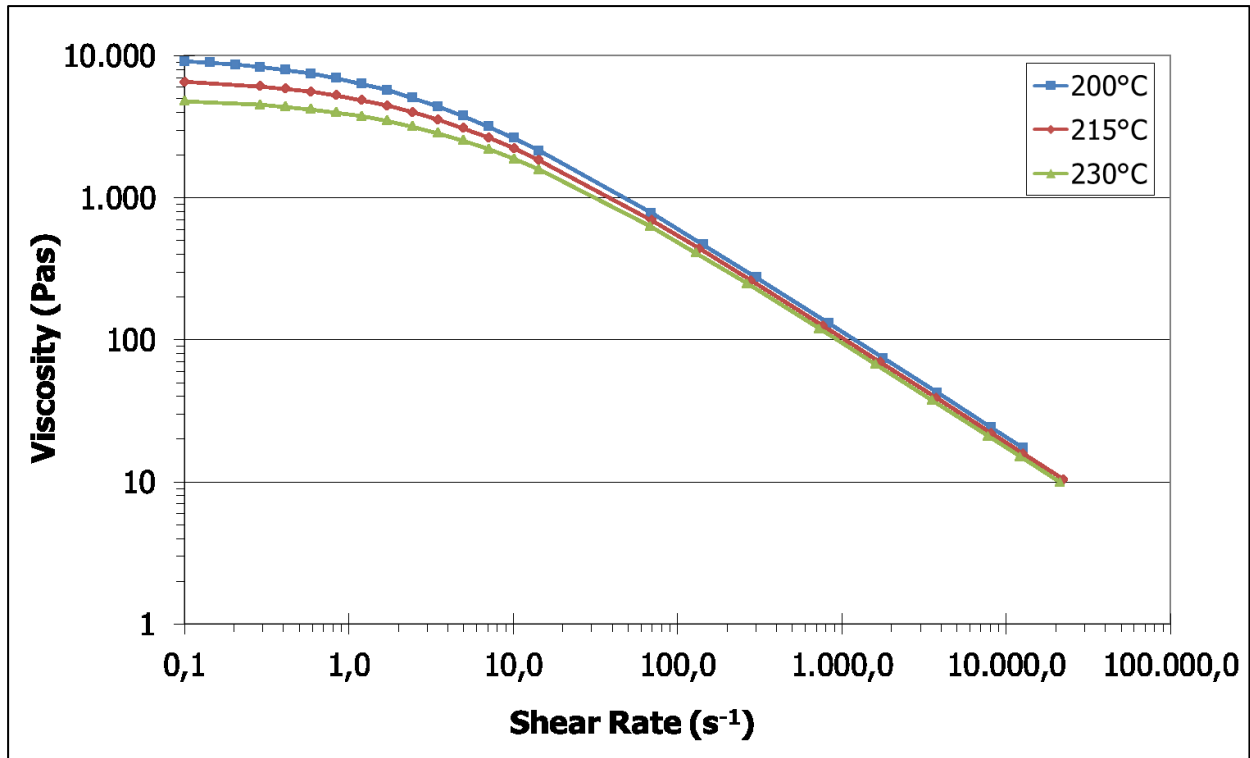
Wortberg, J., & Kaczmarek, D. (2004). *Kunststoff-Maschinenführer - Chapter Extruder und Extrusionsanlagen*. Munich: Carl Hanser Verlag.

Zhang, X.-M., Feng, L.-F., Chen, W.-X., & Hu, G.-H. (2009). Numerical Simulation and Experimental Validation of Mixing Performance of Kneading Discs in a Twin Screw Extruder. *Polymer Engineering and Science*, 49, 1772-1783.

16 Appendix

Material Data - PP Bormed™ DM55pharm

Viscosity

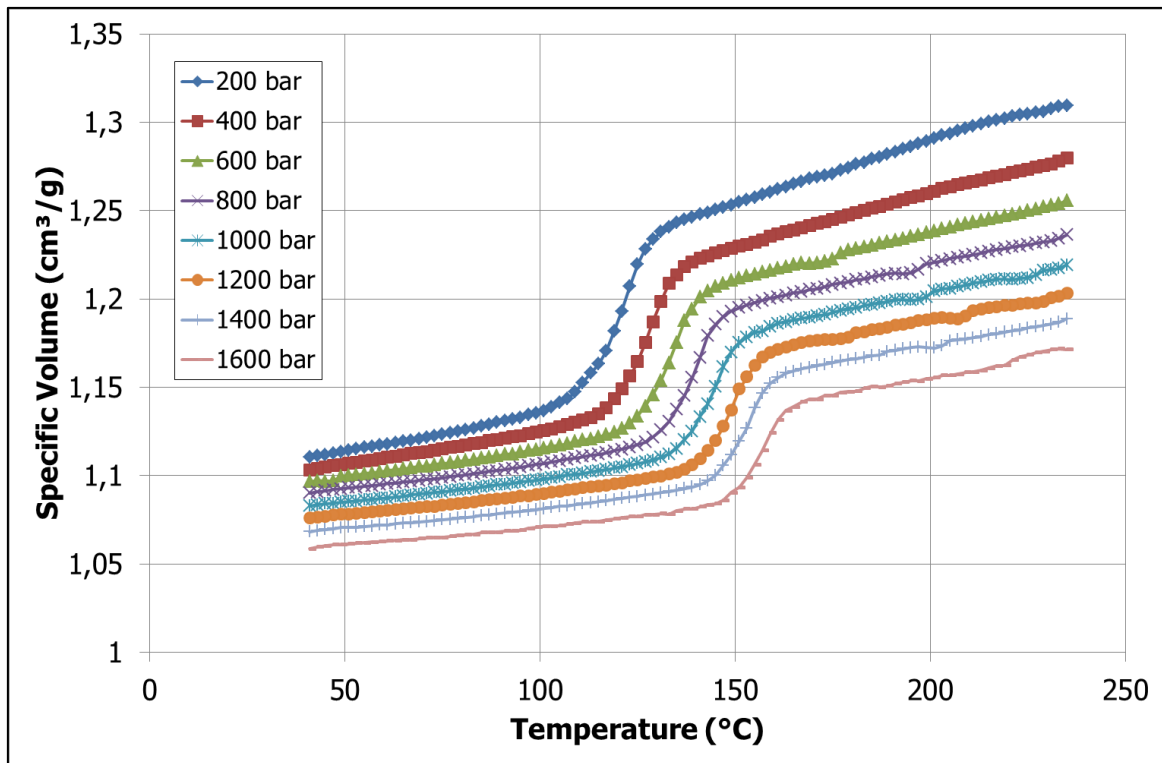


DM55 Unfilled

A _T -Factor, Arrhenius model:	$a_T = e^{\left(\frac{\Delta U_\tau}{R} \cdot \left(\frac{1}{T} - \frac{1}{T_0}\right)\right)}$	
Cross model with temperature shifting	$\eta = \frac{a_T \cdot A}{1 + (B \cdot a_T \cdot \dot{\gamma})^C}$	
Shear rate range: $\dot{\gamma} = 0,1 \text{ s}^{-1}$ to $\dot{\gamma} = 10.000 \text{ s}^{-1}$		
Cross constants	T_0 (K)	ΔU_τ (kJ/mol)
A= 7018 (Pas)	488.15	45.35
B= 0.27740 (s)		
C= 0.74576 (/)		

pVT

DM55 Unfilled

*Coefficients for solid state*

K1	38372	cm ³ bar/g
K2	0.41579	cm ³ bar/g
K3	1133.2	bar
K4	34714	bar
K5	2.79 E ⁻⁶	cm ³ /g
K6	0.084	1/°C
K7	0.0024	1/bar

Coefficients for melt region

K1	22655	cm ³ bar/g
K2	1.4277	cm ³ bar/g
K3	1999.7	bar
K4	19443	bar

Coefficients for transition region

K8	126.11	°C
K9	0.024601	°C/bar

DSC

DM55 Unfilled

